Dissertation zur Erlangung des Doktorgrades
der Fakultät für Biologie
der Ludwig-Maximilians-Universität München

Structural, biochemical and biophysical characterisation of human transcription factor RBP-Jκ

von

Karen Henning

München, im April 2006

Erklärung:

Diese Dissertation wurde im Sinne der Promotionsordung von Dr. Matthias Wilmanns, an der Außenstelle des Europäischen Laboratoriums für Molekularbiologie (EMBL) in Hamburg betreut und von PD Dr. Bettina Kempkes vor der Fakultät vertreten.

Ehrenwörtliche Versicherung

Diese Dissertation wurde selbstständig und ohne unerlaubte Hilfe angefertigt.

München, den 20. April 2006

Karen Henning

eingereicht am	28. April 2006
Erstgutachter	PD Dr. Bettina Kempkes (GSF Munich)
Zweitgutachter	Prof. Dr. Dirk Eick (GSF Munich)
Mündliche Prüfung	19. Oktober 2006

Table of Contents

Table of Contents i

List of Abbreviations iv

1 Introduction 1

1.1 RBP-Jκ 1

1.2 Protein interaction partners of RBP-Jκ 3

1.2.1 Cellular interaction partners 3

1.2.2 Viral interaction partners 10

1.3 Interaction of RBP-Jκ with Notch1 and EBNA2: structural aspects 13

1.3.1 Structure of RBP-Jκ 13

1.3.2 Structural information about Notch1 14

1.3.3 EBNA2 15

1.3.4 Common and distinct features of Notch and EBNA2 17

1.4 Open questions 19

1.5 Scope of this thesis 20

2 Materials and Methods 22

2.1 Materials 22

2.1.1 Bacterial Strains 22

2.1.2 Cell lines 22

2.1.3 Plasmids 23

2.1.4 Oligonucleotides 24

2.1.5 Antibodies 28

2.1.6 Enzymes 28

2.1.7 Peptides 29

2.1.8 Chemicals 29

2.1.9 Crystallisation screens 31

2.1.10 Laboratory equipment 31

2.1.11 Synchrotron radiation sources 32

2.1.12 Software 32

2.1.13 Kits, columns and other material 33

2.2 Methods 34
2.2.1 Bacterial cell culture 34
2.2.2 Eucaryotic cell culture 37
2.2.3 DNA manipulation and analysis 39
2.2.4 Methods for the analysis of proteins and DNA/protein interactions 42
2.2.5 Expression and purification of proteins 45
2.2.6 Isothermal titration calorimetry (ITC) 54
2.2.7 Small angle X-ray scattering (SAXS) 63
2.2.8 Circular dichroism (CD) 67

3 Results 71

3.1 Expression and purification of human RBP-Jκ, Notch1 and EBNA2 constructs 71
3.1.1 Expression and purification of full-length human RBP-Jκ and RBP-Jκ fragments 71
3.1.2 Expression and purification of Notch^{Ram} and Notch^{RamANK} 83
3.1.3 Expression and purification of EBNA2 proteins 85
3.2 Biochemical and biophysical characterization of the interaction of RBP-Jκ with Notch^{Ram} or Notch^{RamANK} or EBNA2 87
3.2.1 Binary complexes of RBP-Jκ with DNA and comparison of recombinant RBP-Jκ proteins expressed in *E.* coli and insect cells 87
3.2.2 Formation of ternary complexes with RBP-Jκ, DNA and Notch^{Ram} or Notch^{RamANK} 99
3.2.3 Contribution of the ANK domain to RBP-Jκ binding 103
3.2.4 The affinity of EBNA2$^{259-435}$ to nRBP$^{full-length}$ is two orders of magnitude higher than that of Notch^{RamANK} 117
3.3 Crystallization trials of RBP-Jκ bound to DNA, peptides derived from Notch^{Ram} or EBNA2 and Notch^{Ram} or Notch^{RamANK} 131

4 Discussion 138

4.1 Importance of RBP-Jκ in the context of Epstein-Barr virus infections 138
4.2 The binding properties of recombinant RBP-Jκ depend on the expression system 139
4.3 The conserved part of RBP-Jκ has the same binding properties for DNA or Notch proteins as its full-length counterpart 140
4.4 The ankyrin repeats of Notch-IC do not detectably contribute to RBP-Jκ binding 140

4.5 The minimal RBP-Jκ binding site in EBNA2 (CR5 and CR6) does not account for its strong binding affinity 145
4.6 Impact of the stronger binding affinity of EBNA2$^{259-435}$ compared to that of Notch^{RamANK} on the cellular and Epstein-Barr viral system 147
4.7 Further experiments and outlook 149

Summary 151

Zusammenfassung 153

References 155

Acknowledgements 166

Lebenslauf 167

List of Abbreviations

Å	Ångstrøm
aa	amino acids
ADAM	family of proteins with disintegrin and metalloprotease function
ANK	domain of hNotch1 comprising seven ankyrin repeats
APS	ammonium persulfate
ATP	adenosine triphosphate
bp	base pair(s)
BSA	bovine serum albumin
CD	circular dichroism spectropolarimetry
CIR	CBF-1 interacting repressor
Cp	Epstein-Barr viral C-promoter
DNA	desoxyribonucleic acid
dNTP	3'-desoxyribonucleoside-5'-triphosphate
dpm	disintegration per minute
DTT	1,4-dithio-DL-threitol
EBNA	Epstein-Barr virus nuclear antigen
EBV	Epstein-Barr virus
E. coli	*Escherichia coli*
EDTA	ethylenediamine tetra-acetic acid
EMSA	electrophoretic mobility shift assay
FCS	fetal calf serum
GCN5	family of histone acetyltransferases
GST	glutathione-S-transferase
h(rs)	hour(s)
HDAC	histone deacetylase
HEPES	4-(2-hydroxyethyl)-1-piperazine-ethane-sulfonic acid
6xHis	hexahistidine affinity purification tag
HRP	horseradish peroxidase
HSV	Herpes simplex virus
IPTG	isopropyl-β-D-thiogalactopyranoside
I(s)	scattering intensity
I(0)	forward scattering intensity
ITC	isothermal titration calorimetry
K_a	molar association constant
K_d	molar dissociation constant
kbp	kilo base pairs
kDa	kilo Dalton
l	litre
LB	Luria Bertani bacterial growth medium
LMP	Latent Membrane Protein
LMP1P	Epstein-Barr viral LMP1 promoter
LMP2AP	Epstein-Barr viral LMP2A promoter
mA	Milliampere
min	minute(s)
MR	molecular replacement
M***r***	relative molecular mass
mRNA	messenger RNA
N	stoichiometry

Ni-NTA	nickel nitrilotriacetic acid
NLR	Notch-Lin region
NLS	nuclear localisation signal
NMR	nuclear magnetic resonance spectroscopy
Notch-IC	Notch intracellular domain
$Notch^{Ram}$	construct including the hNotch1-Ram domain
$Notch^{RamANK}$	construct including the hNotch1-Ram and ankyrin domain (ANK)
$nRBP\text{-}J^{aa\text{-}aa}$	RBP-Jκ construct expressed in insect cells and purified under native conditions
O.D.	optical density
$oli\text{-}Cp^{bp}$	double-strand DNA oligonucleotide derived from the C-promoter
$oli\text{-}LMP1P^{36}$	double-strand DNA oligonucleotide derived from the LMP1-promoter
$oli\text{-}LMP2AP^{54}$	double-strand DNA oligonucleotide derived from the LMP2A-promoter
PAA	polyacrylamide
PABP2	polyadenylate-binding protein 2
PAGE	polyacrylamide gel electrophoresis
PBS	phosphate buffered saline
PCAF	p300/CBP associated factor
PCR	polymerase chain reaction
PDB	Protein Data Bank
PEG	polyethylene glycol
PEST	amino acid sequence labelling a protein for rapid degradation
pI	isoelectric point
PMSF	phenylmethylsulfonylfluoride
PNK	polynucleotide kinase
poly-dIdC	nucleic acid polymer composed of desoxy-inosine and desoxy-cytidine
p(r)	distance distribution function
pRB	phosphorylated retinoblastoma protein
PRP45	SKIP homologue in *S. cerevisiae*
PU.1/Spi-1	transcription factor belonging to the Ets family
PVDF	polyvinylidene fluoride
R	gas constant, 8.314 J/mol/K
Ram	RBP association molecule; domain in hNotch1
RBP-Jκ	recombination signal binding protein-J, identical to CBF-1
R_g	radius of gyration
rpm	revolutions per minute
$rRBP^{aa\text{-}aa}$	RBP-Jκ construct expressed in *E.* coli, purified and refolded
RT	room temperature
s	momentum transfer vector, $s=4\pi\sin(\theta)/\lambda$, where 2θ is the scattering angle and $\lambda=1.5$Å is the incident x-ray wavelength
SAP30	Sin3-associated polypeptide p30; component of human histone deacetylase complex
SAXS	small-angle x-ray scattering
SDS	sodium dodecyl sulfate
SKIP	ski-interacting protein
SMAD	family of signal transduction proteins (mothers against DPP homolog)

SMRT	corepressor protein (silencing mediator of retinoic acid and thyroid hormone receptors)
SNW	conserved region in SKIP (serine-asparagine-tryptophane)
SRCD	synchrotron radiation circular dichroism spectropolarimetry
TAD	Notch intracellular transactivation domain
TAE	tris-acetate-EDTA buffer
TBE	tris-borate-EDTA buffer
TCEP	Tris-(2-carboxyethyl)-phosphine hydrochloride
TE	10mM Tris-HCl, 1mM EDTA, pH7.5
TEMED	N, N, N',N'-tetramehylethylendiamine
TEV	tobacco etch virus protease
tev	TEV cleavage site, Glu-Asn-Leu-Tyr-Phe-Gln*Gly
TF	transcription factor
Tris	Tris-hydroxymethyl-aminomethane
UV	ultra-violet light
V	Volt(s)
VUV	vacuum ultra-violet

1 Introduction

In order to multiply, pathogenic organisms or particles, such as bacteria or viruses, often interfere with cellular transcription regulation to successfully establish infection. They use different regulatory proteins which function like their cellular equivalents by specifically binding to the promoter regions of their target genes, the initiation and regulation points for the transcription process, to control their expression (for a recent review on eucaryotic promoters see (Smale and Kadonaga, 2003)).

Transcriptional regulation must occur as soon as cells need to react to different environments and therefore to different signals which elicit specific responses that depend on the organ or organism to which the cells belong. Regulation depends on specific transcriptional repressors or activators, which are brought to the nucleus where they are activated via the signal transduction pathways leading from the cell surface to the nucleus. Different stimuli thus lead to the production of different signalling proteins, which transfer the signal via a varying number of intermediate proteins to the nucleus. The last protein in this regulatory chain binds specifically to regulatory elements in the promoter region of its target genes, leading to repression or activation of transcription of the corresponding gene.

The present work focuses on the human transcription factor RBP-Jκ and its direct interaction partners upstream of the signal transduction pathway. The best examined cellular interaction partner of RBP-Jκ is Notch1. A viral equivalent of this protein, EBNA2, is a key component in establishing the latency phase, leading to cell immortalization in host cells infected by the Epstein-Barr virus, which can cause infectious mononucleosis and is also associated with certain types of cancer.

1.1 RBP-Jκ

The transcription factor RBP-Jκ (recognition signal binding protein Jκ, also called CBF-1 for Cp-binding factor 1) belongs to the family of CSL proteins (human C promoter binding factor, *Drosophila melanogaster* Suppressor of Hairless and *Caenorhabditis elegans* Lag-1), members of which are evolutionarily conserved from nematodes to fruit flies and humans. They have a high sequence identity and bind to a core DNA sequence CGTGGGAA (Tun et al., 1994). Originally it was mistakenly identified as a protein involved in the recombination events necessary for the creation of antibody variety.

Human RBP-Jκ is ubiquitously expressed and mediates cellular as well as viral signal transduction in the cell. Apart from the DNA core sequence in the promoters of its target genes the protein binds to various protein interaction partners, such as the corepressor complexes SMRT/NcoR/HDAC1 and CIR/HDAC2/SAP30 (Hsieh et al., 1999; Kao et al., 1998; Zhou and Hayward, 2001). A complex containing the intracellular domain of the Notch receptor and the scaffolding protein SKIP serves as an activator complex to enhance transcription of RBP-Jκ target genes (Zhou et al., 2000). Accordingly RBP-Jκ can act as transcriptional repressor (Dou et al., 1994; Hsieh et al., 1996; Waltzer et al., 1995) or activator (Kopan et al., 1996; Struhl and Adachi, 1998; Tamura et al., 1995) depending on its interaction partners or complexes.

RBP-Jκ target genes have been studied in *D. melanogaster*, where several have been found (Jarriault et al., 1995; Jennings et al., 1994; Lecourtois and Schweisguth, 1995; Wettstein et al., 1997). RBP-Jκ binds to regulatory elements in the promoters of *E(spl)* genes (*Enhancer of Split*). These genes code for basic helix-loop-helix proteins (HLH) acting as transcriptional repressors of differential factors. They negatively regulate expression of proneural genes of the achaete-scute complex, which leads to inhibition of the differentiation of neuroblasts.

Furthermore, RBP-Jκ regulates the expression of the control genes *eyeless*, *vestial* and *distal-less*, which are responsible for the correct formation of eyes, wings and extremities (reviewed in (Bray and Furriols, 2001)).

In vertebrates, RBP-Jκ regulates genes of the *HES* family (*Hairy Enhancer of Split*), which are homologues of the *E(spl)* genes (Lecourtois and Schweisguth, 1995). *HES1* is known to repress the expression of CD4, which is involved in T-cell development. RBP-Jκ binding sites have been found in the promoters of *HES1* and *HES5* (for a review see (Iso et al., 2003)). The vertebrate homologue of Eyeless, Pax6, is also involved in eye development.

RBP-Jκ binding sites have been found not only in cellular but also in viral promoters, for example in the Epstein-Barr virus genome, where they are present in promoters controlling the expression of immediate early genes.

In mammalian promoters the last five base pairs of the binding site for RBP-Jκ (GGGAA) can overlap with the first four of the binding site of the transcription factor NFκB (GGGA). This combination has been found in the promoters of many genes, such as those encoding interleukin 6, major histocompatibility complex class1 (MHCI) and interferon β, leading to the hypothesis that repression of genes whose promoters contain this sequence overlap could also simply be counteracted by displacement of RBP-Jκ (Goodbourn and Maniatis,

1988; Kannabiran et al., 1997; Miyazawa et al., 1998; Plaisance et al., 1997; Shirakata et al., 1996).

1.2 Protein interaction partners of RBP-Jκ

RBP-Jκ possesses interaction sites for numerous proteins exhibiting different functions. The primary structure of RBP-Jκ and the binding regions of the most important interaction partners (coactivators or corepressors) introduced in the section below are shown in Figure 1.1.

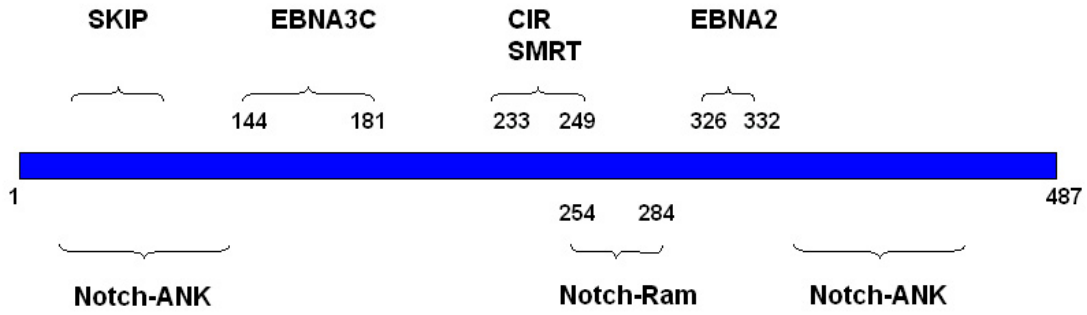

Figure 1.1: Primary structure of RBP-Jκ with the binding regions of corepressors and coactivators introduced in section 1.2. Precise limits are only given if the binding region has been exactly determined, other binding regions are indicated by braces.

1.2.1 Cellular interaction partners

Coactivators

Notch1

Notch proteins were discovered in fruit flies lacking one allele of the corresponding Notch gene, which display a phenotype with notches at the edges of the wings. A knockout of the gene is lethal in the embryonic state. To date, four members of the Notch receptor family have been identified in rodents and humans. All of them, Notch1 to Notch4, shown in Figure 1.2, bind to RBP-Jκ with different affinity, but their function is non-redundant (Mumm and Kopan, 2000). Many cellular processes from embryonic development and differentiation to immortalisation of various tissues types rely on signal transduction involving members of the Notch receptor family.

The loss of RBP-Jκ expression in mice is lethal to embryos at 10.5 days of gestation, an earlier stage than observed with Notch knock-out mice, suggesting that RBP-Jκ does not only function as a downstream target of Notch but also plays a unique role in development (Amakawa et al., 1993; Oka et al., 1995).

The human Notch1 receptor is the major upstream binding partner of RBP-Jκ and regulates its transactivation activity. It is a transmembrane receptor with a single membrane spanning region. The N-terminal extracellular domain of this 300 kDa molecule contains 36 EGF tandem repeats, which play an important role during ligand binding. At the C-terminal end of the EGF repeats there are three cysteine-rich NL regions (Notch-Lin-12; LNR), which are believed to negatively regulate the activity of the Notch intracellular domain (Mumm and Kopan, 2000).

The intracellular region C-terminal to the transmembrane segment of Notch, which interacts directly with RBP-Jκ, is called RAM (RBP-Jκ Association Molecule). The following seven ankyrin repeats, which are flanked by a nuclear localization sequence (NLS), mediate interactions with various proteins (Lubman et al., 2004). The glutamine-rich OPA domain forms an important part of the intrinsic transactivation domain (TAD) of the protein (Kurooka et al., 1998; Milner et al., 1996). The C-terminal PEST sequence is probably involved in the degradation of the protein for rapid termination of the signal (Kurooka et al., 1998).

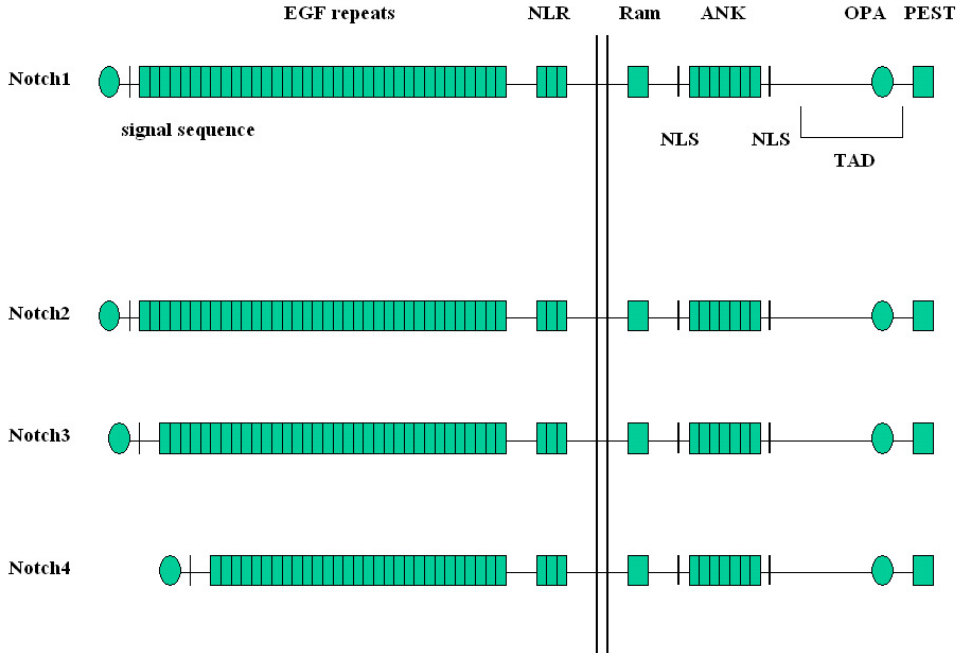

Figure 1.2: The four members of the Notch receptor family. The different protein domains are indicated at the top. Extracellular portion: N-terminal signal sequence followed by different numbers of EGF repeats and three NLRs (Notch-LIN regions); intracellular portion: Ram domain, followed by seven ankyrin repeats, flanked by a nuclear localization signal (NLS); the transactivation domain (TAD) including the glutamine-rich OPA sequence is located at the C-terminus. A PEST sequence labels the protein for rapid degradation.

The activity of Notch proteins is regulated via posttranslational proteolysis. They are processed in the trans-Golgi by a furin-like convertase and presented on the cell surface as a dimer. The functional receptor consists of a 180 kDa N-terminal unit and a 120 kDa C-terminal unit, which associate through a calcium dependent, non-covalent bond.

As illustrated in Figure 1.3, a number of different transmembrane proteins belonging to the DSL family of conserved proteins (Delta, Serrate, Lag-2) located on the surface of neighbouring cells can serve as ligands mediating intercellular interactions. Upon ligand-binding a two-step proteolytic cleavage takes place, which results in the release of the intracellular domain (Notch-IC) of the receptor. The first processing step occurs in the extracellular part of Notch, at the N-terminus of the transmembrane segment and involves a metalloprotease belonging to the ADAM family (a disintegrin and metalloprotease), followed by cleavage directly at the C-terminus of the transmembrane domain. Notch-IC possesses a nuclear localization sequence and translocates to the nucleus where it binds RBP-Jκ, which is present in different complexes with transactivation or repression functions (for recent reviews see (Hayward, 2004; Lai, 2002)).

To form activation complexes Notch-IC displaces corepressors such as e.g. histone deacetylases (HDAC1 and HDAC6) or the SMRT corepressor complex from RBP-Jκ, which leads to upregulation of a number of target genes. The Notch signal transduction pathway is highly conserved throughout eucaryotic organisms.

The homologues of Notch and RBP-Jκ in *D. melanogaster* are the expression products of the *Notch* and *Suppressor of Hairless* (*Su(H)*) genes, respectively, and the signalling pathway is also conserved in C. *elegans* where it involves the RBP-Jκ homologue Lag-1 and the Notch homologue Lin-12 (Roehl et al., 1996).

Notch is expressed in uncommitted proliferative cells during development and is believed to maintain the proliferative capacity of immature cells in the adult. Whereas in *D. melanogaster* the protein is only expressed in proliferating tissues, vertebrates also express it in differentiated tissues such as the adult brain or mature B- and T-cells.

In vertebrates, the activated Notch gene inhibits neuronal and muscular differentiation and promotes adipogenesis. It plays an important role in hemapoietic differentiation: It is expressed in CD34-positive hematopoietic precursors as well as in lymphoid, myeloid and erythroid precursor populations and in B- and T-cells in the peripheral blood. Notch1 and Notch2 influence granulocyte differentiation and mediate cytokine specificity (Bigas et al., 1998; Li et al., 1998; Milner et al., 1996). Whereas Notch1 plays an important role during the induction of T-cell maturation it simultaneously inhibits B-cell differentiation. It

influences the decision between CD4- and CD8-cells, the two functional T-cell subgroups, as well as between cells expressing the αβ- and γδ-receptors in favour of the CD8- and γδ-expressing populations (Robey et al., 1996; Washburn et al., 1997). Upon interaction with RBP-Jκ and NFκB, Notch1 represses the activity of the E47 protein, which is an essential transcription factor during early B-cell development. Notch proteins influence the decision of these cells for self-renovation or differentiation. This function predestines aberrant Notch proteins for an important role as oncogenes in cancer development. In fact, constitutively activated Notch has been found in a subset of T-cell leukemias and lymphomas in humans, cats and mice (Ellisen et al., 1991; Girard et al., 1996; Rohn et al., 1996).

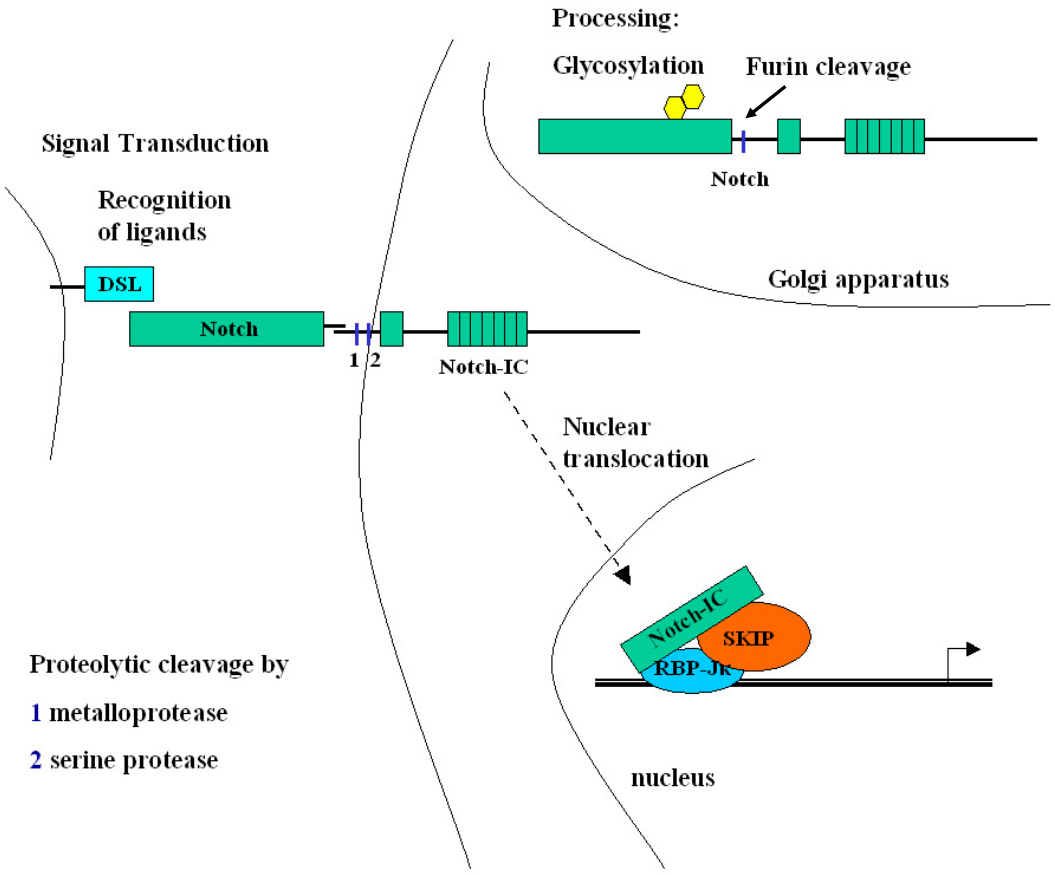

Figure 1.3: Simplified scheme of the processing of Notch and of signal transduction via the Notch1-receptor. Before insertion into the cell membrane the Notch protein is processed in the Golgi apparatus, where the N-terminal extracellular part of the protein is glycosylated and the pro-protein is proteolytically cleaved into the future extracellular and intracellular portions. When inserted into the membrane both parts associate at the C-terminus of the extracellular and the N-terminus of the intracellular part through a calcium dependent, non-covalent bond. Upon binding of a ligand belonging to the DSL family to the extracellular part of Notch the latter is proteolytically cleaved in two steps by a metalloprotease and a serine protease. The resulting intracellular domain translocates to the nucleus where it displaces corepressors from RBP-Jκ thus enabling transactivation of RBP-Jκ target genes.

SKIP as a link between transcription and splicing

SKIP is a 60-80 kDa protein, which is expressed ubiquitously albeit in low abundance in the cell and is preferentially located in the nucleus. It is highly conserved and can be found throughout lower eucaryotes, plants, fungi and animals. A search in the Pfam protein domain database (Bateman et al., 2000) yields only one known domain in the amino acid sequence of SKIP, the SNW domain. This acronym stands for the absolutely conserved amino acid motif SNWKN. The remaining protein consists of N- and C-terminal domains separated by species-specific inserts.

The three-dimensional structure of SKIP is so far unknown, but the protein may take part in various interactions depending on its functional status or way of assembly.

SKIP is a constituent of many complexes that form at or bind close to the sites of preinitiation complex assembly, where it facilitates the correct sequence of events by bringing signalling partners into the vicinity of the appropriate target. It may also serve as scaffold for proteins with low mutual binding affinities at low concentrations. SKIP could also serve as decelerator for the regulatory components on their way through the nucleus, providing a means of compartmentalization by creating non-physically separated reaction compartments by binding to some interaction partners.

Notch-IC binds to RBP-Jκ and this complex displaces the SMRT/HDAC corepressor complex allowing transcription to start from RBP-Jκ controlled promoters. This replacement seems to be assisted by SKIP, since its presence is necessary for Notch-IC to effectively activate CSL promoters (Leong et al., 2004). This was proven by mutation studies which revealed that after deletion/mutation of the fourth ANK repeat of Notch-IC, which binds to SKIP, Notch activity was abrogated. Apart from the physical interaction with Notch-ANK (Zhou et al., 2000), SKIP also binds to the N-terminal part (exons 1-5) of RBP-Jκ, SMRT, mSin3A, CIR and HDAC2. The Notch-IC mimicking Epstein-Barr virus protein EBNA2 binds to SKIP with its CR5 region.

SKIP does not act as a general transcription factor. Human SKIP was found to coregulate only at certain promoters, whereas in *Drosophila* it associates only with a subset of transcriptionally active puffs of salivary polytene chromosomes.

The function of SKIP proteins in the cell is not restricted to transcription and human SKIP was found among the ~100 protein constituents of speckles involved in splicing usually observed in higher eucaryotes (Nagai et al., 2004). The avidity of SNW proteins to splice factors U2, U4 and U5 and snRNAs and connectivity maps of their components suggest that these novel particles represent a part of the spliceosome or a temporary assembly

arising at a certain stage of its function (Nagai et al., 2004). Furthermore, SNW interacts with PABP2 (poly adenosine binding protein) and both proteins colocalize in nuclear speckles (Kim et al., 2001). PABP2 engages the nuclear export machinery and may contribute to mRNA export. It accompanies spliced mRNA on its route to the cytoplasm, where it is replaced by PABP1. Snw1p, the SKIP homologue in *S. pombe*, binds to the small subunit of the heterodimeric splicing factor U2AF, which shuttles continuously between nucleus and cytoplasm (Ambrozkova et al., 2001). This mechanism is independent of mRNA binding.

Mastermind as coactivator

Mastermind (MAML) was first identified in *Drosophila* and implicated as important positive regulator of Notch signalling (Artavanis-Tsakonas et al., 1995; Helms et al., 1999; Smoller et al., 1990; Petcherski and Kimble, 2000). In *Drosophila* the *mastermind* gene encodes a glutamine-rich nuclear protein. Mammalian MAML was shown to stabilize and participate in the DNA-binding complex of Notch-IC and RBP-Jκ during the activation of target promoters (Wu et al., 2000). A short protein fragment at the N-terminus of Mastermind comprising about 75 aa is required for binding the RBP-Jκ-Notch-IC complex (Nam et al., 2003). Mastermind plays dual roles of both activating Notch target gene transcription through the direct binding of CBP/p300 and promoting hyperphosphorylation and degradation of Notch-IC (Fryer et al., 2004; Wallberg et al., 2002).

Corepressors

The corepressor CIR

Indirect evidence has implicated a corepressor in RBP-Jκ-mediated transcriptional repression. Yeast two-hybrid screens were used to identify a 450 aa protein, called CIR (CBF1 interacting protein), as corepressor and link between RBP-Jκ and histonedeacetylase complexes such as HDAC2-mSin3-SAP3 (Hsieh et al., 1999). The protein has a highly charged, serine-rich C-terminus. A 561 aa CIR homologue with a high sequence homology in the N-terminal part (aa 1-150) but not in the C-terminus exists in *C. elegans*, is also highly charged and contains numerous serines. In general, the protein is expressed at high levels in many different tissues such as heart, skeletal muscle or pancreas. The region responsible for RBP-Jκ interaction lies between aa 1 and 121. Within RBP-Jκ the interaction site with CIR could be mapped to aa 233 to 249 by yeast two-hybrid screens

(Hsieh et al., 1999). The protein also interacts with other RBP-Jκ binding proteins such as e.g. SKIP.

The corepressor SMRT

SMRT (silencing mediator of retinoic acid and thyroid hormone receptors) can form complexes with N-CoR and mSin3A as well as histonedeacetylase 1 (HDAC1) (Alland et al., 1997). Yeast two-hybrid and *in vitro* interaction assays proved the interaction of SMRT with RBP-Jκ and the direct interaction was confirmed by GST-pull-down assays (Kao et al., 1998). Like CIR, it antagonizes the Notch-IC-mediated activation of RBP-Jκ and shares the same binding region on RBP-Jκ (amino acids 233 to 251) (Hsieh et al., 1999; Kao et al., 1998; Zhou and Hayward, 2001). In complex with other proteins (e.g. CIR and SKIP) SMRT appears to be responsible for the direction and relocalization of RBP-Jκ to the nucleus.

The LIM protein KyoT2

KyoT2 and its homologue KyoT1 share the first 167 aa. Whereas KyoT1 contains 280 aa, KyoT2 consists of only 194 aa. The different C-terminal portion of KyoT2 was shown to interact with RBP-Jκ. The protein is expressed in various tissues, such as heart, lung, liver, brain and skeletal muscle. It negatively regulates transcription by association with RBP-Jκ and expulsion of Notch-IC from RBP-Jκ (Taniguchi et al., 1998).

The corepressor SHARP

SHARP belongs to the Spen (split ends) family of proteins, which contain RNA recognition motifs (RRMs) in the N-terminal part. It was originally identified as SMRT-associated protein in a yeast two-hybrid screen and implicated in nuclear receptor signalling (Shi et al., 2001). Its role as interaction partner of RBP-Jκ linking RBP-Jκ to HDAC corepressor complexes was only recently discovered (Oswald et al., 2002). Binding of Notch-IC and SHARP to RBP-Jκ is mutually exclusive; binding of SHARP to RBP-Jκ reduces transactivation. The expression of SHARP overlaps with that of Notch, but the protein is also expressed in other tissues, suggesting other functions beside the modulation of Notch-signalling.

1.2.2 Viral interaction partners

So far eight human Herpesviruses, which infect different organs (Varicella zoster), the lymphatic system (Epstein-Barr) or the central nervous system, are known. The Epstein-Barr virus (EBV), which belongs to the family of gamma Herpesviruses, is distributed throughout the world with up to 95 % of the population being seropositive. An outbreak of the disease can, however, be effectively impeded by a functional cellular immune system, which prevents the uncontrolled reproduction of infected cells. As already mentioned, the virus can cause infectious mononucleosis and is associated with cancers in immunocompromised individuals.

It infects either B-lymphocytes or T-cells and has the ability to reside latently in the organism. In this state the production of infectious particles is inhibited and the cells survive. The virus can repeatedly change from the latent state to the infectious cycle.

For EBV up to nine different proteins are synthesized during latent infection, six of which are necessary for establishing and maintaining of the non-productive cycle in B-cells *in vitro* and the immortalisation of the cells (EBNA1, EBNA2, EBNA3A and EBNA3C, EBNA-LP (leader protein) and LMP1 (latent membrane protein 1). In tissue culture EBNA3B and LMP2A/B are not essential for the immortalisation of B-cells (reviewed in Robertson, 2005).

EBNA2

EBNA2 (Epstein-Barr-Virus nuclear antigen 2) is the major viral interaction partner of RBP-Jκ and is responsible for the immortalisation of B-cells upon infection with Epstein-Barr-Virus. It was characterized after reintroduction of a lost DNA fragment spanning EBNA2 and EBNA-LP (Bornkamm et al., 1982; Dambaugh et al., 1984; Dillner et al., 1986; Hennessy and Kieff, 1985; Mueller-Lantzsch et al., 1985) into the transformation defective Epstein-Barr virus strain P3HR1 (Hinuma et al., 1967; Miller et al., 1974), leading to a restoration of the transformation activity (Cohen et al., 1989; Hammerschmidt and Sugden, 1989).

EBNA-LP induces the switch of resting B-cells from G_0 to G_1 as well as synthesis of EBNA2. The presence of both proteins is sufficient to immortalize these cells through expression activation of cyclin D2, which causes continuous cell division. EBNA-LP also binds to the tumour suppressor proteins RB and p53, but this does not influence their regulatory function (Modrow, 2003).

EBNA2 is essential not only for establishing latency and immortality (Cohen et al., 1989; Hammerschmidt and Sugden, 1989) but also for maintenance of B cell immortalization (Kempkes et al., 1995).

Two subtypes of EBV are known: Whereas type 1 has a high transformation rate, induction of transformation in B-lymphocytes by type 2 is reduced. Since both subtypes are found in *ex vivo* established cell lines from B-cell lymphomas a different potential to create tumours is unlikely. In type 1 the sequence of EBNA2 is 491 aa long, whereas that of type 2 has 443 aa. Major differences are found in a relatively hydrophobic domain in the centre of the protein. In contrast, both proteins contain a proline-rich region and repeats of Arg/Lys-Gly (for an overview of the primary structure of EBNA2 see Figure 1.4). Both proteins are phosphorylated, have a molecular mass of 75 to 88 kDa, and accumulate in the nucleus in the form of oligomeric complexes. EBNA2 does not bind DNA directly but acts as transactivator by binding to RBP-Jκ (Grossman et al., 1994; Henkel et al., 1994; Waltzer et al., 1994; Zimber-Strobl et al., 1994) and Pu-1 (Laux et al., 1994). It is likely to act as the viral equivalent of the constitutively active cellular Notch receptor (for a comparative reaction scheme see Figure 1.7) (Johannsen et al., 1995; Sakai et al., 1998). Binding to RBP-Jκ was mapped to the region between aa 252 and 425 which contains the conserved regions CR5, CR6 and CR7 (Ling et al., 1993), where CR6 holds an important function since a double mutation of tryptophans 323 and 324 abolishes the ability of EBNA2 to interact with RBP-Jκ (Ling et al., 1993).

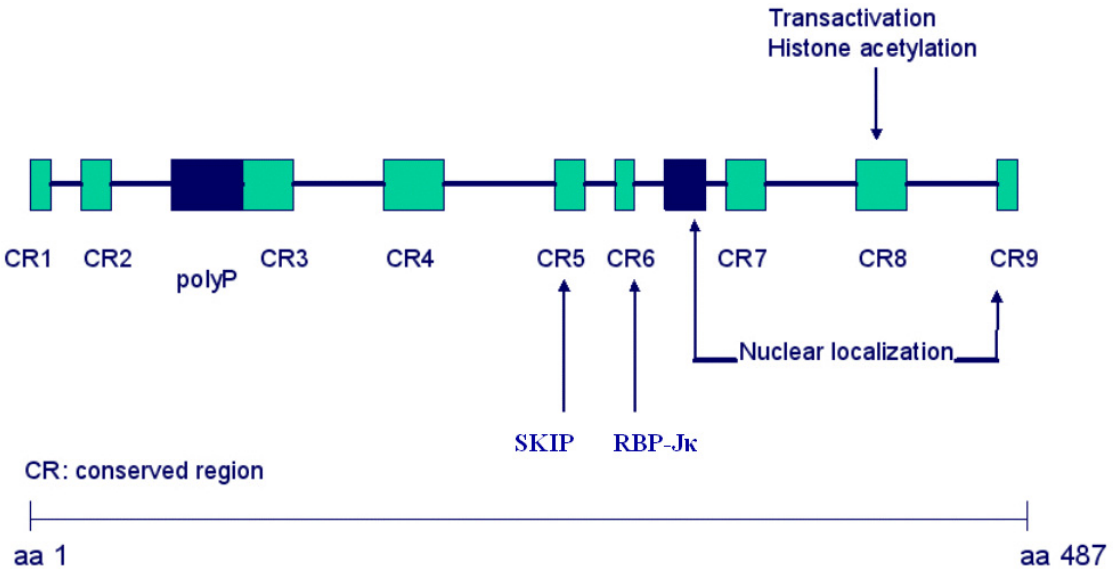

Figure 1.4: Primary structure and functional units of EBNA2 (after (Kempkes, 2002)). The conserved regions are depicted as boxes, in the case of CR5 and CR6 the interaction partners are also indicated.

EBNA2 induces the C-promoter, which regulates the expression of EBNA proteins as well as the promoters of the latent membrane proteins LMP1, LMP2A- and LMP2B (Fahraeus et al., 1990; Sung et al., 1991; Woisetschlaeger et al., 1990; Zimber-Strobl et al., 1991). In addition, it enhances the synthesis of the cellular proteins CD21 and CD23 (Calender et al., 1987; Cordier et al., 1990; Wang et al., 1987) as well as of the proto-oncogene c-fgr (Knutson, 1990). CD23 is a weak IgE binding receptor expressed on EBV-transformed B-cells and primary B-lymphocytes stimulated by antigens. A secreted isoform of CD23 acts as B-cell growth factor and contributes to the activation and proliferation of B-lymphocytes in the course of EBV infection. EBNA2 possesses a strong transactivation domain through which it is able to interact with constituents of the RNA-polymerase transcription initiation complex. It is also known to interact with human SKIP protein, being involved in e.g. chromatin remodelling or splicing (for a recent review on viral interactions with components of the Notch pathway see Hayward, 2004).

EBNA3A, EBNA3B and EBNA3C

The three proteins belonging to the EBNA3 family of Epstein-Barr virus proteins consist of 944 (EBNA3A), 938 (EBNA3B) and 992 aa (EBNA3C), respectively. EBNA3A and EBNA3B are distantly homologous to EBNA3C. The genes encoding the three proteins are tandemly organized in the EBV genome indicating that they evolved from a common ancestor by gene duplication (reviewed in Robertson, 2005).

EBNA3C can transactivate some EBNA2-regulated genes (Allday and Farrell, 1994; Murray et al., 1988; Wang et al., 1990), was shown to associate with RBP-Jκ in human lymphoblasts (Robertson et al., 1995) and can block EBNA2 transactivation of the LMP1 and LMP2 promoters in transient transfection assays (Le Roux et al., 1994; Marshall and Sample, 1995; Robertson et al., 1995). The protein possesses a glutamine- and proline-rich domain which can functionally substitute for the EBNA2 acidic domain in transcriptional activation (Cohen and Kieff, 1991; Marshall and Sample, 1995).

Like EBNA3C, EBNA3A and EBNA3B can specifically block EBNA2 activation of the LMP2 promoter in transient transfection assays (Le Roux et al., 1994), indicating competition for a similar binding site on RBP-Jκ. In GST-pull-down assays all three proteins bind GST-RBP-Jκ, although this assay shows the affinity of EBNA3A for GST-RBP-Jκ to be only slightly above background (Robertson et al., 1995). The source of the respective protein may play an important role, since *in vivo* expressed EBNA3A was later shown to have a similar affinity for RBP-Jκ as the other two proteins, whereas the *in vitro*-

translated EBNA3A interacts only weakly (Robertson et al., 1995). The binding region within the EBNA3 proteins could be narrowed to the amino terminal domain (Robertson et al., 1995; Zhao et al., 1996). By binding to RBP-Jκ all three proteins alter the ability of RBP-Jκ to recognize its cognate DNA sequence, thus altering its transactivation activity. All three proteins compete with EBNA2 as well as Notch-IC, but most probably do not bind to the same region. The interaction site of EBNA3C on RBP-Jκ was mapped to the region encompassing aa 144 to 178 (Zhao et al., 1996).

1.3 Interaction of RBP-Jκ with Notch1 and EBNA2: structural aspects

1.3.1 Structure of RBP-Jκ

The crystal structure of the RBP-Jκ homologue in *C. elegans*, Lag-1, was solved at 2.85 Å resolution (Kovall and Hendrickson, 2004) yielding the model in Figure 1.5. Alignment of CSL-proteins of different organisms revealed that a portion of about 425 aa is conserved throughout all organisms. The structural genomics approach which was used and which included RBP-Jκ homologues from different organisms revealed only the structure of the *C. elegans* homologue of RBP-Jκ bound to a 13 bp double-strand DNA, derived from the mammalian HES-1 promoter.

The structure of Lag-1 includes three distinct domains, displaying considerable similarity to already known structures: Lag-1 contains two domains resembling those of members of the Rel transcription factor family, the N-terminal domain (NTD) and the C-terminal domain (CTD), corresponding to Rel-homology regions RHR-N and RHR-C (Nam et al., 2003). In contrast with the situation in Rel-proteins they are, however, separated by a modified β-trefoil domain (BTD), which is inserted where the junction between the two domains of a Rel transcription factor would be. The protein does not form a beads-on-a-string system but parts of the domains are structurally integrated into others. DNA-binding occurs via the NTD and the BTD, whereas the CTD does not contribute to the binding.

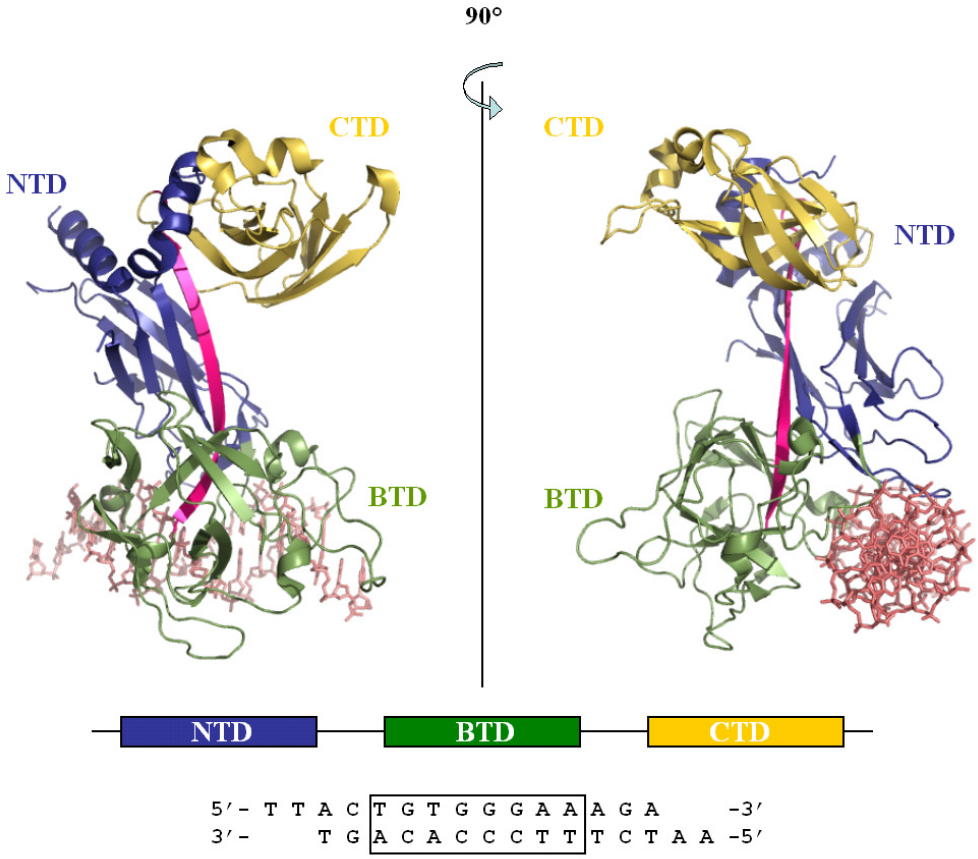

Figure 1.5: Ribbon structure of C. *elegans* Lag-1 (PDB-code 1TTU). The domain organisation is depicted in blue for the N-terminal domain (NTD), yellow for the C-terminal domain (CTD) and green for the β-trefoil domain (BTD). The β-strand bridging BTD and CTD is coloured magenta. The sequence of the DNA with the framed core binding sequence and 5'-single-strand double base overhangs is depicted at the bottom of the figure. The DNA sequence was derived from the mammalian HES-1 promoter.

1.3.2 Structural information about Notch1

The domain organization of Notch1 is shown in Figure 1.1. Structural details are only known for the ankyrin domain (ANK), consisting of seven ankyrin repeats (Ehebauer et al., 2005; Zweifel et al., 2003), and the extracellular ligand binding region (Zweifel et al., 2005).

Various analyses have been carried out to map the exact interaction site of Notch-IC with RBP-Jκ. The amino acids involved in the interaction with Notch-Ram are highlighted in Figure 1.9 below (section 1.3.4).

In the case of the Ram domain the crucial amino acids participating in the interaction with RBP-Jκ could be mapped. Peptide arrays with Ram fragments containing between five and twenty five amino acids revealed that a stretch of five amino acids around a conserved tryptophan is sufficient to mediate the interaction with RBP-Jκ (B. Kempkes, unpublished data). Extensive analysis of the differential binding of RBP-Jκ point mutations (Fuchs et al., 2001; Tani et al., 2001) further narrowed the number of amino acids involved in binding to amino acids Lys456, Leu 457, Val458, Ala465, Asp440, Asn441 and Phe 442. According to the Lag-1 crystal structure amino acids Lys456 to Val458 and Ala465 form a hydrophobic pocket suitable for hydrophobic interactions. This study could, however, not define the role of the different amino acids, i. e. whether they are directly involved in the interaction or if their mutation causes a conformational change, which abolishes the interaction.

Since an interaction or at least a role of the ankyrin repeats had been described, it was also tried to map that interaction (Tani et al., 2001). On the side of the ankyrin repeats a mutation in the fourth repeat resulted in loss of transactivation activity. Mutational analysis suggested that Arg397, Lys391, Arg472, Phe498, Glu499 and Glu433 contribute to the interaction with RBP-Jκ.

1.3.3 EBNA2

So far no structural information is available for EBNA2. A secondary structure prediction (Figure 1.6) obtained using the program PHD (Rost, 1996) shows why it may be difficult to approach this problem.

The protein is predicted to contain long stretches of low complexity regions, depicted as loops (L), without defined secondary structure. This might make it difficult to crystallize even a truncated form containing the binding region because this region does not contain any detectable secondary structure element.

As in the case of the initially unfolded Ram domain of Notch-IC, folding may occur upon binding to RBP-Jκ or other protein interaction partners. The RBP-Jκ binding motif of EBNA2 was mapped to two crucial tryptophans in CR6. When aligned with Notch-Ram (Figure 1.7) this motif has a detectable similarity with the region crucial for Ram-RBP-Jκ interaction. This similarity in the binding motif does not necessarily contradict the assumption of slightly different binding sites of Notch-Ram and EBNA2 on RBP-Jκ. The low number of conserved amino acids comprises mostly hydrophobic residues, so that a

coincidence could also be due to a similar binding mode involving hydrophobic interactions.

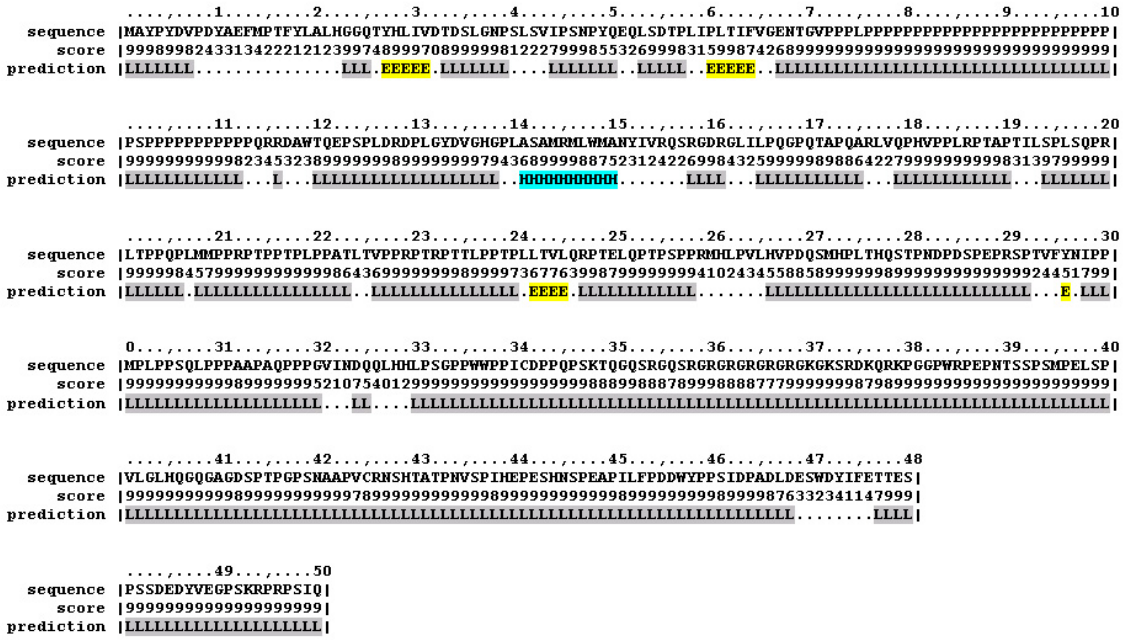

Figure 1.6: Secondary structure prediction based on the EBNA2 sequence with the program PHD. Low complexity regions, i. e. loop structures are highlighted in light grey, α-helices in turquoise and β-sheets in yellow. The score gives the likelihood of the prediction; letters below the score indicate predicted secondary structure elements; E= β-strand, H=α-helix, L=loop region.

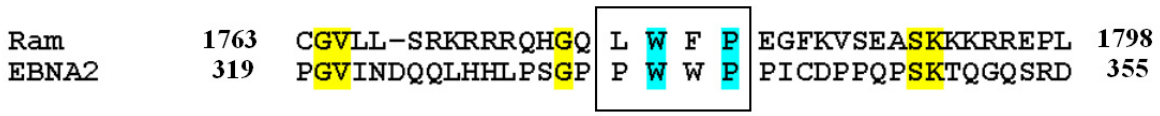

Figure 1.7: Manual alignment of the primary structures of the regions of Notch-Ram and EBNA2 interacting with RBP-Jκ. The conserved binding motif is highlighted by a box, conserved amino acids within in turquoise. Identical amino acids in the surrounding region are indicated by a yellow background.

1.3.4 Common and distinct features of Notch and EBNA2

Both EBNA2 and Notch-IC abolish RBP-Jκ repression and activate transcription of responsive promoters through a combination of abolition of repression and the positive effect of an endogenous activation domain.

In contrast to Notch1, which needs a ligand to be activated by the sequential cleavage steps, which set free its intracellular (IC) domain, EBNA2 is already constitutively active after expression. Similarities can be found in the mode of action of activated (constitutively active) Notch (Notch-IC), occurring in aberrant chromosomal translocations, and EBNA2. Chromosomal translocations that cause expression of a truncated from of Notch are found in a subset of acute T-cell lymphoblastic lymphoma as well as EBNA2 expression is found in immunoblastic B-cell lymphomas. The two proteins have no obvious sequence homology apart from two conserved amino acids (ΦWΦP) in the main RBP-Jκ interacting domain Ram (Notch-IC) and CR6 (EBNA2) (Nam et al., 2003). Whereas Notch-IC is predicted to contain a high percentage of secondary structure elements, EBNA2 is mainly composed of low complexity regions with long proline-rich sequences. The polyproline stretches should, in particular, result in a high flexibility of EBNA2. Their function is essentially still unknown.

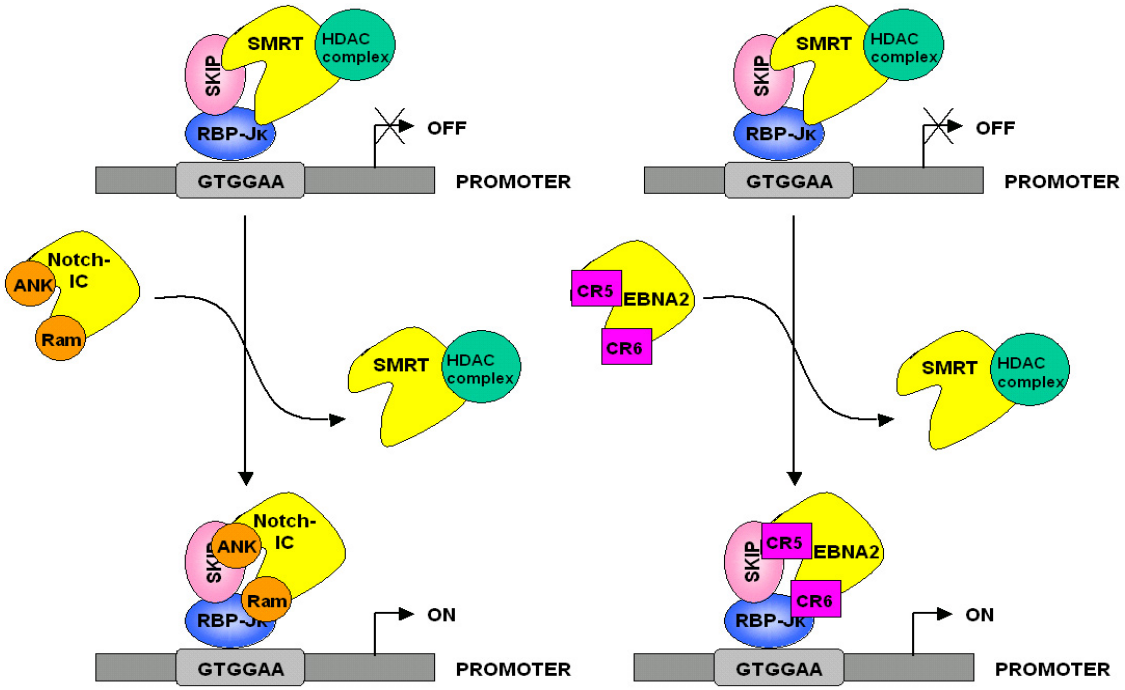

Figure 1.8: Analogous action of Notch1 and EBNA2 in the displacement of corepressor complexes from RBP-Jκ on the example of the SMRT corepressor complex (figure based on Zhou et al., 2000).

The set of proteins interacting with Notch-IC and EBNA2 is remarkably similar in function: Both proteins interact with a number of others belonging to the basal transcription machinery. EBNA2 binds to TFIIH, TATA box binding protein (TBP) associated factor TAF40, TFIIB and the co-activator p100, which interacts with TFIIE (Tong et al., 1995a; Tong et al., 1995b). The EBNA2 transactivation domain interacts with histone acetyltransferases (HATs) p300/CBP and PCAF, whereas besides p300/CBP Notch-IC binds to PCAF and GCN5. Both proteins bind to SKIP, a transcriptional coactivator involved in various other cellular processes (see section 1.3.2). The similarity between the action of Notch-IC and EBNA2 on RBP-Jκ is illustrated in Figure 1.8 on the example of the displacement of the SMRT corepressor complex from RBP-Jκ to activate transcription.
Notch-IC activates target genes involved in developmental processes, like the *hairy enhancer of split complex E(spl)* related genes *Hes1* and *Hes5* (Lecourtois and Schweisguth, 1995), *Hey1*, *Hey2* and *HeyL* (Maier and Gessler, 2000), *ERBB-2* (Chen et al., 1997), *NFκB* (Oswald et al., 1998) and *hairy-related transcription factor* (HRT) (Nakagawa et al., 2000). Recently, strong hints for the activation of c-myc by Notch-IC were also found (Gordadze et al., 2001). EBNA2 responsive elements can be found within the viral Cp (Sung et al., 1991; Woisetschlaeger et al., 1990), LMP1 and LMP2A promoters (Fahraeus et al., 1990; Zimber-Strobl et al., 1991). Both Notch-IC and EBNA2 activate the expression of cellular CD21 and CD23 (Gordadze et al., 2001; Hofelmayr et al., 2001). All these responsive elements contain at least one RBP-Jκ binding site with varying sequences resulting in more or less tight binding of RBP-Jκ to DNA as well as of Notch-IC and EBNA2 to RBP-Jκ. The two overlapping sets of target genes activated by Notch and EBNA2, are presently being characterized in more detail using micro-arrays (Maier et al., submitted).
Figure 1.9 displays amino acids of RBP-Jκ known to interact with Notch-Ram and EBNA2. Apart from the conserved ΦWΦP motif, which is present in both proteins, the interaction sites appear to be sufficiently different to imply that despite similarities in the binding mode, different mechanisms may be involved in the differential activation of the specific target genes of Notch-Ram and EBNA2.

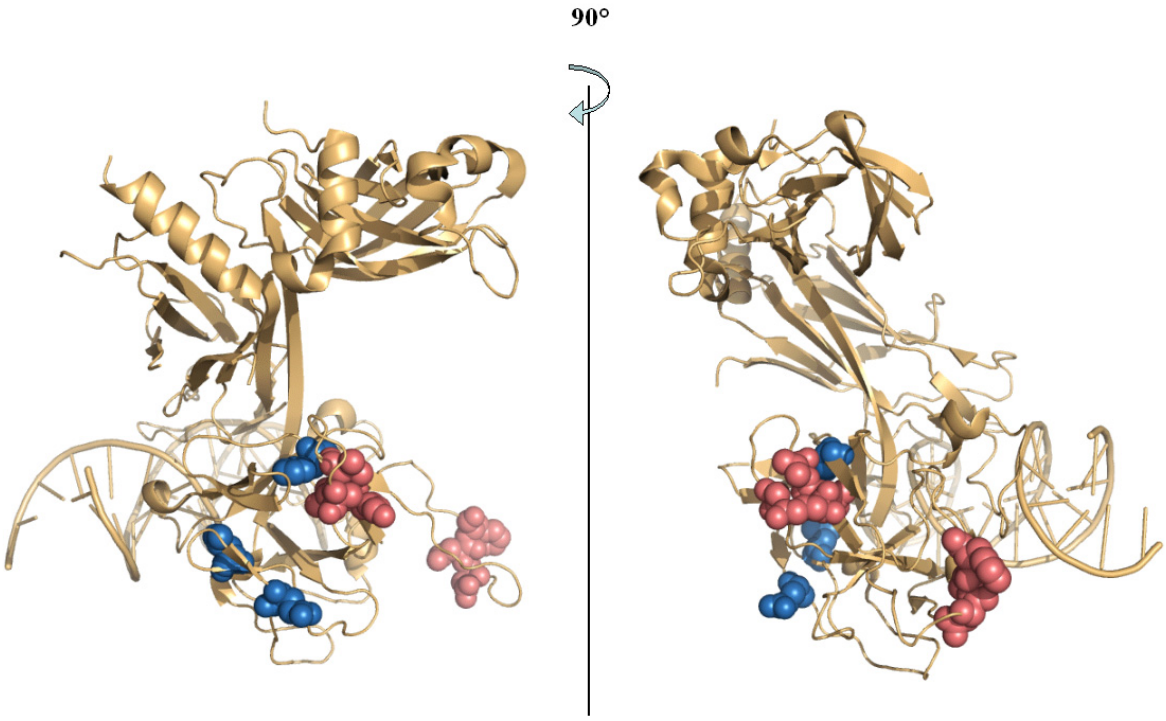

Figure 1.9: Amino acids crucial for the binding of Notch-Ram (Lys456, Leu457, Val458, Ala465, Asp440, Asn441 and Phe442; red) and EBNA2 (Phe425, Leu510 and Gln517; blue) mapped onto the crystal structure of Lag-1 bound to DNA. The views are rotated by 90º. The Figure was created using Pymol (http://www.pymol.org).

1.4 Open questions

The question regarding the interchangeability of Notch-Ram and EBNA2 is still not satisfactorily answered. The obvious differences in the binding mode resulting from various mutation analyses should be studied in more detail. This may also lead to predictions about the transactivation mechanism, which in addition to a common set of activated or repressed genes enables the differentiated regulation of certain target genes. Examination of the functionally similar development of regulatory proteins in cells and viruses is an important issue towards the understanding of physical interactions of proteins in the context of transcriptional regulation.

Controversial results have been obtained concerning the role of the ankyrin repeats in the interaction of Notch-IC with RBP-Jκ. A direct approach to examine the interaction would

answer this question more clearly than the indirect reporter assay methods and EMSAs (electrophoretic mobility shift assay) with protein mixtures, which have hitherto been used. Some structural questions have been answered by the publication of the crystal structure of the RBP-Jκ homologue of C. elegans, Lag-1, bound to DNA (Kovall and Hendrickson, 2004). The two proteins have a high sequence identity, which speaks for a similar overall structure. In the present work, differences have, however, been found, which cannot be explained yet. The crystal structure of a quaternary complex including C. elegans Lag-1 bound to DNA, Notch-RamANK and Mastermind (Nam et al., 2006; Wilson and Kovall, 2006), which was published soon after the completion of the present work, provides insight into the interplay between different activators on RBP-Jκ, but does not clarify whether ANK is able to bind RBP-Jκ by itself or only in the presence of coactivators such as Mastermind.

1.5 Scope of this thesis

The aim of this work was to characterise the physical interactions between RBP-Jκ and its protein and DNA interaction partners and, if possible, determine the high resolution crystal structure of the protein in complex with different interaction partners.

The low resolution models of RBP-Jκ in complex with DNA or Notch comprising the Ram and ANK domain in solution obtained by small angle X-ray scattering represent a first important step towards the structural characterization of RBP-Jκ and its complexes. The question as to whether the Notch ankyrin repeats participate in the interaction with RBP-Jκ could be unambiguously answered using ITC (isothermal titration calorimetry) and EMSA (electrophoretic mobility shift assay) data.

Crystallographic studies were aimed at gaining insight into structural aspects of the protein-nucleic acid interactions as well as understanding the protein-protein interactions of RBP-Jκ with Notch-Ram. The conditions where RBP-Jκ is likely to crystallize could be narrowed down for both a binary complex of DNA-RBP-Jκ and a ternary complex of DNA-RBP-Jκ-Ram. No adequate crystals of either of the complexes could, however, be obtained so far but this can at least partly be understood in the light of the small angle scattering results.

During the work it became apparent that the properties of RBP-Jκ expressed in procaryotic (*E. coli*) and eucaryotic expression systems (recombinant baculovirus in insect cells) differed. This provided the opportunity to compare the properties and activity of both

purified proteins by various biochemical and biophysical assays, such as circular dichroism (CD) spectroscopy, EMSA and ITC.

Truncation mutants were designed, expressed in two different expression systems and characterized biochemically and biophysically to study the domain structure of RBP-Jκ in relation to that of Lag-1. Different binding properties of protein fragments derived from the full-length interaction partners were determined using ITC and EMSA.

Although the viral protein EBNA2 and cellular Notch-IC protein are known to fulfil similar functions in the cell it was found, rather surprisingly, that EBNA2 has a much higher binding affinity to RBP-Jκ than Notch-IC.

2 Materials and Methods

2.1 Materials

2.1.1 Bacterial Strains

Strains used for plasmid amplification

Strain	Genotype
E. coli DH5a	F-, *lac*I-, *rec*A1, *end*A1, *hsd*R17, Δ(*lac*ZYA-*arg*F), U169, F80d*lac*ZΔM15, *sup*E44, *thi*-1, *gyr*A96, *rel*A1 available at the EMBL
E. coli DH10 Bac	F-, *mcr*A, Δ(*mrr-hsdRMS-mcrBC*), Φ80*lac*ZΔM15, Δ*lacX74*, *deoR*, *rec*A1, *end*A1, *ara*D139, Δ(ara,leu)7697, *gal*U, *gal*K, λ, *rps*L, *nup*G, /bMON14272/pMON7124

Strains used for protein expression

Strain	Genotype
E. coli BL21(DE3)RIL	F-, argU, ileY , leuW (Cam)
E. coli BL21(DE3)PlysS	B, F^-, *dcm*, *omp*T, *hsd*S($r_B^-m_B^-$), *gal*, λ(DE3), pLysS Cam
E. coli Rosetta(DE3)PlysS	F^-, *omp*T, *hsd*SB($r_B^-m_B^-$), *gal*, *dcm*, (DE3), *arg*U, *arg*W, *ile*X, *gly*T, *leu*W, *pro*L, *met*T, *thr*T, *tyr*U, *thr*U (Cam)

2.1.2 Cell lines

2.1.2.1 Mammalian cell lines

DG 75	EBV negative Burkitt's lymphoma cell line (Ben-Bassat et al., 1977)
SM261	RBP-J$\kappa^{-/-}$ cell line derived from DG75 (Maier et al., 2003)

2.1.2.2 Insect cell lines

High Five™ (H5)	cell line derived from *Trichoplusia ni* egg cell homogenates, (Invitrogen, Carlsbad, CA, USA)
SF21	cell line isolated from *Spodoptera frugiperda* (Fall Armyworm) ovarian insect cells
expresSF+ (SFplus)	derived from Sf9, (Protein Sciences Corporation, Meriden, CT, USA)

2.1.3 Plasmids

Plasmids provided for this work

pEBNA2	EBNA2	aa 259 to aa 435, comprises CR5 to CR7; K. Fuchs, GSF Munich
PSV180	EBNA2	aa 291 to aa 355, comprises CR5 to CR6; S. Valencia, GSF Munich
pVK60	human RBP-Jκ	full-length in pETM11; V. Kapetaniou, GSF Munich
pVK91	human RBP-Jκ	full-length in pETM30; V. Kapetaniou, GSF Munich

Plasmids produced for this work

pKH1	human RBP-Jκ	RBP-Jκ aa 157 to 333 in pETM11
pKH2	human RBP-Jκ	RBP-Jκ aa 100 to 188 in pETM11
pKH3	human RBP-Jκ	RBP-Jκ aa 165 to 348 in pETM11
pKH4	human RBP-Jκ	RBP-Jκ aa 100 to 333 in pETM11
pKH5	human RBP-Jκ	RBP-Jκ aa 63 to 487 in pETM11
pKH6	human RBP-Jκ	RBP-Jκ aa 74 to 487 in pETM11
pKH11-7	human RBP-Jκ	RBP-Jκ aa 32 to 333 in pETM11
pKH11-8	human RBP-Jκ	RBP-Jκ aa 32 to 435 in pETM11
pKH11-9	human RBP-Jκ	RBP-Jκ aa 157 to 435 in pETM11
pKH11-10	human RBP-Jκ	RBP-Jκ aa 12 to 431 in pETM11
pKH11-11	human RBP-Jκ	RBP-Jκ aa 12 to 435 in pETM11
pKH11-12	human RBP-Jκ	RBP-Jκ aa 12 to 452 in pETM11
pKH11-13	human RBP-Jκ	RBP-Jκ aa 28 to 431 in pETM11
pKH11-14	human RBP-Jκ	RBP-Jκ aa 28 to 435 in pETM11
pKH11-15	human RBP-Jκ	RBP-Jκ aa 28 to 452 in pETM11
pKH11-16	human RBP-Jκ	RBP-Jκ aa 63 to 431 in pETM11

pKH11-17	human RBP-Jκ	RBP-J aa 63 to 435 in pETM11
pKH11-18	human RBP-Jκ	RBP-J aa 63 to 452 in pETM11
pKH11-19	human RBP-Jκ	RBP-J aa 74 to 431 in pETM11
pKH11-20	human RBP-Jκ	RBP-J aa 74 to 435 in pETM11
pKH11-21	human RBP-Jκ	RBP-J aa 74 to 452 in pETM11
pKH11-22	human Notch-Ram	Notch1 aa 1768 to 1861 in pETM11
pKH11-23	human Notch-RamANK	Notch1 aa 1768 to 2122 in pETM11
pKH24.1	human RBP-Jκ	RBP-J aa 28 to 432 in pFastBac-HTa
pKH25.1	human RBP-Jκ	full-length in pFastBac-HTa
pKH30-5	human RBP-Jκ	RBP-J aa 63 to 487 in pETM30
pKH30-6	human RBP-Jκ	RBP-J aa 74 to 487 in pETM30
pKH30-7	human RBP-Jκ	RBP-J aa 32 to 333 in pETM30
pKH30-8	human RBP-Jκ	RBP-J aa 32 to 435 in pETM30
pKH30-9	human RBP-Jκ	RBP-J aa 157 to 435 in pETM30

2.1.4 Oligonucleotides

Oligonucleotides used for cloning

Primers used to generate PCR products for the cloning of RBP-Jκ constructs

Numbers in the name of the primer correspond to the first amino acid for forward primers (_f) or the last one for reverse primers (_r) in the corresponding construct; enzyme names indicate the restriction site introduced

RBP_1_Nco_f	ATG AGC CAT GGC GCC TGT TGT GAC
RBP_487_Kpn_r	ATT CGG TAC CTT AGG ATA CCA CTG TGG CTG TA
oRBP_12_Nco_f	GAG CCA TGG ATC GGC CTC CAC CTA AAC GAC T
oRBP_17_Nco_f	GAG ATT CCA TGG ATC GAC TTA CTA GGG AAG CTA TG
oRBP_28_Nco_f	GAG CCA TGG ATA AAG AGC GAG GGG ATC AAA CA
oRBP_32_Nco_f	GAG CCA TGG ATC AAA CAG TAC TTA TTC TTC ATG CA
oRBP_63_Nco_f	GAG CCA TGG GCA GTG GAT GGA AGA AAA AAA AAG AAC A
oRBP_74_Nco_f	GAG CCA TGG AAC GCG ATG GTT GTT CTG AAC AAG AGT CT
oRBP_100_Nco_f	GAG CCA TGG TGC AGC AGC TAA ACT TGG AAG GAA AGA ACT ATT GCA CA

oRBP_157_Nco_f	GAG CCA TGG TGA AGA AGC AGT CAT TGA AAA ATG CTG ACT TAT GCA TTG CCT
oRBP_165_Nco_f	GAG CCA TGG TGG ACT TAT GCA TTG CCT CAG GAA CAA AGG TGG CTC T
oRBP_188_Kpn_r	GGA ATT CGG TAC CTT ATC TGG TAC TAA CTG TCT GGG ATC GTA GTC GAT TAA ACA
oRBP_333_Kpn_r	GGA ATT CGG TAC CTT AAG GGC CCA TTC CCT CAT
oRBP_348_Kpn_r	GGA ATT CGG TAC CTT ACT GAA CGGC TCT CTA CCA CAG GCA CAG GAG TGA CT
oRBP_431_Kpn_r	GGA ATT CGG TAC CTT AGT AGG TAA AGG TAA GGC TGG TG
oRBP_433_Kpn_r	GGA ATT CGG TAC CTT ATG GTG TGT AGG TAA AGG TAA GG
oRBP_435_Kpn_r	GGA ATT CGG TAC CTT ATG GTT CTG GTG TGT AGG TAA AGG
oRBP_452_Kpn_r	GGA ATT CGG TAC CTT ATG AAT TGG CTC GAA GGA TTG CT
oRBP_487_Kpn_r	GGA ATT CGG TAC CTT AGG ATA CCA CTG TGG CTG TAG ATG ATG TGA CAC TGG T

Primers used to generate PCR products for the cloning of Notch constructs

Numbers in the name of the primer correspond to the first amino acid for forward primers (_f) or the last one for reverse primers (_r) in the corresponding construct; enzyme names indicate the restriction site introduced

Notch_1768_Pci_f	CAT GAC ATG TCC CGC AAG CGC CGG C
Ram_1861_Kpn_r	ATT CGG TAC CTT AAT CCA GGT GCT GCT GAG TCC
RamANK_2075_Kpn_r	ATT CGG TAC CTT AGT AGC TGC CCT CCC GGG
RamANK_2122_Kpn_r	ATT CGG TAC CTT AGC TGC GCA CCA GGT TGT ACT
Notch_2075_Pci_f	ATG AGA CAT GTT TAG CTA CGA GAC CGC CAA G
Notch_2508_Kpn_r	GAA TTC GGT ACC TTA GTG CTC AGG CAC CTG TAG

Oligonucleotides used to form binary complexes with RBP-Jκ

The core RBP-Jκ binding sequence is underlined in each oligonucleotide.

Oligonucleotides derived from the C-promoter; without single-stranded overhangs

Cp_f	GAT CTG GTG TAA ACA CGC CGT GGG AAA AAA TTT ATG
Cp-r	GAT CCA TAA ATT TTT TCC CAC GGC GTG TTT ACA CCA

RI_f	GAT CTG GTG TAA ACA CGC CGT GGG AAA AAA TTT ATG GAT C
RI_r	GAT CCA TAA ATT TTT TCC CAC GGC GTG TTT ACA CCA GAT C
RI_30_f	TGT AAA CAC GCC GTG GGA AAA AAT TTA TGG
RI_30_r	CCA TAA ATT TTT TCC CAC GGC GTG TTT ACA
RI_26_f	TAA ACA CGC CGT GGG AAA AAA TTT AT
RI_26_r	ATA AAT TTT TTC CCA CGG CGT GTT TA
RI_22_f	AAC ACG CCG TGG GAA AAA ATT T
RI_22_r	AAA TTT TTT CCC ACG GCG TGT T
RI_20_f	ACA CGC CGT GGG AAA AAA TT
RI_20_r	AAT TTT TTC CCA CGG CGT GT
RI_18_f	CAC GCC GTG GGA AAA AAT
RI_18_r	ATT TTT TCC CAC GGC GTG
RI_16_f	ACG CCG TGG GAA AAA A
RI_16_r	TTT TTT CCC ACG GCG T
RI_14_f	CGC CGT GGG AAA AA
RI_14_r	TTT TTC CCA CGG CG
RI_12_f	GCC GTG GGA AAA
RI_12_r	TTT TCC CAC GGC
RI_10_f	CCG TGG GAA A
RI_10_r	TTT CCC ACG G

Oligonucleotides derived from the C-promoter; with single base single-stranded overhangs

RI_26_f_A	A TAA ACA CGC CGT GGG AAA AAA TTT AT
RI_26_r_T	T ATA AAT TTT TTC CCA CGG CGT GTT TA
RI_25_f_A	A TAA ACA CGC CGT GGG AAA AAA TTT A
RI_25_r_T	T TAA ATT TTT TCC CAC GGC GTG TTT A
RI_24_f_A	A AAA CAC GCC GTG GGA AAA AAT TTA
RI_24_r_T	T TAA ATT TTT TCC CAC GGC GTG TTT
RI_23_f_A	A AAC ACG CCG TGG GAA AAA ATT TA
RI_23_r_T	T TAA ATT TTT TCC CAC GGC GTG TT
RI_22_f_A	A AAC ACG CCG TGG GAA AAA ATT T
RI_22_r_T	T AAA TTT TTT CCC ACG GCG TGT T
RI_21_f_A	A ACA CGC CGT GGG AAA AAA TTT

RI_21_r_T	T AAA TTT TTT CCC ACG GCG TGT
RI_20_f_A	A ACA CGC CGT GGG AAA AAA TT
RI_20_r_T	T AAT TTT TTC CCA CGG CGT GT
RI_17_f_T	T CAC GCC GTG GGA AAA AA
RI_17_r_A	A TTT TTT CCC ACG GCG TG
RI_16_f_T	T ACG CCG TGG GAA AAA A
RI_16_r_A	A TTT TTT CCC ACG GCG T
RI_15_f_T	T ACG CCG TGG GAA AAA
RI_15_r_A	A TTT TTC CCA CGG CGT
RI_14_f_T	T CGC CGT GGG AAA AA
RI_14_r_A	A TTT TTC CCA CGG CG

Oligonucleotides derived from the C-promoter; with double base single-stranded overhangs

RI_23_f_AA	AA AAC ACG CCG TGG GAA AAA ATT TA
RI_23_r_TT	TT TAA ATT TTT TCC CAC GGC GTG TT
RI_22_f_AA	AA AAC ACG CCG TGG GAA AAA ATT T
RI_22_r_TT	TT AAA TTT TTT CCC ACG GCG TGT T
RI_21_f_AA	AA AAC ACG CCG TGG GAA AAA ATT
RI_21_r_TT	TT AAT TTT TTC CCA CGG CGT GTT
RI_20_f_AA	AA ACA CGC CGT GGG AAA AAA TT
RI_20_r_TT	TT AAT TTT TTC CCA CGG CGT GT
RI_19_f_AA	AA ACA CGC CGT GGG AAA AAA T
RI_19_r_TT	TT ATT TTT TCC CAC GGC GTG T
RI_18_f_AA	AA CAC GCC GTG GGA AAA AAT
RI_18_r_TT	TT ATT TTT TCC CAC GGC GTG
RI_17_f_AA	AA CAC GCC GTG GGA AAA AA
RI_17_r_TT	TT TTT TTT CCC ACG GCG TG
RI_13_f_AA	AA CGC CGT GGG AAA A
RI_13_r_TT	TT TTT TCC CAC GGC G
RI_13_f_TT	TT GCC GTG GGA AAA A
RI_13_r_AA	AA TTT TTC CCA CGG C

Oligonucleotides derived from the LMP1 promoter

SM615-LMP1wt	GGT CCC CGG GGG GCA AGC TGT GGG AAT GCG GTG GCC
SM615-LMP1wt-as	GGC CAC CGC ATT CCC ACA GCT TGC CCC CCG GGG ACC

Oligonucleotides derived from the LMP2A promoter

O54-sense	CTC GCG ACT CGT GGG AAA ATG GGC GGA AGG GCA CCG
O54-anti	CCT GGA ACT ATT TTC CCA CGG TGC CCT TCC GCC CAT

Oligonucleotides derived from the mammalian HES-1 promoter

Cele_13_f_TT	TT ACT GTG GGA AAG A
Cele_13_r_AA	AA TCT TTC CCA CAG T

DNA-oligonucleotides to test unspecific binding of RBP-Jκ

Un_f	CCA TGA ATC CTA CAG TAC
Un_r	GTA CTG TAG GAT TCA TGG

2.1.5 Antibodies

Primary antibodies (provided by E. Kremmer, GSF Munich)

	Species	**isotype**
α-EBNA2, WWP-K 6C8	Rat	IgG 2a
α-GST 2C8	Mouse	IgG 1
α-RBP-Jκ 7A11 (Western blotting)	Rat	IgG 2b
α-RBJκ 6E7 (immunoprecipitation)	Rat	IgG 2b
α-Ram, ICN 5B5	Rat	IgG 2b

Conjugated antibodies

species	**target**	**conjugate**	**Manufacturer**
Goat	α-rat	IgG-HRP	Santa Cruz Biotechnology, Santa Cruz, CA, USA
Goat	α-mouse	IgG-HRP	GE Healthcare (Amersham Biosc.), Munich, DE

2.1.6 Enzymes

Alkaline shrimp phosphatase	Boehringer, Mannheim, DE
Klenow fragment	Roche, Mannheim, DE

Kod polymerase	Invitrogen, Carlsbad, CA, USA
Proteinase K	Roche, Mannheim, DE
Restriction enzymes	New England Biolabs, Ipswich, MA, USA
Subtilisin	Roche, Mannheim, DE
Taq polymerase	Peqlab Biotech. GmbH, Erlangen, DE
TEV protease	G. Stier, EMBL
Trypsin	Roche, Mannheim, DE

2.1.7 Peptides

Peptide	**derived from**
QLWFP	Notch-Ram
RQHGQLWFPEGE	Notch-Ram
PSGPPWWPPI	EBNA2
RPSGPPWWPPIE	EBNA2

2.1.8 Chemicals

Acetic Acid	Roth, Karlsruhe, DE
Agarose	Invitrogen, Carlsbad, CA, USA
Amphotericine B	Sigma Aldrich, Taufkirchen, DE
Ampicillin	Roth, Karlsruhe, DE
Arabinose	Sigma Aldrich, Taufkirchen, DE
Arginine	Sigma Aldrich, Taufkirchen, DE
β-Mercaptoethanol	Sigma Aldrich, Taufkirchen, DE
Bacto agar	Invitrogen, Carlsbad, CA, USA
Bovine serum albumine	New England Biolabs, Ipswich, MA, USA
Bradford Reagent	Biorad, Hercules, CA, USA
Chloramphenicol	Sigma Aldrich, Taufkirchen, DE
Complete protease inhibitor cocktail, EDTA-free	Roche, Mannheim, DE
Dithiothreitol	Roth, Karlsruhe, DE

DNA markers	Fermentas, St Leon-Rot, DE
DNTP	Roche, Mannheim, DE
EDTA	Roth, Karlsruhe, DE
Ethidium bromide	Sigma Aldrich, Taufkirchen, DE
Fetal calf serum	PAA Laboratories, Cölbe, DE
Glycerol	Roth, Karlsruhe, DE
Glycine	Sigma Aldrich, Taufkirchen, DE
Guanidinium Hydrochloride	Roth, Karlsruhe, DE
HEPES	Roth, Karlsruhe, DE
Hydrochloric Acid	Roth, Karlsruhe, DE
Imidazole	Roth, Karlsruhe, DE
IPTG	Roth, Karlsruhe, DE
Kanamycin	Roth, Karlsruhe, DE
LB broth (Lennox)	Roth, Karlsruhe, DE
Lipofectin	Invitrogen, Carlsbad, CA, USA
Nickel sulfate	Sigma Aldrich, Taufkirchen, DE
Magnesium Cloride	Sigma Aldrich, Taufkirchen, DE
Magnesium Formate	Hampton Res., Aliso Viejo, CA, USA
MES	Roth, Karlsruhe, DE
Pefabloc	Pentapharma, Basel, CH
Penicillin/Streptomycine	Invitrogen/Gibco, Carlsbad, CA, USA
Polyethyleneglycol	Sigma Aldrich (Fluka), Taufkirchen, DE
Polyethyleneglycol 3350	Sigma Aldrich (Fluka), Taufkirchen, DE
Polyethyleneglycol 4000	Sigma Aldrich (Fluka), Taufkirchen, DE
Polyethyleneglycol 5000 MME	Sigma Aldrich (Fluka), Taufkirchen, DE
Polyethyleneglycol 8000	Sigma Aldrich (Fluka), Taufkirchen, DE
Polyethyleneglycol	Sigma Aldrich (Fluka), Taufkirchen, DE
Potassium Chloride	Sigma Aldrich, Taufkirchen, DE
Protein Standard for size exclusion chromatography	Biorad, Hercules, CA, Hercules, CA, USA
SDS	Sigma Aldrich (Fluka), Munich,DE
SF900 medium	Invitrogen, Carlsbad, CA, USA
Silicon grease	Dow Corning, Wiesbaden, DE

Sodium Chloride	Roth, Karlsruhe, DE
Sodium Hydroxide	Roth, Karlsruhe, DE
TCEP	Sigma Aldrich, Taufkirchen, DE
TNM medium	Sigma Aldrich, Taufkirchen, DE
Tris-hydroxymethyl-aminomethane	Omni Lifesciences, Vista, CA, USA
XTRA Blue Xgal solution	Qbiogene, Morgan Irvine, CA

2.1.9 Crystallisation screens

All crystallisation screens used (Additive Screen 2; Crystal Screen 1 and 2; Grid Screens Ammonium Sulfate, MPD, PEG 6000 and Na-Malonate; Natrix Screen; PEG/Ion Screen) were purchased from Hampton Research, Aliso Viejo, CA, USA

2.1.10 Laboratory equipment

Air Fuge	Beckman Coulter, Krefeld, DE
Äkta Explorer	GEHC* (Amersham Pharmacia), Munich, DE
Äkta Prime	GEHC (Amersham Pharmacia), Munich, DE
Äkta Purifier	GEHC (Amersham Pharmacia), Munich, DE
Bacteria shaker Multitron	Infors, Bottmingen, CH
CD spectrometer	Jasco GmbH, Gross-Umstadt, DE
Flow hood work bench	Heraeus Instruments, Langenselbold, DE
Gel documentation system ChemiDoc	Biorad, Hercules, CA, USA
Gel electrophoresis units (DNA) Mini-Sub cell GT	Biorad, Hercules, CA, USA
Gel electrophoresis units (protein) X Cell Sure Lock	Invitrogen, Carlsbad, CA, USA
Centrifuge 5810 R	Eppendorf AG, Hamburg, DE
Centrifuge 5415 R	Eppendorf AG, Hamburg, DE
Centrifuge 5415 D	Eppendorf AG, Hamburg, DE
Centrifuge Allegra	Eppendorf AG, Hamburg, DE
Centrifuge Avanti J-20 XP	Beckman Coulter, Krefeld, DE

Centrifuge RC 26 Plus	Sorvall, Langenselbold, DE
Counter QC 4000 XER	Bioscan, Washington DC, USA
Incubator for bacteria cultures	Heraeus Instruments, Langenselbold, DE
Insect cell incubator Multitron	Infors, Bottmingen, CH
Mammalian cell incubator	Heraeus Instruments, Langenselbold, DE
Rotors GSA, SA300, SS34	Sorvall, Langenselbold, DE
Rotor JLA 8.1000	Beckman Coulter, Krefeld, DE
Rotor JA 25.50	Beckman Coulter, Krefeld, DE
PCR machine Mastercycler Gradient	Eppendorf AG, Hamburg, DE
PH-Meter Seven Easy	Mettler Toledo, Giessen, DE
Spectrophotometer BioPhotometer	Eppendorf AG, Hamburg, DE
Thermomixer Comfort	Eppendorf AG, Hamburg, DE
Ultrasonic Cell Disrupter Sonoplus HD 2200	Bandelin electronic, Berlin, DE
UV transilluminator	Angewandte Gentechnologische Systeme GmbH, Heidelberg, DE
Water purification system	Millipore GmbH, Schwalbach, DE
X-ray film developer	GEHC (Amersham Biosc.), Munich, DE

*GEHC: GE Healthcare

2.1.11 Synchrotron radiation sources

Source	Instrument	Technique
BESSY Berlin		X-ray crystallography
CLRC Daresbury	12.1	Circular Dichroism
EMBL Hamburg at DESY	X33	SAXS
EMBL Hamburg at DESY	BW7B	X-ray crystallography

2.1.12 Software

BLAST	http://blast2srs.embl.de
Clone Manager	Sci Ed Central, www.scied.com
ClustalW	www.ebi.ac.uk/clustalw/

Entrez Pubmed	www.ncbi.nlm.nih.gov/entrez/query.fcgi
FoldIt	http://iubio.bio.indiana.edu:7780/archive/00000038/
MODELLER	http://salilab.org/modeller/
PestFind	http://bioweb.pasteur.fr/seqanal/interfaces/pestfind.html
Pfam	www.sanger.ac.uk/Software/Pfam/
PHD	www.embl-heidelberg.de/predictprotein/predictprotein.html
PDB Protein Data Bank	www.pdb.org
Protein parameter tool	www.expasy.org/tools/protparam.html
Pymol	www.pymol.org
Rasmol	www.umass.edu/microbio/rasmol/

2.1.13 Kits, columns and other material

ECL Western Blotting detection reagent	GEHC* Amersham Biosc., Munich, DE
HiTrap Chelating 1 ml	GEHC Amersham Biosc., Munich, DE
HiTrap Chelating 5 ml	GEHC Amersham Biosc., Munich, DE
Hybond N+ nylon membrane	Millipore GmbH, Krefeld, DE
QIAquick Gel Extraction Kit	Qiagen, Hilden, DE
QIAquick PCR purification Kit	Qiagen, Hilden, DE
QIAquick Spin Mini Kit	Qiagen, Hilden, DE
Superdex 75 10/30, size excl. column	GEHC Amersham Biosc., Munich, DE
Superdex 75 16/60, size excl. column	GEHC Amersham Biosc., Munich, DE
Superdex 200 10/30, size excl. column	GEHCAmersham Biosc. Munich, DE
Superdex 200 16/60, size excl. column	GEHCAmersham Biosc., Munich, DE
Whatman paper	Biometra, Goettingen, DE
X-ray film	Eastman Kodak Co., USA

Plastic laboratory-ware were purchased from Greiner GmbH, Frickenhausen, DE, NUNC GmbH, Wiesbaden, DE, Eppendorf AG, Hamburg, DE.

*GEHC: GE Healthcare

2.2 Methods

2.2.1 Bacterial cell culture

Maintenance and propagation of bacteria

Bacteria were cultured at 37 °C on LB-agar plates in an incubator or in liquid LB-medium in a shaker. Transformed bacteria were selected by adding the appropriate antibiotics to agar or LB-medium (kanamycin 50 µg/ml, chloramphenicol 34 µg/ml, ampicillin 50 µg/ml). For liquid cultures 100 to 1000 ml LB-medium were inoculated with a single bacterial colony picked from an agar plate.

Glycerol stocks for long-term storage were only prepared for plasmids transformed into DH5a to be able to regrow cultures quickly for DNA preparation. Aliquots of 700 µl of culture (OD_{600} = 0.6) were mixed with 300 µl glycerol and stored at -80 °C.

LB-medium: 1% (w/v) Bacto-Tryptone; 0.5% (w/v) Bacto-yeast extract; 0.5% (w/v) NaCl

LB-agar: LB-medium; 1.5% (w/v) Bacto-agar

Preparation of competent bacteria

A sample from a frozen bacterial stock was spread out onto an LB-agar plate and grown overnight. A single colony was used to inoculate 5 ml of LB-medium overnight at 37 °C. 200 ml LB-medium containing 20 mM $MgSO_4$ and 10 mM KCl were inoculated with 1 ml of the overnight culture in a 1 l flask. The cells were fermented at 37 °C up to an OD_{600} of 0.6-0.7. Bacteria were kept on ice for 10 minutes and pelleted at 3500 rpm (rotor GSA, Sorvall, Langenselbold, DE) for 10 minutes at 4 °C. The medium was discarded and the pellet resuspended in 20 ml of ice-cold 0.1 M $CaCl_2$. The bacteria were then pelleted at 3500 rpm for 20 minutes at 4 °C and resuspended in 4 ml of ice-cold 0.1 M $CaCl_2$. After another centrifugation step (as above) the cells were resuspended in 2 ml cold 10 % glycerol. Aliquots of 100 µl bacteria suspension were flash-frozen in liquid nitrogen and stored at -80 °C.

Heat shock transformation

100 µl of competent cells stored at -80 °C were thawed on ice. 10 to 100 ng of plasmid DNA or 10 µl of ligation mix were added and the bacteria-DNA mix incubated on ice for 30 minutes. Following a 45 sec heat shock at 42 °C the mix was incubated on ice for 2 minutes. 500 µl LB-medium were added and the cells were incubated at 37 °C in a shaker for one hour. If a ligation product was transformed the cells were centrifuged at 2000 rpm (centrifuge 5810 R, Eppendorf AG, Hamburg, DE) for 1 minute, the supernatant discarded until 50 µl were left

and spread onto an agar plate containing the appropriate antibiotics. The LB-agar plates were incubated at 37 °C for 16 to 18 hours.

For the transformation of pre-existing plasmids an aliquot of the culture of transformed bacteria was plated out onto an agar plate containing the appropriate antibiotics.

Heat shock transformation of recombinant baculo-virus vectors

A recombinant Bacmid (rBacmid) is produced when, after ligation of the gene of interest into a baculo-virus pFASTBAC vector and transformation of the ligation product into DH10Bac *E. coli* cells the gene of interest including possible tags recombines into a baculo-viral genome present in DH10Bac cells. The new recombinant artificial baculo-virus genome is called rBacmid (for a scheme of rBacmid production see Figure 2.1).

Transformation of a recombinant baculo-virus vector into DH10Bac follows a modified version of the protocol described before. An aliquot of competent DH10Bac cells stored at – 80 °C was thawed on ice. 1 ng of baculo-virus vector was mixed with 25 µl competent cells and incubated on ice for 30 min. Following a 45 sec heat shock at 42 °C the mix was incubated on ice for 2 minutes. 200 µl LB-medium were added and the cells were incubated at 37 °C in a shaker for four hours. 20 µl of the culture were plated on agar containing 50 µg/ml kanamycin, 10 µg/ml gentamicin, 40 µg/ml tetracycline, 40 µg/ml IPTG and 1 mg/ml Bluogal and incubated at 37 °C for 48 to 72 hours until blue and white colonies could be distinguished.

Isolation of plasmid DNA

Single colonies obtained from transformation of bacteria with ligation reactions or plasmid DNA were used to inoculate 5 ml of LB-medium with the appropriate antibiotics. The culture was grown overnight at 37 °C and harvested by centrifugation at 4000 rpm (Allegra centrifuge, Eppendorf) for 10 minutes. The QIAquick Spin Mini Kit (QIAGEN) was used according to the manufacturer's instructions.

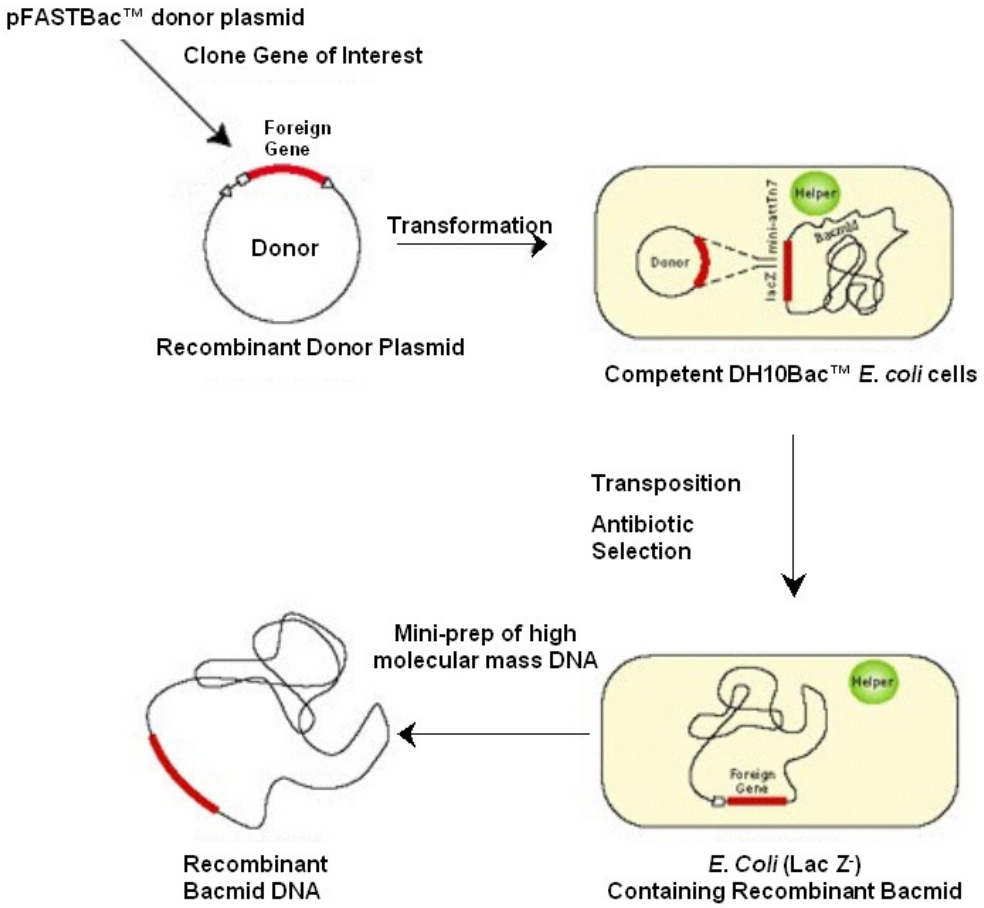

Figure 2.1: Scheme for the production of a recombinant Bacmid (rBacmid). The gene of interest is ligated into an appropriate baculo-virus transfer vector. The recombinant vector is transformed into competent DH10Bac *E. coli* cells containing one copy of a baculo-virus genome and helper plasmids expressing a recombinase. The recombination sites flanking the gene of interest in the vector enable it to recombine into the viral genome to form a recombinant Bacmid. Clones containing the rBacmid are visualized by blue-white selection, since successful recombination destroys the β-galactosidase gene expressed to metabolise a chromogenic substrate such as BluoGal™ contained in the agar into a blue substance colouring the bacteria. The insertion of a gene destroys the reading frame of β-galactosidase resulting in white bacteria.

Isolation of rBacmid-DNA

As described in Figure 2.1 successful recombination of the gene of interest into the baculo-virus genome results in the destruction of the reading frame of the β -galactosidase gene. Bacterial clones containing a recombinant Bacmid are therefore incapable of converting a chromogneic substrate such as BluoGal™ into a blue substance and thus remain white.

To amplify and isolate rBacmid-DNA two white DH10Bac colonies were picked and inoculated into 2 ml of medium and grown overnight at 37 °C in a shaker. Cell lysis and

separation of rBacmid-DNA from proteins and cell debris was carried out using buffers P1, P2 and N3 supplied with the QIAquick Spin Mini kit (QIAGEN) according to the manufacturer's instructions. Since the desired rBacmid is very large (16 kbp), miniprep columns are not suitable for DNA purification. A clear lysate containing rBacmid-DNA was obtained by a centrifugation step. The rBacmid-DNA was precipitated by addition of 3 volumes of 100% ethanol and by centrifugation at 16100 g and 4 °C for 30 minutes. The DNA pellet was washed with 500 µl of 70% ethanol, dried under a sterile bench and dissolved in 50 µl of MilliQ water.

P1: 50 mM Tris-HCl, pH 8.0, 10 mM EDTA, 100 µg/ml RNase A
P2: 200 mM NaOH, 1% SDS (w/v)
N3: 3.0 M potassium acetate, pH 5.5

2.2.2 Eucaryotic cell culture

Mammalian cell culture
Cultivation of cells in suspension

DG75 cells were grown in suspension culture in RPMI containing 10% (v/v) FCS, 2mM L-glutamine and 100 U/ml penicillin/streptomycine. They were kept at 37 °C in a 5% CO_2, water saturated atmosphere.

Cells were counted in a Neubauer chamber in a 1:1 solution in trypan blue to exclude dead cells. As soon as the culture had reached a density of $1x10^6$/ml they were split 1:4 to 1:6.

Insect cell culture

Cultivation of suspension and adherent cells
Adherent cells

High Five™ cells, SF21 and SFplus cells were grown in monolayer cultures with TNM media + 10% FCS. Cells were grown in 5, 10 or 25 ml cell culture bottles, where they grow as monolayer with a duplication time of 12 hours. When confluent, the cells were split according to the desired confluence level and incubated until 70 to 80% confluency for infection or up to 100 % for propagation.

TNM medium: 51 g TNM-FH powder (Sigma) per litre medium were dissolved in deionised H_2O, supplemented with 0.35 g/l $NaHCO_3$, adjusted to pH 6.2 and filtered through a sterile filter into a sterile bottle.

Suspension cultures

SFplus cells were grown in suspension in flasks holding 300 ml of SF900 medium supplemented with 1.25 µg/ml amphotericin and 100 U/ml penicillin/streptomycin. After reaching a density of $2x10^6$ cells/ml they were split 1:2 or infected with the appropriate recombinant baculo-virus.

SF900 medium: 38.4 g SF900 powder (Sigma) per litre medium were dissolved in deionised H_2O, supplemented with 0.8 ml insect cell supplement (Invitrogen) and 0.35 g/l $NaHCO_3$, adjusted to pH 6.2 and filtered through a sterile filter into a sterile bottle.

Production of a recombinant baculo-virus

rBacmid transfection

SF21 cells in 6-well plates holding $9x10^5$ cells/well were used for transfection. The cells were washed twice with 2 ml TNM medium without any supplements. The medium was then discarded and replaced by a mix of 6 µl Cellfectin and 5 µl rBacmid-DNA (200 ng) in 200 µl TNM only. After 45 min 800 µl TNM only were added and the mix was incubated for five hours at 27 °C. The mix was replaced by 2 ml of TNM + FCS. The supernatant, which contains the primary virus (P1), was collected after 72 hours.

Virus production

To produce a larger amount of virus, SF21 cells were grown in TNM+FCS media to 60-70% confluence in 25 ml plates and infected with 600 µl of P1 virus. Depending on the appearance of the cells after infection the supernatant containing the secondary virus (P2) was taken 48-72 hours after infection.

2.2.3 DNA manipulation and analysis

Cloning of recombinant plasmids

Constructs for protein expression in bacteria

Primers for any DNA fragment of interest were designed with an NcoI- or, if this site was present in the fragment, a PciI-restriction site at the 5'-end of the forward primer and a KpnI-restriction site at the 5'-end of the reverse primer. The DNA fragment was amplified by PCR and digested with the appropriate restriction enzymes (NEB) according to the manufacturer's instructions. It was ligated into a linearized pETM11 vector (G. Stier, EMBL Heidelberg) with flanking sites for NcoI and KpnI. Chemically competent *E. coli* DH5α bacteria were transformed with the ligation product and spread onto an agar plate containing the appropriate antibiotic.

Constructs for protein expression in insect cells

The DNA fragments encoding the protein of interest amplified by PCR were ligated into the baculo-virus shuttle vector pFastBac-Hta, containing a 6xHis-Tag. The multiple cloning site included the commonly used NcoI and KpnI sites, which were used to cut both vector and fragment. Competent DH10Bac cells were transformed according to the protocol in section 2.2.1. After 48 to 72 hours the colonies are visible and can be distinguished on the basis their blue and white colour. After isolation of Bacmid-DNA the presence of the insert was verified by restriction digestion with NcoI and KpnI.

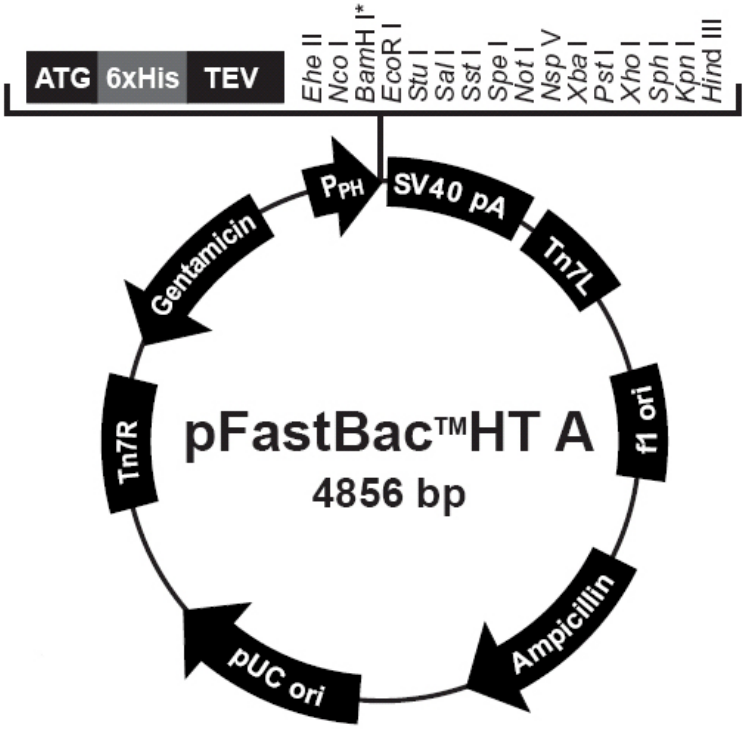

Figure 2.2: Map of the baculovirus vector pFastBac-HT A indicating features important for cloning and replication. The vector contains an N-terminal 6xHis tag separated from the gene of interest by a TEV cleavage site. Within the multi-cloning site both full-length RBP-Jκ and a truncated fragment containing aa 28 to 432 were ligated between NcoI and KpnI restriction sites.

Polymerase chain reaction

To check the presence of an insert Taq polymerase (Roche, Mannheim, DE) was used according to the manufacturer's instructions.

Kod polymerase (Invitrogen, Carlsbad, CA, USA) was used to amplify DNA fragments intended for cloning. The kit delivered with the polymerase was used according to the manufacturer's instructions.

Annealing of single-stranded oligonucleotides

Equal molar ratios of single-stranded complementary oligonucleotide were mixed in 10 mM Tris, pH 8.0 and 1 mM $MgCl_2$. The solution was heated to 95 ºC for 10 minutes in a heat block and then left to gradually cool down to room temperature by switching the heat block off. The final concentration of annealed oligonucleotides was 0.5 nM/µl in each case.

Radioactive labelling of DNA

End-labelling with γ-^{32}P-ATP using T4 polynucleotide kinase

End-labelling was used for oligonucleotides derived from the C-promoter containing an RBP-Jκ binding site, which were shortened to lengths of 14 to 24 bp. Before labelling the oligonucleotide pairs were annealed.

20 pMol of oligonucleotide ends were incubated with 2 µl of 10x buffer for T4-polynucleotide kinase (Roche, Mannheim, DE) and 1 µl kinase (Roche, Mannheim, DE). The reaction mixture was made up to 15 µl with H_2O and 5 µl γ-^{32}P-ATP added to make a final volume of 20 µl. It was then incubated at 37 °C for 30 min and separated from free γ-^{32}P-ATP using Nick™ columns (GE Healthcare, Amersham Pharmacia, Munich, DE) for oligonucleotides longer than 20 bp or Nap™ columns (GE Healthcare, Amersham Pharmacia, Munich, DE) for oligonucleotides shorter than 21 bp according to the manufacturer's instructions. 100 µl fractions were collected and the three most strongly labelled fractions as determined with a QC4000 XER counter (Bioscan, Washington DC, USA) were used further.

Fill-in with radioactive dCTP using Klenow fragment

The oligonucleotides derived from the Epstein-Barr viral Cp, LMP1P and LMP2AP were annealed and treated with Klenow-polymerase to fill up the overhangs with cold dATP/dTTP/dGTP and radioactive dCTP.

6.6 pM of double-strand oligonucleotide were added to 2 µl of 10x buffer 2 (restriction buffer 2, NEB), 2 µl dATP, dGTP, dTTP (0.5 mM each) and 2 µl Klenow polymerase (Roche, Mannheim, DE). The reaction mixture was made up to 15 µl with H_2O. 5 µl of dCTP were added to make the reaction volume 20 µl. It was then incubated for 1 h at 37 °C. To separate free radioactive nucleotides the labelled oligonucleotide was purified using Nick™ purification columns (GE Healthcare, Amersham Pharmacia, Munich, DE) according to the manufacturer's instructions. 100 µl fractions were collected and the three most strongly labelled fractions as determined with a QC4000 XER counter (Bioscan, Washington DC, USA) were used for experiments.

NEB2: 10 mM Tris-HCl, pH 7.9, 50 mM NaCl, 10 mM $MgCl_2$, 1 mM DTT

2.2.4 Methods for the analysis of proteins and DNA/protein interactions

Protein quantification
Purified proteins

5 µl of protein solution were mixed with 95 µl UV cocktail. The absorption of the mixture was measured at 280 nm after defining a blank with 5 µl of the corresponding buffer. The protein concentration was calculated according to Lambert-Beer's Law:

$$E = \varepsilon \cdot c \cdot l$$

with E being the extinction at 280 nm, ε the calculated molar extinction coefficient and l the pathlength of the cuvette.

UV cocktail: 50 mM Na_3PO_4, pH 8.0; 6 M guanidinium hydrochloride

Protein mixtures

10 µl of the protein solution were mixed with 990 µl Bradford reagent (Biorad, Hercules, CA). The absorption of the solution was determined at 600 nm. For calibration, a BSA stock solution was diluted to concentrations of 0.1, 0.2, 0.5, 0.8, 1.0 and 1.2 mg/ml. 10 µl of each dilution were added to 990 µl of Bradford reagent and the absorption measured at 600 nm.

SDS-polyacrylamide gel electrophoresis (SDS-PAGE)

SDS-PAGE separates proteins according to their molecular mass on a polyacrylamide gel. The individual charge of each protein is neutralized by addition of sodium dodecylsulfate (SDS) to the protein sample. The negatively charged SDS molecules denature and coat each protein molecule producing a layer of negative charges resulting in the migration of coated proteins towards the cathode in an electric field applied to the polyacrylamide gel.

Samples were mixed with 4x LDS sample buffer (Invitrogen, Carlsbad, CA, USA) and applied to polyacrylamide gels (12% or 5 to 20% gradient gels) cast with Tris-Tricine buffer. The gel was run at 12.5 V/cm for 90 minutes.

LDS sample buffer: 10%Glycerol, 141 mM Tris Base, 106 mM Tris HCl, pH 8.5, 2% lithiumdodecylsulfate (LDS), 0.51 mM EDTA, 0.22 mM SERVA® Blue G250, 0.175 mM Phenol Red

Native polyacrylamide gel electrophoresis

Electrophoretic mobility shift assay (EMSA) using radioactive isotopes

The following reaction was set up to form binary DNA-protein or ternary protein-protein-DNA complexes: 5 µl binding buffer were mixed with 2 µl poly-dIdC and 2 µl BSA to produce the binding mix. This was made up, with the desired amount of protein (0.01 to 250 ng) and H_2O, to 18 µl and incubated for 5 minutes at room temperature, followed by addition of 2 µl ^{32}P labelled oligonucleotide (radioactivity calculated for and diluted to $3x10^4$ counts/(µl·s)). The final mixture was incubated for 30 minutes at room temperature and loaded onto a 4% polyacrylamide gel in TBE buffer. The gel was run at 6.5 V/cm for 3 hours, dried and exposed to an X-ray film.

Buffer 4x BB: 40 mM Hepes, pH 7.9, 4 mM EDTA, 800 mM KCl; 16% Ficoll
poly dIdC: 1mg/ml poly dIdC in TE buffer and 100 mM NaCl
BSA: 1 mg/ml in H_2O

Electrophoretic mobility shift assay with non-radioactive detection

Check for the presence of binary protein-DNA and ternary protein-protein-DNA complexes

Oligonucleotides were incubated with 10 µg of the respective protein for 30 minutes at room temperature in buffer N. The complexes were loaded onto an 8% polyacrylamide gel in TBE buffer (Invitrogen, Carlsbad, CA, USA) and run for 75 minutes at 10 V/cm. The gels were stained with ethidium bromide to visualise the DNA and Coomassie Brilliant blue for protein bands.

Buffer N: 20 mM Tris-HCl, pH 8.0; 100 mM NaCl; 1 mM DTT; 1 mM $MgCl_2$
Coomassie Brilliant Blue staining solution: 30 % ethanol, 10 % acetic acid, 0.1 % Coomassie Briliant Blue R (Sigma)

Estimation of the binding affinity of proteins to DNA, other proteins and peptides

5 µg of protein were incubated with the appropriate amount of DNA, other protein and/or peptide with 5µl buffer BB and 2 µl BSA in a total volume of 20 µl for 30 minutes at room temperature. The samples were applied to an 8% polyacrylamide gel in TBE buffer and run

for 6 hours at 6.5 V/cm. The gels were stained with ethidium bromide to visualise the DNA and Coomassie Brilliant blue or Safe Stain for protein bands.

Buffer 4x BB: 40 mM Hepes, pH 7.9, 4 mM EDTA, 800 mM KCl; 16% Ficoll
BSA: 1 mg/ml in H_2O

Western blotting and immunodetection of proteins

Proteins separated by SDS-PAGE were transferred to a PVDF membrane in a transfer unit (TE 22 Mini Tank Transfer Unit, Hoefer, San Francisco, CA, USA) filled with transfer buffer. The blotting sandwich consisted of the gel placed on top of two pieces of Whatman 3MM filter paper and a sponge and overlaid with the PVDF membrane, pre-washed in methanol and equilibrated in transfer buffer. An additional layer of filter paper and a sponge placed on top of the membrane completed the blotting sandwich. The transfer was carried out at 400 mA for 1 hour.

Following transfer the membrane was incubated in blocking buffer to block all non-specific binding sites. The primary antibody (cell supernatant) was diluted to its correct working concentration (1:5) in blocking buffer and applied to the membrane for one hour at room temperature. The membrane was then washed three times for 10 minutes with PBS-T, before applying the peroxidase-conjugated secondary antibody for 1 hour at room temperature. This antibody is specific for the isotype of the primary antibody used. It was diluted according to the manufacturer's instructions in PBS-T. The membrane was washed three times for 10 minutes with 50 ml PBS-T and the blot was developed using ECL reagents A and B (GE Healthcare, Amersham Pharmacia, Munich, DE) according to the manufacturer's instructions. An X-ray film was exposed to the blot to detect protein antibody complexes by the appearance of bands of the appropriate molecular mass.

Transfer buffer: 25% methanol; 25 mM Tris, pH; 0.2 M glycine; 0,1% SDS
Blocking buffer: 1x PBS; 0.05% Tween-20; 5% fat-free milk powder
PBS-T: 1x PBS; 0.05% Tween-20

Immunoprecipitation of recombinant proteins

500 ng of recombinant protein in 300 µl equilibration buffer were incubated with 50 µl of antibody for 1 h on ice. 20 µl of preequilibrated protein G-beads were added and the mixture left rocking for 1 h. The beads were sedimented at 800 g and washed 3 times with

equilibration buffer. SDS sample buffer was added to elute the bound protein from the beads and to separate recombinant protein and antibody and the mixture was boiled for 10 minutes in a thermomixer.

The results were analysed by SDS-PAGE, Western Blotting and immunodetection (see above).

Limited proteolysis

10 µg of pure protein in cleavage buffer CB were incubated with 0.1 µg trypsin between 30 seconds and 2 hours at room temperature. The reaction was stopped with SDS sample loading buffer containing 10 mM ß-mercaptoethanol and boiled for 10 min. Samples were analysed by SDS-PAGE.

CB: 50 mM Tris, pH 8.0, 150 mM NaCl, 1 mM EDTA and 2 mM ß-mercaptoethanol

Dynamic light scattering

Monodispersity is a measure of the homogeneity of a molecular species, and therefore of the sample quality. High monodispersity is correlated with the likelihood of a sample crystallizing. Dynamic light scattering allows one to estimate the size of macromolecules in solution (their hydrodynamic radius) and their monodispersity.

A sample of 25 µl protein solution with the desired concentration, which could be recovered after the measurements, was pipetted into a quartz cuvette put into a Temperature Controlled Microsampler (Wyatt Technology Corp., Santa Barbara, CA, USA) and the DLS measured at 4 ºC with a Dyna Pro 99 (Wyatt Technology Corp., Santa Barbara, CA, USA). At least 15 data points were taken in each case.

2.2.5 Expression and purification of proteins

Proteins expressed in bacteria

Expression test

A 1 ml overnight culture grown from a single colony of freshly transformed bacteria on an agar plate was used to inoculate 50 ml of LB-medium supplemented with the appropriate antibiotics. The 50 ml culture was grown at 37 °C until an OD_{600} of 0.6 was reached. After induction with 2 mM IPTG the culture was incubated at 37 °C for 3 hours. Aliquots of 0.5 ml culture suspension were taken before and after induction, pelleted by centrifugation, lysed and analysed by SDS-PAGE.

Overexpression of recombinant proteins

A 10 ml overnight culture grown from a single colony of freshly transformed bacteria on an agar plate was used to inoculate 1 l of LB-medium supplemented with the appropriate antibiotics. The 1 l culture was grown at 37 °C until an OD_{600} of 0.6 was reached and subsequently induced with 0.5 mM IPTG or 1% arabinose. After induction the culture was grown at 20 °C for 13 to 15 hours. The cells were harvested by centrifugation at 5000 rpm (rotor JLA 8.1000, Beckman Coulter, Krefeld, DE) for 15 minutes. After washing the pellet with cold PBS and another centrifugation step (as above) the pellets were frozen at -20 °C and stored until needed.

Optimisation of expression conditions to promote soluble expression

Expression conditions for different proteins can be optimised in order to promote the solubility of the overexpressed recombinant protein by changing one or more variables, e.g. expression temperature, expression host, additives in the medium or expression time. Table 2.1 lists variables having been changed alone or pair wise to promote soluble expression of proteins expressed into inclusion bodies under standard expression conditions.

The coexpression of chaperones as achieved in the bacterial strains listed in table 2.2 together with the protein of interest may promote proper folding of the protein. These strains were therefore used to test whether the solubility of the protein of interest could be increased.

Temperature (°C) before Induction → after induction	**Additives**	**IPTG (mM)**	**Expression time (hrs)**	**Expression host**
37	50 mM Tris-HCl pH 7.4	1	20	BL21(DE3)PlysS
37→30	0.5 -5 % Glucose	0.5	2	BL21(DE3)RIL
37→25	5 mM $MgCl_2$	0.1	4	BL21(DE3)
37→20	5% ethanol		6	RosettaRIL
37→18			10	RosettaPLysS

Table 2.1: Variables in protein expression changed to promote soluble expression; single changes or a combination of changes were applied

Strain	Chaperones expressed
BL21(DE3)cc1	DnaK, DnaJ, GrpE
BL21(DE3)cc2	DnaK, DnaJ, GrpE, ClpB
BL21(DE3)cc3	GroESL
BL21(DE3)cc4	DnaK, DnaJ, GrpE, GroESL (large amounts)
BL21(DE3)cc5	DnaK, DnaJ, GrpE, GroESL (small amounts)

Table 2.2: *E. coli* strains used to improve solubility of RBP-Jκ. The five strains are stably transformed with different combinations of genes coding for bacterial chaperones known to promote protein folding (kind gift of Prof. B. Bukau, University of Heidelberg, Germany).

Solubility screens to solubilise proteins under non-denaturing conditions

Depending on the properties of the overexpressed protein certain components in the lysis buffer may promote its solubility. The screen summarized in table 2.3 was used to check the solubility of otherwise insoluble proteins.

After lysis (200 µl/ml cell culture) and sonication the suspension was centrifuged at 20 krpm (rotor SA300) at 4 °C for 45 minutes. The remaining pellet was solubilized in the same volume 6 M guanidinium hydrochloride. Both fractions were analysed by SDS-PAGE to estimate the percentage of protein in the soluble and insoluble fraction.

pH **50 mM NaCl** **5 mM EDTA** **1mg/ml lysozyme** **50 mM**	**Salt** **50mM Tris, pH 7.5** **5 mM EDTA** **1 mg/ml lysozyme**	**Urea** **50mM Tris, pH 7.5** **50mM NaCl** **5mM EDTA** **1 mg/ml lysozyme** **up to 3 M urea**	**Detergent** **20 mM Tris, pH 7.5** **50 mM NaCl** **1 mg/ml lysozyme**	**Stabiliser** **20 mMTris, pH7.5** **50 mM NaCl** **1 mg/ml lysozyme**
Na-Acetate, pH 5	0.1 M NaCl	0.5 M urea	0.2 % NP40	10 % glycerol
MES, pH 6	0.5 M NaCl	1-6 M urea in steps of 1 M	0.2 % Triton X-100	50 % glycerol
Tris-HCl, pH 7	1 M NaCl		0.2 % Tween20	
Tris-HCl, pH 8	0.1 M KCl		0.2 % dodecylmaltoside	
Tris-HCl, pH 9	1 M KCl			

Table 2.3: Screen to check the solubility of a protein in different buffer conditions designed by J. Perry (UCLA, CA, USA); different parameters are subsequently changed. The first row lists the basic components of the buffer; each column lists the extent of the changed parameter.

Purification of proteins under native conditions

His-tagged proteins

Pellets were thawed on ice and resuspended in 40 ml buffer LBB per 1 l of cell culture (6-8 g wet cell weight). The cell walls were disrupted by sonication on ice (probe TT34 of the HD2200 generator (Bandelin electronic, Berlin, DE) for 3 x 4 minutes with 30% total sonication time and 50% maximum energy output). The lysate was clarified by centrifugation at 20 krpm (rotor SS34, Sorvall, Langenselbold, DE) for 40 minutes at 4 °C, passed through a 45 µm sterile filter and applied to 3.5 ml of Ni-NTA beads equilibrated with buffer LBB, followed by gentle mixing at 4 °C for one hour. The mix of lysate and Ni-NTA beads was applied to an empty Biorad column (Hercules, CA, USA), where the lysate flowed through whereas the Ni-beads were assembled to form a column. The beads were washed with 5 column volumes of buffer LIB (low imidazole wash), 5 column volumes of buffer HSB (high salt wash) and another 5 column volumes of buffer LIB. The protein bound to the Ni-NTA beads was eluted with buffer EB. 2 ml fractions were collected and analysed on an SDS-PAGE. The fractions containing the desired protein were pooled and TCEP was added to a final concentration of 2 mM to quantitatively reduce random disulfide bridges. The protein concentration was determined and the sample flash frozen in liquid nitrogen before storage at -80°C.

Buffer LBB: 50 mM Tris-HCl, pH 8.0; 150 mM NaCl; 800 mM urea, 1 µg/ml DNase, Complete mini EDTA free protease inhibitor cocktail according to manufacturer's instructions

Buffer LIB: Buffer LBB + 5 mM imidazole

Buffer HSB: Buffer LBB + 500 mM NaCl

Buffer EB: Buffer LBB + 400 mM imidazole

GST-tagged proteins

Pellets were thawed on ice and resuspended in 40 ml buffer LBB per 1 l of cell culture (6-8 g wet cell weight). The cell walls were disrupted by sonication on ice (probe TT34 of the HD2200 generator (Bandelin electronic, Berlin, DE) for 3 x 4 minutes with 30% total sonication time and 50% maximum energy output). The lysate was clarified by centrifugation at 20 krpm (rotor SS34, Sorvall, Langenselbold, DE) for 40 minutes at 4 °C, passed through a 45 µm sterile filter and applied to 3 ml of GST-beads equilibrated with buffer LBB, followed by gentle mixing at 4 °C for one hour. The mix of lysate and GST-beads was centrifuged at 300g for 10 minutes to sediment the beads. The beads were washed 3 times with 5 column volumes of buffer LBB containing 300 mM NaCl. The protein bound to the GST-beads was

eluted with 2x 3ml buffer GEB. The elution fractions were analysed on an SDS-PAGE. The fractions containing the desired protein were pooled and TCEP was added to a final concentration of 2 mM to quantitatively reduce random disulfide bridges. The protein concentration was determined and the sample flash frozen in liquid nitrogen before storage at -80°C.

Buffer GEB: Buffer LBB + 30 mM reduced glutathione

Purification of proteins from inclusion bodies under denaturing conditions followed by refolding

Pellets from 2l of bacterial culture were resuspended in buffer LBR, sonicated with probe TT34 of the HD2200 generator (Bandelin electronic, Berlin, DE) for 3 x 4 minutes with 30% total sonication time and 50% maximum energy output and centrifuged at 4 °C for 40 minutes at 20 krpm (rotor SS34, Sorvall, Langenselbold, DE). The supernatant was discarded and the pellet containing the inclusion bodies resuspended in buffer RR and incubated for at least 30 minutes at room temperature. The solution with the solubilized inclusion bodies was clarified by centrifugation at 4 °C for 40 minutes at 20 krpm and filtered through a 45 µm sterile filter. After application to 5 ml Ni-NTA beads pre-equilibrated with buffer RR the beads were washed with 10 column volumes of buffer RW. The sample was eluted using the minimum amount (5-10 ml) of buffer RE.

Since the standard refolding protocol depicted in Figure 2.3 (a) did not result in soluble and functional protein the refolding screen listed in table 2.3 was applied. It consists of 16 conditions varying in the content of guanidinium hydrochloride, sodium chloride, arginine and glycine.

The highest ratio of soluble:insoluble protein combined with the lowest possible content of denaturing agents defined condition 13 as optimal for refolding in all cases (changed protocol shown in Figure 2.3 (b)).

The purified protein solution resulting from the affinity purification was rapidly diluted in refolding buffer 13 in 1:20 ratio. The solution was stirred slowly overnight at 4 °C and frozen at -80 °C.

Buffer LBR: 50 mM Tris, pH 8.0; 150 mM NaCl ; 1 µg/ml DNase, Complete mini EDTA free protease inhibitor cocktail according to manufacturer's instructions

Buffer RR: 40 mM Tris, pH 8.0; 500 mM KCl; 6 M guanidinium hydrochloride

Buffer RW: 40 mM Tris, pH 8.0; 40 mM KCl; 5.7 M guanidinium hydrochloride; 30 mM imidazole

Buffer RE: 40 mM Tris, pH 8.0; 40 mM KCl ; 4.7 M guanidinium hydrochloride; 300 mM imidazole

Refolding buffer 13: 50 mM Tris, pH 9.0; 1 M arginine; 150 mM NaCl; 1% glycine

Purification of binary DNA-protein complexes and ternary protein-protein-DNA complexes using size exclusion chromatography

Size exclusion chromatography was carried out on an Äkta Explorer (Amersham Pharmacia). One or two proteins and DNA were mixed in appropriate ratio. Depending on the size of the column the solution was concentrated to 1 ml (Superdex 16/60) or 200 µl (Superdex 10/30) and applied to the column, which was equilibrated in GF buffer. Fractions of 1 ml or 200 µl, respectively, were collected and analysed by SDS-PAGE.

GF buffer: 50 mM Tris-HCl, pH 8.0; 100 mM NaCl; 2 mM DTT

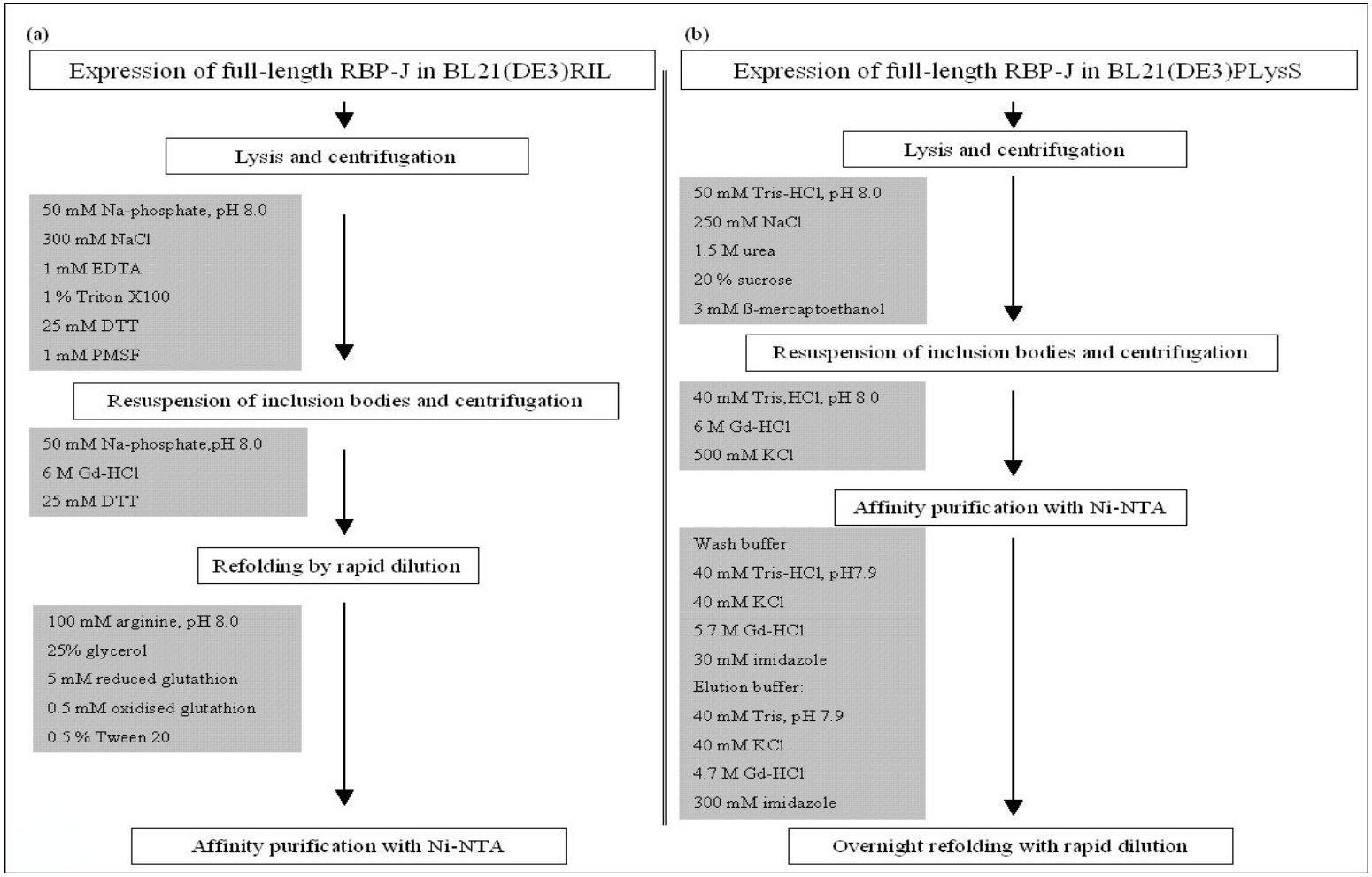

Figure 2.3: Flow charts of refolding procedures based on rapid dilution. **(a)** Standard refolding protocol and **(b)** adapted refolding protocol.

	1	**2**	**3**	**4**
Tris-HCl, pH 7.5	50 mM Tris	50 mM Tris 250 mM Gd-HCl 250 mM L-Arginine 150 mM NaCl 0.5% Glycine	50 mM Tris 500 mM Gd-HCl 500 mM L-Arginine 200 mM NaCl 1% Glycine	50 mM Tris 1 M Gd-HCl 1 M L-Arginine 300 mM NaCl 2% Glycine
	5	**6**	**7**	**8**
Tris-HCl, pH 8.0	50 mM Tris 0 mM Gd-HCl 250 mM L-Arginine 200 mM NaCl 2% Glycine	50 mM Tris 250 mM Gd-HCl 0 mM L-Arginine 300 mM NaCl 1% Glycine	50 mM Tris 500 mM Gd-HCl 1000 mM L-Arginine 0 mM NaCl 0.5% Glycine	50 mM Tris 1000 mM Gd-HCl 500 mM L-Arginine 150 mM NaCl 0% Glycine
	9	**10**	**11**	**12**
Tris-HCl, pH 8.5	50 mM Tris 0 mM Gd-HCl 500 mM L-Arginine 300 mM NaCl 0.5% Glycine	50 mM Tris 250 mM Gd-HCl 1000 mM L-Arginine 200 mM NaCl 5% Glycine	50 mM Tris 500 mM Gd-HCl 0 mM L-Arginine 150 mM NaCl 2% Glycine	50 mM Tris 1000 mM Gd-HCl 250 mM L-Arginine 0 mM NaCl 1% Glycine
	13	**14**	**15**	**16**
Tris-HCl, pH 9.0	50 mM Tris 0 mM Gd-HCl 1000 mM L-Arginine 150 mM NaCl 1% Glycine	50 mM Tris 250 mM Gd-HCl 500 mM L-Arginine 0 mM NaCl 2% Glycine	50 mM Tris 500 mM Gd-HCl 250 mM L-Arginine 300 mM NaCl 0% Glycine	50 mM Tris 1000 mM Gd-HCl 0 mM L-Arginine 200 mM NaCl 0.5% Glycine

Table 2.4: Refolding screen consisting of 16 conditions. Conditions differ by the concentration of guanidine-HCl, NaCl, L-arginine and glycine. The most suitable condition for refolding combines the lowest concentration of denaturing agents with the best soluble:insoluble protein ratio.

Proteins expressed in insect cells

Overexpression of proteins

SFplus cells grown in suspension were cultivated until their density reached $2x10^6$ cells/ml. 4 ml of P2 virus supernatant were added to infect the cells. Depending on their appearance the cells were harvested 48 to 72 hours after infection. After centrifugation at 1000 g at 4 ºC for 15 minutes the pellet was washed with ice-cold PBS and centrifuged again. It was frozen and stored at -20 ºC until needed.

Purification of overexpressed proteins

A cell pellet from 300 ml of cell culture was thawed on ice. After resuspension in LBI buffer the solution was sonicated with probe TT34 of the generator HD2200 (Bandelin electronic, Berlin, DE) for 2 minutes with 30% total sonication time and 50% maximum energy output until no more intact cells were visible under the microscope and centrifuged at 20 krpm (rotor SS34, Sorvall, Langenselbold, DE) for 40 minutes at 4 ºC. The supernatant was passed through a 45 µm filter and applied to 3.5 ml Ni-NTA beads pre-equilibrated with LBI buffer. The mixture of lysate and beads were gently mixed at 4 ºC for 1 hour and then applied to an empty Biorad column (Hercules, CA), where the lysate flowed through whereas the Ni-beads were assembled to form a column. The beads were washed with 5 column volumes of LII buffer (low imidazole wash), 5 column volumes of buffer HSI (high salt wash) and another 5 column volumes of LII buffer. The protein bound to the Ni-NTA beads was eluted with EI buffer. 2 ml fractions were collected and analysed by SDS-PAGE. The fractions containing the desired protein were pooled, TCEP added to a final concentration of 2 mM, the protein concentration determined and the sample flash frozen in liquid nitrogen before storage at -80°C.

Buffer LBI: 50 mM Tris-HCl,pH 8.0; 300 mM NaCl; 5 % glycerol; 2.5 mM MgCl2; 1mM ß-Mercaptoethanol; 1 µg/ml DNase, Complete mini EDTA free protease inhibitor cocktail according to manufacturer's instructions

Buffer LII: Buffer LBI + 5 mM imidazole

Buffer HSI: Buffer LBI + 500 mM NaCl

Buffer EI: Buffer LBI + 400 mM imidazole

Preparation of nuclear extracts

50 ml of DG75 cell culture were centrifuged at 300g at 4 ºC and washed with 5 ml cold PBS. After another centrifugation step as above the cells were resuspended in 3-4 pellet volumes (usually about 300 µl) of buffer A and kept on ice for 60 minutes to make the cells swell. The mixture was subsequently homogenized using a DOUNCE-homogenizer (Wheaton). The suspension was centrifuged for 10 seconds at 16100 g and the pellet was washed with 300 µl buffer A without resuspending it, followed by resuspension in 300 µl buffer B. The mix was kept on ice for 30 minutes, vortexed and centrifuged at 4 ºC for 20 minutes at 16100 g. The protein concentration of the supernatant and of the nuclear extract was determined and aliquots were shock frozen in liquid nitrogen.

Buffer A: 10 mM HEPES, pH 7.9; 10 mM KCl; 1.5 mM $MgCl_2$, prior to use add 5 mM DTT and 5mM Pefabloc (Pentapharma, Basel, CH)

Buffer B: 20 mM HEPES, pH 7,9; 25% glycerol; 420 mM NaCl, 1.5 mM $MgCl_2$; 0.8 mM EDTA; prior to use add 5 mM DTT and 5 mM Pefabloc (Pentapharma, Basel, CH).

2.2.6 Isothermal titration calorimetry (ITC)

Introduction

Isothermal titration calorimetry is used to study interactions between molecules (reviewed in (Pierce et al., 1999)). These can be protein-ligand (e.g. peptides or DNA) interactions as well as protein-protein interactions. Not only can the overall binding of two molecules easily be detected, but the stoichiometry n, the binding affinity (K_a) and the enthalpy (ΔH) and entropy (ΔS) changes of a given reaction can also be determined in a straightforward manner. The total concentration of all but one of the reactants remains constant throughout the experiment. Non-linear least square fitting of the calorimetric data from a single experiment, where heat is the only dependent variable, allows an estimation of the thermodynamic parameters. The method has many advantages, when compared to others such as surface plasmon resonance (SPR) or analytical ultracentrifugation. For SPR the protein must be attached to a surface, which depending on the binding site on the protein could potentially interfere with the binding of the ligand or interacting protein. In the case of ultracentrifugation pressure may interfere with the equilibrium.

Whereas other methods only give mostly qualitative evidence of binding, ITC allows one to separate the enthalpic and entropic contributions to the binding affinity.

The ITC device consists of two identical cells located inside an adiabatic jacket. The reference cell is kept at constant temperature (Figure 2.4). During the measurement the temperature difference between the two cells is measured and a cell feedback (CFB) or differential power is applied to maintain them at the same temperature. An endothermic reaction causes a positive feedback, because heat must be supplied to the sample cell to keep its initial temperature, whereas an exothermic reaction results in a negative feedback, because heat must be extracted to lower the temperature to its initial value.

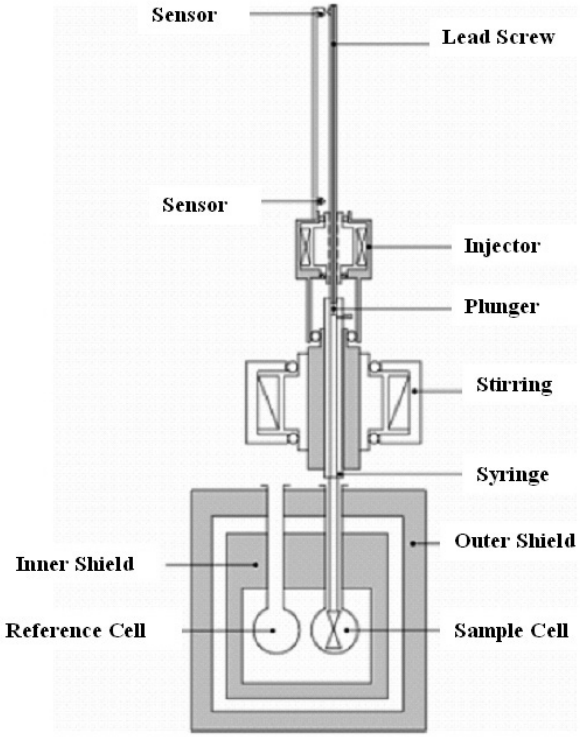

Figure 2.4: Schematic view of the VP-ITC device (Microcal, USA) taken from the VP-ITC manual.

The feedback system is usually based on a Peltier element, where the heat Q, which is absorbed or dissipated during a time t, depending on the direction of the current is proportional to the current (I):

$$Q = P \cdot I \cdot t$$

where P is the Peltier factor, which depends on the materials used in the element. Unlike the Joule effect, which is proportional to the square of the current

$$Q = R \cdot I^2 \cdot t$$

(R: resistance), the Peltier effect is proportional to the current and changes sign (-/+) when the current changes direction.

During the ITC measurement small volumes of the ligand are injected into a large volume of the protein solution at time intervals allowing the solution to reach equilibrium.

The entropy of the reaction (ΔS) and the Gibbs free energy (ΔG) can be calculated using Gibbs equation:

$$\Delta G = -RT\,lnK = \Delta H - T\Delta S$$

As the reaction is done a constant pressure $\Delta H = Q$, where Q is the total heat absorbed or dissipated during the reaction.

In addition it is possible to determine the heat capacity of binding at constant pressure (ΔC_p) from two ITC measurements carried out at different temperatures:

$$\Delta C_p = \frac{\Delta H_{T_2} - \Delta H_{T_1}}{T_2 - T_1}$$

with $T_1 < T_2$.

This parameter is a good indicator of changes in hydrophobic interactions. The value is negative if hydrophobic contacts are formed and positive if they are broken.

Beside hydrophobic interactions, protonation plays a role in molecular interactions. It can be characterized to some extent by carrying out the experiment with buffers having different enthalpies of ionisation. A less exothermic ΔH in a buffer displaying a higher heat of ionisation than in a buffer with a lower heat of ionisation indicates that protons are taken up as sample and ligand interact.

ITC is used to measure the heat evolved or absorbed when e.g. a protein and a ligand are mixed. In general, the ligand, which has about ten-fold higher concentration than the protein is titrated in small volumes into a large volume of protein solution. The method is non-destructive so that the protein and the ligand can be recovered after the measurement.

The time integral of the measured CFB is a direct measurement of the heat absorbed or dissipated which is directly proportional to the extent of binding.

The binding reaction corresponds to an equilibrium:

$$M_1 + M_2 \rightleftharpoons M_1M_2$$

where M_1 and M_2 represent the macromolecule and its ligand. The strength of the interaction is described by the association (K_a) or dissociation constant (K_d):

$$K_a = \frac{[M_1M_2]}{[M_1][M_2]} = \frac{1}{K_d}$$

where $[M_1]$ and $[M_2]$ are the concentrations of each molecule and $[M_1M_2]$ that of the complex. These constants are related to the Gibbs free energy of association ΔG_a and dissociation ΔG_d ($=-\Delta G_a$), respectively. They can be expressed in terms of the corresponding change of enthalpy (ΔH) and entropy (ΔS) during the reaction:

$$\Delta G_a = -RT \ln K_a = \Delta H_a - T\Delta S_a$$
$$\Delta G_d = -RT \ln K_d = \Delta H_d - T\Delta S_d$$

where R is the gas constant (1.9872 $kcalK^{-1}Mol^{-1}$) and T the absolute temperature.

The sequence of injections is continued until the heat change is zero or remains constant at a very low level, which may be due to dilution effects. This means that the protein molecule is saturated with ligand and the concentration of complex has reached its maximum.

Prerequisites

ITC experiments require large amounts and volumes of sample. The MicroCal VP-ITC device (MicroCal LLC, Northampton, MA, USA) requires 1.6 ml of protein solution with a concentration of 10-100 µM and 300 µl ligand solution with a concentration of 100 to 1000 µM. Both concentrations must be exactly known. All solutions should be degassed and made with identical buffers as differences in buffer composition and pH may give large heat changes and lead to spurious results.

Controls

To test the sensitivity and accuracy of the VP-ITC device two kinds of control runs were carried out:

Methanol run to test sensitivity

The cell is filled with degassed water, the syringe with a 2.5% methanol/water solution. The experimental parameters of the run are provided by the manufacturer and stored in the computer. The only detectable signal should be the heat dissipated when methanol is diluted into water. Since the concentration of methanol in the cell increases with every injection, this heat should decrease after each injection. Typical results obtained in methanol runs are shown in Figure 2.5.

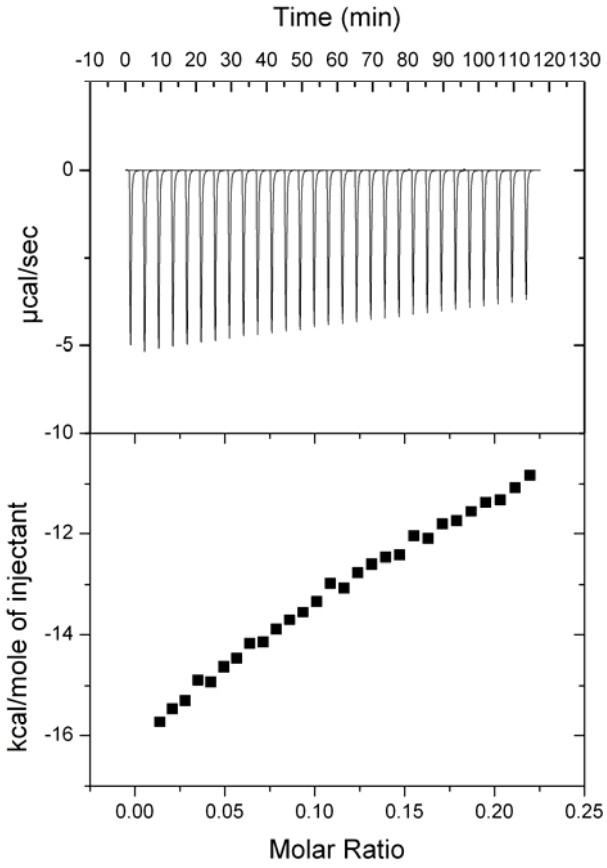

Figure 2.5: Exemplary data set of a methanol run.

Rnase-2'CMP Experiment

2'CMP solution (ca. 2.0 – 2.2 mM): 10 mg 2'CMP were dissolved in 5.5 ml 50 mM potassium acetate solution, followed by addition of another 5.5 ml potassium acetate buffer, pH 5.5. The pH was adjusted to 5.5 with 50 mM acetic acid. The concentration of 2'CMP was determined by absorption at 260 nm after 20-fold dilution of the solution in 0.2 M Tris-HCL, pH 7.0, using an extinction coefficient of 7400 cm^{-1} M^{-1} (c=A/(7400 x l)).

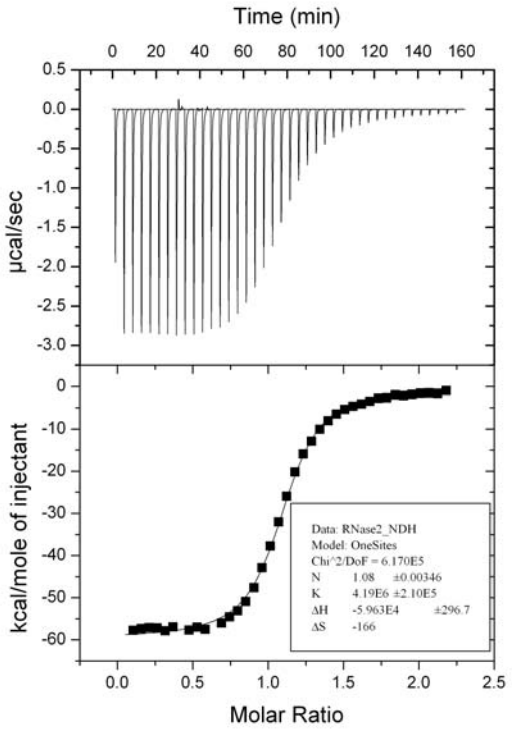

Figure 2.6: Exemplary data set of an RNase-2'CMP run

RNase solution (ca. 0.06 mM): 20 mg RNase A were dissolved in 20 ml potassium acetate buffer, pH 5.5. The solution was dialyzed against two changes of 500 ml potassium acetate buffer at 4 ˚C for three hours per change (dialysis tubing: Spectra/Por, cut-off 6-8000, Sigma). The concentration is determined spectrophotometrically using an extinction coefficient of 9800 cm^{-1} M^{-1} at 280 nm (c=A/(9800 x l); c: concentration, A: absorbance at 280 nm; l: pathlength in cm).

The experimental parameters are provided by the manufacturer and stored in the computer. Figure 2.6 displays the results obtained with the RNase-2'CMP run. The sigmoidal binding curve derived from the set of ligand injections indicates the saturation of the available binding sites upon addition of more ligand. The binding constant can be calculated from the slope of the curve combined with the concentrations of the components.

Experiment

RBP-Jκ protein in complex with DNA (16 to 20 bp) was concentrated to about 22 to 35 µM. Protein solution (1.8 ml) was filled into the sample cell, which had been cleaned and flushed with the appropriate buffer. The ligand solution, which had a concentration between 250 µM and 0.5 mM, was filled into the syringe according to the manufacturer's

instructions. The syringe was assembled into the sample cell. The experimental conditions (temperature of the cell: 15 to 30 °C, desired number of injections, stirring speed: 290 rpm, injection parameters: filter period 2 s, duration 2.4 s and equilibration options: Fast Equilibration, Auto) were set on the user interface provided by the manufacturer. A sequence of 50 to 70 injections of 3 to 6 µl separated by 300-second intervals to allow equilibration was used to determine the binding curve. Figure 2.7 displays exemplary datasets of experiments carried out with an nRBP$^{full\text{-}length}$-J-DNA binary complex and Notch^{Ram} **(a)** and Notch^{RamANK} **(b)** as ligand.

The ability of the components to form complexes was tested with non-radioactive EMSA before and after the experiment.

Evaluation

The recorded data was evaluated using the program ORIGIN, adjusted to the needs of microcalorimetry and provided by the manufacturer. ORIGIN uses the measured concentrations of protein and ligand to calculate the binding constants, the enthalpy and entropy changes and the stoichiometry of the reaction. The results are visualised on a graph depicting the reaction curve and a table displaying the calculated values.

The differential power or heat flow, which had to be applied to or extracted from the sample cell during each injection, compared to the power applied to the reference cell is measured and displayed in µcal/s. Given the information on the concentration of both reactants and the injection volume, the ORIGIN program calculates the enthalpy ΔH from the changes in the differential power after each injection and displays it as kcal/M of injectant in a graph containing the integrated data from all injections.

The heat measured is determined by integrating the current in the Peltier element over time

$$q_i = \int_{t_i}^{t_i+1} PIdt$$

The heat associated with the change of state after each injection (q_i) is proportional to the increment in the concentration of the complex after injection in the calorimetric cell, which has a volume V, $[M_1M_2]$ is the concentration of complex and ΔH the enthalpy of binding:

$$q_i = V\Delta H([M_1M_2]_i - [M_1M_2]_{i-1}$$

A general model of binding including multiple, noninteracting binding sites quantifies cumulative heat of binding with:

$$Q = \frac{V_0[M]_t \sum (n_i \Delta H_i K_{ai}[L])}{1 + K_{ai[L]}}$$

with V_0 being the volume of the cell, ΔH_i the enthalpy change at each injection and $[M]_t$ is the total macromolecule concentration including bound and free fractions, K_a is the binding constant and [L] is the free ligand concentration.

Before normalizing the heat of binding to the ligand concentration, a volume correction is made to account for dilution of the macromolecule at each injection. The baseline is subtracted and the area under the peak is integrated.

To determine n, K_a and ΔH_b as the enthalpy of binding per mole of ligand the above equation is represented in terms of the binding constant and total ligand concentration $[L]_t$ to obtain the quadratic

$$Q = \frac{n[M]_t \Delta H V_0}{2} \left\{ 1 + \frac{[L]_t}{n[M]_t} + \frac{1}{nK_a[M]_t} - \left[(+\frac{[L]_t}{n[M]_t} + \frac{1}{nK_a[M]_t})^2 - 4\frac{[L]_t}{n[M]_t} \right]^{\frac{1}{2}} \right\}$$

The n, K_a and ΔH_b parameters are then optimised with the routines provided in the ORIGIN software.

As the reaction takes place at constant pressure and temperature the entropy change in the system can be calculated from the enthalpy change

$$\Delta S = -\frac{\Delta H}{T}$$

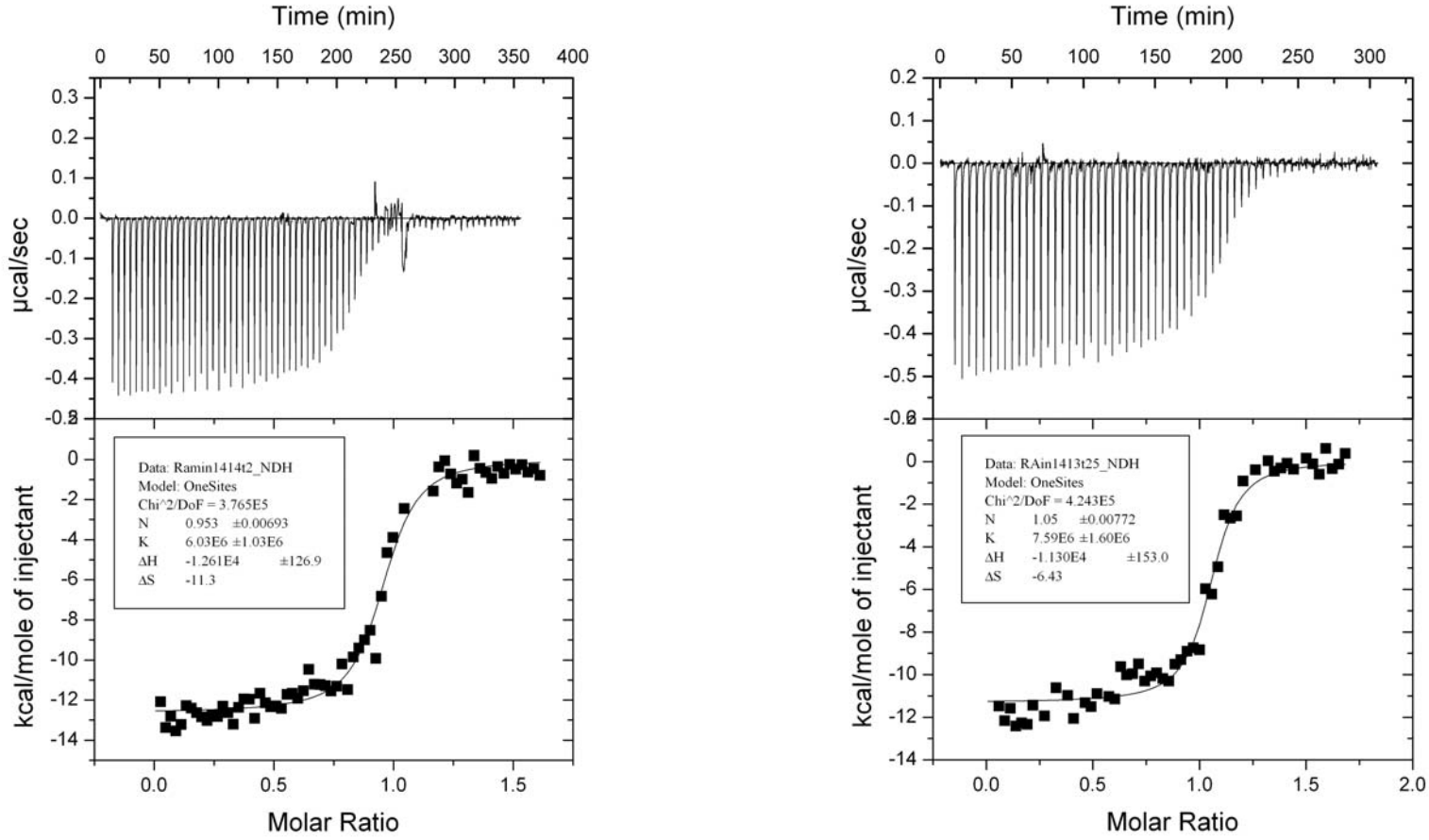

Figure 2.7: Exemplary datasets of unprocessed (top) and processed data (bottom) of experiments carried out with an RBP-Jκ-DNA binary complex and Notch^{Ram} (left panel) and Notch^{RamANK} (right panel) as ligand.

2.2.7 Small angle X-ray scattering (SAXS)

Introduction

Small angle X-ray scattering experiments allow one to obtain low resolution (1-100 nm) structural information on proteins and their complexes in solution, as well as on microemulsions or polymers. For monodisperse solutions the method can provide information on the shape and size of macromolecules or oligomers.

Experimental setup

The basic experimental setup is illustrated in Figure 2.8. An X-ray beam generated by a generator or a synchrotron source is diffracted by a monochromator to select an appropriate wavelength band and may be focussed on the detector using mirrors. The sample is usually contained in a cell with mica windows or in a capillary. The small angle scattering (scattering angle $2\theta < 10$ degrees) is transmitted through a vacuum flight path to a detector. The distance between sample and detector can be varied depending on the required angular range.

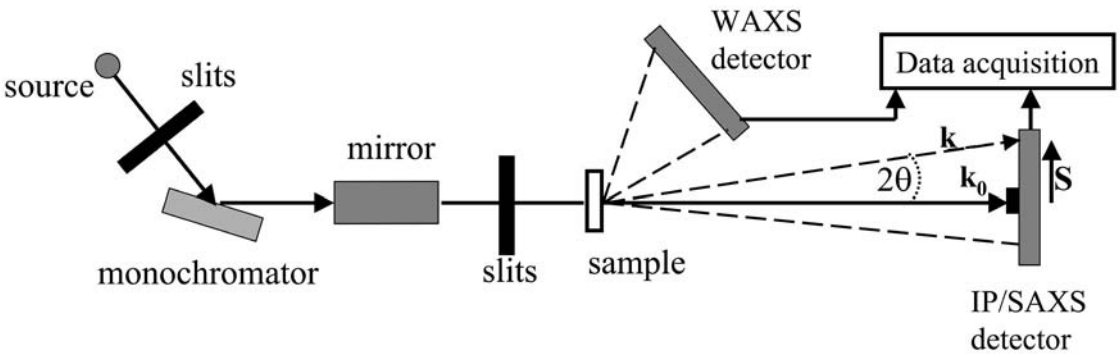

Figure 2.8: Basic layout of a small angle X-ray scattering (SAXS) instrument. The detector used in our measurements was an imaging plate (IP).

The scattering process

The incident X-rays, which are characterised by the wave-vector k_0 and the wavelength, $\lambda = \frac{2\pi}{|k_0|}$ hit the sample and are scattered at angles 2θ corresponding to a wave-vector k.

The momentum transfer S (often also referred to as Q, in the literature) is defined by the difference of the wave vectors:

$$\left|\vec{S}\right| = \left|\vec{k} - \vec{k}_0\right| = \frac{4\pi}{\lambda}\sin\theta$$

The differential scattering cross-section dσ/dΩ of the sample in a given direction is the ratio between the energy scattered per unit solid angle dΩ and unit time and the intensity (energy per unit area and time) of the incident radiation.

The experiment results in a plot of the differential scattering cross-section as a function of momentum transfer S or scattering angle 2θ.

Monodisperse solutions of proteins are composed of isolated particles with a volume V_P which can be represented by an assembly of atoms (or scattering centres) at distances $\vec{r}_i$ from the origin. Waves with a mean amplitude b_i originate from the scattering centres and interfere. Depending on the phase difference, $\vec{S}\cdot\vec{r}_i$, constructive or destructive interference occurs. The detector records the intensity, which is related to the differential scattering cross-section:

$$\left(\frac{d\sigma}{d\Omega}\right) = N_P \cdot \left|\sum_i \overline{b}_i \cdot e^{i\vec{S}\vec{r}}\right|^2 = N_P K^2 \cdot P(S) \cdot SF(S)$$

where N_P is the number density of molecules in the sample, K the contrast factor corresponding to the difference between the average electron density of the solute and of the solvent. P(S) is the formfactor of the molecules and SF(S) the structure factor of the solution, which reflects the arrangement of the molecules relative to each other. For ideal monodisperse solutions (i.e. with negligible intermolecular interactions) this function is uniformly equal to one.

Fourier transformation of the intensity yields the distance distribution function p(r),

$$p(r) = \frac{r^2}{2\pi}\int_0^\infty \left(\frac{d\sigma}{d\Omega}\right)\cdot S^2 \cdot \frac{\sin(Sr)}{Sr} dS$$

To extract the shape of the molecules from the measured differential scattering cross-section indirect methods have to be used because of the spherical averaging in solution and

the loss of phase information due to the fact that only intensities rather than amplitudes and phases are measured.

For monodisperse solutions the molecular mass and radius of gyration can easily be obtained from a plot of the logarithm of the intensity vs S^2. Indeed, as shown by Guinier (see e.g. (Guinier, 1939)) the scattering at small angles can be approximated by:

$$I(s) = I(0)\exp(-Rg^2S^2/3)$$

By linear extrapolation to zero angle a plot of I(S) vs S^2 will thus yield I(0), the forward scattering which is proportional to the molecular mass of the solute, and its slope gives the radius of gyration Rg, which is a measure for the extension of a molecule. It is defined by:

$$R_g^2 = \frac{\int_0^\infty p(r) \cdot r^2 dr}{2\int_0^\infty p(r) dr}$$

Experiment

After purification, the sample was concentrated, centrifuged in an Airfuge (Beckman Coulter, Krefeld, DE) at about 30 krpm for 20 minutes and the concentration was determined spectrophotometrically. 70 µl of sample, needed for each measurement, were carefully filled into a cell with mica windows to avoid air bubbles. Each measurement of a protein sample was bracketed by two buffer measurements. The data were recorded on the double focusing beamline X33 using an imaging plate scanner (mar345 Image Plate Detector; Marresearch GmbH, Norderstedt, DE). Each sample was exposed to X-rays for three minutes in the 64-bunch mode of the DORIS III storage ring.

Evaluation

Data processing

Recorded data were normalised to incident beam intensity, corrected for detector response, buffer background subtracted, scaled to protein concentration and extrapolated to infinite dilution following standard procedures implemented in the program PRIMUS (Konarev et al., 2003).

Porod analysis (Porod, 1982) was used to estimate the excluded particle volume and the radius of gyration R_g of the solute was evaluated using the Guinier approximation (see e.g. (Koch et al., 2003)) and the indirect transform program GNOM (Svergun, 1992).

Model building

Low-resolution models of the binary RBP-Jκ-DNA and the ternary RBP-Jκ-DNA-Notch^{RamANK} complex were built *ab initio* from the X-ray scattering data using the program DAMMIN (Svergun, 1999). This program initially represents the protein-DNA or protein-protein-DNA complex as a collection of dummy atoms (DA) and builds a chain-compatible spatial distribution of these DAs into the search volume, by simulated annealing. When the number of residues is known, DAMMIN can fit the scattering data to 10 to 15Å resolution.

Model evaluation

A model for the DNA-RBP-Jκ binary complex was created starting from the Lag-1-DNA binary complex structure. The program BUNCH (Petoukhov and Svergun, 2005) was used to preliminarily check whether addition of the missing portions at the N- and the C-terminus of the protein, compared to the Lag-1 structure, led to a theoretical scattering curve, which could be fitted to the experimental scattering curve.

After confirmation five bodies were created, corresponding to the binary complex, the two segments added at the N- and the C-terminus, the Notch^{Ram} domain and the Notch-ANK domain. The body corresponding to ANK was built with a merged PDB-file created from the recently solved structure of the six ankyrin repeats of hNotch1 (Ehebauer et al., 2005) extended with another repeat to create the seven repeats contained in Notch_IC. For the body corresponding to Notch^{Ram} a dummy molecule of the same size as the Ram domain with preferably α-helical structure was taken.

Of the two models taken into account one assumed a participation of the ankyrin repeats in the binding, the other did not. Both, however, included the available information about the interaction of RBP-Jκ with Ram.

The program SASREF (Petoukhov and Svergun, 2005) combined the bodies to obtain a model of the binary and ternary complexes whose theoretical scattering curves fitted the experimental data for both complexes, with any given restraint, e.g. the necessity for certain amino acids to interact. The chi-value, calculated for each dataset, serves as

indicator of the quality of the fit and represents the level of confidence with which two data sets are correlated. It is calculated as:

$$\chi^2 = \frac{1}{n-1}\sum_{j=1}^{n}\left[\frac{\langle c(s)\rangle I_{DR}(s_j) - cI_{\exp}(s_j)}{\sigma(s_j)}\right]^2$$

where I_{exp} is the experimental intensity specified at n points s_j, j=1, …n, $\sigma(s_j)$ is the corresponding standard deviation, and c is a scaling coefficient.

2.2.8 Circular dichroism (CD)

Introduction

Circular dichroism is based on the interaction of optically active substances with circularly polarized light, whereby the refractive index and absorption coefficients depend on the polarization (left or right).

Optical activity results from structural asymmetry (enantiomorphism) in molecules resulting in different molar extinction coefficients for left and right circularly polarized light. The measurement yields the difference between the two:

$$\Delta\varepsilon = \varepsilon_L - \varepsilon_R$$

displayed as ellipticity θ

$$\theta(\lambda) = const.(\varepsilon_L - \varepsilon_R)\cdot c \cdot d$$

where d is the thickness of the cuvette and c the sample concentration. The CD spectrum thus represents the ellipticity θ as a function of the wavelength λ.

CD spectroscopy can be used to determine whether a protein is folded and if so which secondary structure elements are present. Good CD measurements give ratios of secondary structure elements, which are 95% reliable.

The useful range for conventional CD measurements extends from 190 to 250 nm (far UV range). Within this range the peptide bonds in a protein act as chromophores, where $n \rightarrow \pi^*$ and the $\pi \rightarrow \pi^*$ transitions take place and a signal can be detected if there is a regular, folded environment. The region below 190 nm to about 160 nm (vacuum UV range) provides further information but the requirements regarding sample buffer and concentration and intensity of the light source are considerably higher and the measurements can only be performed on a synchrotron radiation source.

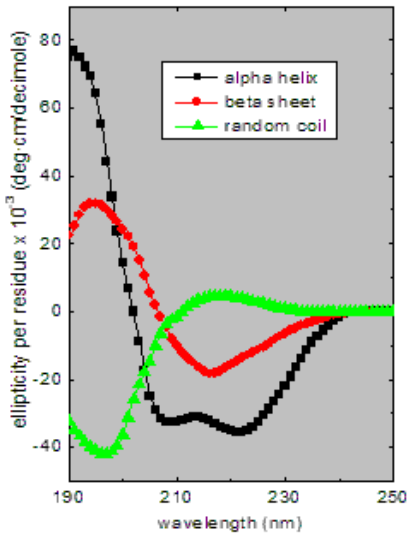

Figure 2.9: Characteristic spectra of secondary structure elements (taken from www. AP lab.com/circular_dichroism.htm)

Spectra of proteins or peptides consisting of a single type of secondary structure element (α-helix, β-sheet, random coil) are displayed in Figure 2.9. To evaluate the secondary structure of a protein a linear combination of spectra of the three structural elements is fitted to its CD spectrum, which yields the ratio of the contributions of the different secondary structure elements.

Experiment

Conventional CD experiments were carried out on a J-810 spectropolarimeter (Jasco GmbH, Gross-Umstadt, DE). Samples were dialysed overnight against 10 mM Tris, pH 8 and concentrated to 22 µM for protein complexes and 50 µM for Notch^{RamANK}. Spectra were recorded between 160 and 230 nm at 4 ºC in 0.5 nm steps with 1 second integration time in a 1 mm quartz cuvette. After subtraction of the buffer background and the DNA signal the data were scaled to molar ellipticity using the equation:

$$[\theta] = \frac{100(signal)}{Cnl}\left[\frac{\deg \cdot cm^2}{dmol}\right]$$

with [θ] = mean residue ellipticity in deg cm² dmol-1
signal = unprocessed output in mdeg
C = protein concentration in mM
n = number of amino acids
l = cell pathlength in cm

Secondary structure content and ratios were calculated using the software of the spectropolarimeter.

SRCD spectra were recorded at beamline CD12 of the CLRC Daresbury Laboratory's Synchrotron Radiation Source (Clarke and Jones, 2004). Prior to measuring protein spectra, a (+)-10-camphosulphonic acid (CSA) spectrum was measured for ellipticity calibration (Woody, 1995). CSA was used at 1mg/ml in a 0.1mm quartz cuvette (Hellma, Müllheim, DE).

Before the measurement RBP-Jκ was dialysed against 10 mM Tris, pH 8 and 300 mM NaBr, which gives a lower absorption signal than NaCl. RBP-Jκ in complex with DNA was dialysed against 10 mM Tris, pH 8. Both samples were concentrated to the maximum possible. About 30µl of sample were needed to fill a 0.1 mm path-length quartz cuvette. For samples with lower concentrations a 0.2 mm cuvette was used. Spectra were measured over the range of 170 nm to 250 nm, with 1 nm and 0.5 nm intervals, respectively, and 1 second integration time. No radiation damage due to the high photon flux at the beamline could be detected after several measurements with the same sample. The spectra were corrected for buffer background and DNA signal and scaled against the CSA ellipticity calibration and converted to molar ellipticity (in deg cm^2 $dmol^{-1}$).

Data analysis

A modified version of the program SELCON (Sreerama & Woody, 1993; Clarke & Jones, 1999) was used to determine the secondary structure content using the data range from 180 to 230 nm. SELCON uses a singular value decomposition algorithm to assign secondary structure by comparison with a basis set of spectra from proteins of known structure, repeated iteratively to self-consistency.

The original version of the other program used, CONTIN, implemented the ridge regression algorithm of Provencher & Glockner, 1981 (Provencher and Glockner, 1981). The latest version incorporates the locally linearised model (Van Stokkum et al., 1990) in selecting basis set proteins from the reference database.

3 Results

3.1 Expression and purification of human RBP-Jκ, Notch1 and EBNA2 constructs

3.1.1 Expression and purification of full-length human RBP-Jκ and RBP-Jκ fragments

3.1.1.1 *E. coli* as expression host for RBP-Jκ and truncation constructs

E. coli is presently the most frequently used expression host because it is easy to handle and yields high amounts of protein. One major drawback is, however, that the overexpressed recombinant proteins are often insoluble or non-functional. Since such difficulties are not predictable and can in many cases be overcome *E. coli* remains the expression system of first choice.

Individual proteins require different expression conditions. Whereas some can be expressed in E. coli in soluble and functional form using a standard protocol others require different conditions, subcloning to different expression vectors or expression in a different expression host than E. coli.

In this work the priority was to express full-length functional RBP-Jκ in E. coli with sufficient yield to carry out crystallization studies.

Expression in soluble form can be promoted by changing expression conditions, e. g. parameters such as temperature, concentration of inducing agent, buffer added to the LB medium (for a more detailed overview see table 2.1). When this fails one can try to express a truncated form of the protein and optimize the conditions as above. If necessary, one may try to solubilize the expressed protein in different buffers.

3.1.1.2 Purification of full-length RBP-Jκ

The plasmids pVK60 and pVK91 (section 2.1.3), comprising full-length RBP-Jκ cloned into pETM11 (N-terminal 6xHis-tag) and pETM30 (N-terminal 6xHis-tag and GST-tag) were kindly provided by Bettina Kempkes at GSF in Munich. Initial expression of the VK60 and VK91 proteins was carried out as described in section 2.2.5. Figure 3.1 illustrates the generally high levels of expression obtained with His-and GST-tagged full-length RBP-Jκ. Besides facilitating purification an N-terminal GST-tag fused to the protein of interest, as the case in VK91, promotes its solubility. The solubility of both VK60 and

VK91 could neither be increased by changing expression parameters (tables 2.1 and table 2.2) nor by using different buffers during the biological pulping of the bacterial cells (table 2.3), so that different approaches such as refolding or expression of truncated RBP-Jκ proteins were used to obtain sufficient amounts of functional protein. Unless indicated otherwise, further efforts to promote soluble expression or solubility studies concentrated on VK60, since both the His-tagged and the His-GST-tagged proteins were expressed as inclusion bodies and were thus insoluble.

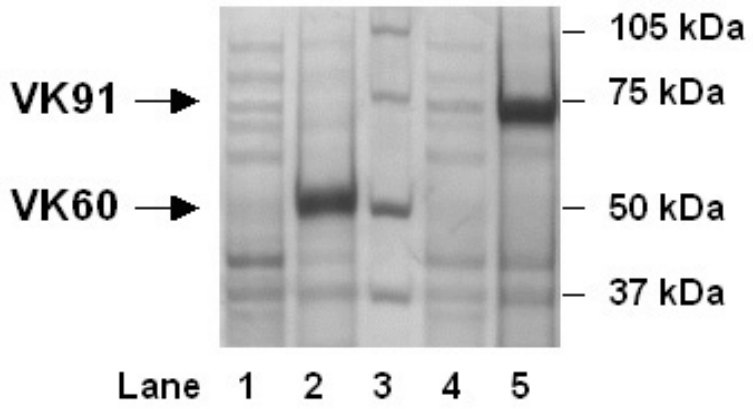

Figure 3.1: Analysis of the induction of full-length RBP-Jκ fused to a 6xHis-tag (VK60) and a GST-tag (VK91). The expression pattern before induction (lanes 1 and 4) is compared to that 2 hrs after induction with 1 mM IPTG (lanes 2 and 5). Lane 3: Protein marker (Biorad).

Purification of soluble VK60

Independently of the expression host and growing conditions, both RBP-Jκ fused to a His-tag and to a GST-tag and all deletion mutants listed in table 3.1 expressed into inclusion bodies. Despite extensive solubility studies the yield never exceeded 5% of the total amount of overexpressed recombinant protein. A small amount of protein could finally be purified using a lysis buffer containing 1.6 M urea and 20 % sucrose. Urea at concentrations of 1.6 M does not completely denature proteins but promotes solubilization, whereas sucrose stabilises the solubilized protein. The small amount of protein recovered after affinity purification did not suffice, however, for crystallization trials nor DNA binding studies. It was used to form a binary complex to compare its DNA-binding properties to those of RBP-Jκ expressed in insect cells. Since no substantial differences were observed during the purification process of His-tagged and GST-tagged RBP-Jκ further effort was focused on the His-tagged protein (VK60) and its truncated versions.

Purification of VK60 under denaturing conditions followed by refolding

To find a suitable refolding buffer a refolding screen was used as shown in Figure 2.3(b). The full-length His-tagged protein was affinity-purified before refolding. Following the procedure described in Materials and Methods (section 2.2.4) large amounts of pure protein could be obtained as illustrated in Figure 3.2. Using the *E. coli* strain BL21(DE3)PlysS as expression host up to 120 mg of protein could be extracted from 1 l of cell culture.

The refolding screen consisted of the 16 conditions listed in table 2.4 in section 2.2.4 , which differ by their concentrations in guanidinium hydrochloride, salt, arginine and glycine. The aim was to find conditions where most of the protein would remain soluble after addition to the respective buffer and stirring overnight (app. 10 hrs) at 4 °C. The amount of guanidinium hydrochloride also had to be adjusted so that no or close to no denaturant was left in the final refolding solution.

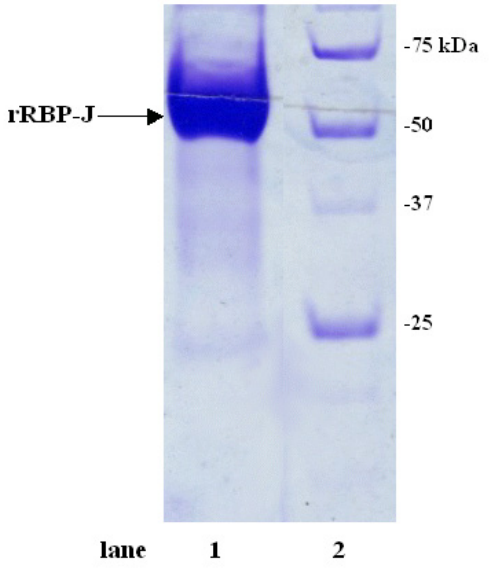

Figure 3.2: SDS PAGE analysis of the elution fraction of Ni-affinity purified VK60 (7.7 µg, lane 1), which was subsequently subjected to refolding. Lane 2: Protein marker (Biorad)

The samples corresponding to each of the different conditions were centrifuged after rapid dilution of the protein solution in the refolding buffer and overnight stirring. The pellets were resuspended in the same volume of 8 M urea as the original sample. Samples of the resuspended pellets and the supernatants were analysed by SDS-PAGE to estimate the ratio of soluble and insoluble protein after refolding. Figure 3.3 shows the results for the pellet fraction (right lane) and the supernatant (left lane) for each condition. Condition 13 (1M arginine, 150 mM NaCl and 1% glycine in Tris-HCl, pH 9.0) yielded the highest ratio of

soluble to insoluble protein for VK60 and all other insoluble RBP-Jκ truncations and at the same time corresponds like condition 1 to zero concentration of denaturant. Condition 13 was therefore used for all subsequent purifications of VK60 and insoluble RBP-Jκ truncations (refolded VK60 will from here on be referred to as $rRBP^{full\text{-}length}$).

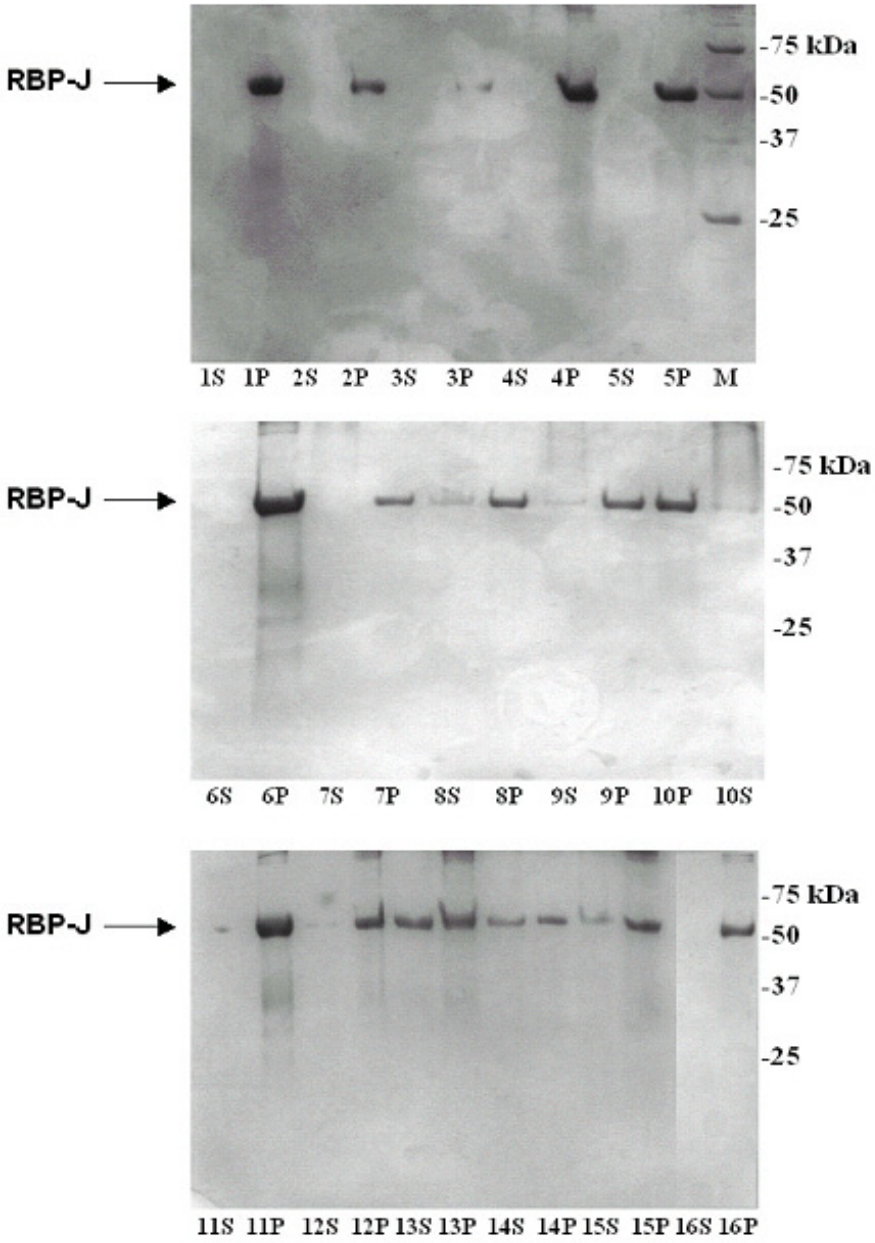

Figure 3.3: SDS PAGE analysis of the refolding screen consisting of 16 conditions with full-length RBP-Jκ (VK60) to find the optimal refolding condition by comparison of the highest soluble:insoluble protein ratio. In each case 15 µl of the soluble fraction and the pellet dissolved in the same volume as the soluble fraction were applied to allow comparison. The labels refer to the refolding conditions for the pellets (P) and the supernatants (S) preceded by the number of the corresponding condition. Of all suitable conditions, i. e. those containing the smallest amount of denaturing agents, condition 13 (50 mM Tris-HCl, pH 9.5, 1 M arginine, 150 mM NaCl, 1% glycine) gave the highest soluble:insoluble protein ratio for VK60.

The refolded protein could be shock frozen in liquid nitrogen and indefinitely stored at -80 degrees.

3.1.1.3 Truncation constructs

Truncation constructs were designed to promote solubility of the protein, based on the knowledge available at the time. The amount of soluble full-length protein obtained from natively purified RBP-Jκ did not suffice to carry out binding studies nor crystallisation trials. Table 3.1 lists all designed truncation constructs including their size and domains.

Truncation constructs comprising one or more known functional domains of RBP-Jκ

The constructs belonging to group 1 in table 3.1 (a) were based on the results of mutational analyses of RBP-Jκ (Chung et al., 1994) where the DNA binding ability of point mutants of the protein was analysed using electrophoretic mobility shift assays (EMSA). As a result of this study these constructs were no longer considered useful, because they did not include the complete DNA-binding domain.

Truncation constructs according to putative laternative starting points RBP-Jκ for translation

Additional methionines within the amino acid sequence may indicate the presence of alternative starting points for translation of the protein. Two such methionines were found in RBP-Jκ at positions 89 and 99. Truncated proteins expressed with these amino acids as starting points should still be able to bind DNA and Notch^{Ram} (Chung et al., 1994; Fuchs et al., 2001; Sakai et al., 1998). Figure 3.4 illustrates an initial solubility screen with both proteins showing their presence in the insoluble fraction.

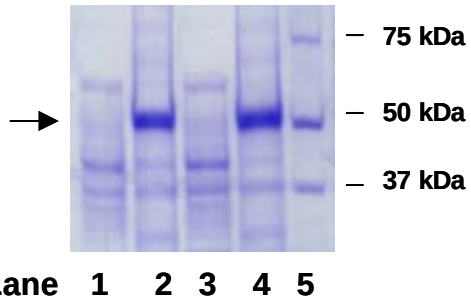

Figure 3.4: Analysis of the solubility of truncated RBP-Jκ proteins RBP63-487 (KH5, lanes 1 and 2) and RBP74-487 (KH6, lanes 3 and 4). Bacterial pellets of 1 ml of culture were lysed in 1 ml buffer and the solution was centrifuged. The resulting pellet was dissolved in 1 ml 8 M urea. 10 µl of the supernatant (lanes 1 and 3) and 10 µl of the dissolved insoluble portion (lanes 2 and 4) were analysed by SDS-PAGE. The arrow indicates differences in the soluble and insoluble fractions.

(a) Group 1

Protein	Molecular mass (kDa)	Number of amino acids	Amino acid range	Theoretical pI	Domains included
VK60	58	513	1-487	8.29	All
KH1	20	202	157-333	4.8	Ram binding DNA binding
KH2	10	114	100-188	9.9	SAB domain
KH3	20	209	165-348	4.7	Ram binding DNA binding
KH4	26	259	100-333	6.3	Ram binding DNA binding SAB domain

(b) Group 2

Protein	Molecular mass (kDa)	Number of amino acids	Range	Theoretical pI	Domains included
KH5	46	450	63-487	5.6	Ram binding DNA binding SAB domain
KH6	47	439	74-487	6.0	Ram binding DNA binding SAB domain

(c) Group 3

Protein	Molecular mass (kDa)	Number of amino acids	Range	Theoretical pI	Domains included
KH7	37	327	32-333	7.6	N-RHR linker
KH8	49	430	32-435	6.4	N-RHR linker C-RHR
KH9	35	304	157-435	5.5	C-RHR

(d) Group 4

Protein	Molecular mass (kDa)	Number of amino acids	Range	Theoretical pI	Domains included
KH12	50	466	12-452	8.3	All
KH13	46	429	28-431	6.7	All
KH14	46	433	28-435	6.4	All
KH15	48	450	28-452	7.1	All

Table 3.1: Truncated proteins designed based on information available at the time; the number of amino acids include 26 aa for the 6xHis-tag and a linker with a TEV cleavage site. **(a)** Designs according to mutational analysis; SAB: strong ANK binding **(b)** Constructs designed from putative alternative starting points of hRBP-Jκ translation starting at aa 64 and 74, respectively; **(c)** Designs assuming that RBP-Jκ belongs to the Rel familiy of transcription factors, which contain two domains (N-RHR and C-RHR) separated by an unusually long linker in the case of RBP-Jκ; **(d)** Constructs based on the alignment of primary structures of RBP-Jκ homologues from different species (see Figure 3.5); constructs which did not express in *E. coli* or did not bind DNA are not listed.

Neither of the constructs described as group 2 in table 3.1 formed binary complexes with oligonucleotides derived from Cp (for an example see Figure 3.8, lanes 6 and 7).

Truncation constructs designed assuming that RBP-Jκ is a member of the familiy of Rel-transcription factors

Using bioinformatical methods (a combination of sequence alignment with CLUSTALW and secondary structure prediction with PHD with the fold recognition program 3D-PSSM (Fischer et al., 1999; Kelley et al., 2000) it was discovered that RBP-Jκ belongs to the family of Rel transcription factors (Nam et al., 2003). These proteins consist of two domains called N-RHR (**R**el **H**omology **R**egion) and C-RHR, which are connected by a short linker. In the case of RBP-Jκ the linker consists of 125 aa and is thus unusually long. The design of the three truncations of group 3 in table 3.1(c) was based on this information. None of the three truncations fused to a His-tag resulted in soluble expression. An SDS-PAGE analysing the induction of the generally well expressed but insoluble proteins is shown in Figure 3.5.

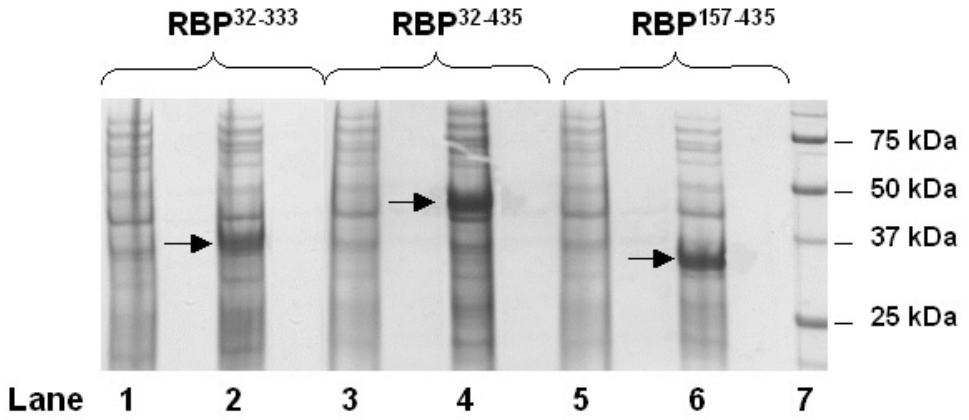

Figure 3.5: Analysis of the induction of RBP-Jκ truncation mutants belonging to group 3 in table 3.1. All fragments are fused to a 6xHis-tag. The expression pattern before induction (lanes 1, 3 and 5) of RBP^{32-333} (KH7), RBP^{32-435} (KH8) and $RBP^{157-435}$ (KH9) is compared to that 2 hrs after induction with 1 mM IPTG (lanes 2, 4 and 6). Induction bands of the corresponding proteins are indicated by arrows. Lane 7: Protein marker (Biorad).

Truncation constructs designed based on alignments with homologues of the protein family from other species

The structure of C. *elegans* Lag-1 has been recently solved (Kovall and Hendrickson, 2004) and is described in the introduction. The corresponding PDB file (PDB-code 1TTU) does not contain all amino acids in the construct used. Three amino acids are not visible at the

N- terminus and another three cannot be found at the C-terminus. In total, the construct is 63 aa shorter than full-length human RBP-Jκ, but includes the conserved part. Figure 3.6 shows an alignment of human RBP-Jκ with *C. elegans* Lag-1 highlighting the borders chosen for the deletion according to the visible amino acids in the Lag-1 structure.

The approach applied to solve the structure of C. *elegans* Lag-1 is based on a sequence alignment of RBP-Jκ homologues of different organisms shown in Figure 3.6. This alignment served as template for the design of RBP-Jκ truncations, which are more likely to crystallise. The truncation constructs based on sequence alignment are listed as group 4 in table 3.1(d). They differ from each other by only a few amino acids, but a great variety was designed to enhance the chances for crystallisation, since many cases are known, where a difference of a few amino acids determines success in crystallisation.

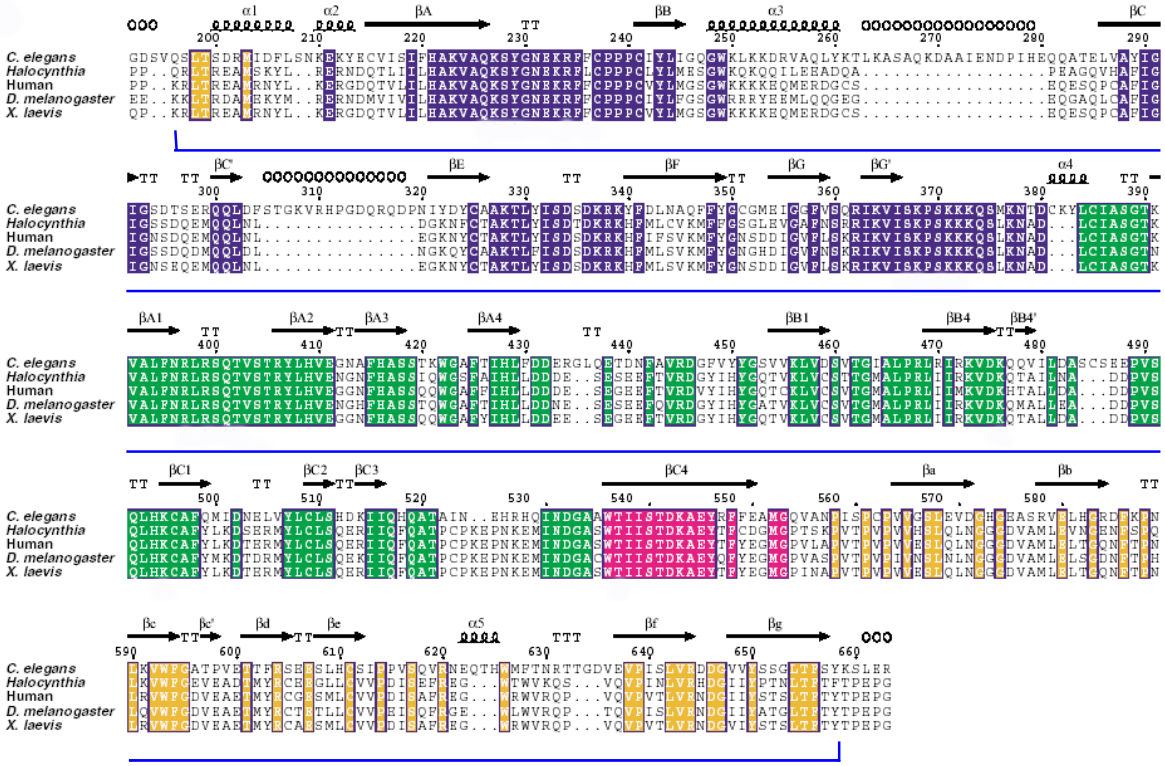

Figure 3.6: Alignment of homologs of the CSL family (C. *elegans*, Halocynthia, human, D. melanogaster, and Xenopus laevis) showing the most conserved region of the proteins (from (Kovall and Hendrickson, 2004)). These regions were cloned and expressed and the crystal structure of the protein derived from C. *elegans* was solved at 2.85 Å resolution (Kovall and Hendrickson, 2004). The boundaries of the three distinct domains are coloured in blue for the N-terminal domain, green for the β-trefoil domain and orange for the C-terminal domain. Residues belonging to the bridging βC4 strand are coloured in magenta. Blue brackets indicate the borders of the truncation construct expressed in insect cells (nRBP$^{28\text{-}432}$), which ist described in section 3.1.1.4 below.

Activity test of purified protein: DNA binding

RBP-Jκ is a transcription factor, which specifically binds to an 8-base pair core sequence, which is conserved among many species. To establish the DNA-binding activity of any RBP-Jκ construct purified in this work and especially to judge its successful refolding a 40 bp double-strand DNA oligonucleotide derived from Cp was used. After determining the protein concentration by measuring absorption at 280 nm an equimolar amount of DNA was added to the solution and a non-radioactive EMSA was run after incubation for 10 minutes at room temperature. DNA binding was detected by staining the gels with ethidium bromide and Coomassie Brilliant Blue. The theoretical pI of full-length RBP-Jκ is 8.29 so that RBP-Jκ without DNA should not enter the native gel run at pH 8.0. None of the constructs used could be visualized on a native gel without DNA. In contrast full-length RBP-Jκ and truncated proteins bound to DNA enter the native gel and result in a band, which can be stained with both ethidium bromide and Coomassie Brilliant blue, therefore proving the formation of a binary complex. Figure 3.7 shows a native gel with a binary $rRBP^{full\text{-}length}$-DNA complex subsequently stained with ethidium bromide and Coomassie Brilliant blue.

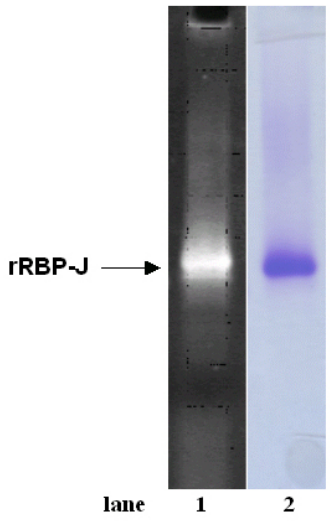

Figure 3.7: Analysis of the DNA binding activity of $rRBP^{full\text{-}length}$ by non-radioactive EMSA. The gel containing the binary complex formed with 1.5 µg $rRBP^{full\text{-}length}$ obtained after Ni-affinity purification and an equimolar amount of oli-Cp^{40} was successively stained with ethidium bromide (lane 1) and Coomassie Brilliant Blue (lane 2).

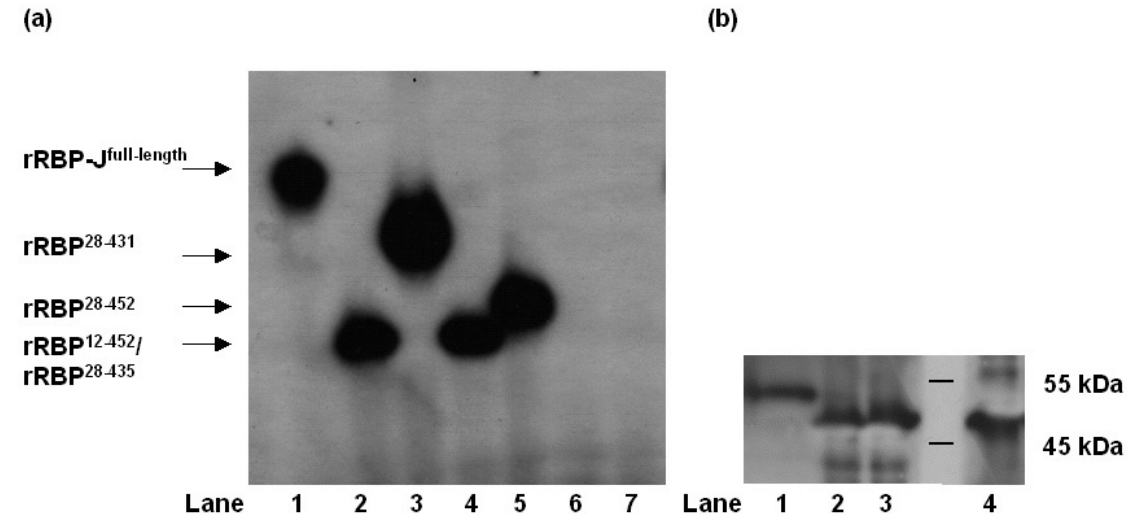

Figure 3.8: (a) Analysis of the DNA-binding activity of truncated RBP-Jκ proteins (5 ng each) listed in table 3.1(d) by radioactive EMSA. All proteins were expressed in E. *coli* and refolded in condition 13. Arrows on the left side indicate the binary complexes of RBP-Jκ and DNA. Lane 1: rRBP$^{full-length}$; lane 2: rRBP$^{12-452}$ (KH11-12); lane 3: rRBP$^{28-431}$(KH11-13); lane 4: rRBP$^{28-435}$ (KH11-14); lane 5: rRBP$^{28-452}$ (KH11-15); lanes 6 and 7: negative controls, truncated variants of RBP-Jκ with putative alternative starting points, which do not bind DNA (rRBP$^{64-487}$ and rRBP $^{74-487}$, see table 3.1(b)). **(b)** Western blot analysis of 5 ng of the truncated proteins belonging to group 4 after refolding (table 3.1): rRBP$^{12-452}$ (lane 1), rRBP$^{28-432}$ (lane 2), rRBP$^{28-435}$ (lane 3), rRBP$^{28-452}$ (lane 4).

All of the truncation constructs in table 3.1(d) expressed as inclusion bodies and the refolding protocol described for full-length RBP-Jκ thus had to be applied in all cases. The result of the DNA-binding activity tested in an EMSA with radioactively labelled oligonucleotides derived from Cp, is depicted in Figure 3.8. Full-length refolded RBP-Jκ was taken as positive control (lane 1) and constructs corresponding to truncated RBP-Jκ variants with putative alternative starting points, which do not bind DNA, as negative control (lanes 6 and 7). Although all refolded truncation constructs bind DNA they offer no advantage as they all expressed as inclusion bodies.

Activity test of purified rRBP$^{full-length}$: Ternary complex formation

It was attempted to form ternary complexes with DNA and proteins derived from hNotch1 as described in section 2.2.5. No ternary complex was detected by size exclusion chromatography of the mixture of the two proteins and DNA in the case of rRBP$^{full-length}$. Binding conditions including a range of pH (5.5 to 9) and salt concentrations (50 to 300 mM) were tried out – without success - to promote ternary complex formation. No shift of

the binary RBP-Jκ-DNA complex was observed on non-radioactive EMSA gels in the presence of $Notch^{Ram}$ or $Notch^{RamANK}$ protein suggesting that the refolded RBP-Jκ expressed in *E. coli* either is only partially refolded or lacks crucial posttranslational modifications.

3.1.1.4 Baculovirus-infected insect cells as alternative expression system

Insect cells process translated proteins in a similar way to mammalian cells. Although in some cases posttranslational modifications are applied differently, the system provides many advantages for overexpression of soluble recombinant proteins with the help of recombinant baculoviruses. Since only insufficient soluble expression could be obtained with *E. coli* as expression host and some of the refolded proteins did bind DNA but not protein interaction partners derived from hNotch (see below), the expression system was changed to obtain fully active RBP-Jκ.

Constructs and viruses

A construct coding for full-length RBP-Jκ (pKH25.1) as well as a final truncation construct comprising aa 28 to 432 of human RBP-Jκ (pKH24.1), designed according to the alignment shown in Figure 3.6 and the residues visible in the electron density map of *C. elegans* Lag-1 were cloned into the baculovirus vector pFastBac-HTa, displayed in Figure 2.2. These constructs were transformed into competent DH10 bacteria containing the Baculovirus genome as episome. The gene of interest, fused with a 6xHis-tag, recombined within the virus genome. The isolated viral DNA was then transfected to SF21 cells. The primary virus (P1) could be harvested in the cell medium after five days. Taking the truncation construct pKH24.1, coding for $nRBP^{28-432}$, (see section 2.1.3) as an example, the control PCR in Figure 3.9 shows the presence of the gene of interest in the Bacmid-DNA, the primary virus.

Purification

After infection with a baculovirus encoding either KH25.1 or the truncation mutant pKH24.1 SFplus cells express the protein within two days. Harvest took place after 48 hours depending on the appearance of the cells.

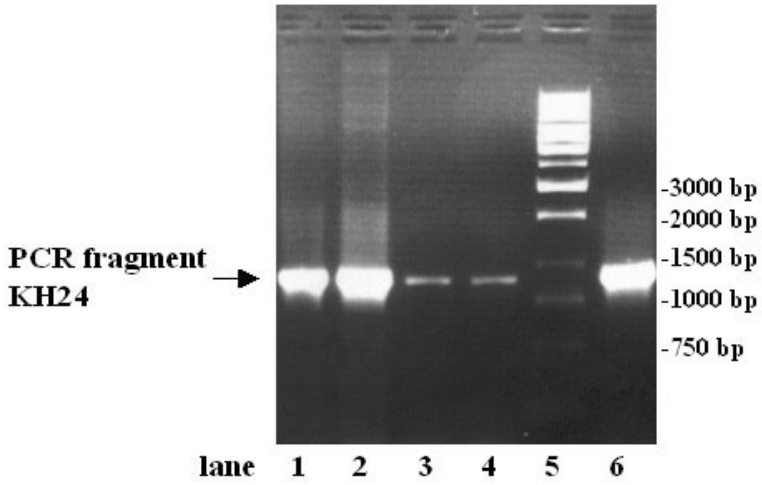

Figure 3.9: Control PCR proving the presence of the KH24 PCR fragment in the Bacmid DNA and in the primary baculovirus; lanes 1 and 2: two clones of the Bacmid DNA (pKH24.1 and pKH24.2), lanes 3 and 4: primary virus derived from clones in lanes 1 and 2 (P1-24.1 and P1-24.2), lane 5: Gene Ruler™ 1 kb DNA ladder (Fermentas), lane 6: positive control (pVK60).

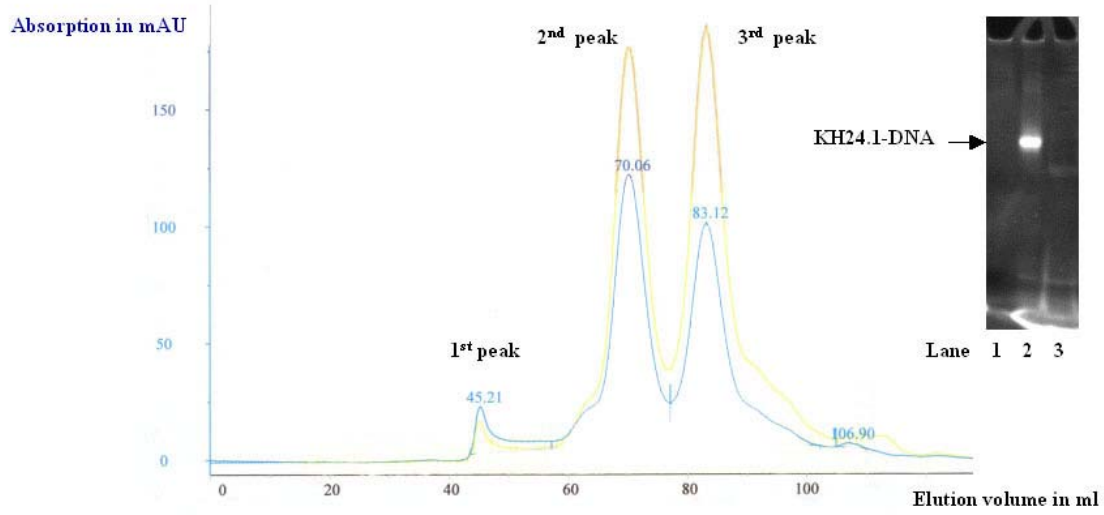

Figure 3.10: Final purification of a binary complex of nRBP$^{28-432}$ bound to a 22 bp oligonucleotide derived from Cp with double A and T overhangs at each 5´end. Size exclusion chromatography was carried out using a Superdex 200 16/60 column (Amersham Pharmacia). Peak fractions were pooled, concentrated and analysed by non-radioactive EMSA. The 1st peak corresponds to the void volume of the column and presumably contains aggregated protein, the 2nd peak contains the binary nRBP-DNA complex, and the 3rd one is free excess DNA. Blue curve: absorption at 280 nm, red curve: absorption at 254 nm. Non-radioactive EMSA stained with ethidium bromide: Lane 1: 1st peak; lane 2: 2nd peak containing the binary complex; lane 3: 3rd peak. Red curve: absorption at 260 nm; blue curve: absorption at 280 nm.

Both KH25.1 and KH24.1 were completely soluble and were purified following the procedure described in Section 2.5.2. From here on both proteins will be referred to as $nRBP^{full\text{-}length}$ for KH25.1 and $nRBP^{28\text{-}432}$ for KH24.1. After the first purification step using Ni-NTA the proteins were about 80% pure. After complexation with DNA they were further purified using size exclusion chromatography. TEV protease was applied to the complex before this last step depending on further use. An exemplary size exclusion chromatogram for $nRBP^{28\text{-}432}$ bound to DNA is shown in Figure 3.10.
Depending on the time after infection and the cell density, 5 to 9 mg of pure protein could be obtained from 300 ml of cell culture.

3.1.2 Expression and purification of $Notch^{Ram}$ and $Notch^{RamANK}$

Two truncations comprising the Notch-Ram and –RamANK domains have been designed for the present work. An overview of their arrangement within Notch is illustrated in Figure 3.11.

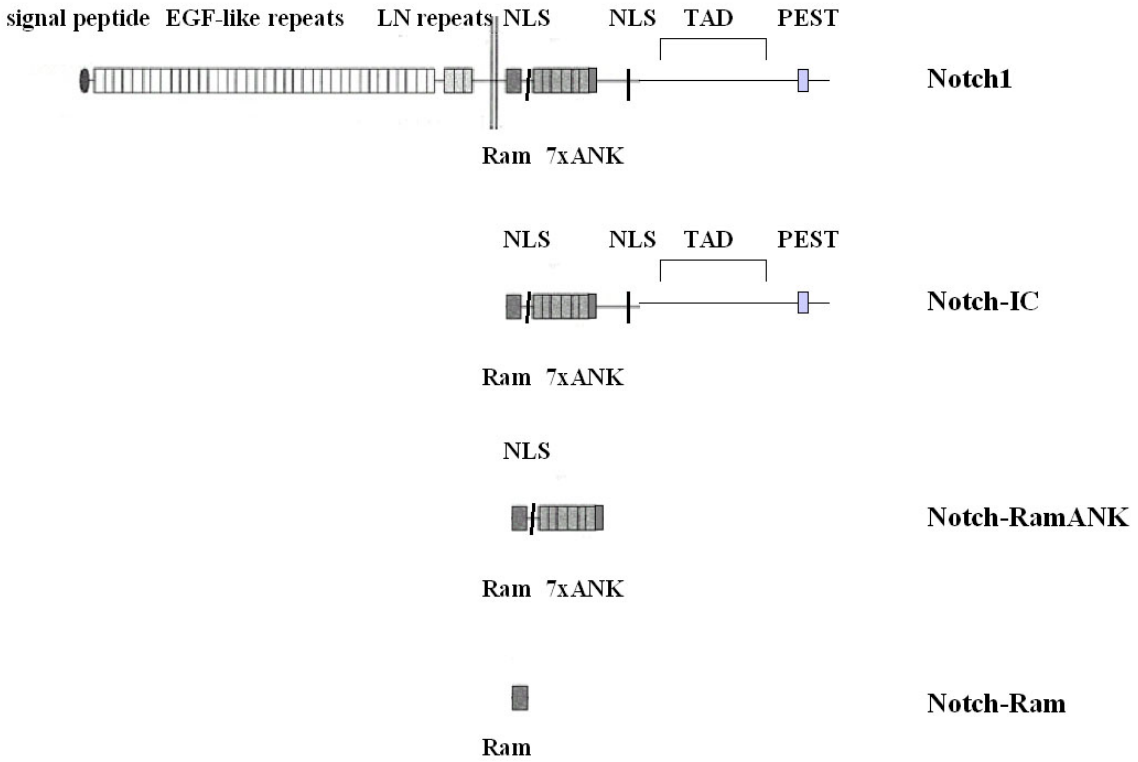

Figure 3.11: Overview of the arrangement and location of the truncated proteins designed for the present work. Notch-IC was not used, but is mentionned here because it represents the part of Notch which binds RBP-Jκ *in vivo*.

Notch^{Ram}

The expression construct and its properties

The human Notch^{Ram} domain (aa 1768-1861) comprises about 100 amino acids. The EXPASY protein parameter tool (Gasteiger et al., 2005) predicts a molecular mass of 11.3 kDa and a theoretical pI of 5.62. The PHD secondary structure prediction tool (Rost, 1996)reveals that it does not contain any secondary structure element with an average reliability of 0.9. This was confirmed previously (Nam et al., 2003) and in our study by CD spectroscopy (see below).

Expression and purification

Transformed into the expression host BL21(DE3)PlysS the protein expressed in high levels and could be purified in the native state. The procedure followed a standard protocol using a two-step purification. After application to Ni-NTA, low imidazole and high salt washing steps, the protein could be eluted in large amounts. SDS-PAGE analysis showed it to be about 80% pure. After overnight TEV cleavage size exclusion chromatography with a Superdex 75 16/60 column (Amersham Pharmacia) was used to purify the protein to about >95% purity. Figure 3.12 displays the SDS-PAGE analysis of the size exclusion chromatography peak showing pure and homogenous Notch^{Ram} protein. The pure protein was used for binding experiments with Isothermal Titration Calorimetry, electrophoretic mobility shift assays and for crystallization trials.

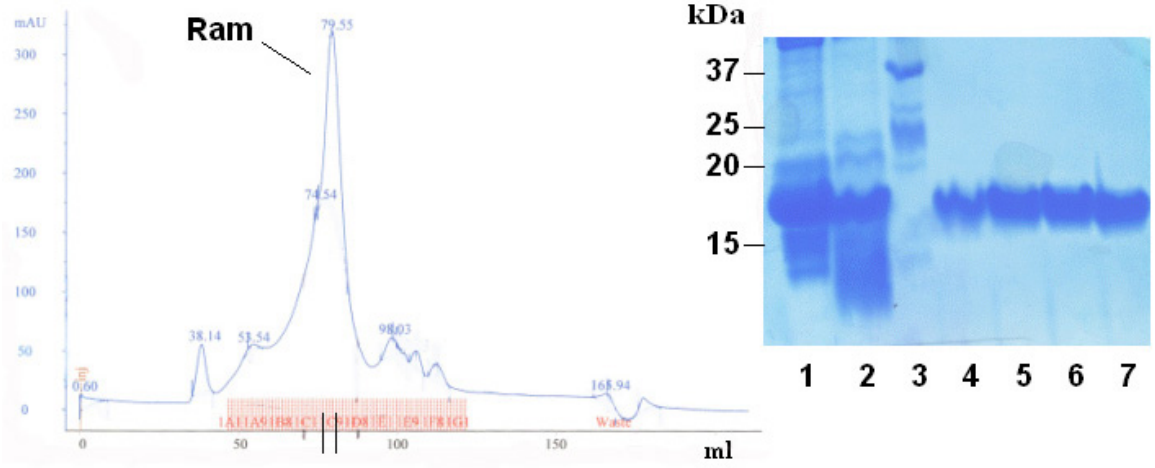

Figure 3.12: Final purification of Notch^{Ram} using size exclusion chromatography; the chromatogram shows a run with a Superdex 75 16/60 column. Four fractions of the major peak were analysed by SDS-PAGE: lane 1: elution fraction from Ni-NTA resin; lane 2: fraction after overnight TEV cleavage at 4 °C; lane 3: protein marker (Biorad); lanes 4 to 7: fractions C7 to C10 from size exclusion chromatography as indicated by black dashes.

Notch^{RamANK}

The expression construct and its properties

Cloning of the RamANK domain of Notch1 was unsuccessful until alternative cleavage sites (Acc651 and PciI) were used to clone it into pETM11. The C-terminal end of the Ram domain is followed by seven ankyrin repeats (further referred to as ANK) which were reported to be involved in the binding of the Notch-IC domain to RBP-Jκ (Tani et al., 2001). On average each of the ANK repeats consist of about 25 to 30 aa which fold up to a tightly packed helical structure involved in signal transduction processes. The Notch^{RamANK} construct cloned from the human Notch1 receptor possesses 364 aa and has a theoretical molecular mass of 40.3 kDa. The ExPASy protein parameter tool predicts a theoretical pI of 4.87 for the protein.

Expression and purification

Transformed into BL21 (DE3)PlysS the protein could be expressed in high amounts and purified in the native state using the same protocol as for the Notch^{Ram} protein. After purification using Ni-NTA the protein was about 70% pure and was further processed in the same manner as the Notch^{Ram} protein.

3.1.3 Expression and purification of EBNA2 proteins

EBNA2 constructs EBNA2$^{259-435}$ (KF214), comprising CR5 to CR7, and EBNA2$^{291-355}$ (SV180), including CR5 and CR6 (for a graphical overview of the constructs designed and cloned by S. Valencia, GSF Munich, see Figure 3.13) were overexpressed in *E. coli* BL21(DE3)PLysS as expression host. Purification followed the protocol described in section 2.2.4. As illustrated in Figure 3.14 both proteins were highly soluble and >90 % pure after the GST-affinity step.

```
MAYPYDVPDYAEFMPTFYLALHGGQTYHLIVDTDSLGNPSLSVIPSNPYQEQLSDTPLIP 60

LTIFVGENTGVPPPLPPPPPPPPPPPPPPPPPPPPPPPPSPPPPPPPPPPPQRRDAWT 120

QEPSPLDRDPLGYDVGHGPLASAMRMLWMANYIVRQSRGDRGLILPQGPQTAPQARLVQP 180

HVPPLRPTAPTILSPLSQPRLTPPQPLMMPPRPTPPTPLPPATLTVPPRPTRPTTLPPTP 240

LLTVLQRPTELQPTPSPPRMHLPVLHVPDQSMHPLTHQSTPNDPDSPEPRSPTVFYNIPP 300

                CR5                          CR6
MPLPPSQLPPPAAPAQPPPGVINDQQLHHLPSGPPWWPPICDPPQPSKTQGQSRGQSRGR 360

                                    CR7
GRGRGRGRGKGKSRDKQRKPGGPWRPEPNTSSPSMPELSPVLGLHQGQGAGDSPTPGPSN 420

AAPVCRNSHTATPNVSPIHEPESHNSPEAPILFPDDWYPPSIDPADLDESWDYIFETTES 480

PSSDEDYVEGPSKRPRPSIQ 500
```

Figure 3.13: Sequence of full-length EBNA2 with the truncated constructs EBNA2$^{259-435}$ (KF214), highlighted in blue and EBNA2$^{291-355}$ (SV180), underlined, used in the present work. The conserved regions (CR) included in the different constructs are framed.

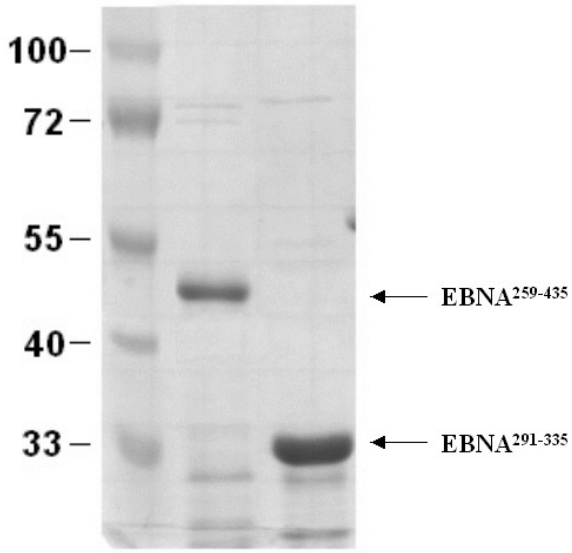

Figure 3.14: SDS-PAGE analysis of the one-step purification of proteins derived from EBNA2; lane 1: protein marker (Fermentas), lane 2: EBNA2$^{259-435}$ (0.5 µg), lane 3: EBNA2$^{291-335}$ (1 µg).

3.2 Biochemical and biophysical characterization of the interaction of RBP-Jκ with Notch^{Ram} or Notch^{RamANK} or EBNA2

3.2.1 Binary complexes of RBP-Jκ with DNA and comparison of recombinant RBP-Jκ proteins expressed in *E.* coli and insect cells

Influence of reducing agents on the quality of purified RBP-Jκ

Full-length human RBP-Jκ contains 13 cysteines, which are unlikely to form disulphide bridges in the reducing environment of the nucleus, but may well form random intra- or intermolecular disulphide bridges in solution, which may lead to unspecific aggregation, especially at higher concentrations. Furthermore, because of the susceptibility of the SH-group to oxidation exposure to oxygen may change the properties of the protein.

For these reasons and to guarantee a uniform and monodisperse protein solution it is essential to add sufficient amounts of reducing agents.

Dithiothreitol (DTT, see Figure 3.15(a)) is a commonly used reducing agent during and after the protein purification process. DTT is, however, easily oxidized when exposed to oxygen, and the reaction is reversible, i. e. reduced thiols can be re-oxidized.

Since all attempts at producing a homogenous protein solution using common working concentrations of DTT (1-10 mM) failed, a less commonly used reducing agent, Tris(2-carboxyethyl)phosphine (TCEP, see Figure 3.15(b) (Burns et al., 1991)), which stoichiometrically and irreversibly reduces disulphide bridges according to the reaction in Figure 3.16(a) was tried out as alternative. Figure 3.16 compares the reaction mechanisms of both substances.

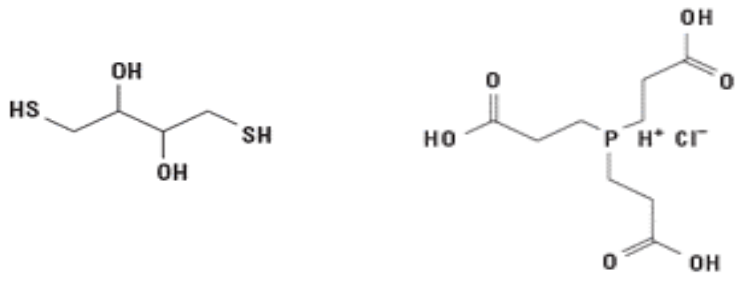

(a) **(b)**

Figure 3.15: Chemical formula of the reducing agents **(a)** dithiothreitol (DTT); **(b)** Tris(2-carboxyethyl)phosphine (TCEP).

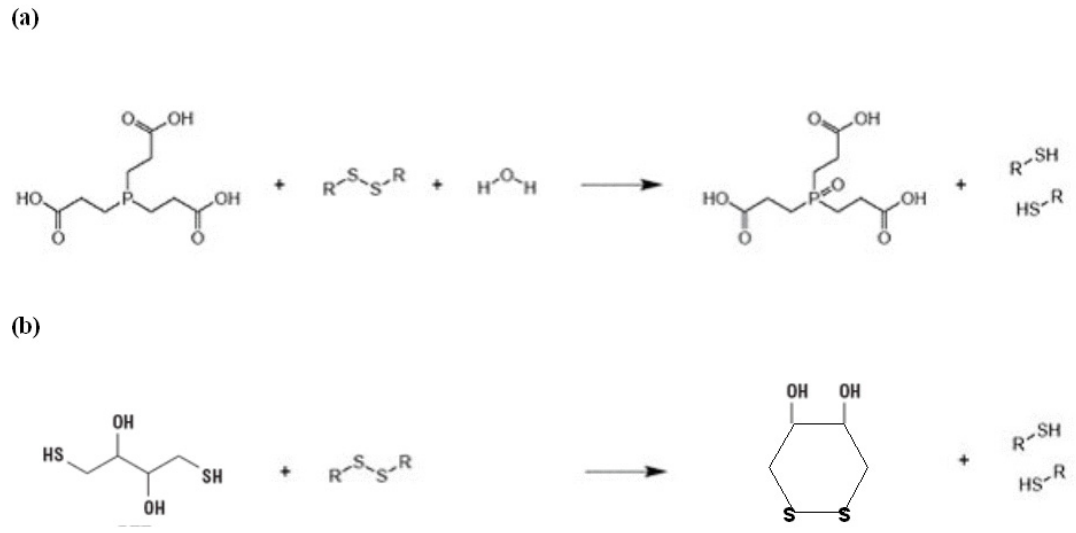

Figure 3.16: (a) Irreversible reaction of TCEP with thiols; **(b)** reversible reaction of DTT with thiols.

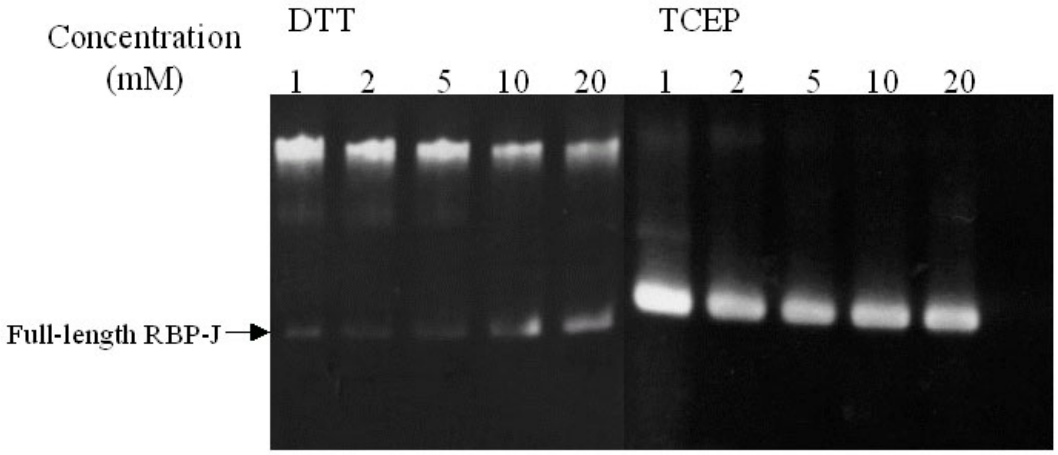

Figure 3.17: Comparison of the reducing abilities of dithiothreitol (DTT) and Tris(2-carboxyethyl)phosphine (TCEP) on a complex of nRBP$^{full\text{-}length}$ with a oli-Cp^{20} by non-radioactive EMSA. Left panel: Increasing concentrations (1 to 20 mM) of DTT added to the preformed binary complex; right panel: increasing concentrations (1 to 20 mM) of TCEP added to the preformed binary complex.

Whereas with DTT a second band of a binary nRBJ$^{full\text{-}length}$-DNA complex located above the band of the monomeric 1:1 complex on a non-radioactive EMSA gel was always obtained (see Figure 3.17), addition of 2 mM TCEP resulted in a single band corresponding to the native 1:1 nRBP-DNA complex.

Since monodispersity is an essential prerequisite for crystallization and X-ray small angle scattering as well as reliable binding studies using non-radioactive EMSA or isothermal titration calorimetry and virtually any biophysical characterisation technique (e.g. CD spectroscopy), DTT was replaced by TCEP during and after purification of RBP-Jκ proteins.

A surprising observation, which has apparently not been described before and remains unexplained, was made when binary and ternary complexes with RBP-Jκ were purified on a size exclusion column in a buffer containing 5 mM TCEP. Whereas the usual elution volume of the binary complex is at about 70 ml in a Superdex 200 16/60 size exclusion column, binary complexes formed with two different oligonucleotides eluted after nearly one column volume (about 120 ml), when TCEP was present in the buffer (Figure 3.18(a) and (b)), which could be shown with non-radioactive EMSA (Figure 3.18(c). The same result was obtained when a molecular mass standard (Biorad) containing five proteins of different molecular masses was run on the same column in the same buffer (Figure 3.18(d).

Following page:

Figure 3.18: Changed elution profiles of binary DNA-nRBP$^{full\text{-}length}$ complexes in the presence of 2 mM TCEP in the gel filtration buffer. (a) Elution profile of a size exclusion run of nRBP$^{full\text{-}length}$ bound to oli-Cp^{14} on a S200 10/30 size exclusion column (Amersham). Absorption was measured at an elution volume where normally peptides elute. (b) Elution profile of a size exclusion run of nRBP$^{full\text{-}length}$ bound to oli-Cp^{15} on a S200 10/30 size exclusion column (Amersham). The elution profile resembles the one in (a). (c) Analysis of the peaks obtained in (a) and (b) by non-radioactive EMSA. The pure and functional binary complex could be detected in both cases. In the figure nRBP$^{full\text{-}length}$ is abbreviated nRBP. (d) Verification of the altered elution profile of the column depending on the presence of 5 mM TCEP in the gel filtration buffer by a size exclusion run with standard proteins on the same column. Under normal circumstances the void volume of a S200 10/30 column is about 7.5 ml, corresponding to the elution of the first component of the protein standard with a molecular mass of 680 kDa. In the present case the elution profile is shifted by about 6 ml, so that the peak according to protein with the highest molecular mass (680 kDa) appears only at an elution volume of about 13 ml.

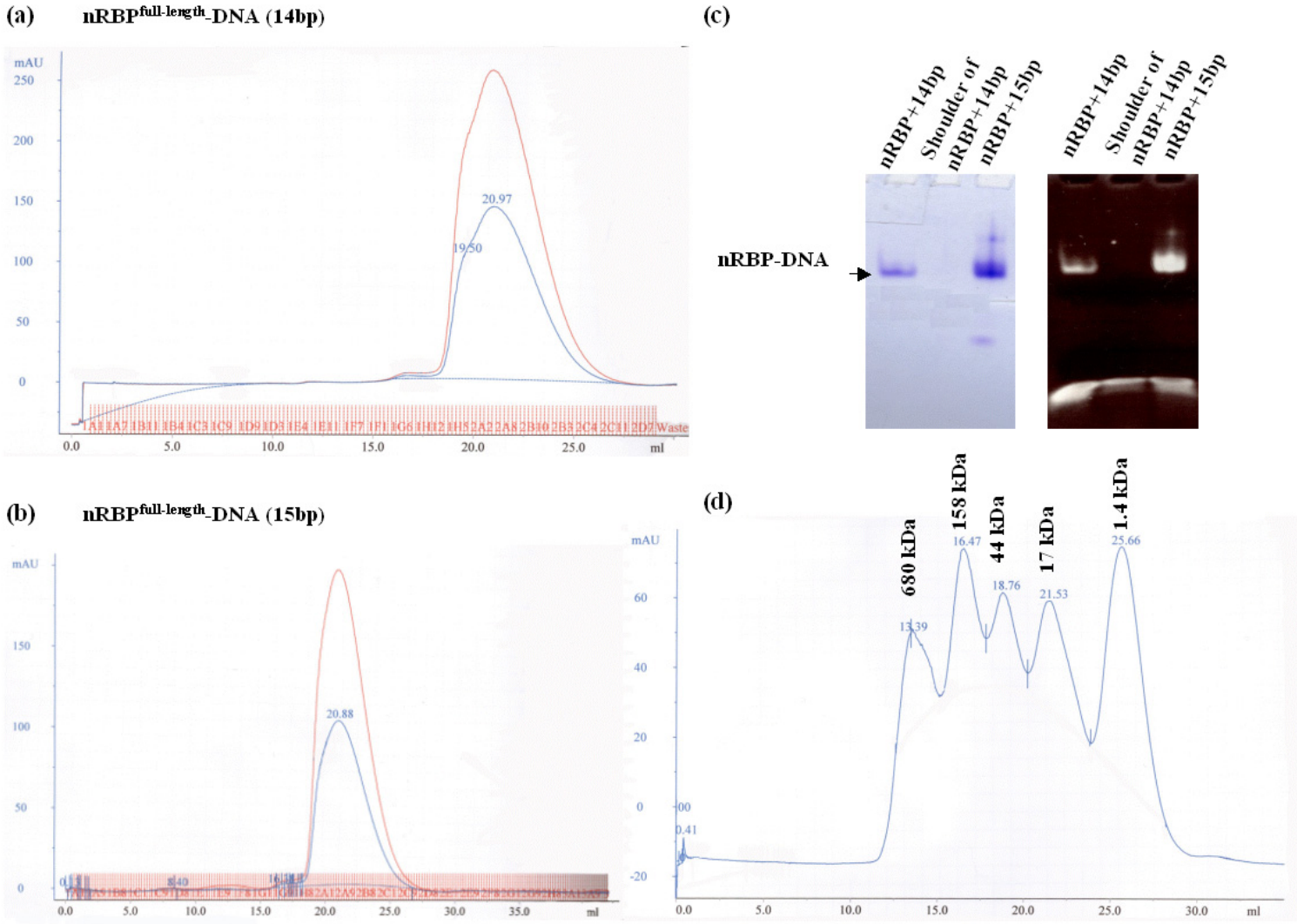
(a)
nRBP^full-length-DNA (14bp)
mAU
20.97
19.50
ml
(b)
nRBP^full-length-DNA (15bp)
mAU
20.88
ml
(c)
nRBP+14bp
Shoulder of nRBP+14bp
nRBP+15bp
nRBP-DNA
(d)
680 kDa
158 kDa
44 kDa
17 kDa
1.4 kDa
16.47
18.76
21.53
25.66
13.39
0.41
ml

The difference in activity of RBP-Jκ expressed in *E.* coli or insect cells is not related to properties measurable with CD spectroscopy, EMSA or mass spectrometry

Post translational modification occurs differently in bacteria and insect cells or mammals. Differences may influence the ability of the overexpressed and purified protein to crystallize. The different properties regarding the binding of other proteins and peptides mentioned above suggest major differences between RBP-Jκ expressed in *E. coli* and in insect cells. Besides incomplete refolding of the protein expressed in bacteria, posttranslational modifications may be the cause for the different binding properties.

Mass spectrometry provides a means of comparing the total mass of both proteins with their theoretical mass.

The molecular mass of His-tagged full-length RBP-Jκ calculated with the Expasy protein parameter tool (Gasteiger et al., 2005) is 57.423 kDa. The molecular mass of $nRBP^{full\text{-}length}$ expressed in insect cells obtained by mass spectrometry is 57.419 kDa. The small difference (4 Da) does not correspond to any of the common posttranslational modifications and is most probably not significant. This suggests that the yield of fully functional RBP-Jκ proteins depends on other factors than posttranslational modifications, such as e. g. correct folding.

DNA-binding ability

The ability of RBP-Jκ to bind specifically to an eight base pair double-strand DNA sequence was used to compare the binding mode of $rRBP^{full\text{-}length}$ and $nRBP^{full\text{-}length}$. Oligonucleotides with 14 to 22 base pairs, derived from Cp, were used to determine the DNA-binding ability of $rRBP^{full\text{-}length}$ and of full-length and deleted RBP-Jκ expressed in insect cells ($nRBP^{full\text{-}length}$ and $nRBP^{28\text{-}432}$). The binding affinity of $nRBP^{full\text{-}length}$ and $nRBP^{28\text{-}432}$ purified from insect cells is compared with that of $rRBP^{full\text{-}length}$ purified from *E. coli* in Figure 3.19. The results clearly illustrate that the two proteins purified from insect cells bind to oligonucleotides shorter than 16 bp, whereas the corresponding bands are barely detectable in the case of the refolded protein purified from *E. coli*.

Compared to EMSAs with radiolabelled DNA much higher amounts of protein and DNA are required for native gels, which have to be stained with ethidium bromide and Coomassie Brilliant blue. Figure 3.20 displays an EMSA using radiolabelled DNA for $rRBP^{full\text{-}length}$ and $nRBP^{full\text{-}length}$ expressed in insect cells for comparison. In contrast to the

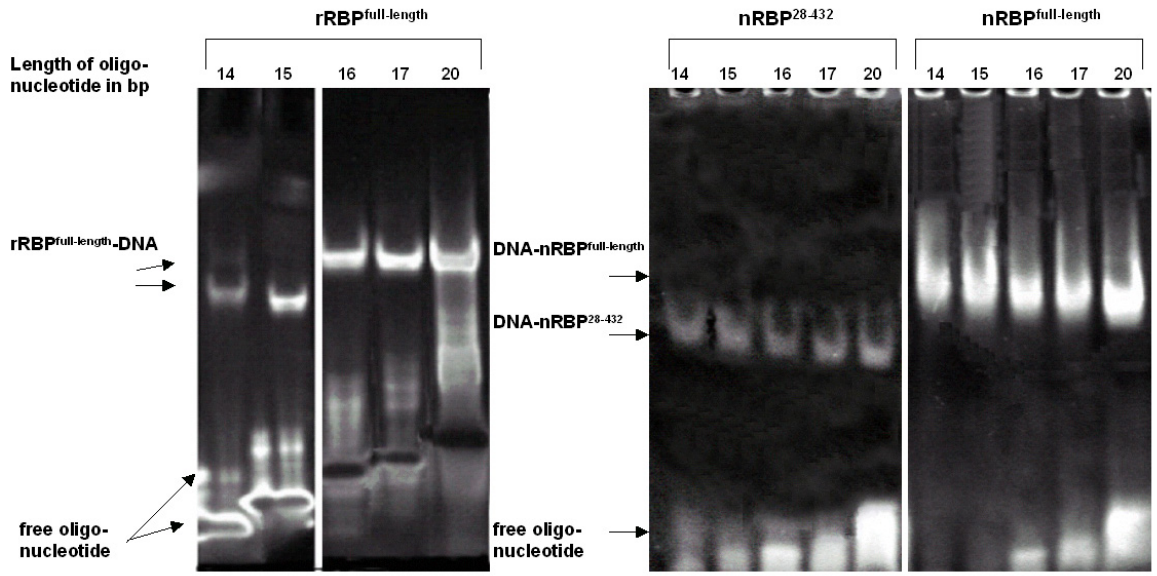

Figure 3.19: Comparison of ability of nRBP$^{28\text{-}432}$, nRBP$^{full\text{-}length}$ and rRBP$^{full\text{-}length}$ to bind DNA of different length using non-radioactive EMSA. Left panel: 10 µg rRBP$^{full\text{-}length}$, right panel: 2 µg nRBP$^{28\text{-}432}$ and 10 µg nRBP$^{full\text{-}length}$ bound to oligonucleotides derived from Cp (oli-Cp^{14}, oli-Cp^{15}, oli-Cp^{16}, oli-Cp^{17} and oli-Cp^{20}).

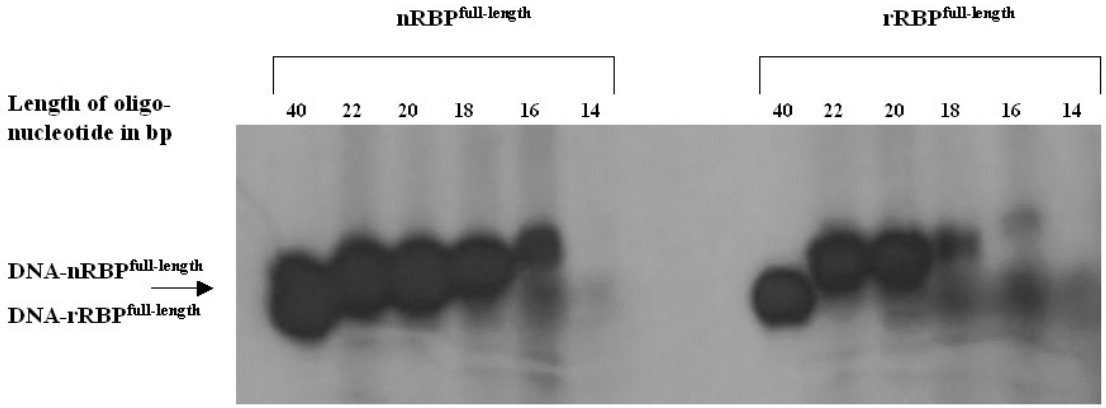

Figure 3.20: Comparison of the ability of nRBP$^{full\text{-}length}$ and rRBP$^{full\text{-}length}$ to bind DNA of different length using radioactive EMSA. The oligonucleotides are derived from Cp (oli-Cp^{40}, prepared with Klenow-fill-in; oli-Cp^{22}, oli-Cp^{20}, oli-Cp^{18}, oli-Cp^{16} and oli-Cp^{14}, all prepared by end-labelling); left panel: nRBP$^{full\text{-}length}$ (1 ng); Right panel: rRBP$^{full\text{-}length}$ (2 ng).

result obtained with the non-radioactive EMSA gel stained with ethidium bromide the protein no longer binds to the shorter oligonucleotides: 14 bp in case of nRBP$^{full\text{-}length}$ and 14 and 16 bp for rRBP$^{full\text{-}length}$.

Both types of assay, the EMSA with radiolabelled oligonucleotides and the one without any label stained with ethidium bromide and Coomassie Brilliant Blue are essentially the same and differ only in the amounts of protein and DNA added. The differences in DNA-binding are clearly seen in the shifts carried out with radiolabelled DNA, where only nanogram amounts of protein and DNA are added. As the binding affinities for the shorter oligonucleotides are lower the equilibrium

$$\text{RBP-J}\kappa + \text{DNA} \rightleftharpoons \text{RBP-J}\kappa\text{-DNA}$$

is shifted towards the left side, which results in amounts of complex too low to detect as is happening in the radioactive EMSA in Figure 3.20.

Biological activity of purified RBP-Jκ on binding sites found in the viral promoters Cp, LMP1P and LMP2AP

Cp has a strong binding site for RBP-Jκ (Ling et al., 1994) so that 1 ng of refolded RBP-Jκ can easily be detected using radioactive EMSA. To compare the binding affinities of proteins expressed in insect cells and $rRBP^{full\text{-}length}$ from *E. coli* an EMSA with radiolabelled oli-Cp^{40} oligonucleotide was made. Figure 3.21(a) displays the results with both $nRBP^{28\text{-}432}$ and $nRBP^{full\text{-}length}$ and with $rRBP^{full\text{-}length}$ as positive control. All three proteins were run on the same gel. The binding affinity of the two proteins purified from insect cells is up to an order of magnitude higher than that of $rRBP^{full\text{-}length}$ purified from *E. coli*.

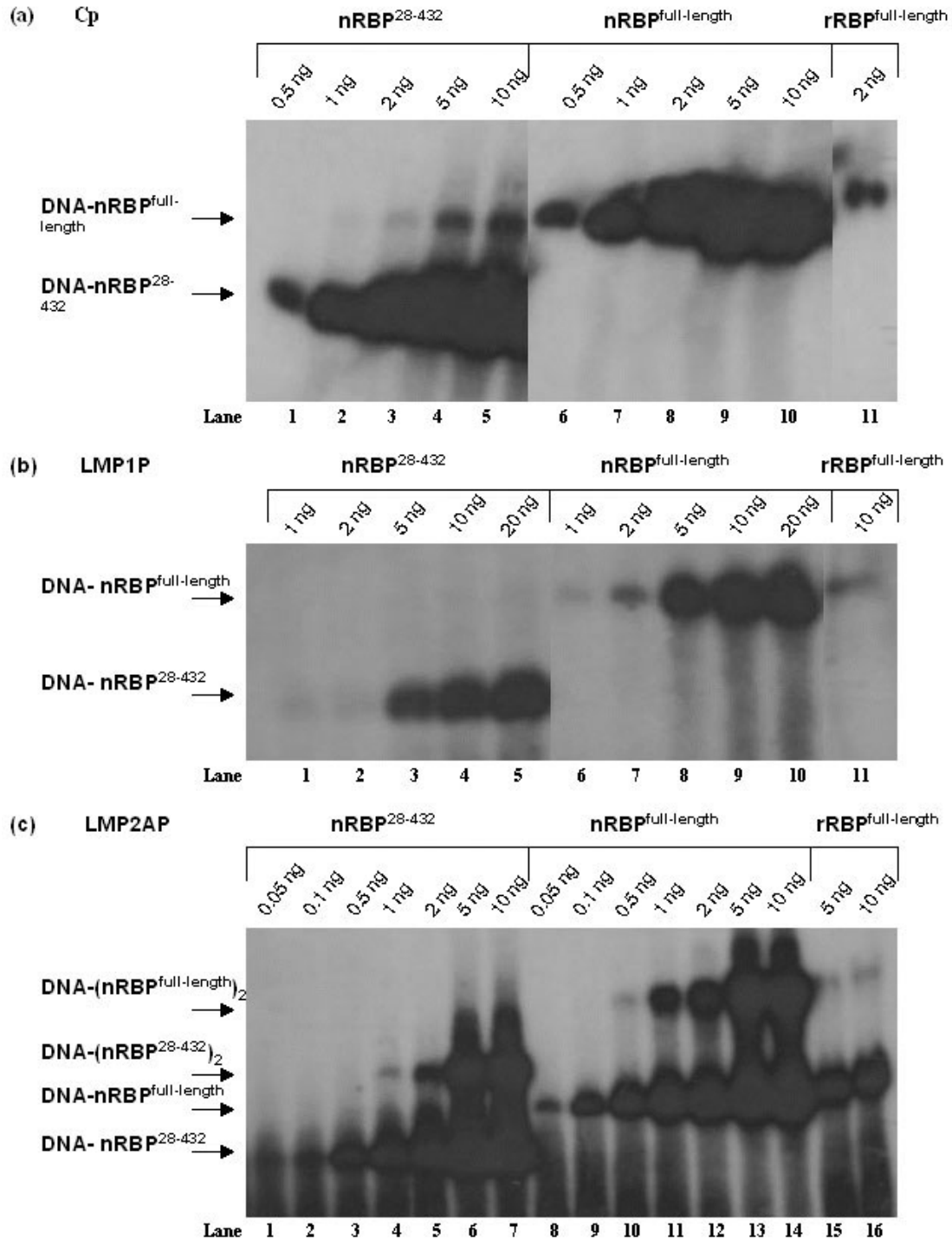

Figure 3.21: Comparison of the affinity of RBP-Jκ expressed in different hosts (nRBP$^{28-432}$, nRBP$^{full-length}$ and rRBP$^{full-length}$) to oligonucleotides derived from different viral promoters using radioactive EMSAs on 4% TBE polyacrylamide gels. **(a)** Cp: 0.5-10 ng of nRBP$^{28-432}$ and nRBP$^{full-length}$ and 2 ng of rRBP$^{full-length}$ were incubated with equal amounts of oli-Cp[40]. **(b)** LMP1P: 1-20 ng nRBP$^{28-432}$ and nRBP$^{full-length}$ and 10 ng rRBP$^{full-length}$ were incubated with equal amounts of a oli-LMP1P[36]. **(c)** LMP2AP: 0.05-10 ng nRBP$^{28-432}$ and nRBP$^{full-length}$ and 5-10 ng of rRBP$^{full-length}$ were incubated with equal amounts of oli-LMP2AP[54].

rRBP$^{full\text{-}length}$ was shown to bind an oligonucleotide derived from LMP1P (oli-LMP1P^{36}) much less tightly than those derived from Cp. Therefore the experiment was carried out using higher amounts of protein than for the corresponding experiment with oli-Cp^{40}. Figure 3.21(b) displays the results of the binding assay with radiolabelled oli-LMP1P^{36}. As in the case of Cp, the binding affinity of both nRBP$^{28\text{-}432}$ and nRBP$^{full\text{-}length}$ is about 10 times higher than that of rRBP$^{full\text{-}length}$.

LMP2AP contains two separate binding sites for RBP-Jκ, which are successively occupied upon addition of increasing amounts of protein. The affinities of both sites are compared in Figure 3.21(c). As shown previously for oligonucleotides derived from LMP1P and Cp the affinity of proteins purified from insect cells for LMP2AP is higher than that of rRBP$^{full\text{-}length}$, the ratio is about an order of magnitude. Moreover, in case of nRBP$^{28\text{-}432}$ and nRBP$^{full\text{-}length}$ the second binding site on LMP2AP is occupied at much lower concentrations than in case of rRBP$^{full\text{-}length}$.

Comparison of the secondary structure of rRBP$^{full\text{-}length}$ and native nRBP$^{full\text{-}length}$

The EMSA results and the many unsuccessful trials to form ternary complexes of rRBP$^{full\text{-}length}$ with DNA and Notch proteins suggested that incomplete refolding may be the cause for the lack of binding of rRBP$^{full\text{-}length}$ to Notch proteins. CD spectroscopy was therefore used to investigate the secondary structure of rRBP$^{full\text{-}length}$ and nRBP$^{full\text{-}length}$ alone and in binary complexes with DNA.

For the complexes the contribution of DNA to the spectra must be subtracted prior to data evaluation. In other words, it is assumed that binding does not alter the contribution of DNA.

The spectra of rRBP$^{full\text{-}length}$ and nRBP$^{full\text{-}length}$ alone and bound to DNA, after subtraction of the contribution of DNA, are displayed in Figure 3.22(a) and (b). For unbound RBP-Jκ the curves match quite well in the range 220-260 nm, but significant differences are observed in the range 185-215 nm..

Similar results are obtained with RBP-Jκ bound to DNA. In the wavelength range from 185 to 215 nm the maxima are inverted and the general shape of the curves differs. As illustrated in Tables 3.2 and 3.3 by the result of the CONTIN evaluation, none of the programs detects more than 5% difference in any of the classes of secondary structure element considered (helix, sheet, turn, random coil).

As the structure of the *C. elegans* homologue Lag-1 mostly consists of β-sheets, one would expect $nRBP^{full\text{-}length}$ to have a higher contribution of β-sheets than refolded $rRBP^{full\text{-}length}$. The results in Table 3.2 and 3.3 confirm that the beta-sheet content of $nRBP^{full\text{-}length}$ is about 5% higher than that of refolded $rRBP^{full\text{-}length}$, both in the free and bound states, and that this increase occurs mainly at the expense of random coils and to a lesser extent α-helices and turns.

The interpretation of CD results requires some caution and it should be noted that none of the programs predicted the content of β-sheets in $nRBP^{full\text{-}length}$ in the range, found in the crystal structure of Lag-1. All programs gave satisfactory results, however, concerning the proportion of secondary structure elements for the reference data collected with lysozyme. The results of the programs sometimes differ considerably from the judgement of human experts, who more easily recognize considerable changes in secondary structure. The computer programs use singular value decomposition to fit the experimental data by linear combinations of sets of curves representing proteins containing only one secondary structure element. Experience shows that the error range is quite large, so that usually a combination of personal judgement and computer analysis are combined to come to a conclusion. In the present case one would definitely conclude that there are major differences in secondary structure between the native and the refolded RBP-Jκ.

Taken together the assays carried out point to differences in the properties of $rRBP^{full\text{-}length}$ and $nRBP^{full\text{-}length}$ without, however, revealing any obvious cause.

(a)

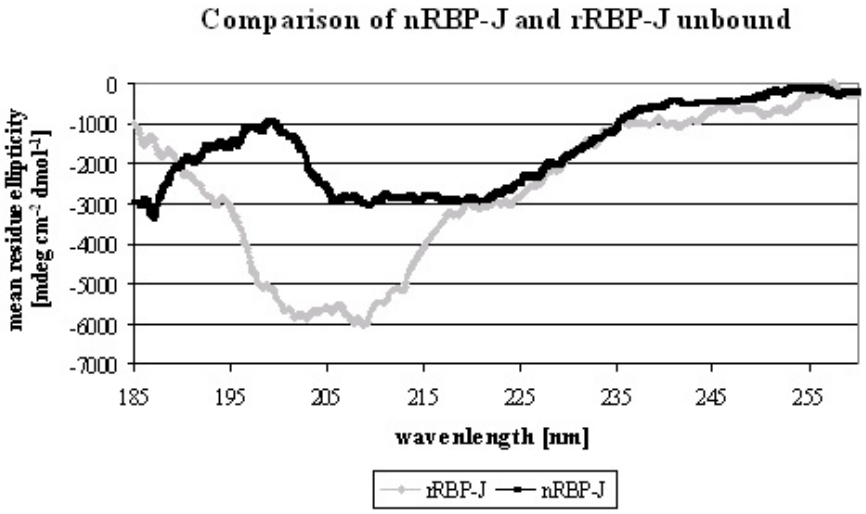

(b)

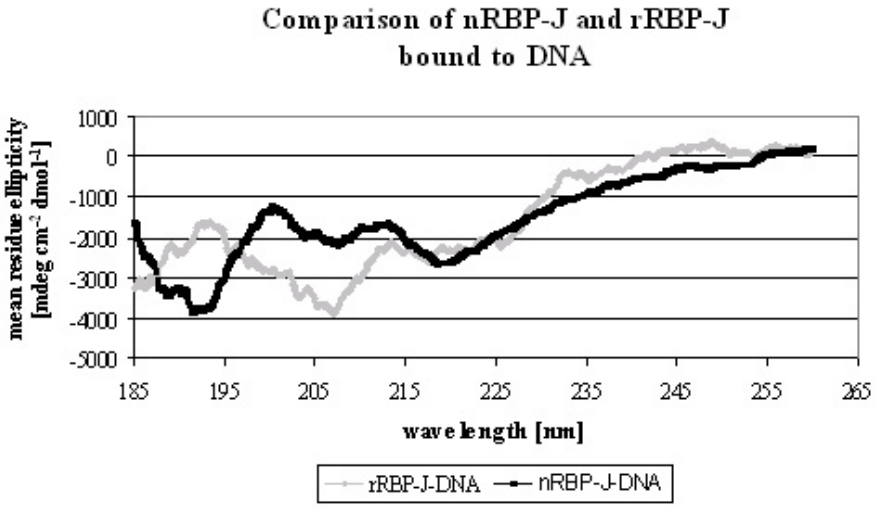

Figure 3.22: CD spectra of **(a)** $rRBP^{full\text{-}length}$ and $nRBP^{full\text{-}length}$ and **(b)** $rRBP^{full\text{-}length}$ and $nRBP^{full\text{-}length}$ bound to DNA; after subtraction of the DNA signal the data was converted from difference ellipticity $\Delta\Phi$ to mean residue ellipticity, which is concentration independent.

rRBP$^{full\text{-}length}$	*α-helix*	*β-sheet*	*Turns*	*Random coil*
Reference set 3	13.4 %	29.3 %	24.8 %	32.6 %
Reference set 4	12.5 %	28.6 %	24.5 %	34.3 %
Reference set 6	9.2 %	24.0 %	19.2 %	47.6 %
Reference set 7	11.2 %	22.7 %	18.3 %	47.8 %
Average	**11.6 %**	**26.2 %**	**21.7 %**	**40.5 %**

nRBP$^{full\text{-}length}$	*α-helix*	*β-sheet*	*Turns*	*Random coil*
Reference set 3	9.9 %	34.6 %	23.4 %	32.0 %
Reference set 4	10.1 %	34.0 %	22.8 %	33.0 %
Reference set 6	7.3 %	30.8 %	19.0 %	43.0 %
Reference set 7	9.1 %	29.2 %	17.9 %	43.8 %
Average	**9.1 %**	**32.2 %**	**20.8 %**	**37.9 %**

Table 3.2: Calculation of secondary structure elements for refolded and native RBP-Jκ with CONTIN. Protein reference sets 3, 4, 6 and 7 were chosen because they are optimized for measurements in the range of 190 to 260 nm.

rRBP$^{full\text{-}length}$**-DNA**	*α-helix*	*β-sheet*	*Turns*	*Random coil*
Reference set 3	9.8 %	32.9 %	24.2 %	33.8 %
Reference set 4	9.9 %	33.0 %	23.3 %	33.0 %
Reference set 6	7.5 %	27.7 %	17.9 %	46.9 %
Reference set 7	8.7 %	27.7 %	17.8 %	45.7 %
Average	**9.0 %**	**27.8 %**	**20.8 %**	**39.9 %**

nRBP$^{full\text{-}length}$**-DNA**	*α-helix*	*β-sheet*	*Turns*	*Random coil*
Reference set 3	9.1 %	35.5 %	22.9 %	31.5 %
Reference set 4	8.0 %	35.7 %	22.8 %	33.5 %
Reference set 6	5.0 %	31.7 %	18.4 %	44.9 %
Reference set 7	6.0 %	30.8 %	16.7 %	46.5 %
Average	**7.0 %**	**33.4 %**	**20.2 %**	**39.1 %**

Table 3.3: Calculation of secondary structure elements for rRBP$^{full\text{-}length}$ and nRBP$^{full\text{-}length}$ bound to DNA with CONTIN.

3.2.2 Formation of ternary complexes with RBP-Jκ, DNA and Notch^{Ram} or Notch^{RamANK}

Both nRBP$^{full\text{-}length}$ and nRBP$^{28\text{-}432}$ were expressed in insect cells because although the corresponding proteins expressed in *E. coli* and refolded (rRBP$^{full\text{-}length}$ and rRBP$^{28\text{-}432}$) bind DNA they did not bind Notch^{Ram} or Notch^{RamANK} (see section 3.2.3), nor peptides derived from Notch^{Ram}. Exemplary ITC data sets collected with nRBP$^{full\text{-}length}$ and the ligands mentionned above are shown in Figure 2.7 in section 2.2.6. Interestingly, this difficulty did not occur with the proteins derived from EBNA2, for which binding to rRBP$^{full\text{-}length}$ can be detected on radioactive EMSAs (data not shown).

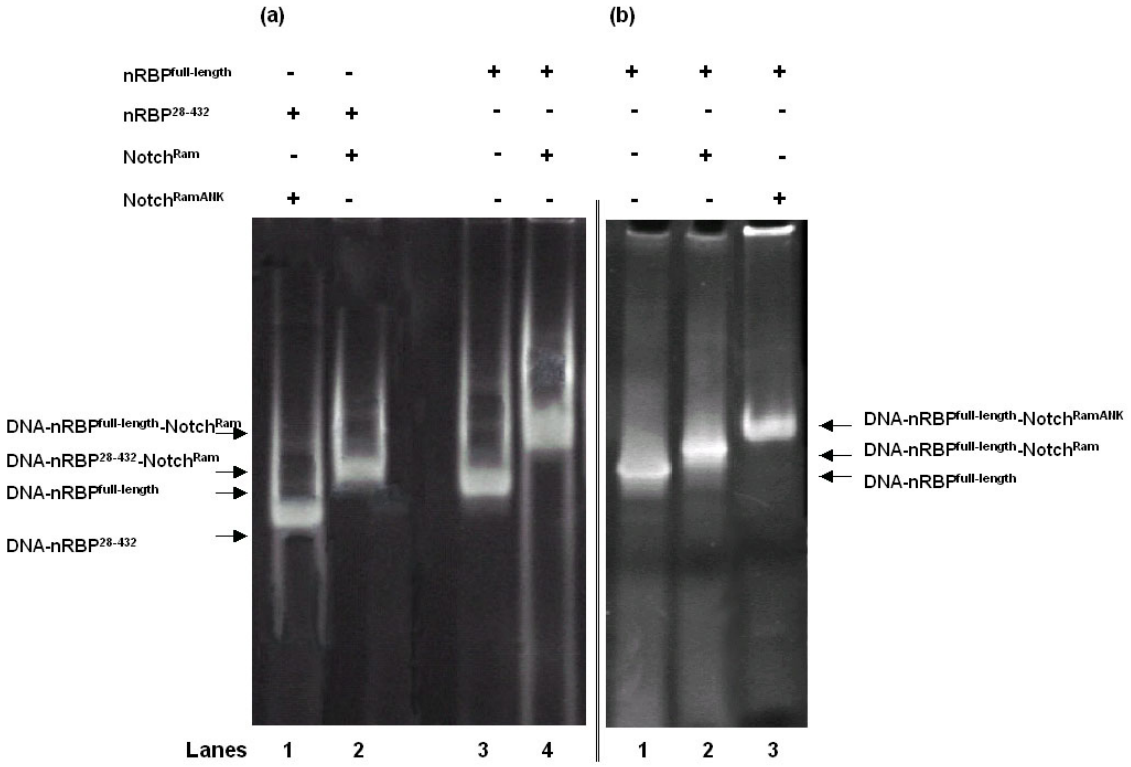

Figure 3.23: Analysis of the ability of nRBP$^{28\text{-}432}$ and nRBP$^{full\text{-}length}$ to form binary and ternary complexes with DNA and proteins derived from human Notch1 (Ram and RamAMK) by non-radioactive EMSA. Analysis was carried out with 2 µg nRBP$^{full\text{-}length}$ or nRBP$^{28\text{-}432}$ and the corresponding amount of oli-Cp^{23} and Notch^{Ram} expressed in *E. coli* to form 1:1:1 complexes. **(a)**: Comparison of the ability of nRBP$^{28\text{-}432}$ and nRBP$^{full\text{-}length}$ to form ternary complexes with DNA and Notch^{Ram}. Lane1: DNA-nRBP$^{28\text{-}432}$; lane 2: DNA-nRBP$^{28\text{-}432}$-Notch^{Ram}; lane 3: DNA-nRBP$^{full\text{-}length}$; lane 4: DNA-nRBP$^{full\text{-}length}$-Notch^{Ram}; **(b)**: Non-radioactive EMSA gel comparing the binary DNA-nRBP$^{full\text{-}length}$ complex (lane 1) with the ternary DNA-nRBP$^{full\text{-}length}$-Notch^{Ram} and DNA-nRBP$^{full\text{-}length}$-Notch^{RamANK} complexes (lanes 2 and 3).

Ternary complexes were formed with $nRBP^{28-432}$ and $nRBP^{full-length}$ as described in section 2.2.5. Prior to the effort to further purify the complex the ability of the components to form complexes was tested by non-radioactive EMSA. Figure 3.23 shows the first trials to form ternary complexes with $Notch^{Ram}$ and $Notch^{RamANK}$. Figure 3.23(a) shows a non-radioactive EMSA with both proteins forming complexes with DNA and $Notch^{Ram}$ proving full activity for both of them in this assay. The binding to $Notch^{RamANK}$ is displayed in Figure 3.23(b).
Size exclusion chromatography and analysis with non-radioactive EMSA showed the presence of ternary complexes after addition of $Notch^{Ram}$ or $Notch^{RamANK}$ proteins (examples are illustrated in Figure 3.24). An exemplary chromatogram is displayed in 3.11 showing the peak of the complex eluting just after the void volume of the column (40 ml). As in the case of the complex formed by nRBP and DNA the elongated DNA molecule causes the complex to elute at a higher volume than expected from its size. To confirm the activity of the ternary complex and exclude aggregation, the peak was analysed with non-radioactive EMSA and subsequently stained with ethidium bromide and Coomassie Brilliant Blue.

Following page:

Figure 3.24: Final purification of ternary complexes formed with $nRBP^{28-432}$, oli-Cp^{19} and protein derived from human Notch1 (Ram and RamANK) using size exclusion chromatography. Blue curves: Absorption at 280 nm; red curves: Absorption at 260 nm. The fractions of the peaks obtained were pooled, concentrated and analysed by SDS PAGE and non-radioactive EMSA. **(a)** Purification of DNA-$nRBP^{28-432}$-$Notch^{Ram}$ on a S75 16/60 size exclusion column (Amersham); the SDS PAGE gel, where a 10 µl sample was applied, shows the presence of both protein components, the non-radioactive EMSA gel shows the supershift caused by binding of $Notch^{Ram}$ to the binary DNA-$nRBP^{28-432}$ complex (10 µl sample obtained from size exclusion chromatography) in comparison to a binary DNA- $nRBP^{28-432}$ complex (1 µg), which was formed prior to the ternary complex. **(b)** Purification of DNA-$nRBP^{28-432}$-$Notch^{RamANK}$ on a S200 16/60 size exclusion column (Amersham); the SDS PAGE gel shows the presence of both protein components in the first two peaks (lanes 1 and 2) and the separated TEV protease applied to cleave of the 6xHis-tag from both protein components (lanes 3 and 4); the non-radioactive EMSA gel shows, however, that only the 2^{nd} peak (lane 2) contains DNA and thus corresponds to a ternary complex.

(a) Purification of DNA-nRBP$^{28-432}$-Notch^{Ram}

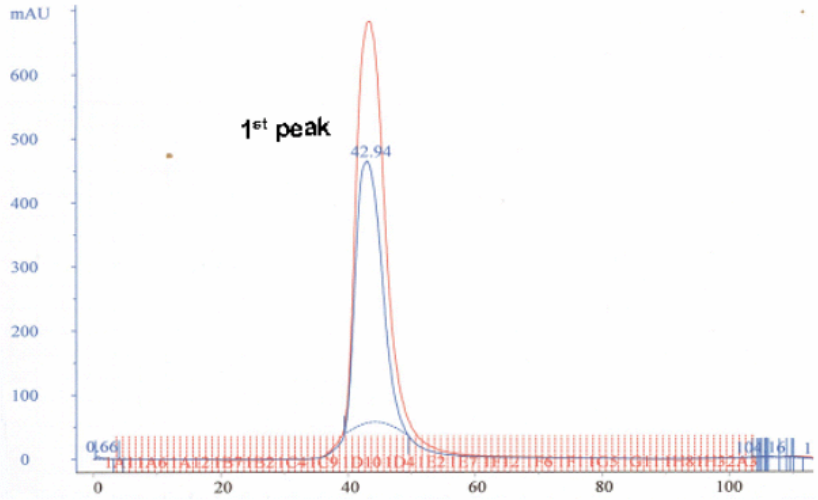

SDS PAGE stained with Coomassie Brilliant Blue

native PAGE stained with Ethidium Bromide

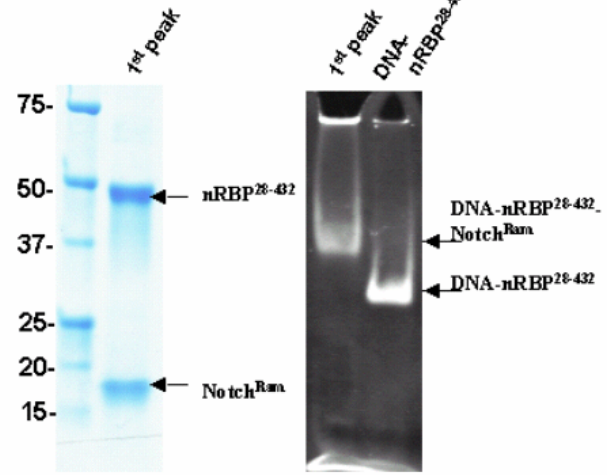

(b) Purification of DNA-nRBP$^{full-length}$-Notch^{RamANK}

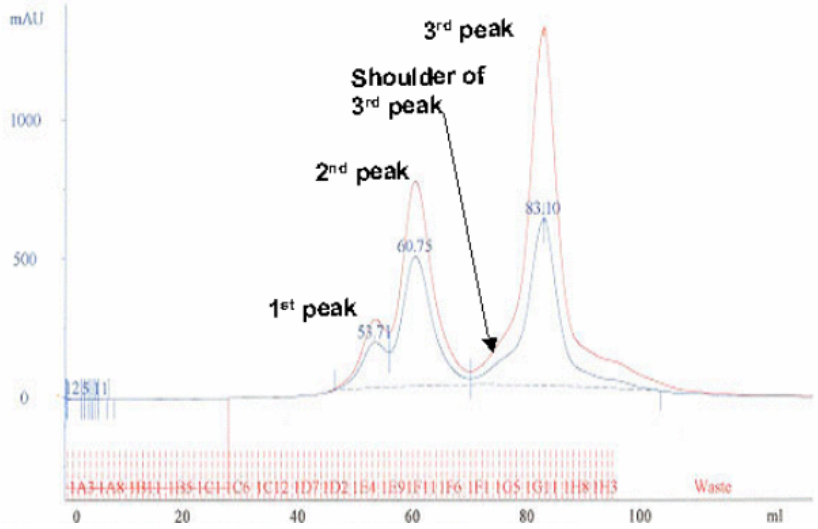

SDS PAGE stained with Coomassie Brilliant Blue

native PAGE stained with Ethidium Bromide

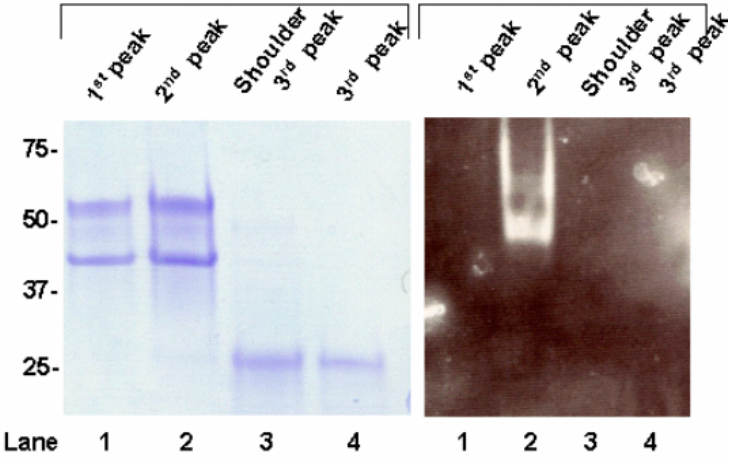

Evidence for the folding of Notch^{Ram} upon binding to nRBP$^{full\text{-}length}$

The Ram domain of Notch1 has previously been reported to be unfolded (Nam et al., 2003). The hypothesis that upon binding to nRBP$^{full\text{-}length}$ Ram folds into a unit consisting of the usual secondary structure elements was verified by CD spectroscopy. For this study the ternary complex of Notch^{Ram} with nRBP$^{full\text{-}length}$ and DNA (oli-Cp^{16})was examined. To calculate the contribution of Notch^{Ram} to the spectrum of the ternary complex the contribution of the binary complex between nRBP$^{full\text{-}length}$ and DNA was subtracted before converting the data into mean residue ellipticity. The spectra obtained are depicted in Figure 3.25, and the results obtained with CONTIN are listed in table 3.4.

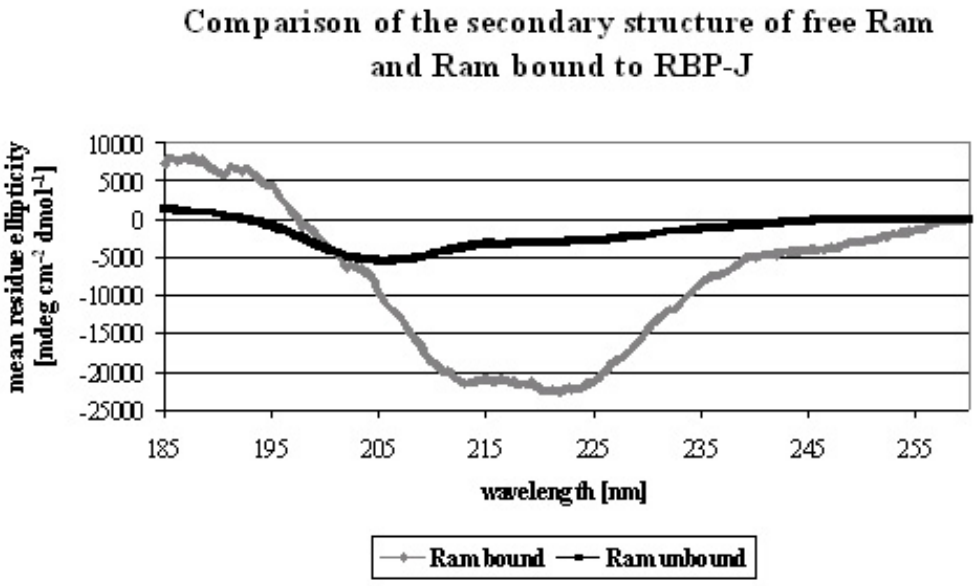

Figure 3.25: CD spectra of free Notch^{Ram} and Notch^{Ram} bound to nRBP$^{full\text{-}length}$-DNA; after subtraction of the contribution of nRBP$^{full\text{-}length}$-DNA to the ternary complex the data was converted from difference ellipticity ΔΦ to mean residue ellipticity.

If turns are considered as fairly unstructured patches the unfolded part of free Notch^{Ram} adds up to about 60 % of the protein. Two thirds of the remaining part (~27 %) correspond to β-sheets and one third (~13 %) to α-helices. Major changes are detected after binding of Notch^{Ram} to nRBP$^{full\text{-}length}$: the contribution of β-sheets drastically diminishes and that of turns also moderately decreases whereas that of α-helices and the percentage of random coils slightly increases. The calculated increase in the proportion of α-helices indicates a major change in the secondary structure of Notch^{Ram} upon binding nRBP$^{full\text{-}length}$. Although,

as already mentioned, one has to be very cautious in the interpretation of secondary structure calculation from CD data, in the present case the changes before and after Ram binding, which are obvious for the human eye are also detected by the programs. Usually one considers a difference of 5 %, in this case between bound and unbound Ram, as significant.

Notch^{Ram} unbound	*α-helix*	*β-sheet*	*Turns*	*Random coil*
Reference set 3	19.2 %	28.2 %	23.2 %	29.4 %
Reference set 4	13.5 %	29.3 %	23.6 %	32.7 %
Reference set 6	10.8 %	24.5 %	17.8 %	47.0 %
Reference set 7	12.2 %	24.1 %	16.6 %	47.1 %
Average	**13.9 %**	**26.6 %**	**20.4 %**	**39.1 %**

Notch^{Ram} bound	*α-helix*	*β-sheet*	*Turns*	*Random coil*
Reference set 3	39.1 %	8.0 %	17.8 %	35.1 %
Reference set 4	35.9 %	8.0 %	22.9 %	33.1 %
Reference set 6	32.4 %	6.2 %	7.7 %	52.7 %
Reference set 7	33.8 %	6.5 %	16.2 %	43.5 %
Average	**35.3 %**	**7.2 %**	**16.2 %**	**41.1 %**

Table 3.4: Calculation of secondary structure elements for free Notch^{Ram} and Notch^{Ram} bound to nRBP$^{full-length}$-DNA with the program CONTIN. Reference sets 3, 4, 6 and 7 were chosen, because they are optimized for measurement in the range of 190 to 260 nm. The average content of secondary structure elements is calculated from the values obtained with all reference sets.

3.2.3 Contribution of the ANK domain to RBP-Jκ binding

RBP-Jκ purified from insect cells binds to Notch^{Ram} or Notch^{RamANK} only at high concentrations

EMSAs with radiolabelled DNA were used to show binding of a binary complex of nRBP$^{full-length}$ and DNA to the Notch constructs. Figure 3.26 shows a representative EMSA with nRBP$^{full-length}$ bound to oli-Cp^{40}. Increasing amounts of Notch^{Ram} or Notch^{RamANK} were added, but only with a 1250-fold excess of Notch^{RamANK} could a supershift be observed,

which given the large excess of ternary complex partner can no longer be considered to be specific. No supershift was observed with the Notch^{Ram} protein. Since EMSAs with radiolabelled oligonucleotides are very sensitive, this indicates that no binding occurred, contradicting the results obtained with non-radioactive EMSA (see e.g. Figure 3.23), size exclusion chromatography (Figure 3.24) and ITC (tables 3.5 and 3.6 below).

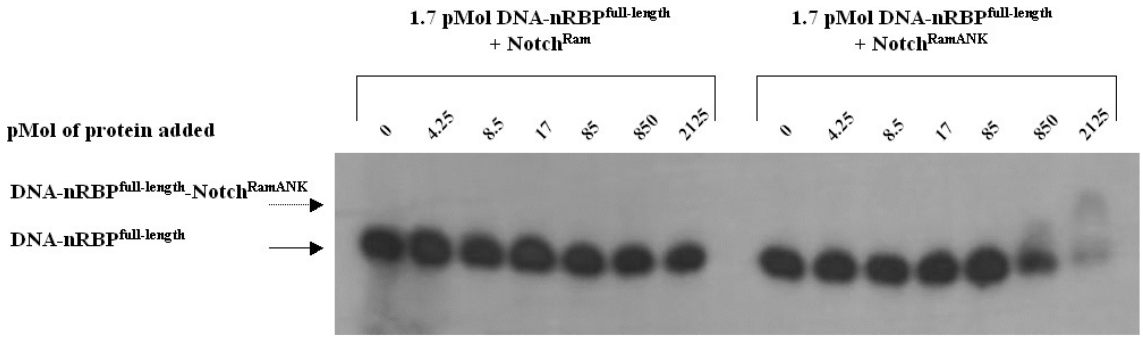

Figure 3.26: Representative EMSA to analyse the ability of nRBP$^{full\text{-}length}$ to form ternary complexes with Notch^{Ram} or Notch^{RamANK} . The assay was carried out using radiolabelled oli-Cp^{40} to form a 1:1 complex with 1.7 pMol nRBP$^{full\text{-}length}$; amounts of ternary complex partner added are indicated at the top of the respective lane. Lanes 1 to 7: attempt to form a ternary complex with nRBP$^{full\text{-}length}$-DNA and increasing amounts of Notch^{Ram}; lanes 8 to 14: ternary complex formation with nRBP$^{full\text{-}length}$-DNA and increasing amounts of Notch^{RamANK}; lanes 1 and 8: binary complex, following lanes. nRBP$^{full\text{-}length}$:Notch-protein ratios: 1:2.5; 1:5; 1:10; 1:50; 1:500; 1:1250

Protein-protein complexes sometimes only form in a narrow range of conditions. Therefore the experiment was repeated with amounts of protein comparable to those used in the non-radioactive EMSA before (µg instead of ng) on a 4 % TBE gel. The radiolabelled oligonucleotide was replaced by a non-labelled one. Before application to the gel, ethidium bromide was added to all samples. Ethidium bromide intercalates into DNA and RNA and can be visualised by its fluorescence upon irradiation with UV light. Other intercalators, such as SybrGreen, are known to change the running properties of the DNA and/or DNA-protein-complexes. Even if pre-incubation with ethidium bromide changed the running properties of the samples it would be expected to do so proportionally and the result would be the same as that obtained with samples stained after the run. The results of the experiment are displayed in the left panel of Figure 3.27. To sharpen the visible bands the experiment was repeated with an 8% TBE gel, as illustrated in Figure 3.27 in the right panel. Not only could the running behaviour of the complexes be improved, but the supershift of the ternary complexes is more clearly visualised.

The ability of nRBP$^{full\text{-}length}$ in a binary complex with DNA to form ternary complexes with Notch^{Ram} or Notch^{RamANK} depends on the concentration of Notch^{Ram} or Notch^{RamANK}. This suggests that one is dealing with an equilibrium corresponding to a relatively low affinity. To check the activity of Notch^{Ram} and Notch^{RamANK} protein, an experiment similar to the one displayed in Figure 3.26 was performed in a non-radioactive EMSA.

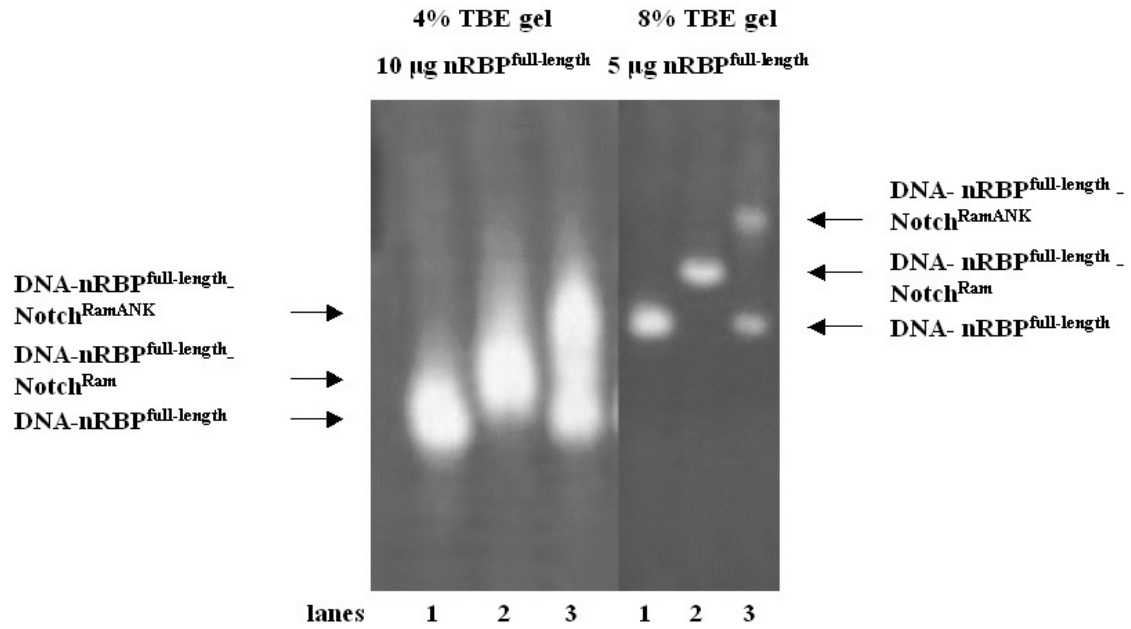

Figure 3.27: Ternary complex formation of nRBP$^{full\text{-}length}$ with oli-Cp^{22} and proteins derived from human Notch1 (Ram and RamANK) analysed on 4% and 8% TBE non-radioactive EMSA gels. Ternary complexes were formed by addition of twice the stoichiometric amount of Notch protein to 10 and 5 µg nRBP$^{full\text{-}length}$ in the 4 % and 8% TBE PAGE gels. Lanes 1: Binary DNA-nRBP$^{full\text{-}length}$ complex; lanes 2: ternary DNA-nRBP$^{full\text{-}length}$-Notch^{Ram} complex; lanes 3: ternary DNA-nRBP$^{full\text{-}length}$-Notch^{RamANK} complex.

As illustrated in Figure 3.28 it was possible to form both ternary complexes with Notch^{Ram} (Figure 3.28(a)) and Notch^{RamANK} (Figure 3.28(b)). In both cases the ternary complex appeared as soon as the corresponding Notch protein was added in 1:1 molar ratio. In this condition about 70% of binary complex formed by nRBP$^{full\text{-}length}$ and DNA was transferred to a ternary complex. When Notch^{Ram} or Notch^{RamANK} was added in 1:2 molar ratio 100% nRBP$^{full\text{-}length}$ bound to DNA was present in the ternary complex. This indicates that both ternary complex partners exhibit between 50 and 100% biological activity, if one assumes that they have the maximum achievable concentration dependent binding affinity.

The additional band in the Coomassie Brilliant Blue stain in Figure 3.28(b) in the lanes where the amount of ternary complex partner exceeds that of binary complex (lanes 5 to 8)

corresponds to free excess Notch^{RamANK} protein which could not bind to nRBP$^{full\text{-}length}$-DNA. A corresponding band could not be detected for the Notch^{Ram} protein in Figure 3.28(a), but there is a smear with increasing intensity as larger amounts of excess protein are added to the binary complex.

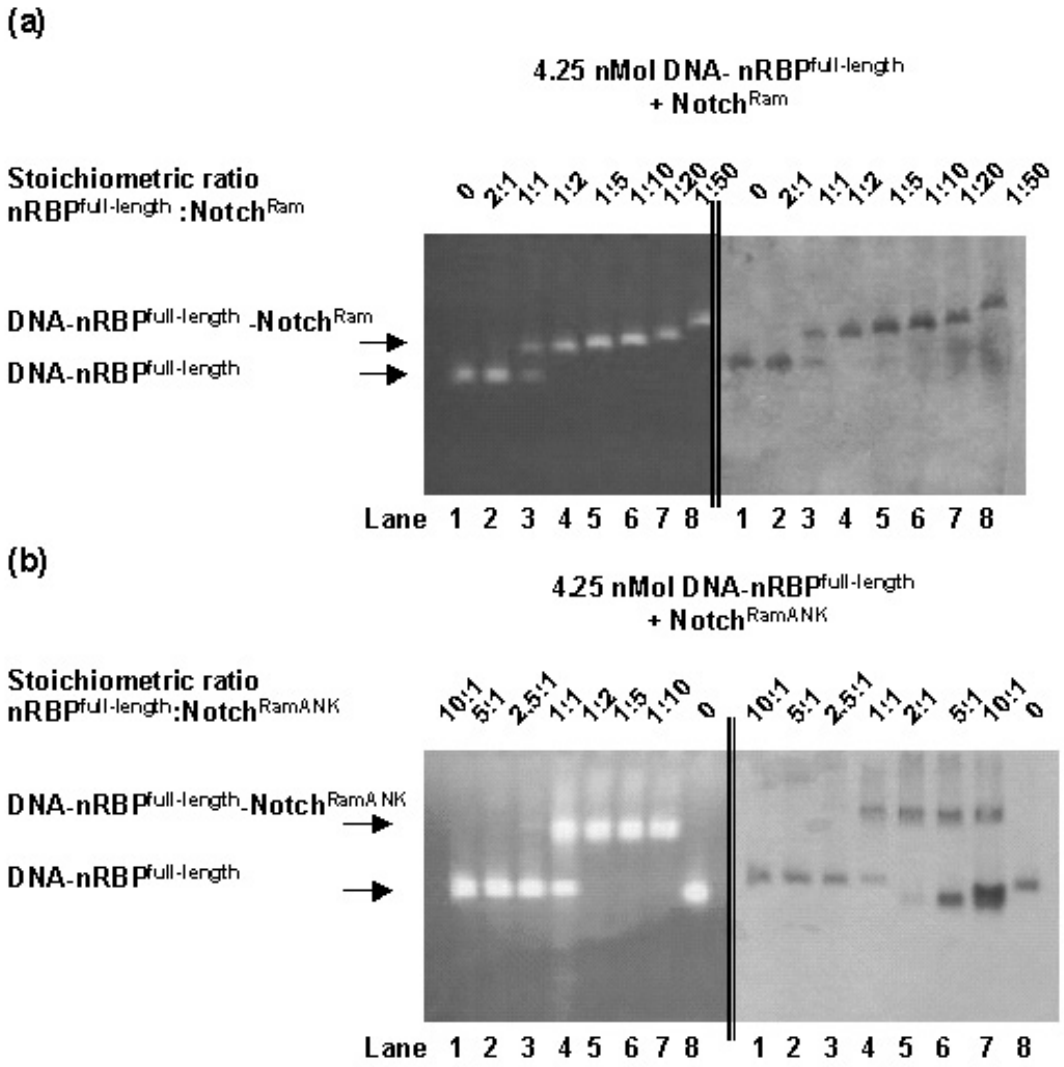

Figure 3.28: Non-radioactive EMSA successively stained with ethidium bromide (left panel) and Coomassie Brilliant Blue (right panel) to study the binding affinity of Notch^{Ram} and Notch^{RamANK} to 4.25 nMol binary complex formed with oli-Cp^{22} and nRBP$^{full\text{-}length}$. The first lane in (a) and the last one in (b) were loaded with DNA- nRBP$^{full\text{-}length}$ without ternary complex partner added. Molar ratios of binary complex:ternary complex partner are indicated at the top of each lane. **(a)** Increasing amounts of Notch^{Ram} are added to 5 µg DNA-nRBP$^{full\text{-}length}$. The ternary DNA-nRBP$^{full\text{-}length}$-Notch^{Ram} complex is visible as soon as Notch^{Ram} is added to DNA-nRBP$^{full\text{-}length}$ in 1:1 stoichiometric ratio. **(b)** Decreasing amounts of Notch^{RamANK} are added to 5 µg DNA-nRBP$^{full\text{-}length}$. As in (a) the ternary DNA-nRBP$^{full\text{-}length}$-Notch^{RamANK} complex is visible as soon as Notch^{Ram} is added to DNA-nRBP$^{full\text{-}length}$ in 1:1 stoichiometric ratio.

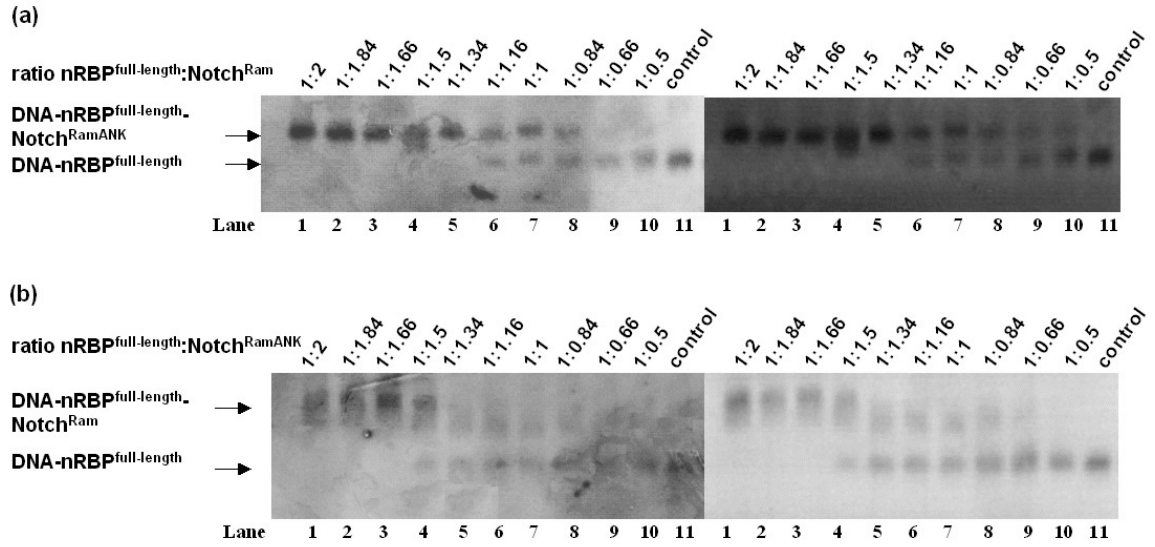

Figure 3.29: Non-radioactive EMSA to determine the amount of protein necessary for Notch^{Ram} and Notch^{RamANK} to bind to 5 µg nRBP$^{full\text{-}length}$, which corresponds to 4.25 nMol. nRBP$^{full\text{-}length}$ was incubated with the stoichiometric amount of oli-Cp^{22} to form a 1:1 complex: **(a)** Notch^{Ram} as ligand; **(b)** Notch^{RamANK} as ligand; gels were successively stained with Coomassie Brilliant Blue (left panel) and ethidium bromide (right panel); stoichiometric ratios between binary complex and ligand are indicated above the respective lane. A control comprising the binary DNA- nRBP$^{full\text{-}length}$ complex was applied in lanes 11.

Luciferase reporter assays and GST pull-down assays have led to the conclusion that the ankyrin domain of Notch-IC participates in the binding to RBP-Jκ, albeit weakly compared to the Ram domain, but sufficiently to possibly have an effect on transactivation efficiency (Kato et al., 1997; Kurooka et al., 1998; Tani et al., 2001). In contrast, in our EMSAs no visible difference could be detected in the binding affinity of Notch^{Ram} and Notch^{RamANK}. As illustrated in Figure 3.28, formation of ternary complex can be detected with both Notch constructs as soon as the Notch:RBP-Jκ stoichiometric ratio is 1:1. RBP-Jκ is quantitatively bound at all ratios above 1:1. To be able to estimate the real difference in a narrower range the experiment illustrated in Figure 3.28 was repeated with a stoichiometric range of nRBP-J$^{full\text{-}length}$:Notch^{Ram} and nRBP-J$^{full\text{-}length}$:Notch^{RamANK} of 1:0.5 to 1:2. The result is displayed in Figure 3.29, where the small difference between the binding affinities becomes even clearer. Here the ternary complex with Notch^{RamANK} is visible at a stoichiometric ratio of 1:0.66, whereas the ternary complex with Notch^{Ram} can already be detected at a ratio of 1:0.5. Visual detection is difficult, however, if only because of the

logarithmic sensitivity of the human eye, so that reliable estimations cannot be made in this range.

The affinities of Notch^{Ram} and Notch^{RamANK} for RBP-Jκ measured by ITC are nearly equal

To confirm the results obtained with EMSA and obtain more quantitative results, ITC experiments were carried out with both Notch proteins. Notch^{Ram} and Notch^{RamANK} were used to titrate the binary nRBP$^{full\text{-}length}$-DNA complex according to the protocol described in section 2.2.6. During the experiment the heat evolved or absorbed is detected, and as the concentration of ligand and protein are known the thermodynamic parameters of the reaction can be calculated.

Each experiment was repeated three times and evaluated as described in section 2.2.6. Except for the first experiment conducted with Notch^{Ram} as ligand (see table 3.5), which yielded a slightly different enthalpy change, all experiments gave similar results for the stoichiometry (N) of the reaction, the binding constant and the enthalpy (ΔH) change. As expected, the stoichiometry of the reaction was 1:1 in both cases. As the experimental errors are of the order of 15 - 20% for the binding constant the small difference observed between the two ligands is not significant.

The results for the experiments conducted with Notch^{RamANK} listed in table 3.6 are based on the assumption that there is a single binding site for the ligands.

If one assumes, however, that there are two binding sites in the case of Notch^{RamANK}, the calculated affinities for nRBP$^{full\text{-}length}$ are the same for both the Ram domain and the ankyrin repeats, in contrast to previous reports in the literature (Kato et al., 1997; Kurooka et al., 1998), which are partly based on *in vivo* assays. The results obtained do not exclude the presence of two similar binding sites, but the shape of the binding curve is incompatible with the existence of two sites with significantly different affinities.

Three of the experiments were carried out at 25 ºC instead of 20 ºC to detect a possible temperature dependence of the parameters characterising the equilibrium but none was found. According to tables 3.5 and 3.6 the values for ΔH and K_a are similar, so that major differences in the binding properties of Notch^{Ram} and Notch^{RamANK} can be excluded.

Models of the binary DNA-RBP-Jκ and ternary DNA-RBP-Jκ-Notch^{RamANK} complexes obtained by small angle x-ray scattering (SAXS)

The high sequence identity between the conserved domains of *C. elegans* Lag-1, for which a high resolution crystal structure is available (Koval et al., 2004), and human RBP-Jκ suggests that the structures of the two proteins should have a very similar secondary structure content and arrangement of elements. Superposition of the conserved domain of

Experiment no.	Ram 1	Ram 2	Ram 3	Ram 4
T (°C)	20	20	25	25
ΔH ± σ(ΔH) [kcal/mole]	-1.08 x 10^4 ±160.2	-1.35 x 10^4 ±233.2	-1.26 x 10^4 ±127	-1.26 x 10^4 ±119
N ± σ(N)	0.988±0.01	1.08±0.008	0.953±0.006	0.952±0.006
K_a ± σ(K_a) [M^{-1}]	6.93 x 10^6 ±1.31x10^6	1.92 x 10^7 ±4.4x10^6	6.03 x 10^6 ±1.03x10^6	6.52 x 10^6 ±1.07x10^6

Table 3.5: Thermodynamic parameters of the binding of Notch^{Ram} to nRBP$^{full-length}$-DNA (16 bp). With a given temperature T the parameters ΔH (enthalpy change) and N (stoichiometry of the reaction) can be calculated.

Experiment no.	RA 1	RA 2	RA 3
T (°C)	20	20	25
ΔH ± σ(ΔH) [kcal/mole]	-1.16 x 10^4±102.2	-1.14 x 10^4±103.5	-1.13 x 10^4±153.0
N ± σ(N)	0.97±0.005	1.01±0.005	1.05±0.008
K_a ± σ(K_a) [M^{-1}]	1.21 x 10^7±2.04x10^6	7.57 x 10^6±1.04x10^6	7.59 x 10^6±1.6x10^6

Table 3.6: Thermodynamic parameters of the binding of Notch^{RamANK} to nRBP$^{full-length}$-DNA (16 bp).

RBP-Jκ (aa 28 to 432) with the Lag-1 structure using the program MODELLER (http://salilab.org/modeller/) resulted in ten models. As the program can only model the same number of amino acids as present in the model structure, the additional N- and C-terminal parts could not be taken into account. Figure 3.30 represents the calculated model with the best statistics superimposed on the Lag-1 structure to visualize the equal overall fold. There are considerable differences in the loop regions, which are the least predictable. Within the DNA-binding region of RBP-Jκ the differences in the loop regions, which

interact mainly with DNA are, however, smaller than those within non DNA-binding loop regions, although the DNA has not been taken into account in the calculation.

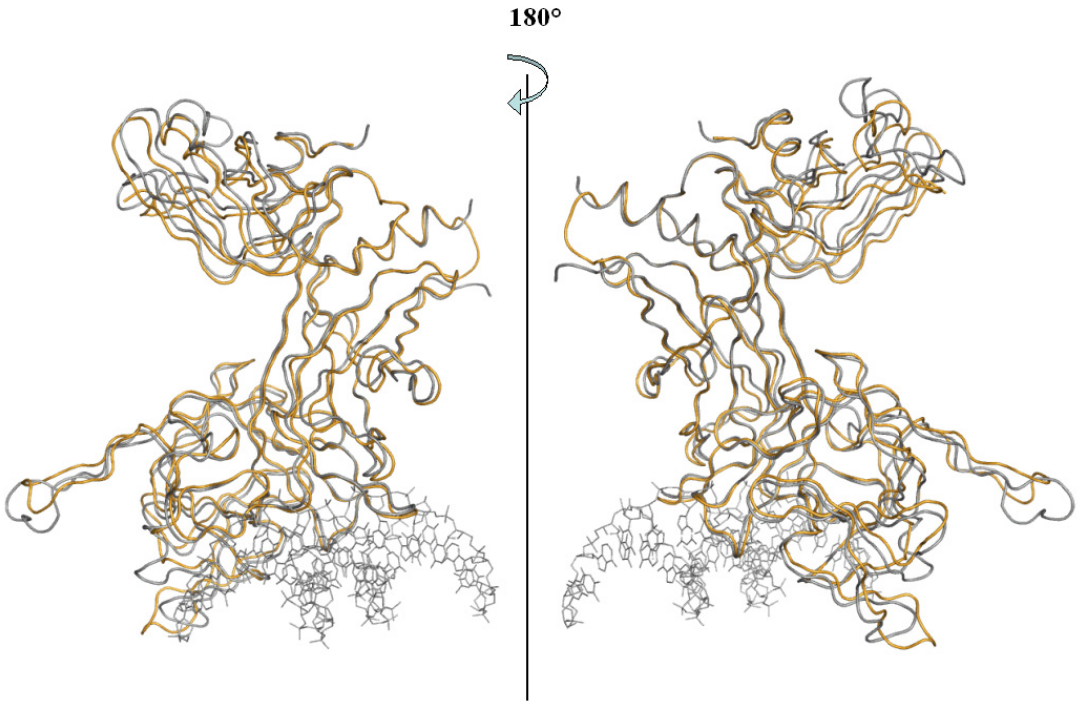

Figure 3.30: Superposition of the Lag-1-DNA crystal structure (grey) and the best model obtained after fitting aa 28 to 432 of human RBP-Jκ (orange) into this crystal structure with MODELLER (http://salilab.org/modeller/). The two views differ by a 180º rotation of the molecule.

Since the DNA binding sites of both proteins are conserved to a higher extent than other loop regions without comparable known interaction sites, this result appears consistent.

These predictions were verified by SAXS. This technique provides low-resolution information on the overall shape of a molecule and can provide useful insights in conformational changes occurring upon binding of interaction partners and the participation of defined parts of the molecules in the interaction.

The experiment was conducted as described in section 2.2.7. The shape, or envelope, of the macromolecule in solution can be calculated *ab initio* from the scattering curve. Additional knowledge, if available, can be used to set up restraints in the calculation of the envelope. For example, in the presence of a complex of molecules one can specify the requirement or exclusion of contacts between amino acids of two different molecules, e. g. as result of mutational analyses.

After *ab initio* calculation of the shape of the binary complex with the program DAMMIN (Svergun et al., 2001) the DNA-Lag-1 binary complex structure model was used as a starting point for the interpretation of the SAXS data. The shape obtained by *ab initio* calculations did not satisfactorily correspond to the Lag-1 model, because DAMMIN does not take into account that DNA contributes twice as much to the scattering intensity, which artificially increases the size of the resulting envelope.

The binary RBP-Jκ-DNA complex studied here consists of full-length RBP-Jκ, which comprises 39 aa more at the N-terminus and 54 more at the C-terminus than the domain conserved in each member of the CSL-family of transcription factors. Calculations with the program BUNCH (Petoukhov and Svergun, 2005) confirmed that addition of two bodies corresponding to the additional portions in nRBP-Jκ at the N- and the C-terminus compared to the model of the binary complex could yield a theoretical scattering curve, which fits the experimental data.

Other information obtained with bioinformatical methods suggested that the additional parts present in nRBP-$J^{full\text{-}length}$ compared to the conserved fragment may be very elongated. Secondary structure predictions with full-length RBP-Jκ (figure 3.31) suggest that the N-terminal first 39 aa, including the His-tag are unfolded. The additional 54 aa present in full-length human RBP-Jκ are predicted on the basis of comparison with the crystallized Lag-1 protein part to contain an eight aa long α-helix, with the remaining stretch being unfolded.

The program SASREF (Petoukhov and Svergun, 2005) is able to calculate theoretical scattering curves from molecules with partially known structure. For the additional portions to be included into the model, the program creates a number of different models and tries to obtain the best fit between the theoretical scattering curve of the complete model and the experimental data. Models of the binary complex calculated with SASREF show indeed, that a theoretical scattering curve calculated from a combination of the binary complex and two additional proteins at the N- and the C-terminus fits when the model has very elongated N- and C- termini (figure 3.32: scattering curves, figure 3.33: model).

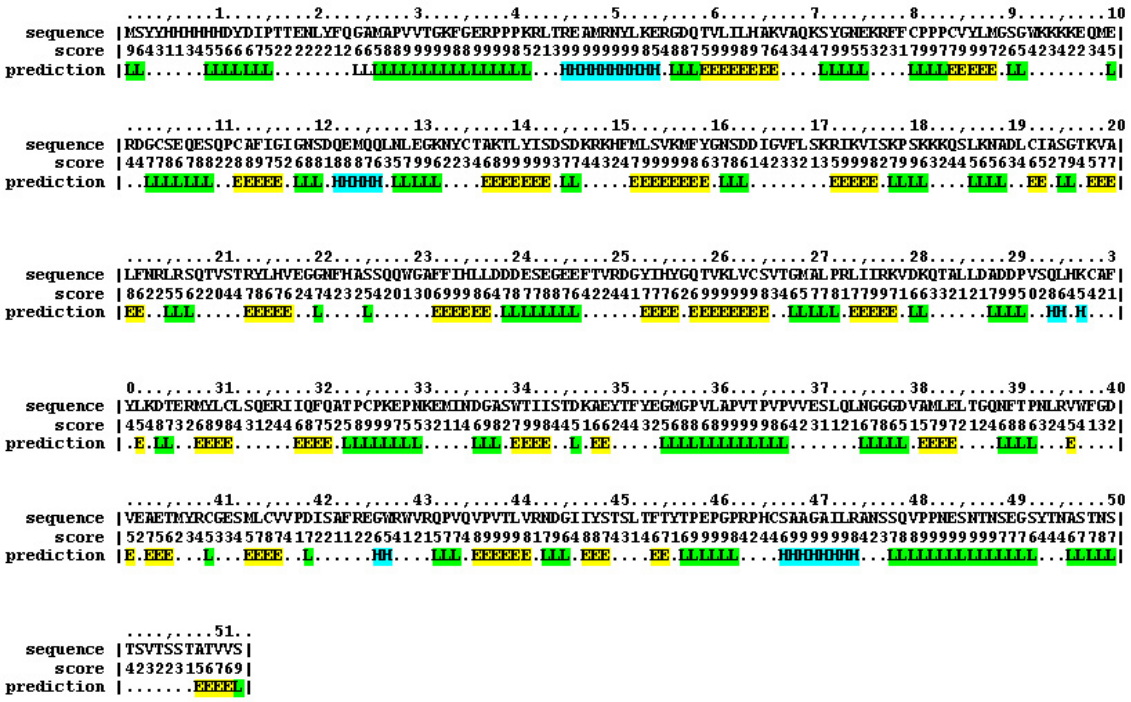

Figure 3.31: Secondary structure prediction for human 6xHis-RBP-Jκ as used for interpretation of the SAXS data. Secondary structure elements are highlighted in green (loops), yellow (β-sheets) or light blue (α-helices). The probability score for the prediction is listed under the aa sequence. A score of five and above predicts the existence of a particular element.

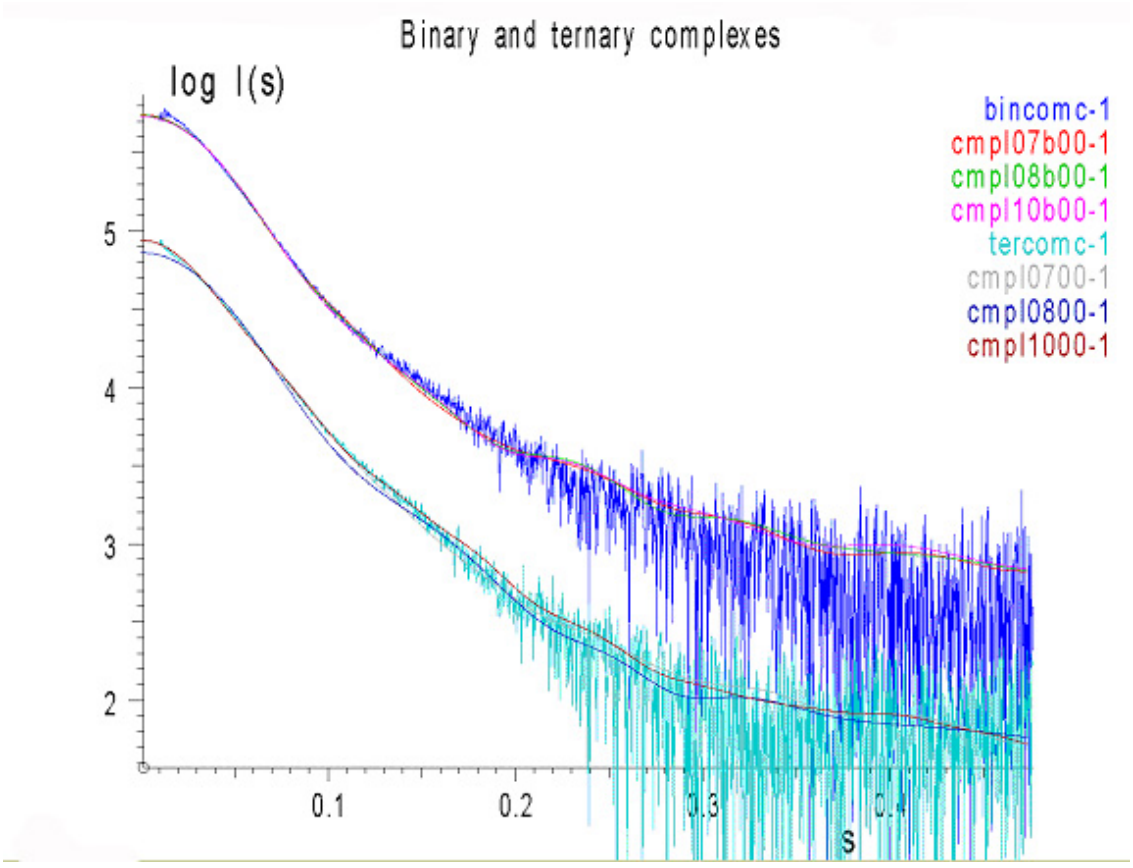

Figure 3.32: Fit of the three best model scattering curves of the binary DNA-nRBP$^{full\text{-}length}$ and the ternary DNA-nRBP$^{full\text{-}length}$-Notch^{RamANK} complex to the experimental scattering data. Blue curve: experimental scattering of the binary complex; red, green and magenta curves: theoretical scattering patterns of the three calculated models. Pale green curve: experimental scattering of the ternary complex; grey, dark blue and brown curves: theoretical scattering curves of three calculated models for the ternary complex. The grey and brown curves are derived from the model assuming that the ankyrin repeats do not participate in binding nRBP$^{full\text{-}length}$. The dark blue curve is derived from the model assuming the interaction of nRBP$^{full\text{-}length}$ with the ankyrin repeats. Theoretical radius of gyration R_g and chi-values for the models of the binary complexes: compl07b R_g=2.95 nm, chi: 2.616; compl08b: R_g=2.94 nm, chi: 2.673; compl09b: R_g=2.91 nm, chi: 3.093. Theoretical radius of gyration R_g and chi values for the models of the ternary complexes: compl07: R_g=4.01 nm, chi: 2.460; compl08: R_g=3.15 nm, chi: 3.663; compl09: R_g=4.08 nm, chi: 2.462.

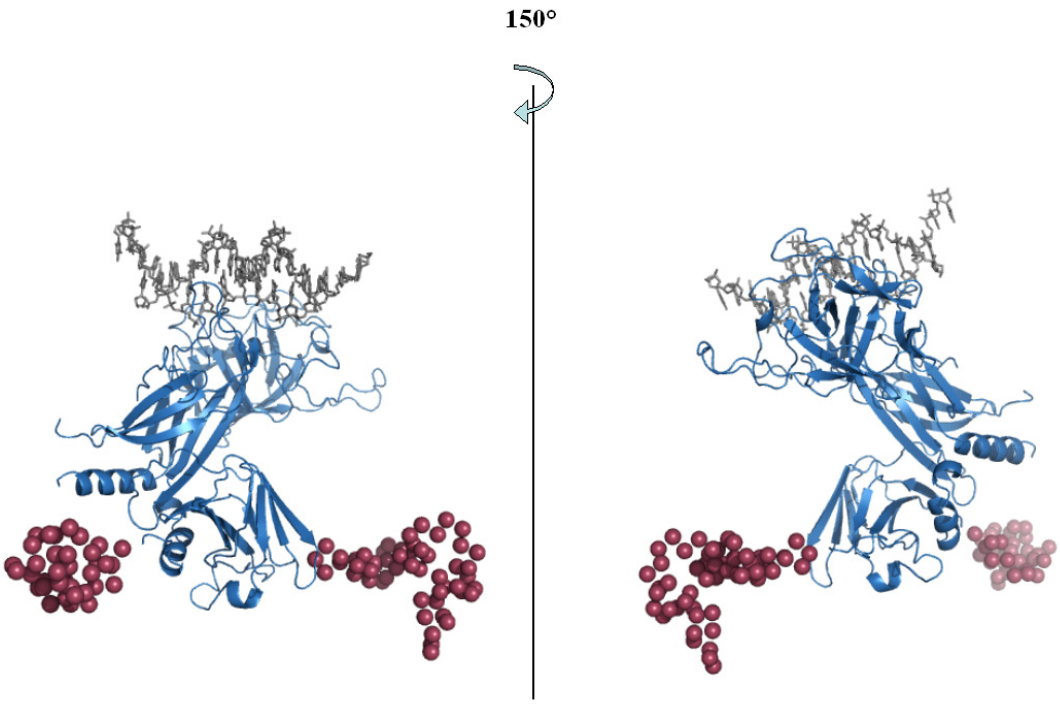

Figure 3.33: Model of the binary DNA-nRBP$^{full\text{-}length}$ complex (cmpl07b from Figure 3.31); blue: nRBP$^{full\text{-}length}$ fitted onto the Lag-1 crystal structure (PDB-code: 1TTU); gray: 16 bp double-strand DNA with a double T- or A-overhang at the 5'-end; red pheres: additional amino acids present in nRBP$^{full\text{-}length}$, but missing in the Lag-1 crystal structure, modeled with SASREF (Petoukhov and Svergun, 2005).

To study conformational changes and the contribution of Ram and the ankyrin repeats to the binding to RBP-Jκ a ternary complex of DNA-nRBP$^{full\text{-}length}$-Notch^{RamANK} was also analyzed by SAXS. Comparison of scattering data of the ternary complex with the results of model calculations using SASREF was used to investigate the role of the ankyrin repeats of Notch^{RamANK} in binding RBP-Jκ, which had been previously found to be at most very weak (see section 3.2.2).

Preliminary calculations showed that a model, where no contribution of the ankyrin repeats to the binding of RBP-Jκ was assumed gave a better fit to the experimental data than the one requiring an interaction of the ankyrin repeats. After fitting Ram by assuming it to adopt mostly α-helical structure and therefore replacing it by a molecule exhibiting such a structure, the stretch consisting of the seven ankyrin repeats was located in such a way that the entire complex was less compact and more elongated than the first one. More exact calculations of the ternary complex were done with SASREF, including the binary complex, Notch-Ram and Notch-ANK, to obtain the best fit to the experimental data. Because of their low complexity the additional portions of the binary complex have not

been taken into account in the calculations for the ternary complex. Even with a very flexible Ram domain it was almost impossible to obtain a model where the ANK domain participates in the interaction with RBP-Jκ. A superposition of the calculated theoretical scattering curves of the different models with the experimental data (see figure 3.32) together with the corresponding chi-values clearly indicates that none of the compact models assuming the participation of the ankyrin repeats in binding RBP-Jκ fits the experimental scattering data (model see figure 3.34). In contrast, an excellent agreement is found for elongated models where the ankyrin repeats point away from the interaction site of Ram with RBP-Jκ (model in figure 3.35).

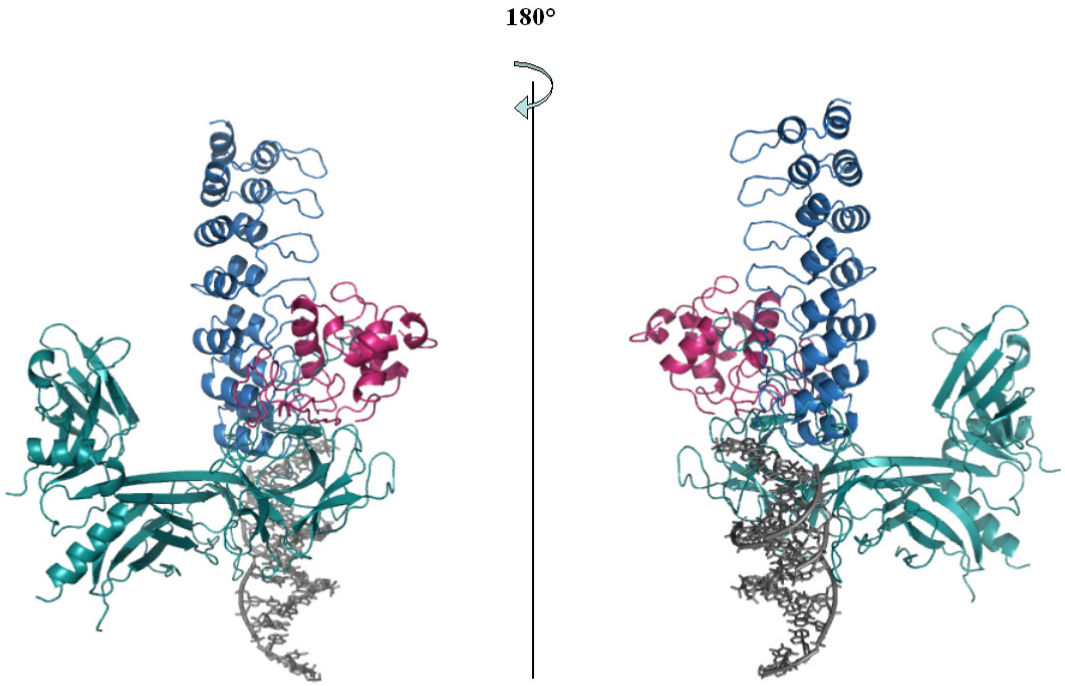

Figure 3.34: Model of the ternary DNA-nRBP$^{full\text{-}length}$-Notch^{RamANK} complex assuming the participation of the ankyrin repeats in the interaction with nRBP$^{full\text{-}length}$; models of this type (e.g. cmpl080 in Figure 3.32) give a much poorer fit to the experimental data than those in Figure 3.35. Green: nRBP$^{full\text{-}length}$ fitted onto the Lag-1 crystal structure (PDB-code: 1TTU); red: α-helical protein structure as dummy molecule representing the Ram domain (PDB-code 1HEW); blue: seven ankyrin repeats created from the crystal structure of six Notch1 ankyrin repeats plus one additional taken from the same structure (PDB-code: 1YYH).

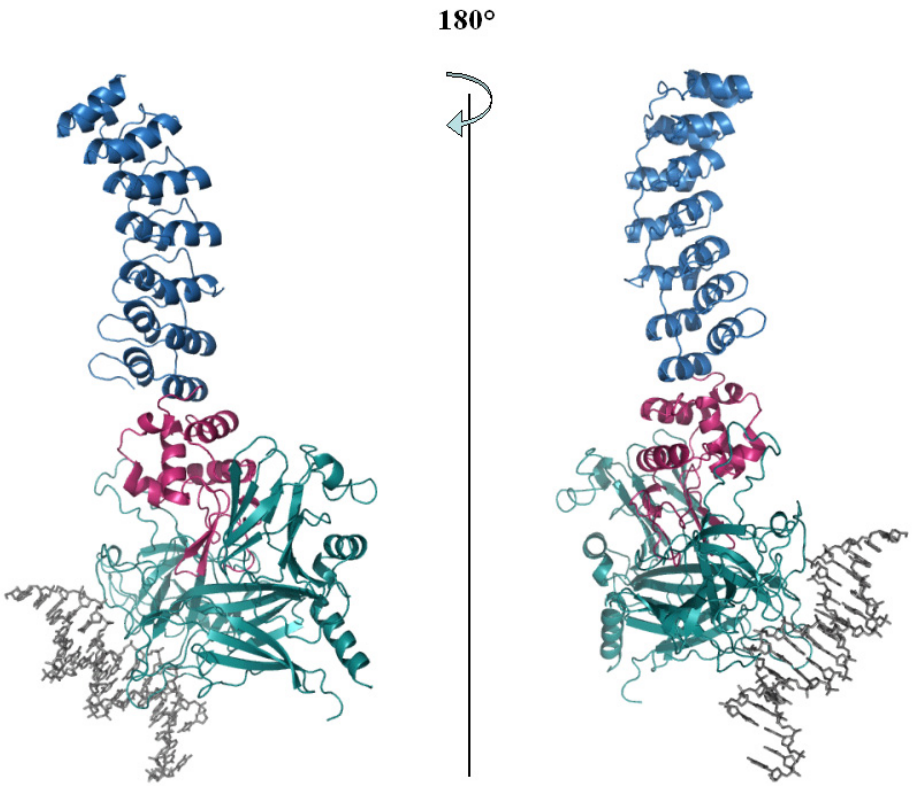

Figure 3.35: Model of the ternary DNA-nRBP$^{full\text{-}length}$-Notch^{RamANK} complex without participation of the ankyrin repeats in the interaction. Models of this type give the best fit to the experimental data (e.g. cmpl070 in Figure 3.32). Green: nRBP$^{full\text{-}length}$ fitted onto the Lag-1 crystal structure (PDB-code: 1TTU); red: dummy molecule representing the Ram domain; blue: seven ankyrin repeats created by extending the crystal structure of six Notch1 ankyrin repeats by one additional unit taken from the same structure (PDB-code: 1YYH).

To ensure that SASREF was not used with too much bias information *ab initio* calculations were carried out with the program DAMMIN. The calculated envelope was superimposed on the model which gave the best fit using SASREF. The superposition reveals a surprisingly accurate fit as illustrated in figure 3.36.

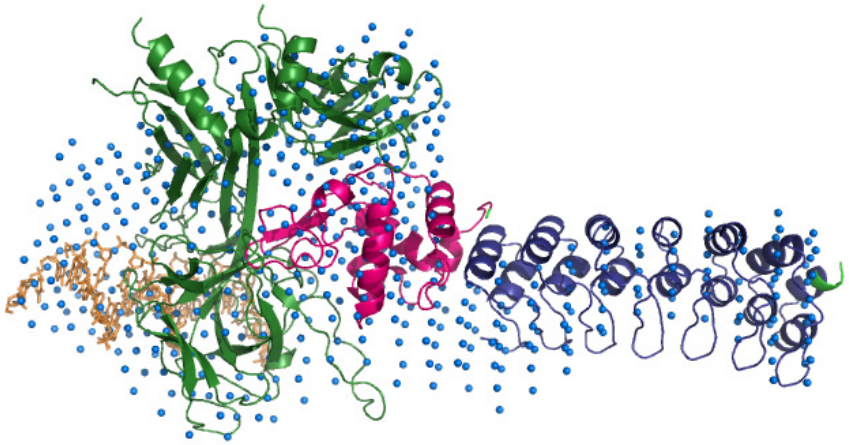

Figure 3.36: Superposition of an *ab initio* calculated envelope of a DNA-nRBP$^{full\text{-}length}$-Notch^{RamANK} ternary complex measured by SAXS and a model created by combining the known structural features. RBP-Jκ is coloured green, the 16 bp double-strand DNA with single-strand two-base overhangs at each 5'-end is coloured yellow; The part of the complex comprising the Notch Ram domain is coloured magenta, the seven ankyrin repeats blue. The envelope calculated *ab initio* from the experimental scattering curve by the program DAMMIN is represented by light blue spheres.

3.2.4 The affinity of EBNA2$^{259\text{-}435}$ to nRBP$^{full\text{-}length}$ is two orders of magnitude higher than that of Notch^{RamANK}

Notch is a cellular transmembrane receptor, which has an intracellular domain that translocates to the nucleus upon activation by its ligands. Due to the lack of expressed ligands under cell culture conditions no Notch-signalling occurs so that usually only very low amounts of Notch-IC can be found in the nucleus. Even after activation only comparably few Notch-IC molecules are present in the nucleus, which are rapidly degraded to quickly terminate the signal. Binding to any interaction partner can thus be expected to be very strong.

EBNA2 is the viral analogue of Notch-IC and regulates the latency phase of Epstein-Barr virus in the cell. The concentrations of the protein in the nucleus are not known, but should be sufficiently high to allow efficient interaction with the appropriate regulatory proteins activating the transcription of EBNA2 target genes.

Since only the Ram domain and the seven ankyrin repeats (ANK) located near the Ram domain of Notch-IC are involved in the binding to RBP-Jκ (Tamura et al., 1995; Tani et al., 2001) it is sufficient to compare binding to EBNA2$^{259-435}$ with constructs comprising the Ram domain and the Ram domain coupled to ANK.

EMSAs were therefore carried out with the available Notch constructs Notch^{Ram} and Notch^{RamANK} and with the EBNA2$^{259-435}$ construct, which contains the conserved CR5 and CR6 regions of EBNA2, the latter of which is involved in RBP-Jκ-binding (Ling et al., 1993), as well as CR7, fused to an N-terminal GST-tag.

To exclude a possible participation of the GST-tag in the binding to nRBP$^{full-length}$ control experiments were carried out with all oligonucleotides used, i. e. oli-Cp^{40}, oli-LMP1P^{36} and oli-LMP2AP^{54}. Binding to DNA alone was checked as well as binding to a binary nRBP$^{full-length}$-DNA complex in comparison with EBNA2$^{259-435}$. The results of these control experiments are shown in Figure 3.37. A supershift of the binary nRBP$^{full-length}$-DNA complex upon binding of EBNA2$^{259-435}$ is clearly visible in all three cases, whereas no supershift can be observed when purified GST (kindly provided by S. Maier, GSF Munich) is added to the binary complex. The experiment also proves that GST alone does not bind to DNA.

As illustrated in Figure 3.26 Notch^{Ram} or Notch^{RamANK} do not bind to nRBP$^{full-length}$ in a radioactive EMSA where up to 10 ng nRBP$^{full-length}$ corresponding to a final concentration of about 8 nM are available. In contrast, binding occurs in gels run under the same conditions but with a larger amount of the two proteins (5 µg nRBP$^{full-length}$ and twofold excess Notch^{Ram} and Notch^{RamANK}) resulting in a final concentration of 4.25 µM nRBP$^{full-length}$ (see Figures 3.28 and 3.29). In contrast, binding of EBNA2$^{259-435}$ to nRBP$^{full-length}$ occurs even when only very small amounts of protein are put into the reaction, as illustrated in Figure 3.37, indicating that its affinity for nRBP$^{full-length}$ is much higher than that of Notch^{RamANK}.

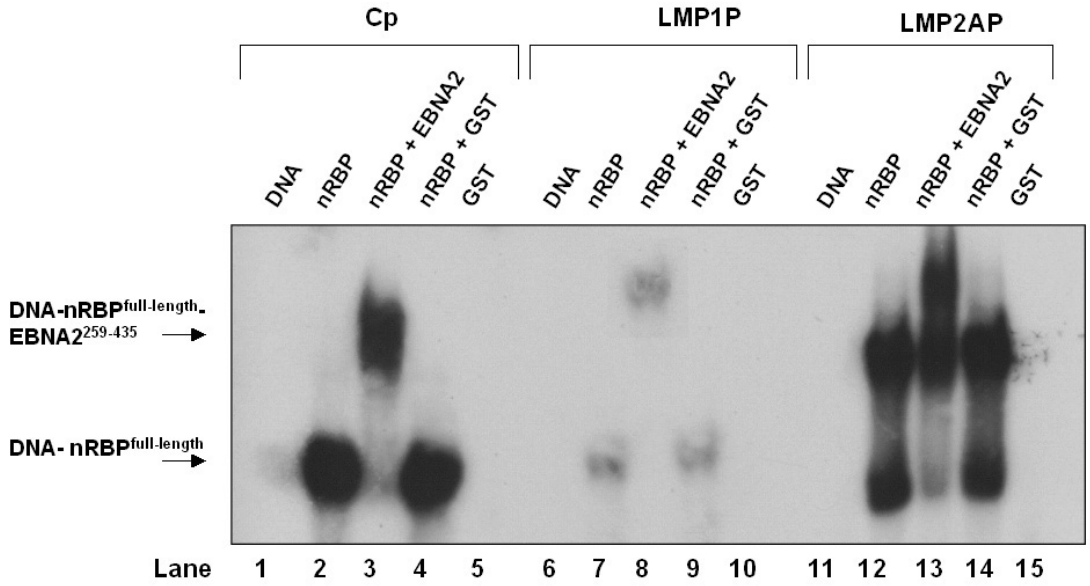

Figure 3.37: Radioactive EMSA to estimate the affinity of EBNA2$^{259-435}$ for a binary DNA-nRBP$^{full-length}$ complex and to examine the capacity of GST to bind to nRBP$^{full-length}$ or DNA in the absence of other components. Binding of GST is tested with radioactively labelled double-stranded DNA oligonucleotides derived from the viral Cp, LMP1P and LMP2AP, as indicated at the top of the figure**.** 5 ng of nRBP$^{full-length}$ were supplemented with equimolar amounts of EBNA2$^{259-435}$ or GST. Arrows mark the binary complex DNA-nRBP$^{full-length}$ and the complex formed by nRBP$^{full-length}$-EBNA2$^{259-435}$. Since it is impossible to distinguish the complex formed with the two binding sites on oli-LMP2AP^{54} occupied by nRBP$^{full-length}$ and the corresponding complex containing one nRBP$^{full-length}$ and one EBNA2$^{259-435}$ spots have not been marked by arrows.

To compare the binding affinities of nRBP$^{full-length}$ and Notch as well as of nRBP$^{full-length}$ and EBNA2$^{259-435}$ directly, radioactive EMSAs were run with amounts of protein comparable to those used for non-radioactive EMSAs stained with ethidium bromide and Coomassie Brilliant Blue. The main difficulty in such an experiment arises from the high amount of protein that can bind DNA, which gives a signal that is too strong for interpretation. To guarantee a detectable and interpretable signal an appropriate amount of non-labelled DNA derived from the same promoter, which competes with the radioactively labelled DNA for the available nRBP$^{full-length}$ molecules, must be added. In the following experiments an amount of non-labelled DNA binding 95% of the available nRBP$^{full-length}$ molecules was therefore added to each sample.

Figure 3.38 shows the interaction of Notch^{RamANK} and EBNA2$^{259-435}$ with nRBP$^{full-length}$ bound to oli-Cp^{40}. In the case of Notch^{RamANK}-nRBP$^{full-length}$ the interaction, which is revealed by the supershift marked nRBP$^{full-length}$-Notch^{RamANK}, is only detectable when 5 µg nRBP$^{full-length}$ (corresponding to a protein concentration of 4.25 µM) and 10 µg Notch (9.5µM) or 1 µg nRBP$^{28-432}$ (0.85 µM) and 2 µg Notch (1.7 µM), respectively, are mixed and run on the gel. With amounts below 1 µg, the binary complex nRBP$^{full-length}$-DNA is visible but the supershift caused by the binding of Notch^{RamANK} disappears. The same series was repeated for nRBP$^{full-length}$ and EBNA2$^{259-435}$. The supershift caused by the binding of EBNA2$^{259-435}$ to nRBP$^{full-length}$-DNA is visible down to 10 ng nRBP$^{full-length}$ (8.5 nM) and 20 ng EBNA2$^{259-435}$ (17.5 nM), respectively. The very different binding behaviour of the interaction partners under the same conditions - amounts of proteins per reaction and constant 1:2 stoichiometric ratio - indicates that EBNA2$^{259-435}$ has a higher affinity for nRBP$^{full-length}$ than Notch^{RamANK}.

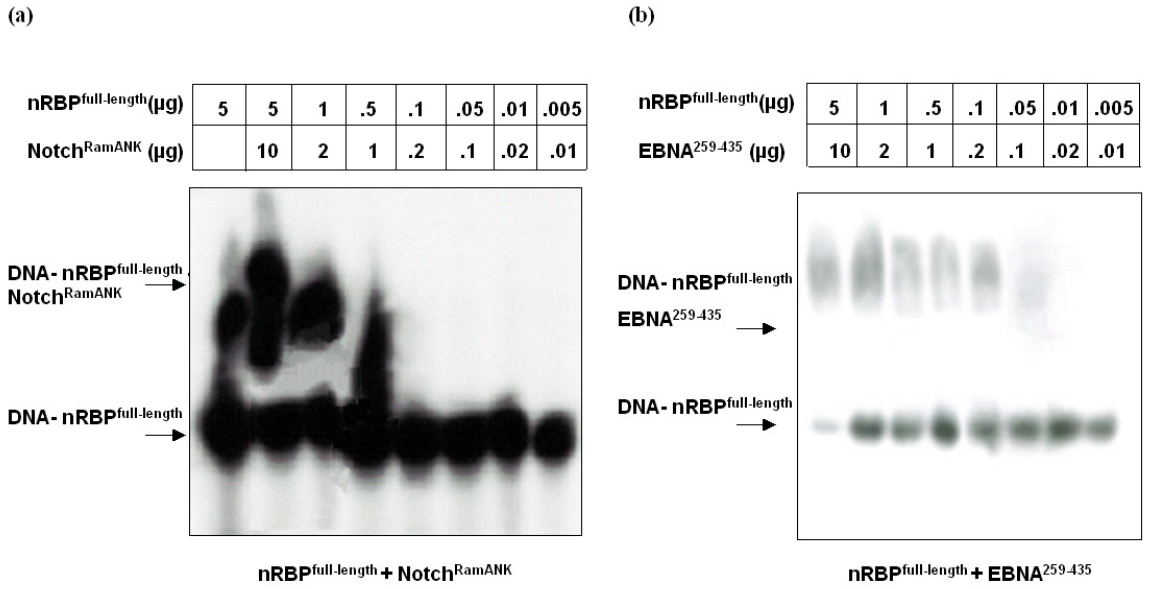

Figure 3.38: Representative EMSA to compare the binding affinity of **(a)** Notch^{RamANK} and **(b)** EBNA2$^{259-435}$ to nRBP$^{full-length}$. Amounts of nRBP$^{full-length}$ and Notch^{RamANK} or EBNA2$^{259-435}$, respectively, taken to form complexes are indicated at the top of each lane. A constant 1:2 molar ratio of the respective proteins (nRBP$^{full-length}$:ternary complex partner) was utilized to form ternary complexes on radioactively labelled oli-Cp^{40} and non-labelled oligonucleotide of the same kind sufficient to bind 95 % of the available protein. The band corresponding to the ternary DNA-nRBP$^{full-length}$-Notch^{RamANK} complex is no longer detectable when less than 500 ng nRBP$^{full-length}$ and 1 µg Notch^{RamANK} are applied, whereas the band

corresponding to the ternary complex DNA-nRBP$^{full\text{-}length}$-EBNA2$^{259\text{-}435}$ is still visible when only 50 ng nRBP$^{full\text{-}length}$ and 100 ng EBNA2$^{259\text{-}435}$ are applied.

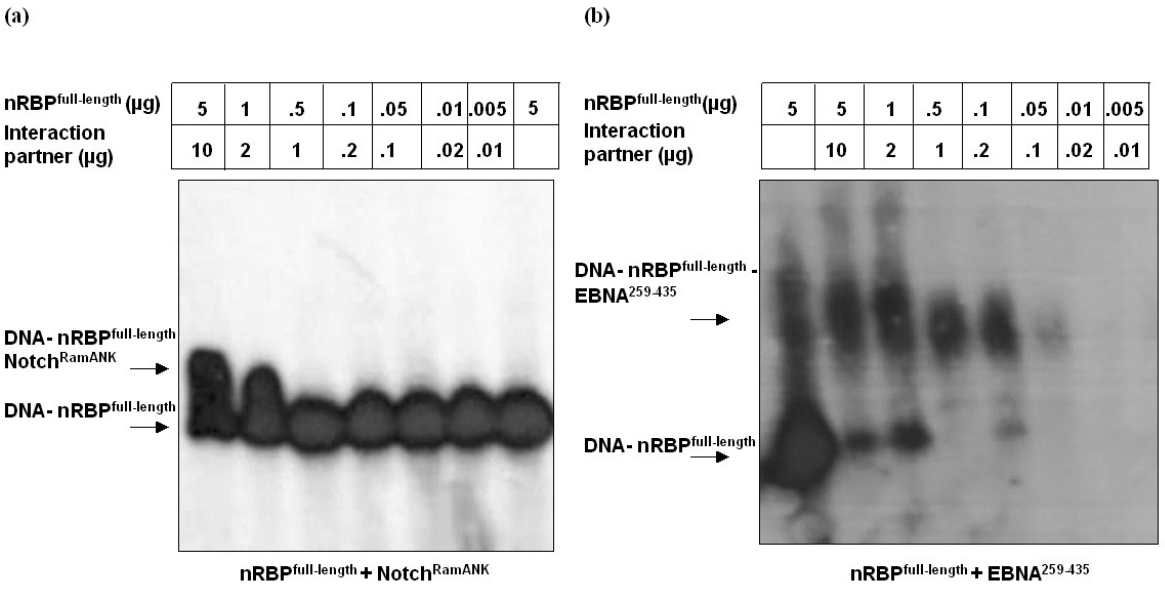

Figure 3.39: Representative EMSA to compare the binding affinity of Notch^{RamANK} **(a**) and EBNA2$^{259\text{-}435}$ **(b)** to nRBP$^{full\text{-}length}$. Amounts of nRBP$^{full\text{-}length}$ and Notch^{RamANK} or EBNA2$^{259\text{-}435}$, respectively, taken to form complexes are indicated at the top of each lane. A constant 1:2 molar ratio of the respective proteins (nRBP$^{full\text{-}length}$:ternary complex partner) was utilized to form ternary complexes on radioactively labelled oli-LMP1P^{36}. The band corresponding to the ternary DNA-nRBP$^{full\text{-}length}$-Notch^{RamANK} complex is no longer detectable when less than 1 µg nRBP$^{full\text{-}length}$ and 2 µg Notch^{RamANK} are applied, whereas the band corresponding to the ternary complex DNA-nRBP$^{full\text{-}length}$-EBNA2$^{259\text{-}435}$ is still visible when only 10 ng nRBP$^{full\text{-}length}$ and 20 ng EBNA2$^{259\text{-}435}$ are applied.

To test whether this behaviour depended on the oligonucleotide to which nRBP$^{full\text{-}length}$ binds, similar experiments were carried out with nRBP$^{full\text{-}length}$ bound to oli-LMP1P^{36}, which is known to bind the nRBP$^{full\text{-}length}$-EBNA2$^{259\text{-}435}$ complex much more tightly than oligonucleotides derived from Cp. As illustrated in Figure 3.39 the same tendency could be observed with the only difference that the ternary complex formed by nRBP$^{full\text{-}length}$-EBNA2$^{259\text{-}435}$-oli-LMP1P^{36} was still detectable when only 20 ng EBNA2$^{259\text{-}435}$ were put into the binding mix. The difference is most striking in the case of oli-LMP2AP^{54}. The left panel of Figure 3.40 shows a series of complexes of RBP-Jκ and Notch^{RamANK} at constant 1:2 molar ratio but with decreasing amounts of the two proteins. At high concentrations

both RBP-Jκ binding sites on oli-LMP2AP[54] are occupied. The lower the amount of protein added, the lower the occupancy of the second binding site on the oligonucleotide. Amounts of nRBP[full-length] below 10 ng result exclusively in binding to a single site in oli-LMP2AP[54]. The supershift caused by binding of Notch[RamANK] is only visible on one binding site.

Amounts of Notch[RamANK] below 1 µg do not cause a supershift of nRBP[full-length] bound to the first binding site, but a faint band corresponding to a supershift can still be observed when 10 ng of EBNA2[259-435] are added to 5 ng nRBP[full-length].

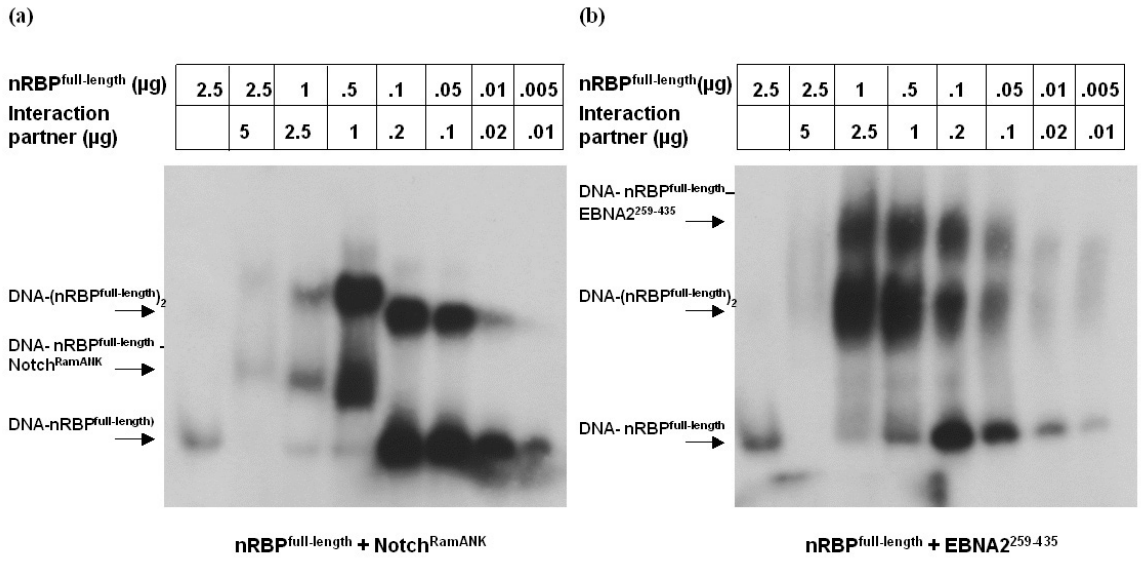

Figure 3.40: Representative EMSA to compare the binding affinity of Notch[RamANK] **(a)** and EBNA2[259-435] **(b)** to nRBP[full-length]. Amounts of nRBP[full-length] and Notch[RamANK] or EBNA2[259-435], respectively, taken to form complexes are indicated at the top of each lane. A constant 1:2 molar ratio of the respective proteins (nRBP[full-length]:ternary complex partner) was utilized to form ternary complexes on radioactively labelled oli-LMP2AP[54]. The band corresponding to the ternary DNA-nRBP[full-length]-Notch[RamANK] complex is no longer detectable when less than 0.5 µg nRBP[full-length] and 1 µg Notch[RamANK] are applied, whereas the band corresponding to the ternary complex DNA-nRBP[full-length]-EBNA2[259-435] is still visible when only 5 ng nRBP[full-length] and 10 ng EBNA2[259-435] are applied.

The EBNA2[259-435] protein used for EMSAs was purified using the N-terminal GST-tag to bind to glutathione sepharose. This tag was not cleaved off since GST is believed not to interfere with the binding of EBNA2[259-435] to nRBP[full-length]. GST is known to form dimers so that two molecules of EBNA2[259-435] bind to one nRBP[full-length] molecule in any case. This

explains why no supershift corresponding to that of Notch^{RamANK} bound to nRBP$^{full\text{-}length}$ on the first binding site of LMP2AP is observed. In contrast, the supershift caused by the EBNA2$^{259\text{-}435}$ dimer binding to nRBP$^{full\text{-}length}$ occupying both binding sites on LMP2AP is still visible when only 5 ng nRBP$^{full\text{-}length}$ and 10 ng EBNA2$^{259\text{-}435}$ are mixed. Native EBNA2 possesses four dimerization domains (CR1 to CR4), which leads to the natural occurrence of the protein as dimer (Harada et al., 2001; Tsui and Schubach, 1994). This function may partly be taken over by the GST-tag in the truncated EBNA2 protein used in the present experiments. The possible cooperative binding of the EBNA2$^{259\text{-}435}$ dimer as well as the role of the GST-tag as substitute for the lacking dimerization domain of EBNA2$^{259\text{-}435}$ still has to be examined.

Binding may depend on the amount of ternary complex partner, i.e. Notch^{RamANK} or EBNA2$^{259\text{-}435}$, in the reaction. Increasing amounts of both proteins added to a constant amount of nRBP$^{full\text{-}length}$ should result in a binding behaviour similar to the one observed when the amounts of both complex partners are altered in the same way. Figure 3.41(a) shows the results of such an experiment carried out with oli-Cp[40]. Increasing amounts of Notch^{RamANK} or EBNA2$^{259\text{-}435}$ were added to 1 µg nRBP$^{full\text{-}length}$. This corresponds to the lowest amount of protein where a supershift could still be observed upon binding of Notch^{RamANK} (see Figure 3.38). The left panel in Figure 3.41(a) displays the series with Notch^{RamANK} and the right one the series with EBNA2$^{259\text{-}435}$. For Notch^{RamANK} a supershift can be observed when 1 µg protein is added to 1 µg nRBP$^{full\text{-}length}$, whereas addition of 0.5 µg EBNA2$^{259\text{-}435}$ causes a supershift although a faint band of binary complex remains. This comparatively small difference does not correspond to the differences observed in Figures 3.38, 3.39 and 3.40. If this behaviour is based on different binding constants a smaller amount of nRBP$^{full\text{-}length}$ with a similar series of increasing amounts of ternary complex partner should reveal the difference more clearly, as confirmed by the results in Figure 3.41(b), where 100 ng nRBP$^{full\text{-}length}$ were used: The supershift caused by Notch^{RamANK} occurs when 1 µg protein is added (corresponding to a concentration of 0.9 µM). In the case of EBNA2$^{259\text{-}435}$ already 100 ng protein (90 nM), the same amount as nRBP$^{full\text{-}length}$ (85 nM), suffice to cause a supershift upon binding to nRBP$^{full\text{-}length}$. The band corresponding to the supershift appears at a different position than that in Figure 3.28, but it is comparable to the one resulting from the trial to form a ternary complex in Figure 3.26. The ternary complex DNA-nRBP$^{full\text{-}length}$-EBNA2$^{259\text{-}435}$ becomes visible when 0.1 µg EBNA2$^{259\text{-}435}$ are added.

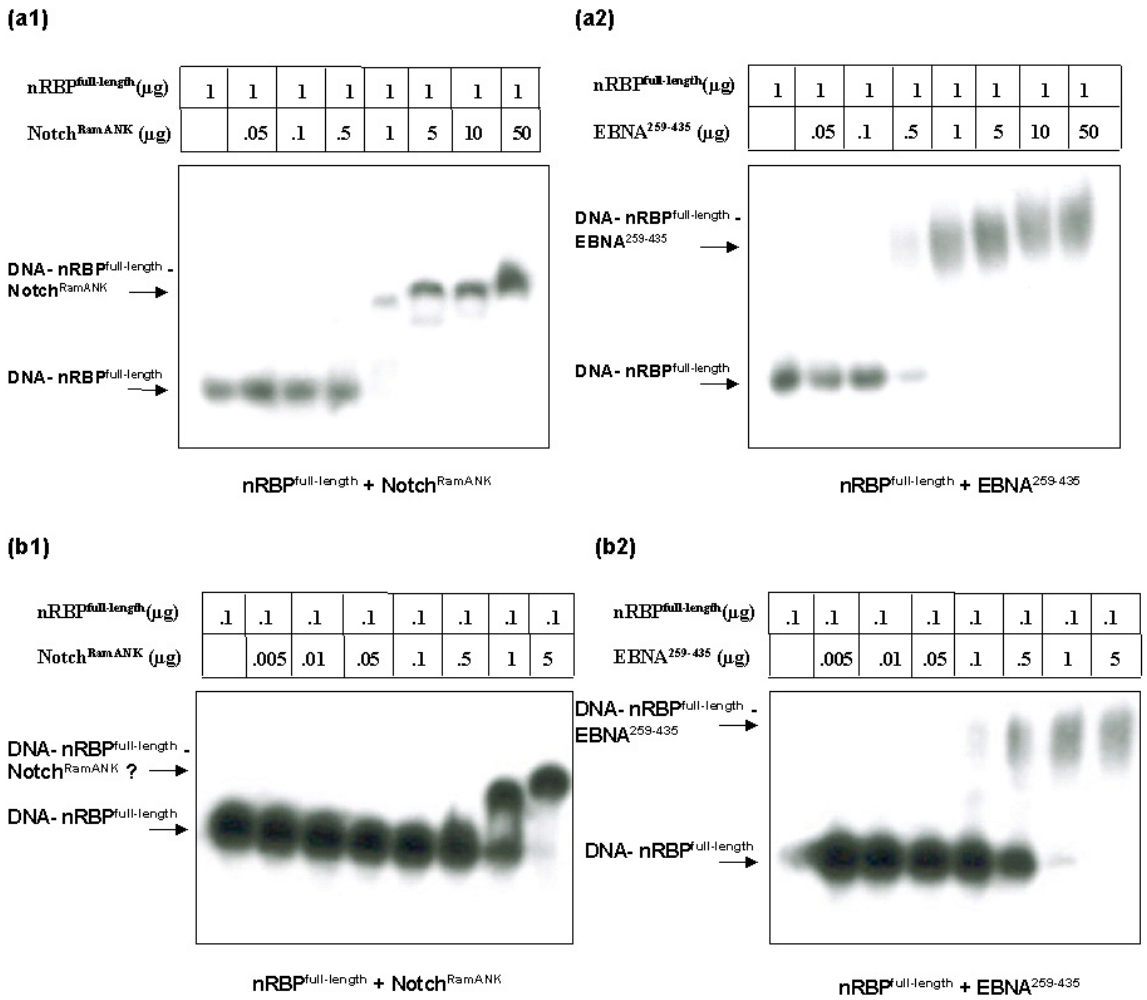

Figure 3.41: Representative EMSA to compare the binding affinity of Notch^{RamANK} and EBNA2$^{259-435}$ to nRBP$^{full-length}$ bound to oli-Cp[40]. Constant amounts of nRBP$^{full-length}$, 1 µg for (a) and 100 ng for (b), and increasing amounts of Notch^{RamANK} (a1 and b1) and EBNA2$^{259-435}$ (a2 and b2) were applied to form ternary complexes. **(a)** Binding of Notch^{RamANK} to the binary complex is visible when 1 µg Notch^{RamANK} is added to 1 µg nRBP$^{full-length}$, a band corresponding to the ternary DNA-nRBP$^{full-length}$-Notch^{RamANK} appears. The ternary complex DNA-nRBP$^{full-length}$-EBNA2$^{259-435}$ becomes visible when 0.1 µg EBNA2$^{259-435}$ are added. **(b)** Binding of Notch^{RamANK} to the binary complex is visible when 1 µg Notch^{RamANK} is added to 1 µg nRBP$^{full-length}$, a band corresponding to the ternary DNA-nRBP$^{full-length}$-Notch^{RamANK} appears upon addition of 100 ng EBNA2$^{259-435}$ and 100 ng nRBP$^{full-length}$.

EBNA2$^{259\text{-}435}$ can displace Notch^{Ram} and Notch^{RamANK} from an nRBP$^{full\text{-}length}$-DNA complex

To check, whether EBNA2$^{259\text{-}435}$ is visible in the 8% TBE-PAGE system and is able to compete with Notch proteins in this system a competition experiment was performed on ternary complexes with Notch^{Ram} and Notch^{RamANK}. Increasing amounts of EBNA2$^{259\text{-}435}$ were added to the corresponding ternary complexes from a substoichiometric ratio of 1:0.5 up to tenfold excess. As indicated by the reduced intensity of the bands of the ternary complex in Figure 3.42 EBNA2$^{259\text{-}435}$ can displace both Notch^{Ram} and Notch^{RamANK} bound to nRBP$^{full\text{-}length}$. The expected ternary complex of EBNA2$^{259\text{-}435}$ bound to nRBP$^{full\text{-}length}$-DNA is not visible as a distinct band in an 8% TBE PAGE gel. The slot of the control lane containing 10 µg EBNA2$^{259\text{-}435}$ stains with ethidium bromide although no DNA is present. Since the bands for the ternary complex with Notch^{Ram} and Notch^{RamANK} are fading, but the one for the binary DNA-nRBP$^{full\text{-}length}$ complex does not intensify it is assumed that the material in the gel slots stained with ethidium bromide corresponds to a new ternary complex formed with EBNA2$^{259\text{-}435}$. The experiment was therefore repeated with radioactive EMSAs on 4 % TBE PAGE gels to visualise the band more clearly.

Direct competition of both ternary complex partners with lower amounts of protein should reveal differences in the ability of the two proteins to displace the other one from its complex with nRBP$^{full\text{-}length}$. The result of the corresponding experiment is shown in Figure 3.43 for Cp. In the left panel (Figure 3.43(a)) increasing amounts of EBNA2$^{259\text{-}435}$ were added to a complex between nRBP$^{full\text{-}length}$ and Notch^{RamANK}. The supershifts caused by Notch^{RamANK} and EBNA2$^{259\text{-}435}$ are easily distiguishable, as the addition of increasing amounts of EBNA2$^{259\text{-}435}$ clearly results in an upward shift of the band containing Notch^{RamANK} in favour of the one containing EBNA2$^{259\text{-}435}$. Already 10 ng EBNA2$^{259\text{-}435}$ added to 1 µg nRBP$^{full\text{-}length}$ and 2 µg Notch^{RamANK} result in a detectable band containing the nRBP$^{full\text{-}length}$-EBNA2$^{259\text{-}435}$ complex bound to the oligonucleotide derived from Cp. Displacement becomes detectable upon addition of 1 µg EBNA2$^{259\text{-}435}$ and is completed when 5 µg EBNA2$^{259\text{-}435}$ are added, which corresponds to a 1:2.5 stoichiometric ratio between Notch^{RamANK} and EBNA2$^{259\text{-}435}$. In contrast, displacement of EBNA2$^{259\text{-}435}$ from a ternary complex with nRBP$^{full\text{-}length}$ starts only after addition of 5 µg Notch^{RamANK} and is not even completed when a 25-fold excess of Notch^{RamANK} is added (Figure 3.43(b)).

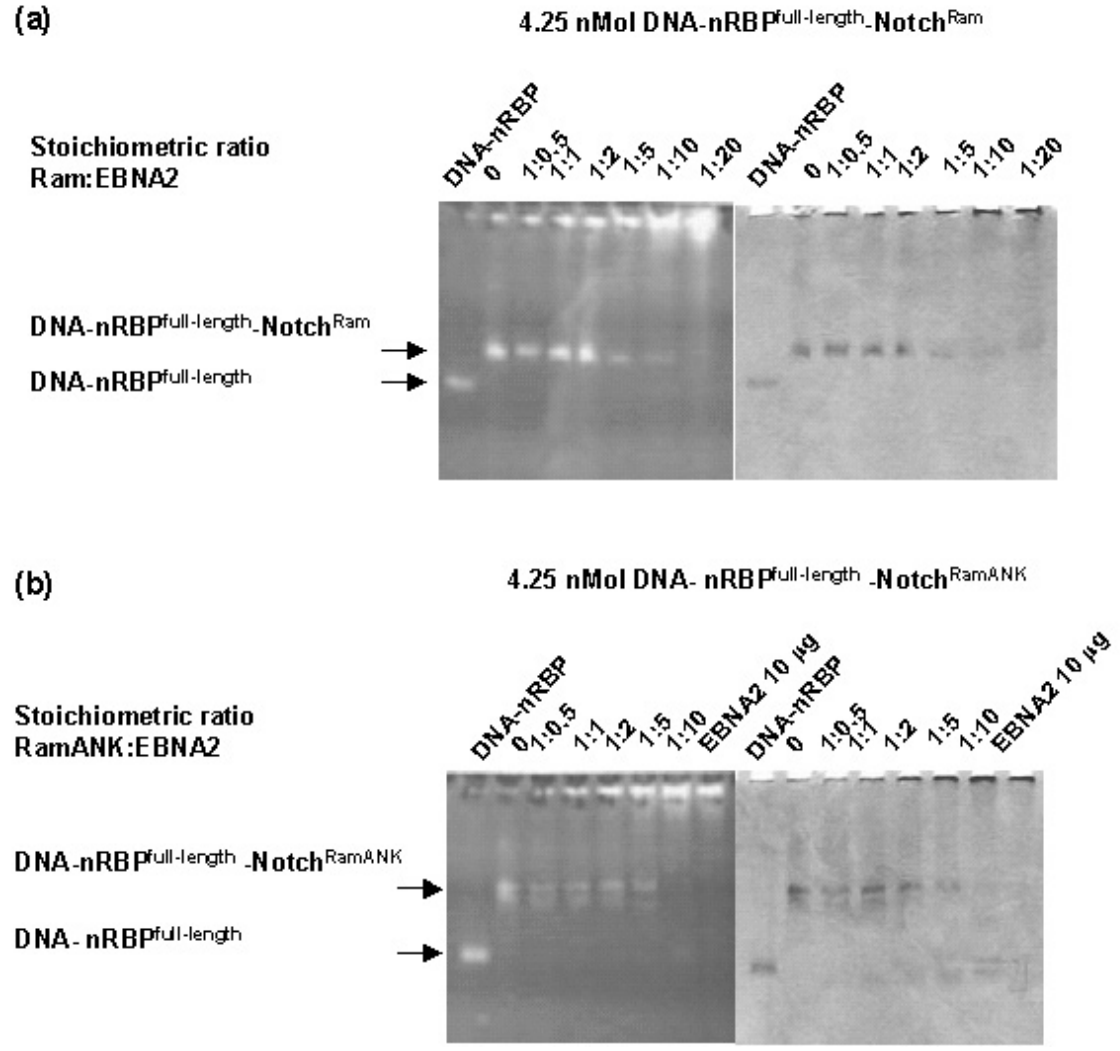

Figure 3.42: Non-radioactive EMSA successively stained with ethidium bromide (left panel) and Coomassie Brilliant Blue (right panel) to study the ability of EBNA2$^{259-435}$ to displace Notch^{Ram} and Notch^{RamANK} from a ternary complex with DNA-nRBP$^{full-length}$ (DNA: oli-Cp^{22}). Increasing amounts of EBNA2$^{259-435}$ were added to a ternary DNA-nRBP$^{full-length}$-Notch^{Ram} **(a)** and DNA-nRBP-Notch^{RamANK} complex **(b)**. In both cases the band corresponding to the ternary complex with Notch^{Ram} or Notch^{RamANK} is fading with increasing amounts of EBNA2$^{259-435}$. Instead an increasing amount of complex, which cannot enter the gel, accumulates in the gel slots. The abbreviations nRBP, RamANK and EBNA2 stand for nRBP$^{full-length}$, Notch^{RamANK} and EBNA2$^{259-435}$.

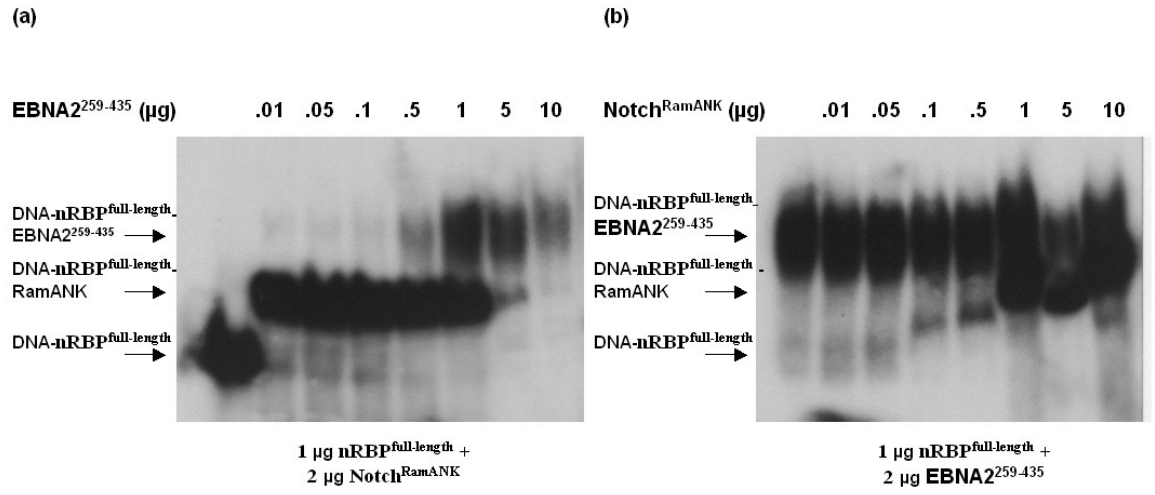

Figure 3.43: EMSA demonstrating the increased ability of EBNA2$^{259\text{-}435}$ to displace Notch^{RamANK} from a ternary complex with DNA-nRBP$^{full\text{-}length}$ compared to that of Notch^{RamANK} with EBNA2$^{259\text{-}435}$. 1 µg nRBP$^{full\text{-}length}$ and 2 µg ternary complex partner were used to form a complex with oli-Cp[40]. The amount of ternary complex partner added to displace the existing one is listed at the top of each lane. **(a)** Displacement of Notch^{RamANK} with increasing amounts of EBNA2$^{259\text{-}435}$; the band corresponding to the ternary complex formed with EBNA2$^{259\text{-}435}$ is visible as soon as the smallest amount of EBNA2$^{259\text{-}435}$ is added. **(b)** Displacement of EBNA2$^{259\text{-}435}$ with increasing amounts of Notch^{RamANK}; a band corresponding to the one observed when a DNA-nRBP$^{full\text{-}length}$-Notch^{RamANK} ternary complex is formed (see e.g. Figure 3.38) appears as soon as 1 µg Notch^{RamANK} is added. This does not result in a significant reduction in the cooresponding band of the DNA-nRBP$^{full\text{-}length}$-EBNA2$^{259\text{-}435}$ complex.

There is a strong band corresponding to the ternary complex formed with EBNA2$^{259\text{-}435}$ and a faint one corresponding to the ternary complex with Notch^{RamANK}, which appears as soon as 0.5 µg Notch^{RamANK} are added. The ability of Notch^{RamANK} to displace EBNA2$^{259\text{-}435}$ from a ternary complex with nRBP$^{full\text{-}length}$ is clearly weaker than the one of EBNA2$^{259\text{-}435}$ to displace Notch^{RamANK}.

The experiment was repeated with oli-LMP1P[36] as binding matrix for nRBP$^{full\text{-}length}$. As mentioned above, oli-LMP1P[36] has a higher affinity for the nRBP$^{full\text{-}length}$-EBNA2$^{259\text{-}435}$ complex than for the complex with Notch^{RamANK} as ternary complex partner. Figure 3.44 illustrates the result of the experiment, which was done under the same conditions and with the same amounts of proteins as indicated in Figure 3.43. As in the case of Cp, 10 ng EBNA2$^{259\text{-}435}$ added to a 200-fold surplus of Notch^{RamANK} result in a faint band corresponding to a supershift of the ternary complex containing EBNA2$^{259\text{-}435}$. Visible

displacement of Notch^{RamANK} from nRBP$^{full\text{-}length}$ occurs when 1 µg EBNA2$^{259\text{-}435}$ is added and is complete in the presence of a 2.5-fold excess. As already found in the experiment shown in Figure 3.43 Notch^{RamANK} is not able to fully displace EBNA2$^{259\text{-}435}$ from nRBP$^{full\text{-}length}$. The first faint band corresponding to a supershift upon formation of a ternary complex containing Notch^{RamANK} appears when 1 µg Notch^{RamANK} is added.
Taken together all these experiments show that EBNA2$^{259\text{-}435}$ has a higher affinity for the binary DNA-nRBP$^{full\text{-}length}$ complex than Notch^{RamANK}.

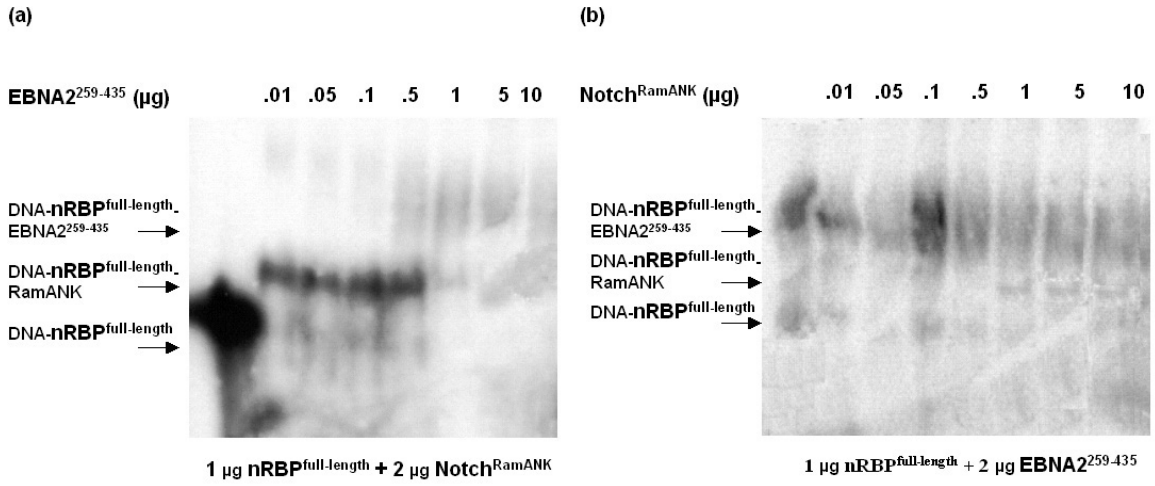

Figure 3.44: Radioactive EMSA demonstrating the higher ability of EBNA2$^{259\text{-}435}$ to displace Notch^{RamANK} from a ternary complex with DNA-nRBP$^{full\text{-}length}$ compared to that of Notch^{RamANK} to displace EBNA2$^{259\text{-}435}$. 1 µg nRBP$^{full\text{-}length}$ and 2 µg ternary complex partner were used to form a complex with oli-LMP1P[36]. The amount of ternary complex partner added to displace the existing one is listed at the top of each lane. **(a)** Displacement of Notch^{RamANK} with increasing amounts of EBNA2$^{259\text{-}435}$; as in Figure 3.43 the band corresponding to the ternary complex formed with EBNA2$^{259\text{-}435}$ is visible as soon as the smallest amount of EBNA2$^{259\text{-}435}$ is added. **(b)** Displacement of EBNA2$^{259\text{-}435}$ with increasing amounts of Notch^{RamANK}; a band corresponding to the DNA-nRBP$^{full\text{-}length}$-Notch^{RamANK} ternary complex appears as soon as 1 µg Notch^{RamANK} is added. This does not result in a visible decrease of the DNA-nRBP$^{full\text{-}length}$-EBNA2$^{259\text{-}435}$ complex.

The unexpectedly weaker binding affinity of Notch^{RamANK} to RBP-Jκ compared to that of EBNA2$^{259\text{-}435}$ gave reasons to check for hints of changes, which might cause the different behaviour. As illustrated in Figure 3.28(b) recombinant Notch^{RamANK} overexpressed and purified from bacteria binds quantitatively to RBP-Jκ and a band corresponding to free Notch^{RamANK} is only visible when excess Notch^{RamANK} is added to the reaction, indicating that the different behaviour is not due to a lack of activity.

No indications of a posttranslational modification within the RBP-Jκ binding regions, i. e. Ram and the seven ankyrin repeats, of Notch1 could be found in the literature.

Proteins from nuclear extracts display the tendency to increase the binding affinity of Notch^{RamANK} to nRBP$^{full\text{-}length}$

The experiments described above were carried out with highly purified recombinant proteins. To exclude the possibility that the lower binding affinity might reflect a requirement for other cellular proteins for efficient binding of Notch^{RamANK} to nRBP$^{full\text{-}length}$, a similar experiment than the one displayed in Figure 3.41(b) was carried out with 2 µg nuclear extract from RBP-Jκ$^{-/-}$ knockout cells (cell line SM261) added to each sample. If any additional proteins were required for stronger binding the supershift band corresponding to Notch^{RamANK} bound to nRBP$^{full\text{-}length}$ should be visible in the presence of even lower amounts of Notch^{RamANK}. A DG75 nuclear extract, and therefore one from SM261 as a cell line derived from DG75, does not contain relevant amounts of Notch1, because virtually no Notch-signalling occurs under cell culture conditions, since Notch ligands such as Delta or Jagged are not expressed (Hofelmayr et al., 1999). Furthermore, if a signal leads to the translocation of Notch1-IC to the nucleus, the protein is rapidly degraded, partly because of its PEST domain labelling it for ubiquitination (Öberg et al., 2001). False positive supershifts can thus be excluded when DG75 nuclear extract is added. Figure 3.45 shows the result of the experiment.

Lanes 4 to 9 display the repeated experiment shown in Figure 3.41(b), left panel, to form a nRBP$^{full\text{-}length}$-DNA-Notch^{RamANK} ternary complex with different amounts of Notch^{RamANK}. As soon as 0.2 µg Notch^{RamANK} are added a band appears which corresponds to the ternary complex. In lanes 10 to 15 2 µg SM261 nuclear extract are added to the mixtures otherwise corresponding to the one in lanes 4 to 9. As clearly visible the band corresponding to the ternary complex is visible when only 10 ng Notch^{RamANK} are added. This experiment was repeated with different setups to confirm this finding (data not shown). This suggests that one or more factors in a nuclear exctract can promote binding of RBP-Jκ and Notch^{RamANK}.

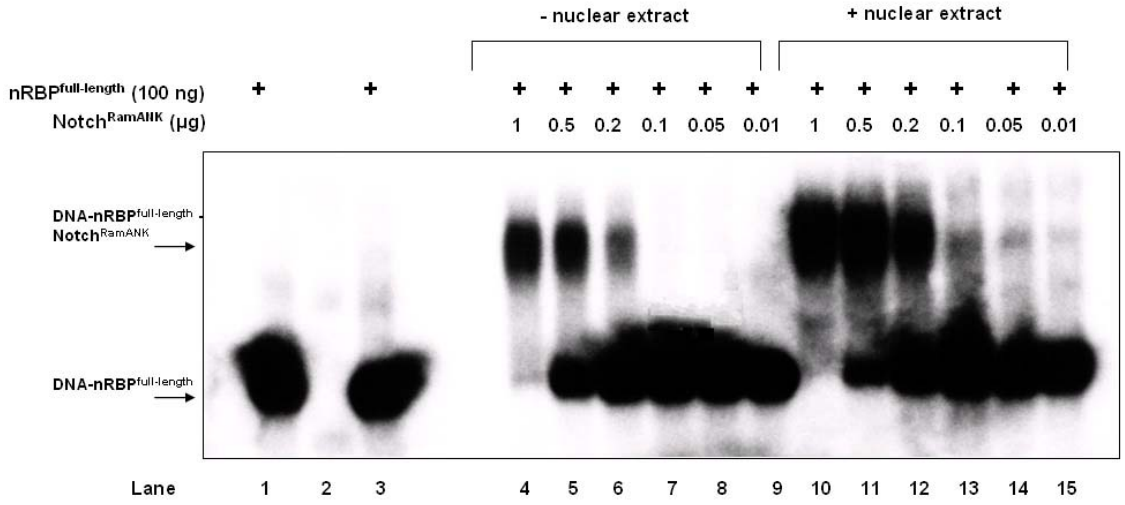

Figure 3.45: Radioactive EMSA to compare the affinity of Notch^{RamANK} to nRBP$^{full\text{-}length}$ in the presence (lanes 4 to 9) or absence (lanes 10 to 15) of 2 µg nuclear extract from RBP-Jκ$^{-/-}$ knockout cells (cell line SM261). Different amount of Notch^{RamANK} are added to 100 ng nRBP$^{full\text{-}length}$ bound to oli-Cp^{40}. The amount of Notch^{RamANK} added is indicated at the top of each lane. Control experiments: Lane 1 represents 100 ng nRBP$^{full\text{-}length}$ alone, lane 2 2 µg nuclear extract and lane 3 a combination of lanes 1 and 2.

3.2.5 EBNA$^{259\text{-}435}$ has a lower affinity to RBP-Jκ than EBNA$^{291\text{-}355}$

The RBP-Jκ binding site on EBNA2 was mapped to the conserved region 6 (CR6). The present work compared the affinity of the two EBNA2 proteins, comprising CR5 and CR6 (EBNA$^{291\text{-}355}$) and CR5 to CR7 supplemented by a short additional N-terminal part (EBNA$^{259\text{-}435}$). ITC experiments were carried out with EBNA2 proteins as ligands, which were titrated to a binary DNA-nRBP$^{full\text{-}length}$ complex. Tables 3.7 and 3.8 list the results of three experiments with EBNA$^{291\text{-}355}$ and two with EBNA$^{259\text{-}435}$. Even if there is a larger scatter in the values for EBNA$^{291\text{-}355}$, one can still clearly see that the affinities of the two proteins for RBP-Jκ differ by one order of magnitude. These data have a higher error than those done with Notch proteins as ligand, which may have been caused by the uncleaved GST-tag, leading to a homodimer. This also explains the stoichiometric ratio of 1:2 of the reaction. Two molecules of GST-EBNA2 bind one molecule RBP-Jκ.

Obviously regions other than CR6 contribute to the binding of RBP-Jκ. Studies to map the region lying within the parts of EBNA2, which are present in EBNA$^{259\text{-}435}$ and also interact with RBP-Jκ, are currently under way (S. Maier, personal communication).

Otherwise the data obtained for EBNA$^{259-435}$ supports previous findings about a higher affinity of EBNA2 for RBP-Jκ.

Experiment no.	**CR67_1**	**CR67_2**	**CR67_3**
T (°C)	20	20	20
ΔH ± σ(ΔH) [kcal/mole]	-7.69 x 10^4 ± 527	-6.07 x 10^4 ± 151	-8.14 x 10^4 ± 412
N ± σ(N)	0.632 ± 0.03	0.647 ± 0.01	0.584 ± 0.005
K_a ± σ(K_a) [M^{-1}]	4.11 x 10^6 ± 2.92x10^5	8.73 x 10^5 ± 1.21x10^5	5.58 x 10^5 ± 1.56x10^5

Table 3.7: Thermodynamic parameters of the binding of EBNA$^{291-355}$ to nRBP$^{full-length}$-DNA (16 bp). With a given temperature T the parameters ΔH (enthalpy change) and N (stoichiometry of the reaction) can be calculated.

Experiment no.	**CR57_1**	**CR57_2**
T (°C)	20	20
ΔH ± σ(ΔH) [kcal/mole]	-1.15 x 10^4 ± 167.3	-1.14 x 10^4 ± 103.5
N ± σ(N)	0.499 ± 0.002	0.412 ± 0.004
K_a ± σ(K_a) [M^{-1}]	1.18 x 10^8 ± 4.48x10^7	3.99 x 10^7 ± 1.05x10^7

Table 3.8: Thermodynamic parameters of the binding of EBNA$^{259-435}$ to nRBP$^{full-length}$-DNA (16 bp). Parameters correspond to those described in table 3.7.

3.3 Crystallization trials of RBP-Jκ bound to DNA, peptides derived from Notch^{Ram} or EBNA2 and Notch^{Ram} or Notch^{RamANK}

Crystallization trials were carried out using the vapour diffusion method with the standard Hampton Research crystal screens or self-made screens combined with the hanging drop method. In the trials that were manually set up a 0.6 µl droplet of solution with different protein concentrations (3, 5 and 8 mg/ml) and the same volume of reservoir solution was used. The total reservoir volume was 0.5 ml. Trials set up using the high throughput crystallization facility had 70 µl reservoir solution and drops composed of 0.3 µl each of protein solution and reservoir solution.

The high throughput facility provides software to evaluate crystal trials. Images of the droplets are taken immediately after the setup of the screen and after several time points.

Manual evaluation of the screens was carried out under a microscope. Generally, the term "hit" is used when small crystals or needles are visible in the drop. In this case the term is used if crystalline precipitate or microcrystals, judged by the eye, were found.

The initial self-made screen combined a pH range from 4.5 to 9 with different concentrations of polyethyleneglycols covering a range of molecular mass (PEG1000 to PEG10000).

Section 2.1.4 lists the different oligonucleotides used in the crystallisation trials aiming at obtaining crystals of binary and ternary complexes of $nRBP^{full\text{-}length}$ and $nRBP^{28\text{-}432}$. Extensive trials with $rRBP^{full\text{-}length}$ expressed in bacteria did not yield any protein crystals.

Ternary complexes with peptide ligands were formed with two peptides derived from EBNA2 comprising 10 or 12 amino acids around the essential WW motif and a dodecapeptide and a pentapeptide derived from $Notch^{Ram}$ including the amino acids essential for binding, which according to the alignment in Figure 1.6 (section 1.3.3) are similar to those in EBNA2. To guarantee that the peptides, which by themselves did not contain charged amino acids, would be soluble one amino acid was added to the N- and C-termini of the dodecapeptides. The amino acid side chains were chosen according to an alignment of the Ram domain and EBNA2 CR6 (see Figure 1.6 in section 1.3.3).

Ternary complexes were formed with both Notch constructs, $Notch^{Ram}$ and $Notch^{RamANK}$, and used in crystallisation trials.

Both for $nRBP^{28\text{-}432}$ and $nRBP^{full\text{-}length}$ screens with protein concentrations of 3 mg/ml rarely resulted in precipitate, whereas heavy precipitates were generally obtained with 8 mg/ml. Depending on the oligonucleotide used up to five times more hits were obtained with $nRBP^{28\text{-}432}$ than with $nRBP^{full\text{-}length}$. Optimization was attempted around all conditions where promising results were obtained.

Optimization of the length of the oligonucleotide

The RBP-Jκ homologue lag-1 was crystallized bound to a 13 bp double-strand oligonucleotide with a double T- or A-overhang at each 5'-end (Kovall and Hendrickson, 2004). The corresponding oligonucleotide adapted to the human RBP-Jκ core binding sequence did not bind to $rRBP^{full\text{-}length}$ and bound only very weakly to either $nRBP^{28\text{-}432}$ or $nRBP^{full\text{-}length}$. Initial trials were thus only set up with $nRBP^{full\text{-}length}$, but they did not yield any useful result. Consequently, oligonucleotides with 15 to 23 base pairs, whose affinity is sufficiently high, were used for crystallization.

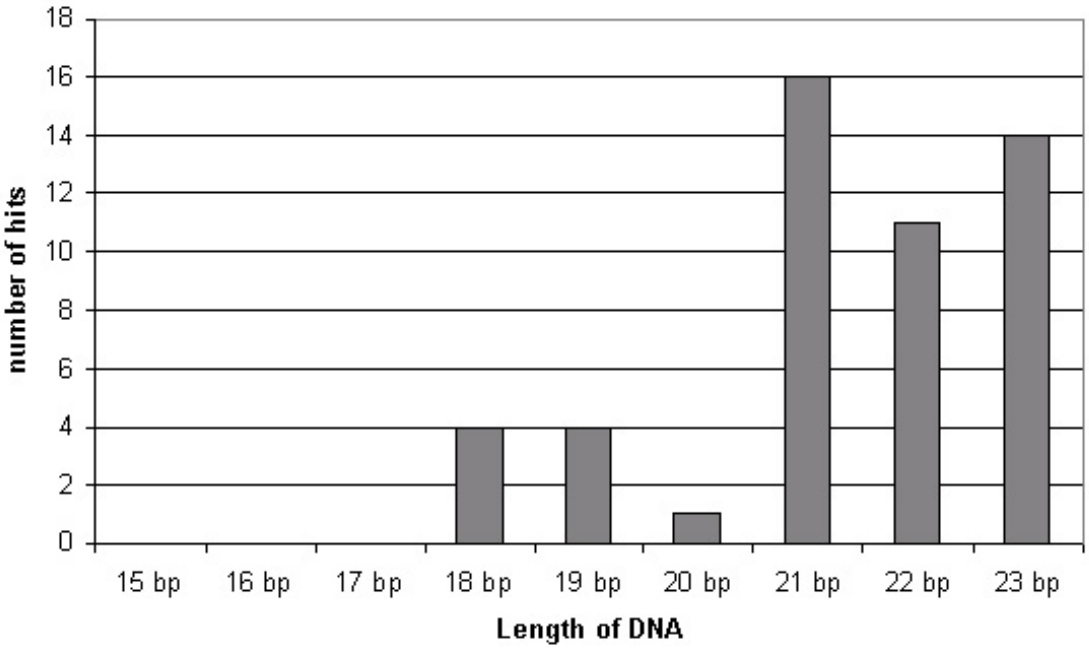

Figure 3.46: Number of promising conditions for binary complexes of nRBP$^{28\text{-}432}$ and nRBP$^{full\text{-}length}$ with oligonucleotides of different lengths.

After extensive studies and comparisons of blunt-ended oligonucleotides with corresponding oligonucleotides with one or two overhanging bases at each 5'-end, it was decided to limit further trials to oligonucleotides with double-overhangs.

As depicted in Figure 3.46 most hits, defined as the occurrence of apparently micro-crystalline precipitates or spherulites, were obtained for oligonucleotides with 21 to 23 base pairs length, but some conditions with 18- or 19-mers yielded additional hits (to compare the oligonucleotides used see section 2.1.4). The conditions for different oligonucleotides only correspond in very few cases. Generally, suitable conditions for one oligonucleotide gave regular or amorphous precipitates for different oligonucleotides.

pH optimum

The hits for both proteins as well as any oligonucleotide or ligand used to form binary or ternary complexes were statistically evaluated to find the pH condition most likely to lead to protein crystals. Figure 3.47 shows the number of hits for pH values between pH 4 and pH 9. Promising conditions were found over the entire range with the highest hit frequency between pH 6.5 and 7.5 (i.e. near the theoretical pI of 8.3 of full-length RBP-Jκ, calculated by ExPASy's protein parameter tool (Gasteiger et al., 2005)).

.

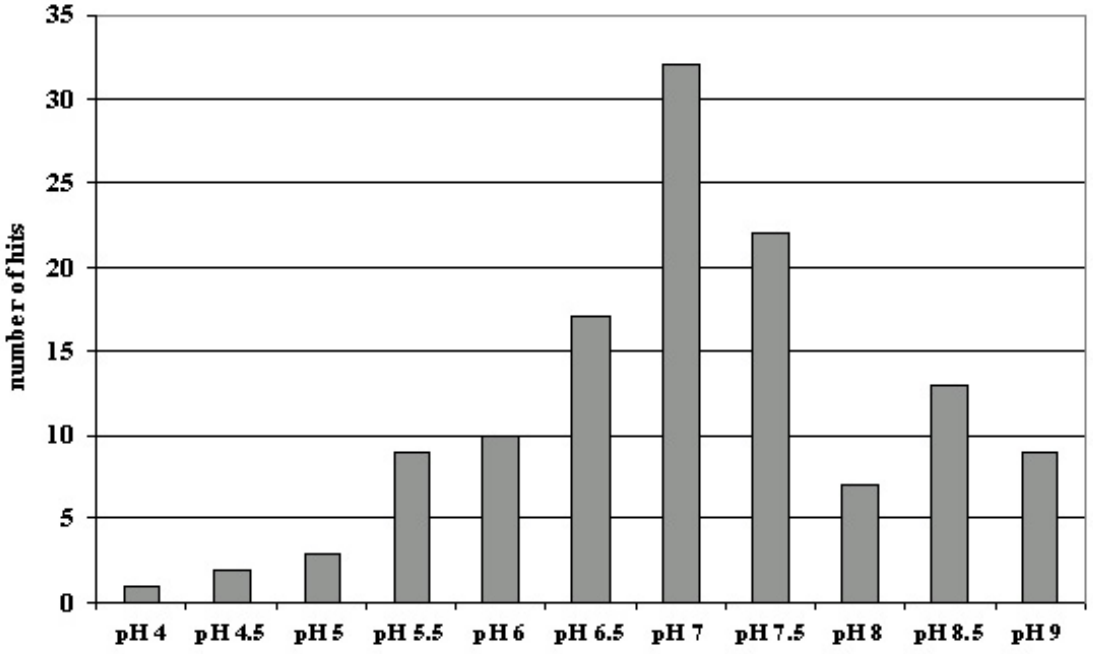

Figure 3.47: Number of promising conditions between pH 4 and 9 in steps of 0.5 pH units.

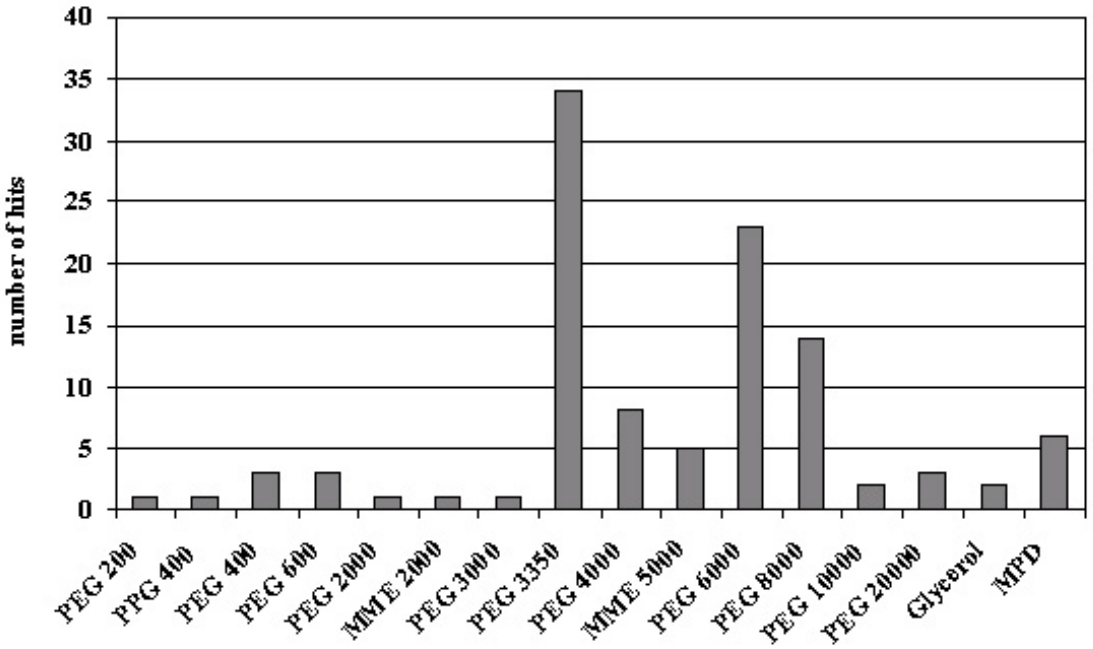

Figure 3.48: Number of promising conditions for polyethyleneglycols (PEG) of different molecular mass, glycerol and MPD as precipitant.

Precipitants

The most promising conditions obtained with both the Hampton Research and self-made screens contained polyethyleneglycols PEG8000 and PEG6000 or PEG3350, which are known to promote crystallization of protein-DNA complexes, as precipitant. Apart from PEGs promising conditions contained only glycerol or MPD (Figure 3.48).

Salts and additives

The Hampton Research screens where usually more than one parameter is altered did not give unambiguous indications concerning the optimal salt or salt concentration to be used for crystallization of binary or ternary complexes with RBP-Jκ. Table 3.9 lists the nature and concentrations of salts found in promising conditions.

Conditions altered using commercially available additive screens resulted in spermine or spermidine as supportive additives. In rare cases ethyleneglycol improved the structure of the precipitate.

Influence of peptides

According to mutational analysis peptides derived from $Notch^{Ram}$ should bind to a hydrophobic pocket on the surface of RBP-Jκ, which may alter the behaviour of the protein in solution. None of the peptides used to form ternary complexes with DNA-RBP-Jκ resulted in an increased number of hits nor did they improve the appearance of conditions, which were judged promising for the binary complex. A chart listing the total number of promising conditions compared with the number obtained with ternary complexes formed with peptides is shown in Figure 3.49.

Influence of Notch proteins

As illustrated in Figure 3.49 a considerable number of promising conditions were obtained with ternary complexes formed with $Notch^{Ram}$. In the case of the 17-bp oligonucleotide the number increased from zero to 17 conditions.

Ternary complexes formed with $Notch^{RamANK}$ did not yield any promising conditions, which is perhaps not surprising in view of the very elongated model established by SAXS as described in section 3.2.3.

Salt	Concentration range [M]
Ammonium acetate	0.05-0.1
Ammonium chloride	1.5
Ammonium nitrate	0.2
Ammonium sulphate	0.1-2.4
Calcium acetate	0.2
Calcium chloride	0.01-0.2
di-ammonium tartrate	0.7
Lithium nitrate	0.2
Lithium sulphate	0.2-1.8
Magnesium acetate	0.15
Magnesium chloride	0.01-0.2
Magnesium formate	0.2-0.5
Magnesium sulphate	0.005-1.8
Potassium chloride	0.1-0.2
Potassium formate	0.1
Potassium nitrate	0.2
Potassium sulphate	0.2
Potassium thiocyanate	0.2-0.5
Sodium acetate	0.2-1.4
Sodium citrate	0.2
Sodium chloride	0.2-3
Sodium fluoride	0.2
Sodium formate	4
Sodium nitrate	1.5
Sodium thiocyanate	0.2
Zinc acetate	0.05

Table 3.9: Salt concentration range of promising crystallization conditions.

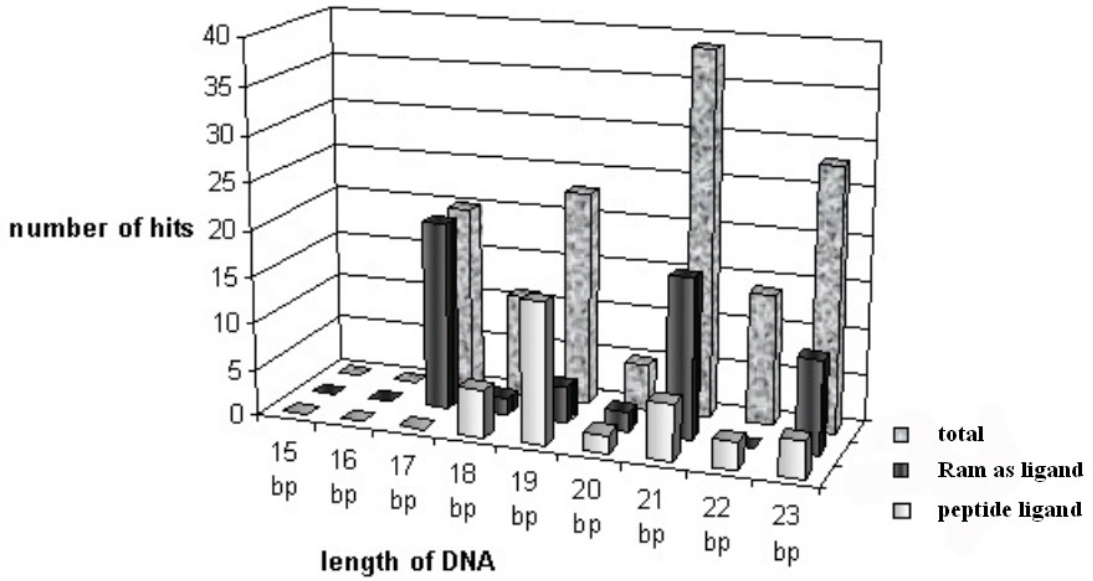

Figure 3.49: Number of conditions, where crystalline precipitate or spherulites were obtained rather than regular or amorphous precipitates as function of the length of the oligonucleotide used for crystallization. The number of total hits is compared with the number obtained with ternary complex formed with peptides or Notch-Ram.

Despite extensive trials none of the conditions identified could be optimized to yield diffracting protein crystals. Most trials resulted in salt or DNA crystals, which both yield characteristic diffraction patterns. The surprising increase in hits with Notch^{Ram} bound to a binary complex formed with a 17-base pair oligonucleotide, which has only recently been put into practice, is currently being examined in more detail.

4 Discussion

4.1 Importance of RBP-Jκ in the context of Epstein-Barr virus infections

RBP-Jκ plays an important role in protein expression in many phyla and is ubiquitously expressed in all human tissues, where it also serves as anchoring point for the Epstein-Barr viral EBNA2 protein. Upon binding of the immediate early EBNA2 protein to RBP-Jκ the latency of the virus in the cell and immortalisation of the cell can be established. The binding mode of EBNA2 mimics that of a cellular protein, the intracellular domain of Notch1 (Notch-IC). Both EBNA2 and Notch1 have been shown to activate or repress expression of a similar set of genes, albeit with some differences. The binding sites of the two proteins on RBP-Jκ differ slightly, but alignments and mutational analyses have shown a conserved ΦWΦP binding motif to be essential for the interactions in both cases.

RBP-Jκ is known to bind a core DNA sequence, where some bases are essential for the binding, but others, mainly located at the border or within the flanking regions of the binding sequence may be altered, which results in weaker but still detectable binding. The resulting binding sites with different affinities for RBP-Jκ allow cells and viruses to differentially regulate responses to signals on the promoters of different target genes, displaying multiple variations of RBP-Jκ binding sites. The DNA sequence interacting with RBP-Jκ can vary at certain positions, i.e. bases may be exchanged. RBP-Jκ binding sites on DNA with different sequences may have different affinities for the protein.

An important question is whether different DNA binding sequences cause changes in the tertiary structure of RBP-Jκ and, if so, how these influence the binding of Notch-IC and EBNA2. Ultimately the question is, of course, whether such information can lead to new approaches for finding selective ways of inhibiting the binding of EBNA2 to RBP-Jκ without affecting that of Notch-IC.

A good understanding of the mechanism and the consequences of the similar, but nevertheless different, binding modes of the two proteins could give rise to new strategies against Epstein-Barr virus infections or at least against the malignant tumours, which this virus may cause.

The present work contributes to a better characterisation of the interactions of Notch1 and EBNA2 with RBP-Jκ using different, complementary biochemical and biophysical methods.

4.2 The binding properties of recombinant RBP-Jκ depend on the expression system

E. coli is a convenient host to express proteins of different origins in view of their large scale purification. A major drawback of this system lies in the possible loss of activity, caused by the absence of specific posttranslational modifications, which normally occur in higher eucaryotes. As the few mammalian expression systems, which have yet been optimised for large scale protein expression, still have major drawbacks the baculovirus system using insect cells as expression host has become important in recent years. The present work illustrates that the choice of expression host is important not only for obtaining soluble protein but can also make a significant difference in the properties of the final product.

After an extensive series of unsuccessful trials to express RBP-Jκ in soluble form in *E. coli*, refolding of the protein expressed into inclusion bodies finally led to a product, which specifically bound DNA, but not the Notch derivatives $Notch^{Ram}$ and $Notch^{RamANK}$, which were expressed in *E. coli* as well. The change to the baculovirus expression system yielded soluble RBP-Jκ, which bound to shorter oligonucleotides than the refolded protein expressed in *E. coli*. Moreover, it did not only generally bind much more strongly to DNA fragments of different lengths, but also bound the Notch proteins $Notch^{Ram}$ and $Notch^{RamANK}$ with similar strength.

The molecular mass determined by mass spectrometry differed by only 4 Daltons from the theoretical value calculated by the ExPaSY protein parameter tool (Gasteiger et al., 2005). As the error on such measurements is of the order of 0.1 Daltons, this difference may be significant but cannot be accounted by any known post-synthetic modification. The enhanced ability to bind both DNA and interacting proteins suggests that several factors play a role. The difference in properties results most probably from the more controlled folding process in insect cells compared to the artificial refolding process applied after complete denaturation of the protein expressed in *E. coli*.

4.3 The conserved part of RBP-Jκ has the same binding properties for DNA or Notch proteins as its full-length counterpart

Alignments of RBP-Jκ homologues from different species revealed a conserved region common to all examined RBP-Jκ proteins. Lag-1, the homologue in *C. elegans*, could be successfully crystallised after truncating the protein at the N- and C-termini (Kovall and Hendrickson, 2004). For the present work a deleted human RBP-Jκ protein, $nRBP^{28-432}$, was designed according to the conserved part, expressed in insect cells and purified in quantities comparable to $nRBP^{full-length}$. The truncated protein was tested for its DNA- and protein-binding ability. Figure 3.21 reveals no substantial difference in the ability of the truncated protein to bind DNA with RBP-Jκ binding sites derived from Epstein-Barr viral promoters. None of the protein interaction partners, $Notch^{Ram}$ and $Notch^{RamANK}$, which were tested on non-radioactive EMSA (Figure 3.23) exhibited different binding properties, supporting the hypothesis that the conserved region is indeed essential and sufficient for the binding properties of RBP-Jκ.

4.4 The ankyrin repeats of Notch-IC do not detectably contribute to RBP-Jκ binding

We also tried to quantify the contribution of the ankyrin domain (ANK) containing seven ankyrin repeats of about 30 amino acids each to the binding affinity of Notch-IC to RBP-Jκ with biochemical (EMSA) and biophysical (ITC) methods in a controlled system. Only proteins >95% pure in well defined buffer conditions were used for the binding assays, so that any influence from unknown sources can be excluded.

No significant differences in the binding affinity could be detected in non-radioactive EMSAs with ternary complexes formed with pure RBP-Jκ, DNA and different amounts of $Notch^{Ram}$ or $Notch^{RamANK}$.

The results obtained with ITC, which are described in section 3.2.3, also clearly indicate that there is no significant difference in the enthalpy change (ΔH=-1.1 to -1.3×10^4 kcal/mole) and the binding constant (6×10^6 to 2×10^7 M^{-1}). As expected, the stoichiometric ratio of the reaction is 1:1 for both ternary complex partners.

The low resolution model of the ternary DNA-nRBP$^{full\text{-}length}$-Notch^{RamANK} complex obtained with SAXS strongly suggests that the ankyrin repeats do not participate in binding RBP-Jκ. The model with the ankyrin domain pointing away from the remaining complex gave a much better fit with much lower errors than the one where the ankyrin repeats contribute to binding to RBP-Jκ. These quantitative data strongly suggest that the contribution of ANK to the binding of RBP-Jκ is negligible.

All experiments taken together suggest that the system is not as simple as what it is reduced to in ITC or even transactivation experiments *in vivo*. It is likely that successful transactivation upon binding of Notch-IC to RBP-Jκ takes places via additional interactions to other proteins involved in the transcription initiation process. As ankyrin repeats are known to mediate protein-protein interactions and interactions with two histone-acetyltransferases have already been detected (Kurooka 2000), they might very well be involved in this function rather than exerting any strong binding to RBP-Jκ.

The affinity of NotchRamANK and RBP-Jκ was shown to be concentration dependent (for comparison see e.g. Figures 3.26 and 3.28). To evaluate the quantitative results obtained with ITC in the context of the expected cellular concentration of RBP-Jκ, this concentration was estimated on the basis of Western blot analyses carried out with DG75 cells. The result of this analysis suggest that under cell culture conditions 25 fg RBP-Jκ can be found in a single cell. Under the assumption that most of the protein is located in the nucleus the calculated final concentration of RBP-Jκ in the nucleus is 3.75 mM, which should be compared with an average concentration of 102 μM assuming RBP-Jκ to be evenly distributed within the cell. Most probably the actual concentration lies somewhere in between these two surprisingly high values. High physiological concentrations of components should suggest a low affinity in the mM range rather than in the low micromolar range as observed in the present work. On the other hand competition of coactivators such as Notch-IC and corepressors for possibly different binding sites on RBP-Jκ may necessitate such a high affinity to successfully enhance the expression of target genes. Assuming a similar concentration for Notch-IC upon activation and translocation the interaction should be possible without the help of other components. However, Notch signals are known to be comparably weak and quickly abrogated by ubiquitination, so that binding without the help of additional components may not occur.

There are some contradictory results in the literature regarding the role of the Notch1 ankyrin (ANK) repeats in binding RBP-Jκ and transactivation of its target genes. Depending on the method applied ANK displayed a more or less strong binding and

transactivation activity. It was even reported that a point mutation within the ANK domain of Notch1 (M1 mutation (Kopan et al., 1994)) results in complete abrogation of transactivation activity of Notch1-RAMIC, while the Ram domain alone was found to lack transactivation ability (Kato et al., 1997; Kurooka et al., 1998). Ram and ANK are both involved in the interaction with RBP-Jκ, whereas ANK was also shown to be necessary for transactivation.

Dumont et al. (2001) found in their study that a GAL4-RamANK fusion protein without the novel transactivation domain (TAD) previously identified by Kurooka et al. (1998) is unable to transactivate GAL4 responsive reporter genes in two different cell lines. The restricted but still significant transactivation of artificial promoter-reporter constructs containing multimerized RBP-Jκ binding sites found in promoters of Hes-1 and Hes-5 by RamANK indicate the presence of two different transactivation mechanisms: Transactivation requires either a transferable TAD possessing the OPA and PEST elements (glutamine- rich and proline-, serine and threonine-rich regions, respectively) or the concerted action of Ram and ANK within an RBP-Jκ protein complex.

One obviously has to distinguish between the ability of Notch constructs to interact with RBP-Jκ and to transactivate. In general, although the different methods applied by different groups partly gave contradictory results, it can be concluded that neither of the two functions on its own suffices for expression of RBP-Jκ target genes.

When this study was effectively completed additional insight in the interaction of the ankyrin repeats with RBP-Jκ was gained from the crystal structure of a quaternary complex of *C. elegans* Lag-1 bound to DNA, RamANK and an additional protein fragment derived from Mastermind (MAML), another transcriptional coactivator (Wilson and Kovall, 2006) and one of the same complex with human proteins without Ram (Nam et al., 2006). The crystal structure of the *C.elegans* proteins, which is depicted in figure 4.1, shows that the ankyrin repeats indeed participate in binding RBP-Jκ at three sites in the third, the fifth and the seventh repeat, the latter of which contains a *C. elegans*-specific insertion. Comparison of the theoretical scattering curve of the crystal structure of the complex composed of proteins from *C. elegans*, excluding Mastermind, with the experimental SAXS data of the according complex with human proteins in solution revealed a poor fit (data not shown), making it unlikely that the conformation of ANK in the crystal structure corresponds to that of the human proteins in solution.

In the crystal structure only a small portion of the Ram domain is visible, because large parts of the domain seem to be very flexible. This does not contradict the findings that Ram

folds up to form mostly alpha-helical structures. However, there is still a considerable portion with low complexity, which most likely is responsible for the less rigid structure of this protein.

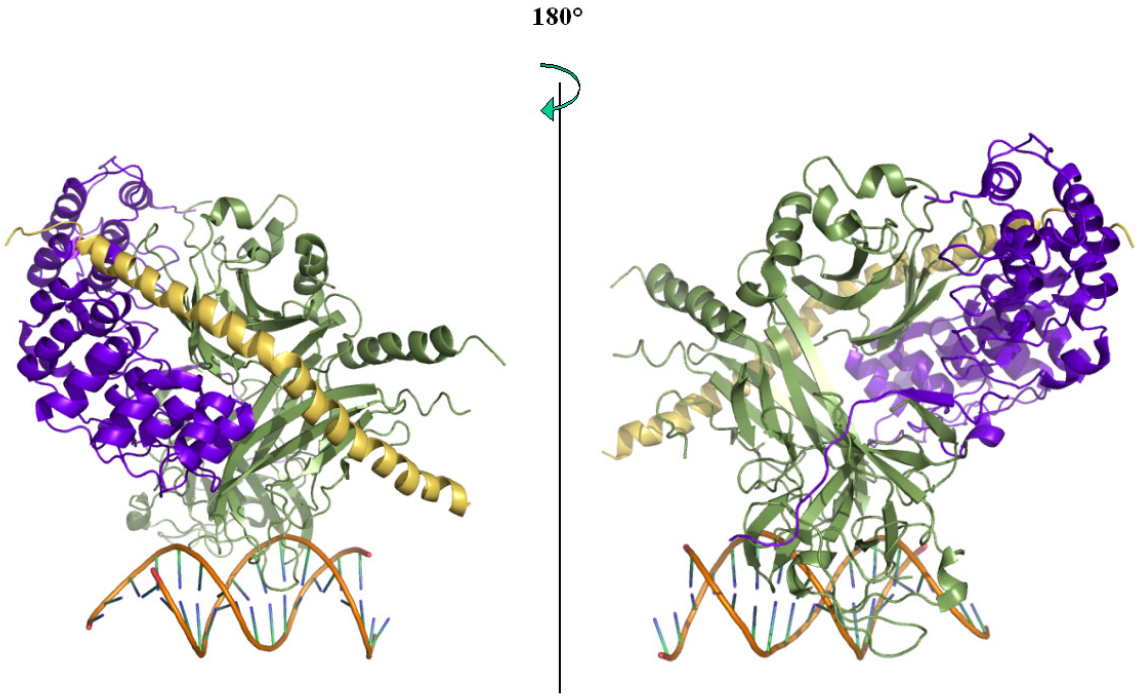

Figure 4.1: Crystal structure of the quaternary complex of the C. elegans proteins Lag-1, Notch-RamANK and Mastermind on DNA. The ribbon structure of Lag-1 is coloured olive, that of RamANK violet and that of Mastermind yellow. The DNA at the bottom of the picture is displayed as sticks representing the bases.

The Mastermind fragment forming two alpha helices is arranged in such a way that it is very well imaginable that by binding of this coactivator to the ternary complex in an unknown sequence the ankyrin repeats are forced into a conformation, where they interact with RBP-Jκ. In this case Mastermind would function as scaffold protein binding RBP-Jκ as well as ANK and its presence may determine the binding and therefore possibly the functionality of the resulting complex. Since a number of such coactivators exist, the conformational changes arising from their binding to RBP-Jκ may well be responsible for the differential transactivation activity of RBP-Jκ. Our results gave rise to the suggestion of a model of the sequence of binding of RBP-Jκ interaction partners which differs from that suggested by Wilson et al. (2006). Figure 4.2 illustrates the differences between this model and the one suggested on the basis of the results obtained in the present work. Whereas the recently published model suggests an equilibrium of ANK domains docked and undocked

on RBP-Jκ after recruitment of Ram (left panel), it is suggested here that ANK can only bind after additional recruitment of MAML (right panel), so that MAML, which interacts strongly with ANK sets the stage for ANK to interact with RBP-Jκ.

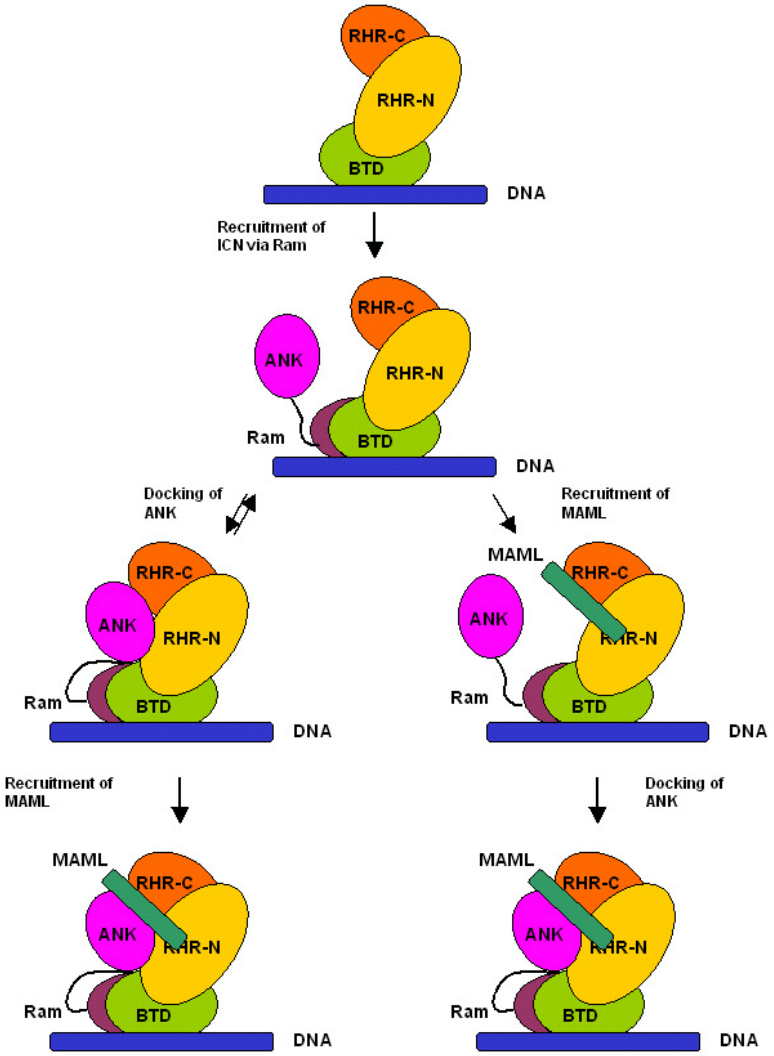

Figure 4.2: Comparison of two models for the sequence of the assembly of Notch-IC, Mastermind (MAML) and RBP-Jκ could take place. Left panel: Model as suggested by Wilson et al. (2006); recruitment of Notch-IC via Ram is followed by docking of ANK to form a high-affinity binding site for MAML. Right panel: Model based on the present work suggesting the necessity of MAML to bind prior to the docking of ANK, thus creating the corresponding high-affinity binding site for ANK.

Our results concerning the possible increase in affinity of RBP-Jκ for Notch after addition of cellular extract strongly supports the latter model. So far no information could be obtained from the authors about whether crystals of a ternary complex have also been

obtained. Both certainly interesting though partly controversial findings encourage to try and unravel the binding meachanism in the context of a physiological environment.

4.5 The minimal RBP-Jκ binding site in EBNA2 (CR5 and CR6) does not account for its strong binding affinity

Many of the results above are still not well established and should be further examined with more controllable methods, but it would not be surprising to find very flexible proteins with functional similarities to EBNA2 in different organisms. This would, of course, considerably complicate the targeting of the protein in the fight against EBV infection resulting in malignant diseases.

The construct used to determine the stronger binding affinity of EBNA2 to RBP-Jκ compared to Notch^{RamANK} comprises aa 258 to 435. The binding properties of full-length EBNA2 have not been determined in the present work, since the regions contributing to the interaction with RBP-Jκ were mapped to the conserved regions CR5 and CR6. There are cases known where the binding of a full-length protein to its interaction partner is weaker than that of a truncated version, e.g. because of the presence of autoinhibitory patches in regulatory proteins involved in signal transduction. Usually, however, the binding affinity increases the smaller the difference in length between the truncation construct and the full-length protein. An EBNA2 construct comprising the minimal RBP-Jκ binding site (EBNA2$^{291-355}$) does not result in a visible supershift when added to nRBP$^{full-length}$-DNA in radioactive EMSAs (S. Maier, GSF, personal communication). In contrast, we could detect binding of this construct to a binary nRBP$^{full-length}$-DNA complex as interaction partner in ITC experiments (section 3.2.5). The binding constant is one order of magnitude lower than that of Notch^{RamANK}, for which binding to nRBP$^{full-length}$-DNA could initially also not be visualized on EMSAs. These experiments indicate that one part of EBNA2, which is included in EBNA2$^{259-435}$ but not in EBNA2$^{291-355}$ and which has not been mapped for the interaction with RBP-Jκ contributes to the binding and enhances affinity.

Secondary structure prediction programs find that a large part of EBNA2 contains low complexity regions and few defined secondary structure elements. The stretches containing multiple prolines in particular introduce considerable flexibility into the protein chain. Although it has been established that most of the poly-proline regions do not contribute to

the transactivation activity of EBNA2 it cannot be excluded that these prolines enable a number of other protein-protein-interactions.

A BLAST similarity search with EBNA2 produces very few homologues in other viruses and finds no significant homologies to cellular proteins. The closest match with 39% sequence identity is found in herpesvirus papio, a virus infecting baboons, followed by cercopithecine herpesviruses 12 and 15. The identical patches include the conserved WW binding motif. Other viruses belonging to the family of gamma herpesviruses do not express similar proteins, although they may have functional analogues, which may display similar structural features despite a very low sequence identity, or even in absence of any identity. It is, however, remarkable that as efficient a protein as EBNA2 would not have evolved or been transferred to other viruses of the same family. This suggests that EBNA2 has appeared quite recently in evolution.

One protein expressed upon infection of cells with human herpesvirus 8 (Kaposi's sarcoma-associated herpesvirus, KHSV) has some non-sequential similarities to EBNA2. Like EBV and a number of other members of the herpes virus family, KHSV displays two alternative life cycle programs upon infection of host cells: latent and lytic infection. Among the products of the limited number of latency genes the gene product LANA (Latency-Associated Nuclear Antigen) is most likely critical for establishing latent KHSV infection. This high molecular mass protein (222 to 234 kDa) has three distinct domains, including a proline-rich one, a characteristic it has in common with EBNA2. Another region comprises long glutamic and aspartic acid-rich repeats as well as a glutamine-rich domain. These features are usually found in low complexity regions of proteins, especially those involved in transcription control. Among the many interactions with proteins involved in transcription (basal transcription factors, histones etc.), which have already been mapped, it was found that LANA interacts with CIR, a repressor protein interacting with RBP-Jκ. LANA also possesses a DNA-binding domain, which is known to bind to a sequence being part of the LMP1 promoter, adding to the common features with EBNA2. Most strikingly, both LANA and EBNA2 interact with RBP-Jκ to regulate latency of the original virus in the host cells (Lan et al., 2005).

In contrast to LANA, RTA (Replication and Transcription Activator) is the critical protein in the switch of HHV-8 from latency to lytic reactivation. Although RTA is the homologue of the EBV BRLF1 gene product, it has some functional similarity with EBNA2, e.g. DNA binding as well as interaction with transcription factors. Before the interaction of LANA and RBP-Jκ was discovered it has been shown to interact with RBP-Jκ to activate

expression of genes, whose products are involved in lytic reactivation (Liang et al., 2002). Its promoter contains RBP-Jκ-binding sites, which were shown to be targeted by LANA to repress lytic reactivation (Lan et al., 2005). If both interactions are indeed present, there must be mechanisms developed for the differential regulation of promoters controlling genes with such different impacts on the life cycle of the original virus. These may be similar to the ones for EBNA2 and Notch-IC binding to RBP-Jκ: slightly different binding sites resulting in different conformational changes enabling RBP-Jκ to bind to the appropriate target promoters.

4.6 Impact of the stronger binding affinity of EBNA2$^{259-435}$ compared to that of Notch^{RamANK} on the cellular and Epstein-Barr viral system

EMSAs proved the higher binding affinity of the EBNA2-truncation EBNA2$^{259-435}$ to RBP-Jκ compared to that of Notch^{RamANK}. Depending on the oligonucleotide used for complex formation with RBP-Jκ the affinity is 20 to 50 times higher than that of Notch^{RamANK}.

The sequence of the oligonucleotide bound to RBP-Jκ has a strong influence on the binding affinity of ternary complex partners of RBP-Jκ. It is possible that the alteration of certain bases causes a conformational change in RBP-Jκ sufficient to influence its binding affinity to other proteins.

EBNA2 is necessary to maintain proliferation in EREB2.5 cells, a conditionally immortalized lymphoblastoid cell line, where EBNA2 is fused to the hormone-binding domain of the estrogen receptor, rendering its activity dependent on estrogen (Kempkes 1995). Independently it was found that Notch-IC, introduced in different ways, was not able to fully substitute for EBNA2 in these cells, when EBNA2 expression was abolished by estrogen depletion (Hofelmayr et al., 2001). Another group found, however, that expression of very high levels of Notch-IC, obtained by repeated selection for EREB2.5 cells expressing higher than average levels of Notch-IC could finally rescue EREB2.5 cells after inactivation of EBNA2 by estrogen depletion (Gordadze et al., 2001). It was found that Notch-IC could not increase the expression of LMP1, another EBV protein necessary to maintain proliferation in EREB2.5 cells, after estrogen depletion. In contrast, cells expressing very high levels of Notch-IC also expressed LMP1 and other proteins usually activated exclusively by EBNA2. These findings could so far not be explained.

Taking into account that different RBP-Jκ binding oligonucleotides result in differences in affinity between the respective ternary complex partners Notch^{RamANK} and EBNA2$^{259-435}$ a possible explanation can be proposed. LMP1 expression is not activated by Notch-IC, but by EBNA2. The RBP-Jκ binding sequence within this promoter corresponds to one used in the present study (Figure 3.39), which showed that EBNA2$^{259-435}$ binds more strongly to RBP-Jκ bound to this sequence than Notch^{RamANK}. The transactivation activity of EBNA2 and the lack of transactivation when Notch replaces EBNA2 could partly be explained by the dependence of the binding affinity of RBP-Jκ for the complex partners on the oligonucleotide in the complex, but probably even more by the generally stronger binding of EBNA2. Binding of two weakly interacting molecules can be enhanced if 1) other proteins are mediating the interaction as scaffolds or 2) the concentration of one or both interaction partners is increased so that the binding equilibrium is driven towards formation of the complex. In the case of Notch-IC overexpressed at unusually high levels exactly this could have been the case. The excess supply of Notch-IC shifts the equilibrium, especially as RBP-Jκ is anyway generally expressed at moderate levels.

Both Notch-IC and EBNA2 were shown to act similarly on several promoters, but also differences have been found, which, apart from the different binding affinity to RBP-Jκ, could arise from their slightly different binding sites on RBP-Jκ resulting in slightly different conformational changes in RBP-Jκ. Furthermore, the most intriguing difference between EBNA2 and Notch, apart from the PEST sequence labeling Notch for rapid breakdown by the ubiquitin-proteasome pathway, lies in the extracellular domain of Notch, which enables a tight control of the expression of all Notch1 target genes. EBNA2 does not possess any such control element.

In general, a signaling protein is involved not only in a single isolated pathway but in several pathways with different feedback loops, creating a complicated and still largely unknown network, which provides the appropriate reaction of cells upon different sets of stimuli. In the present case, only one pathway is examined, excluding the possible influence of others, which could also involve Notch and/or EBNA2.

A set of additional interacting proteins at the transcription initiation level is already known for both EBNA2 and Notch-IC. Components of the basal transcription machinery interact with both proteins (TFIIH, TBP) as well as histone acetyltransferases (EBNA2: p300/CBP and PCAF; Notch-IC: p300/CBP, PCAF and GCN5) and proteins binding to RBP-Jκ (SKIP).

An important question concerns the origin of the generally higher binding affinity of EBNA2$^{259-435}$ compared to Notch^{RamANK} and the impact of this higher affinity on the infection process of Epstein-Barr virus.

Up to 95% of individuals may be infected by EBV depending on the origin of human populations. The high affinity of viral proteins for other cellular proteins may well contribute to high levels of infection as the displacement of the usual interaction partners puts the infected cells into a latency phase rather than resulting in cell destruction upon virus production.

During latency infected resting B-cells do not express EBV proteins. Even in many of the malignant diseases caused by EBV especially EBNA2 is not expressed. It is produced, though, in tumours developed by immunocompromised patients, such as those infected with HIV.

The applicability for only a small percentage of patients whose tumours are caused by EBV together with the findings in the present work, that EBNA2 has a much stronger affinity for RBP-Jκ than Notch-IC raise questions regarding the chances of success of a therapeutic attack at this stage of the viral cycle. Since EBNA2 and Notch-IC bind to at least adjacent sites on RBP-Jκ and compete for the binding a drug will most likely expel Notch-IC rather than EBNA2 from RBP-Jκ.

4.7 Further experiments and outlook

The crystal structure of a ternary complex of RBP-Jκ bound to DNA and Notch^{Ram} or Notch^{RamANK} would confirm the findings described in this work but also unravel further details of the structural changes occurring in Notch^{Ram} upon binding RBP-Jκ. The current state of the work suggests that the formation of suitable protein crystals with Notch^{Ram} as ternary complex partner may essentially be a question of time. Since the proteins seem to be very flexible and according to the SAXS model the ternary complex with Notch^{RamANK} is very extended it may, however, be difficult to obtain crystals which diffract to high resolution.

A three-dimensional structure of EBNA2 would shed light on the contribution of parts of the protein apart from CR6 to binding RBP-Jκ, but several hints of its low complexity and flexibility accounting for its many different interactions suggest that this problem may also require different approaches. A study currently in progress and using radioactive EMSA

(S. Maier, personal communication) aims at the comparison of the affinities of truncated EBNA2 proteins combining CR5 and CR6 (construct EBNA2$^{291-355}$) with adjacent regions present in the construct KF214 (EBNA$^{259-435}$), which was mainly used for the present study. One cannot exclude that the usage of an even larger part of EBNA2 for binding studies will further increase the gap in affinities of EBNA2 and Notch^{RamANK} for RBP-Jκ, thus directing the attention to possible causes for this difference. Only the examination of the whole interactome, which most likely connects RBP-Jκ signal transduction to different regulatory processes such as splicing (in parts already shown with SKIP; see section 1.2.1) will reveal the influence of the binding of other proteins on the affinity of Notch^{RamANK} and EBNA2. The study of binding sites of different transcription factors within the promoters of Notch-IC and EBNA2 target genes and their possible interactions with RBP-Jκ on the one hand or Notch or EBNA2 on the other hand is another approach, which may lead to an explanation for the different binding behaviour.

Summary

RBP-Jκ serves as interaction partner for both cellular and viral proteins. The protein mediates cellular and Epstein-Barr viral signal transduction, which in both cases results in dedifferentiation or immortalization of the cell. The intracellular part of the human Notch1 protein (Notch-IC) and of the Epstein-Barr viral protein EBNA2 binds to RBP-Jκ and expels a corepressor complex to activate transcription. The two proteins have similar functions and their binding regions on RBP-Jκ lie in close vicinity or partially overlap. An important step towards a better understanding of the biology of both signal transduction pathways is to find differences in the properties of Notch and EBNA2, such as binding affinities, stability or binding sites on RBP-Jκ.

The aim of the present work was therefore to characterize the interaction of RBP-Jκ with DNA, proteins and relevant peptides using biochemical, biophysical and structural methods. Expression and purification protocols were developed, which enabled us to obtain sufficiently large amounts of each complex partner. A high biological activity of the individual components was obtained by using different expression systems.

After the characterization of RBP-Jκ expressed in different systems and of potentially more soluble truncations, which may be easier to crystallize, using EMSA and CD spectroscopy, all subsequent studies were carried out with recombinant RBP-Jκ proteins obtained from insect cells. In comparison with RBP-Jκ proteins expressed in bacteria, these had a higher affinity for DNA as well as for Notch proteins. In contrast, according to EMSA, a high biological activity of Notch and EBNA2 proteins expressed in bacteria was found.

There is some controversy in the literature concerning the parts of Notch-IC involved in the binding to RBP-Jκ. The detailed characterization of the interaction of RBP-Jκ with the strongest interacting component, $Notch^{Ram}$, and the naturally occurring fusion of Ram with seven ankyrin repeats, $Notch^{RamANK}$, using isothermal titration calorimetry (ITC), EMSA and small angle x-ray scattering with binary and ternary complexes allowed us to create models, which unambiguously exclude the participation of the ankyrin repeats in the binding of RBP-Jκ in a system consisting only of the highly purified components of the complex. CD spectroscopy revealed that free Ram is largely unfolded and folds into largely α-helical structures upon binding to RBP-Jκ.

Cell biological methods usually provide indirect information about interactions but do not provide quantitative data regarding the strength. The controlled reaction systems developed

in the present study enabled us to detect a 20- to 50-fold higher affinity of EBNA$^{291-355}$ for RBP-Jκ compared to Notch^{RamANK}. Interestingly, first results indicate that the CR6 region of EBNA2, which is described as the most important region interacting with RBP-Jκ cannot account for the higher affinity.

A precise description of the binding sites of the interaction partners would require crystals of RBP-Jκ in complex with proteins from Notch-IC and/or DNA. The many attempts at obtaining suitable crystals were hitherto unsuccessful although we were able to narrow down the area of likely crystallization conditions.

The results obtained by different methods help to clarify the role of the interaction partners of RBP-Jκ in the context of infections by the Epstein-Barr virus, which may lead to malignant tumours because of both the similarities and functional differences of Notch and EBNA2. Furthermore, with the results of the present study the discussion of whether a therapeutic attack on the level of the RBP-Jκ-EBNA2 interaction is useful has to be resumed.

Zusammenfassung

RBP-Jκ dient als Interaktionspartner sowohl für zelluläre als auch für virale Proteine. Hier treffen sich zelluläre und Epstein-Barr-virale Signalübermittlung, die in beiden Fällen zur Dedifferenzierung bzw. Immortalisierung der Zelle führt. Das humane Notch1-Protein bindet an RBP-Jκ und verdrängt einen Korepressorkomplex von RBP-Jκ ebenso wie das Epstein-Barr-Virus Protein EBNA2. Die Funktionen beider Proteine sind ähnlich, auch die Bindestellen an RBP-Jκ liegen nahe beieinander, wenn sie nicht gar überlappen. Einen Unterschied in den Eigenschaften beider Proteine zu finden, sei es Bindungsaffinitäten, Stabilität oder Bindungsstellen an RBP-Jκ, ist ein wichtiger Schritt auf dem Weg zum besseren Verständnis der Biologie beider Signalwege.

Ziel dieser Arbeit war die biochemische, biophysikalische und strukturelle Charakterisierung der Interaktionen von RBP-Jκ mit DNA, Proteinen und relevanten Peptidfragmenten. Zu diesem Zwecke wurden Expressions- und Aufreinigungsprotokolle entwickelt, die es ermöglichen, jeden gewünschten Komplexbestandteils in grossen Mengen und hochrein herzustellen. Die Benutzung unterschiedlicher Expressionssysteme garantiert die maximale biologische Aktivität der individuellen Komponenten.
Nach der Charakterisierung von in unterschiedlichen Systemen exprimiertem RBP-Jκ und Trunkationen, die eine grössere Löslichkeit bzw. leichtere Kristallisierbarkeit versprachen mittels EMSA und CD-Spektroskopie, wurden sämtliche funktionellen Studien mit aus Insektenzellen gewonnenen rekombinanten RBP-Jκ-Proteinen durchgeführt, die im Vergleich mit den bakteriell exprimierten RBP-Jκ-Proteinen sowohl eine grössere Affinität zu DNA, als auch zu Notch-Proteinen aufwiesen. Im Gegensatz dazu wiesen sowohl die verwendeten in Bakterien exprimierten Notch- als auch EBNA2-Proteine ihre volle Aktivität auf.
Die Frage, welche Komponenten des intrazellulären Fragments von Notch1 (Notch-IC) tatsächlich an der Bindung an RBP-Jκ beteiligt sind, wird in der Literatur kontrovers diskutiert. Durch die eindeutige Detektion der rein physikalischen Interaktion von RBP-Jκ mit der stärksten bindenden Komponente, Notch-Ram, sowie der natürlich vorkommenden Fusion von Ram mit sieben Ankyrin-Domänen, $Notch^{RamANK}$, mittels isothermaler Titrationskalorimetrie, EMSA sowie durch Röntgenkleinwinkelstreuungsexperimente mit binären und ternären Komplexen konnten Modelle erstellt werden, die eine Beteiligung der

Ankyrin-Domänen an der Bindung an RBP-Jκ eindeutig ausschliessen. CD-spektroskopische Untersuchungen belegen, dass ungebunden ungefaltetes Notch-Ram sich bei der Bindung an RBP-Jκ in vornehmlich α-helikale Strukturen faltet.

Zellbiologische und daher meist indirekte Nachweismethoden detektieren ausschliesslich die Existenz von Interaktionen, sagen aber wenig über deren Intensität aus. Durch die entwickelten kontrollierten Reaktionssysteme konnte mittels EMSA und isothermaler Titrationskalorimetrie eine 20- bis 50-fach höhere Affinität des verwendeten EBNA2-Proteins im Vergleich zu Notch^{RamANK} detektiert werden. Überdies wurden erste Hinweise erhalten, dass die für EBNA2 in der Literatur als Hauptinteraktionsdomäne beschriebene Region CR6 nicht allein für die um den Faktor 20 bis 50 höhere Affinität zu RBP-Jκ verantwortlich sein kann.

Hinweisen auf die exakte Bindestelle von Notch-IC an RBP-Jκ durch zellbiologische Ansätze wurden durch Kristallisationsversuche nachgegangen, die zur Lösung der dreidimensionalen Kristallstruktur von RBP-Jκ komplexiert mit Notch-IC-Fragmenten und/oder DNA führen sollten. Obwohl dies bislang nicht gelang, konnten die Kristallisationsbedingungen soweit eingeengt werden, dass die Lösung des Problems in grosse Nähe gerückt ist.

Die erhaltenen Ergebnisse helfen, einen Teil der offenen Fragen zur Charakterisierung der RBP-Jκ-Bindungspartner im Zusammenhang mit Infektionen mit dem Epstein-Barr Virus zu beantworten, die sowohl durch die Ähnlichkeit als auch durch die funktionellen Unterschiede der beiden Proteine zu bösartigen Krebserkrankungen führen können.

References

Alland, l., Muhle, R., Hou, H. J., Potes, J., Chin, L., Schreiber-Agus, N., and DePinho, R. A. (1997). Role for N-CoR and histone deacetylase in Sin3-mediated transcriptional repression. Nature *387*, 49-55.

Allday, M. J., and Farrell, P. J. (1994). Epstein-Barr virus nuclear antigen EBNA3C/6 expression maintains the level of latent membrane protein 1 in G1-arrested cells. J Virol *68*, 3491-3498.

Amakawa, R., Jing, W., Ozawa, K., Matsunami, N., Hamaguchi, Y., Matsuda, F., Kawaichi, M., and Honjo, T. (1993). Human Jk recombination signal binding protein gene (IGKJRB): comparison with its mouse homologue. Genomics *17*, 306-315.

Ambrozkova, M., Puta, F., Fukova, I., Skruzny, M., Brabek, J., and Folk, P. (2001). The fission yeast ortholog of the coregulator SKIP interacts with the small subunit of U2AF. Biochem Biophys Res Commun *284*, 1148-1154.

Artavanis-Tsakonas, S., Matsuno, K., and Fortini, M. E. (1995). Notch signaling. Science *268*, 225-232.

Bateman, A., Birney, E., Durbin, R., Eddy, S. R., Howe, K. L., and Sonnhammer, E. L. (2000). The Pfam protein families database. Nucleic Acids Res *28*, 263-266.

Bigas, A., Martin, D. I., and Milner, L. A. (1998). Notch1 und Notch2 inhibit myeloid differentiation in response to different cytokines. Mol Cell Biol *18*, 2324-2333.

Bornkamm, G. W., Hudewentz, J., Freese, U. K., and Zimber, U. (1982). Deletion of the nontransforming Epstein-Barr virus strain P3HR-1 causes fusion of the large internal repeat to the DSL region. J Virol *43*, 952-968.

Bray, S., and Furriols, M. (2001). Notch pathway: Making sense of suppressor of hairless. Curr Biol *11*, R217-221.

Burns, J. A., Butler, J. C., Moran, J., and Whitesides, G. M. (1991). Selective reduction of disulfides by tris-(2-carboxyethyl)-phosphine. J Org Chem *56*.

Calender, A., Billaud, M., Aubry, J. P., Banchereau, J., Vuillaume, M., and Lenoir, G. M. (1987). Epstein-Barr virus (EBV) induces expression of B-cell activation markers on in vitro infection of EBV-negative lymphoma cells. Proc Natl Acad Sci U S A *84*, 8060-8064.

Chen, Y., Fischer, W. H., and Gill, G. N. (1997). Regulation of the ERBB-2 promoter by RBPJkappa and NOTCH. J Biol Chem *272*, 14110-14114.

Chung, C. N., Hamaguchi, Y., Honjo, T., and Kawaichi, M. (1994). Site-directed mutagenesis study on DNA binding regions of the mouse homologue of Suppressor of Hairless, RBP-J kappa. Nucleic Acids Res *22*, 2938-2944.

Clarke, D. T., and Jones, G. (2004). CD12: a new high-flux beamline for ultraviolet and vacuum-ultraviolet circular dichroism on the SRS, Daresbury. J Synchr Rad *11*, 142-149.

Cohen, J. I., and Kieff, E. (1991). An Epstein-Barr virus nuclear protein 2 domain essential for transformation is a direct transcriptional activator. J Virol *65*, 5880-5885.

Cohen, J. I., Wang, F., Mannick, J., and Kieff, E. (1989). Epstein-Barr virus nuclear protein 2 is a key determinant of lymphocyte transformation. Proc Natl Acad Sci U S A *86*, 9558-9562.

Cordier, M., Calender, A., Billaud, M., Zimber, U., Rousselet, G., Pavlish, O., Banchereau, J., Tursz, T., Bornkamm, G., and Lenoir, G. M. (1990). Stable transfection of Epstein-Barr virus (EBV) nuclear antigen 2 in lymphoma cells containing EBV P3HR1 genome induces expression of B-cell activation molecules CD21 and CD23. J Virol *64*, 1002-1013.

Dambaugh, T., Hennessy, K., Chamnankit, L., and Kieff, E. (1984). U2 region of Epstein-Barr virus DNA may encode Epstein-Barr nuclear antigen 2. Proc Natl Acad Sci U S A *81*, 7632-7636.

Dillner, J., Kallin, B., Ehlin-Henriksson, B., Rymo, L., Henle, W., Henle, G., and Klein, G. (1986). The Epstein-Barr virus determined nuclear antigen is composed of at least three different antigens. Int J Cancer *37*, 195-200.

Dou, S., Zeng, X., Cortes, P., Erdjument-Bromage, H., Tempst, P., Honjo, T., and Vales, L. D. (1994). The recombination signal sequence-binding protein RBP-2N functions as a trancriptional repressor. Mol Cell Biol *14*, 3310-3319.

Ehebauer, M. T., Chirgadze, D. Y., Hayward, P., Martinez Arias, A., and Blundell, T. L. (2005). High-resolution crystal structure of the human Notch 1 ankyrin domain. Biochem J *392*, 13-20.

Ellisen, L. W., Bird, J., West, D. C., Soreng, A. L., Reynolds, T. C., Smith, S. D., and Sklar, J. (1991). TAN-1, the human homolog of Drosophila notch gene, is broken by chromosomal translocations in T lymphoblastic neoplasms. Cell *66*, 649-661.

Fahraeus, R., Jansson, A., Ricksten, A., Sjoblom, A., and Rymo, L. (1990). Epstein-Barr virus-encodes nuclear antigen 2 activates the viral latent membrane protein promoter by modulation the activity of a negative regulatory element. Proc Natl Acad Sci U S A *87*, 7390-7394.

Fischer, D., Barret, C., Bryson, K., Elofsson, A., Godzik, A., Jones, D., Karplus, K. J., Kelley, L. A., MacCallum, R. M., Pawowski, K.*, et al.* (1999). CAFASP-1: critical assessment of fully automated structure prediction methods. Proteins *Suppl 3*, 209-217.

Fryer, C. J., White, J. B., and Jones, K. A. (2004). Mastermind recruits CycC:CDK8 to phosphorylate the Notch ICD and coordinate activation with turnover. Mol Cell *16*, 509-520.

Fuchs, K. P., Bommer, G., Dumont, E., Christoph, B., Vidal, M., Kremmer, E., and Kempkes, B. (2001). Mutational analysis of the J recombination signal sequence binding protein (RBP-J)/Epstein-Barr virus nuclearantigen 2 (EBNA2) and RBP-J/Notch interaction. Eur J Biochem *268*, 4639-4646.

Gasteiger, E., Hoogland, C., Gattiker, A., Duvaud, S., Wilkins, M. R., Appel, R. D., and Bairoch, A. (2005). Protein identification and Analysis Tools on the ExPASy server. In The proteomics Protocols Handbook, J. M. Walker, ed. (Totowa, NJ, Humana Press).

Girard, L., Hanna, Z., Beaulieu, N., Hoemann, C. D., Simard, C., Kozak, C. A., and Jolicoeur, P. (1996). Frequent provirus insertional mutagenesis of Notch1 in thymomas of MMTVD/myc transgenic mice suggests a collaboration of c-myc and Notch1 for oncogenesis. Genes Dev *10*, 1930-1944.

Goodbourn, S., and Maniatis, T. (1988). Overlapping positive and negative regulatory domains of the human beta-interferon gene. Proc Natl Acad Sci U S A *85*, 1447-1451.

Gordadze, A. V., Peng, R., Tan, J., Liu, G., Sutton, R., Kempkes, B., Bornkamm, G. W., and Ling, P. D. (2001). Notch1IC Partially replaces EBNA2 Function in B Cells Immortalized by Epstein-Barr Virus. J Virol *75*, 5899-5912.

Grossman, S. R., Johannsen, E., Tong, X., Yalamanchili, R., and Kieff, E. (1994). The Epstein-Barr virus nuclear antigen 2 transactivator ist directed to restonse elements by the J kappa recombination signal binding protein. Proc Natl Acad Sci U S A *91*, 7568-7572.

Guinier, A. (1939). La diffraction des rayons X aux très petits angles: application á l'étude des phénomèns. Ann Phys (Paris) *12*.

Hammerschmidt, W., and Sugden, B. (1989). Genetic analysis of immortalizing functions of Epstein-Barr virus in human B lymphocytes. Nature *340*, 393-397.

Harada, S., Yalamanchili, R., and Kieff, E. (2001). Epstein-Barr virus nuclear protein 2 has at least two N-terminal domains that mediate selb-association. J Virol *75*, 2482-2487.

Hayward, S. D. (2004). Viral interactions with the Notch pathway. Semin Cancer Biol *14*, 387-396.

Helms, W., Lee, H., Ammerman, M., Parks, A. L., Muskavitch, M. A., and Yedvobnick, B. (1999). Engineered truncations in the Drosophila mastermind protein disrupt Notch pathway function. Dev Biol *215*, 358-374.

Henkel, T., Ling, P. D., Hayward, S. D., and Peterson, M. G. (1994). Mediation of Epstein-Barr virus EBNA2 transactivation by recombination signal-binding protein J kappa. Science *265*, 92-95.

Hennessy, K., and Kieff, E. (1985). A second nuclear protein is encoded by Epstein-Barr virus in latent infection. Science *227*, 1238-1240.

Hinuma, Y., Konn, M., Yamaguchi, J., Wudarski, D. J., Blakeslee, J. R., Jr., and Grace, J. T., Jr. (1967). Immunofluorescence and herpes-type virus particles in the P3HR-1 Burkitt lymphoma cell line. J Virol *1*, 1045-1051.

Hofelmayr, H., Strobl, L. J., Marschall, G., Bornkamm, G. W., and Zimber-Strobl, U. (2001). Activated Notch1 can transiently substitute for EBNA2 in the maintenance of proliferation of LMP1-expressing immortalized B cells. J Virol *75*, 2033-2040.

Hofelmayr, H., Strobl, L. J., Stein, C., Laux, G., Marschall, G., Bornkamm, G. W., and Zimber-Strobl, U. (1999). Activated mouse Notch1 transactivates Epstein-Barr virus nuclear antigen 2-regulated viral promoters. J Virol *73*, 2770-2780.

Hsieh, J. J., Henkel, T., Salmon, P., Robey, E., Peterson, M. G., and Hayward, S. D. (1996). Truncated mammalian Notch1 activates CBF1/RBP-Jk-repressed genes by a mechanism resembling that of Epstein-Barr virus EBNA2. Mol Cell Biol *16*, 952-959.

Hsieh, J. J., Zhou, S., Chen, L., Young, D. B., and Hayward, S. D. (1999). CIR, a corepressor linking the DNA binding factor CBF1 to the histone deacetylase complex. Proc Natl Acad Sci U S A *96*, 23-28.

Iso, T., Kedes, L., and Hamamori, Y. (2003). HES and HERP families: multiple effectors of the Notch signaling pathway. J Cell Physiol *194*, 237-255.

Jarriault, S., Brou, C., Logeat, F., Schroeter, E. H., Kopan, R., and Israel, A. (1995). Signalling downstream of activated mammalian Notch. Nature *377*, 355-358.

Jennings, B., Preiss, A., Delidakis, C., and Bray, S. (1994). The Notch signalling pathway is required for Enhancer of split bHLH protein expression during neurogenesis in the Drosophila embryo. Development *120*, 3537-3548.

Johannsen, E., Koh, E., Mosialos, G., Tong, X., Kieff, E., and Grossman, S. R. (1995). Epstein-Barr virus nuclear protein 2 transactivation of the latent membrane protein 1 promoter is mediated by J kappa and PU.1. J Virol *69*, 253-262.

Kannabiran, C., Zeng, X., and Vales, L. D. (1997). The mammalian transcriptional repressor RBP (CBF1) regulates interleukin-6 gene expression. Mol Cell Biol *17*, 1-9.

Kao, H. Y., Ordentlich, P., Koyano-Nakagawa, N., Tang, Z., Downes, M., Kintner, C. R., Evans, R. M., and Kadesch, T. (1998). A histone deacetylase corepressor complex regulates the Notch signal transduction pathway. Genes Dev *12*, 2269-2277.

Kato, H., Taniguchi, Y., Kurooka, H., Minoguchi, S., Sakai, T., Nomura-Okazaki, S., Tamura, K., and Honjo, T. (1997). Involvement of RBP-J in biological functions of mouse Notch1 and its derivatives. Development *124*, 4133-4141.

Kelley, L. A., MacCallum, R. M., and Sternberg, M. J. (2000). Enhanced genome annotation using structural profiles in the program 3D-PSSM. J Mol Biol *299*, 499-520.
Kempkes, B. (2002) Die Rolle des Epstein-Barr Virus nukleären Antigens 2 (EBNA-2) in der B-Zellimmortalisierung, Habilitation, Ludwig-Maximilian-Universität, München.

Kempkes, B., Pawlita, M., Zimber-Strobl, U., Eissner, G., Laux, G., and Bornkamm, G. W. (1995). Epstein-Barr virus nuclear antigen 2-estrogen receptor fusion proteins transactivate viral and cellular genes and interact with RBP-J kappa in a conditional fashion. Virology *214*, 675-679.

Kim, Y. J., Noguchi, S., Hayashi, Y. K., Tsukahara, T., Shimizu, K., and Arahata, K. (2001). The product of an oculopharyngeal muscular dystrophy gene, poly(A)-binding protein 2, interacts with SKIP and stimulates muscle-specific gene expression. Human Molecular Genetics *10*, 1129-1139.

Knutson, J. J. (1990). The level of c-fgr RNA is increased by EBNA-2, and Epstein-Barr virus gene required for B-cell immortalization. J Virol *64*, 2530-2536.

Koch, M. H. J., Vachette, P., and Svergun, D. I. (2003). Small angle scattering: a view on the properties, structure and structural changes of biological macromolecules in solution. Quaterly Reviews of Biophysics *36*, 147-227.

Konarev, P. V., Volkov, V. V., Sokolova, A., Koch, M. H. J., and Svergun, D. I. (2003). PRIMUS: a Windows PC-based system for small-angle scattering data analysis. J Appl Cryst *36*, 1277-1282.

Kopan, R., Nye, J. S., and Weintraub, H. (1994). The intracellular domain of mouse Notch: a constitutively activated repressor of myogenesis directed at the basic helix-loop-helix region of MyoD. Development *120*, 2385-2396.

Kopan, R., Schroeter, E. H., Weintraub, H., and Nye, J. S. (1996). Signal transduction by activated mNotch: importance of proteolytic processing and its regulation by the extracellular domain. Proc Natl Acad Sci U S A *93*, 1683-1688.

Kovall, R. A., and Hendrickson, W. A. (2004). Crystal structure of the nuclear effector of Notch signaling, CSL, bound to DNA. EMBO J *23*, 3441-3451.

Kurooka, H., Kuroda, K., and Honjo, T. (1998). Roles of the ankyrin repeats and C-terminal region of the mouse notch1 intracellular region. Nucleic Acids Res *26*, 5448-5455.
Lai, E. C. (2002). Keeping a good pathway down: transcriptional repression of Notch pathway target genes by CSL proteins. EMBO Rep *3*, 840-845.

Lan, K., Kuppers, D. A., and Robertson, E. (2005). Kaposi´s Sarcoma-associated Herpesvirus Reactivation is regulated by Interaction of Latency-associated nuclear Antigen with Recombination Signal Sequence-Binding protein Jk, the major downstream Effector of the Notch Signaling Pathway. J Virol *79*, 3468-3478.

Laux, G., Adam, B., Strobl, L. J., and Moreau-Gachelin, F. (1994). The Spi-1/PU.1 and Spi-B ets family transcription factors and the recombination signal binding protein RBP-J kappa interact with an Epstein-Barr virus nuclear antigen 2 responsive cis-element. EMBO J *13*, 5624-5632.

Le Roux, A., Kerdiles, B., Walls, D., Dedieu, J. F., and Perricaudet, M. (1994). The Epstein-Barr virus determined nuclear antigens EBNA-3A, -3B, and -3C repress EBNA-2-

mediated transactivation of the viral terminal protein 1 gene promoter. Virology *205*, 596-602.

Lecourtois, M., and Schweisguth, F. (1995). The neurogenic suppressor of hairless DNA-binding protein mediates the transcriptional activation of the enhancer of split complex genes triggered by Notch signaling. Genes Dev *9*, 2598-2608.

Leong, G. M., Subramaniam, N., Issa, L. L., Barry, J. B., Kino, T., Driggers, P. H., Hayman, M. J., Eisman, J. A., and Gardiner, E. M. (2004). Ski-interacting protein, a bifunctional nuclear receptor coregulator that interacts with N-CoR/SMRT and p300. Biochem Biophys Res Commun *315*, 1070-1076.

Li, L., Milner, L. A., Deng, Y., Iwata, M., Banta, A., Graf, L., Marcovina, S., Friedman, C., Trask, B. J., Hood, L., and Torok-Storb, B. (1998). The human homolog of rat Jagged1 expressed by marrow stroma inhibits differentiation of 32D cells through intraction with Notch1. Immunity *8*, 43-55.

Liang, Y., Chang, J., Lynch, S. J., Lukac, D. M., and Ganem, D. (2002). The lytic switch protein of KSHV activates gene expression via functional interaction with RBP-Jk (CSL), the target of the Notch signaling pathway. Genes Dev *16*, 1977-1989.

Ling, P. D., Hsieh, J. J., Ruf, I. K., Rawlins, D. R., and Hayward, S. D. (1994). EBNA-2 upregulation of Epstein-Barr virus latency promoters and the cellular CD23 promoter utilizes a common targeting intermediate, CBF1. J Virol *68*, 5375-5383.

Ling, P. D., Rawlins, D. R., and Hayward, S. D. (1993). The Epstein-Barr virus immortalizing protein EBNA-2 is targeted to DNA by a cellular enhancer-binding protein. Proc Natl Acad Sci U S A *90*, 9237-9241.

Lubman, O. Y., Korolev, S. V., and Kopan, R. (2004). Anchoring notch genetics and biochemistry; structural analysis of the ankyrin domain sheds light on existing data. Mol Cell *13*, 619-626.

Maier, M. M., and Gessler, M. (2000). Comparative analysis of the human and mouse Hey1 promoter: Hey genes are new Notch target genes. Biochem Biophys Res Commun *275*, 652-660.

Marshall, D., and Sample, C. (1995). Epstein-Barr virus nuclear antigen 3C is a transcriptional regulator. J Virol *69*, 3624-3630.

Miller, G., Robinson, J., Heston, L., and Lipman, M. (1974). Differences between laboratory strains of Epstein-Barr virus based on immortalization, abortive infection, and interference. Proc Natl Acad Sci U S A *71*, 4006-4010.

Milner, L. A., Bigas, A., Kopan, R., Brashem-Stein, C., Bernstein, I. D., and Martin, D. I. (1996). Inhibition of granulocytic differentiation by mNotch1. Proc Natl Acad Sci U S A *93*, 13014-13019.

Miyazawa, K., Mori, A., Yamamoto, K., and Okudaira, H. (1998). Transcriptional roles of CCAAT/enhancer binding protein-beta, nuclear factor-kappaB, and C-promoter binding

factor 1 in interleukin (IL)-1beta-induced IL-6 synthesis by human rheumatoid fibroblast-like synoviocytes. J Biol Chem *273*, 7620-7627.

Modrow, S. (2003). Molekulare Virologie (Heidelberg, Spektrum Verlag).

Mueller-Lantzsch, N., Lenoir, G. M., Sauter, M., Takaki, K., Bechet, J. M., Kuklik-Roos, C., Wunderlich, D., and Bornkamm, G. W. (1985). Identification of the coding region for a second Epstein-Barr virus nuclear antigen (EBNA 2) by transfection of cloned DNA fragments. EMBO J *4*, 1805-1811.

Mumm, J. S., and Kopan, R. (2000). Notch signaling: from the outside in. Dev Biol *228*, 151-165.

Murray, R. J., Wang, D., Young, L. S., Wang, F., Rowe, M., Kieff, E., and Rickinson, A. B. (1988). Epstein-Barr virus-specific cytotoxic T-cell recognition of transfectants expressing the virus-coded latent membrane protein LMP. J Virol *62*, 3747-3755.

Nagai, K., Yamaguchi, T., Takami, T., Kawasumi, A., Aizawa, M., Masuda, N., Shimizu, M., Tominaga, S., Ito, T., Tsukamoto, T., and Osumi, T. (2004). SKIP modifies gene expression by affecting both transcription and splicing. Biochem Biophys Res Commun *316*, 512-517.

Nakagawa, O., McFadden, D. G., Nakagawa, M., Yanagisawa, H., Hu, T., Srivastava, D., and Olson, E. N. (2000). Members of the HRT family of basic helix-loop-helix proteins act as transcriptional repressors downstream of Notch signaling. Proc Natl Acad Sci U S A *97*, 13655-13660.

Nam, Y., Sliz, P., Song, L., Aster, J. C., and Blacklow, S. C. (2006). Structural basis for cooperativity in recruitment of MAML coactivators to Notch transcription complexes. Cell *124*, 973-983.

Nam, Y., Weng, A. P., Aster, J. C., and Blacklow, S. C. (2003). Structural requirements for assembly of the CSL.intracellular Notch1.Mastermind-like 1 transcriptional activation complex. J Biol Chem *278*, 21232-21239.

Öberg, C., Li, J., Pauley, A., Wolf, E., Gurney, M., and Lendahl, U. (2001). The Notch intracellular domain is ubiquitinated by the mammalian Sel-10 homolog. JBC *276*, 35847-35853.

Oka, C., Nakano, T., Wakeham, A., de la Pompa, J. L., Mori, C., Sakai, T., Okazaki, S., Kawaichi, M., Shiota, K., Mak, T. W., and Honjo, T. (1995). Disruption of the mouse RBP-J kappa gene results in early embryonic death. Development *121*, 3291-3301.

Oswald, F., Kostezka, U., Astrahantseff, K., Bourteele, S., Dillinger, K., Zechner, U., Ludwig, L., Wilda, M., Hameister, H., Knochel, W.*, et al.* (2002). SHARP is a novel component of the Notch/RBP-Jkappa signalling pathway. EMBO J *21*, 5417-5426.

Oswald, F., Liptay, S., Adler, G., and Schmid, R. M. (1998). NF-kappaB2 is a putative target gene of activated Notch-1 via RBP-Jkappa. Mol Cell Biol *18*, 2077-2088.

Petcherski, A. G. and Kimble, J. (2000). Mastermind is a putative activator for Notch. Curr Biol. *10*, 471-3.

Petoukhov, M. V., and Svergun, D. I. (2005). Global Rigid Body Modeling of Macromolecular Complexes against Small-Angle Scattering Data. Biophys J *89*, 1237-1250.

Pierce, M. M., Raman, C. S., and Nall, B. T. (1999). Isothermal Titration Calorimetry of Protein-Protein Interactions. Methods *19*, 213-221.

Plaisance, S., Vanden Berghe, W., Boone, E., Fiers, W., and Haegeman, G. (1997). Recombination signal sequence binding protein Jkappa is constitutively bound to the NF-kappaB site of the interleukin-6 promoter and acts as a negative regulatory factor. Mol Cell Biol *17*, 3733-3743.

Porod, G. (1982). General Theory. In Small angle scattering, O. Glatter, and O. Kratky, eds. (London, Academic Press).

Provencher, S. W., and Glockner, J. (1981). Estimation of globular protein secondary structure from circular dichroism. Biochemistry *20*.

Robertson, E. S. (Editor) (2005). Epstein-Barr Virus; Laister Academic Press.

Robertson, K. D., Hayward, S. D., Ling, P. D., Samid, D., and Ambinder, R. F. (1995). Transcriptional activation of the Epstein-Barr virus latency C promoter after 5-azacytidine treatment: evidence that demethylation at a single CpG site is crucial. Mol Cell Biol *15*, 6150-6159.

Robey, E., Chang, D., Itano, A., Cado, D., Alexander, H., Lans, D., Weinmaster, G., and Salmon, P. (1996). An activated form of Notch influences the choice between CD4 and CD8 T cell lineages. Cell *87*, 483-492.

Roehl, H., Bosenberg, M., Blelloch, R., and Kimble, J. (1996). Roles of the RAM and ANK domains in signaling by the C. elegans GLP-1 receptor. Embo J *15*, 7002-7012.

Rohn, J. L., Lauring, A. S., Linenberger, M. L., and Overbaugh, J. (1996). Transduction of Notch2 in feline leukemia virus.induced thymic lymphoma. J Virol *70*, 8071-8080.
Rost, B. (1996). Methods in Enzymology *266*, 525-539.

Sakai, T., Taniguchi, Y., Tamura, K., Minoguchi, S., Fukuhara, T., Strobl, L. J., Zimber-Strobl, U., Bornkamm, G. W., and Honjo, T. (1998). Functional replacement of the intracellular region of the Notch1 receptor by Epstein-Barr virus nuclear antigen 2. J Virol *72*, 6034-6039.

Sample, J., Young, L. S., Martin, T., Chatman, T., Kieff, E., Rickinson, A. B., and Kieff, E. (1990). Epstein-Barr virus types 1 and 2 differ in their EBNA3A, EBNA3B, and EBNA3C genes. J Virol *64*, 4084-4092.

Shi, Y., Downes, M., Xie, W., Kao, H. Y., Ordentlich, P., Tsai, C. C., Hon, M., and Evans, R. M. (2001). Sharp, an inducible cofactor that integrates nuclear receptor repression and activation. Genes Dev *15*, 1140-1151.
Shirakata, Y., Shuman, J. D., and Coligan, J. E. (1996). Purification of a novel MHC class I element binding activity from thymus nuclear extracts reveals that thymic RBP-Jkappa/CBF1 binds to NF-kappaB-like elements. J Immunol *156*, 4672-4679.

Smale, S. T., and Kadonaga, J. T. (2003). The RNA Polymerase II Core Promoter. Annu Rev Biochem *72*, 449-479.

Smoller, D., Friedel, C., Schmid, A., Bettler, D., Lam, L., and Yedvobnick, B. (1990). The Drosophila neurogenic locus mastermind encodes a nuclear protein unusually rich in amino acid homopolymers. Genes Dev *4*, 1688-1700.

Struhl, G., and Adachi, A. (1998). Nuclear access and action of notch in vivo. Cell *93*, 549-560.

Sung, N. S., Kenney, S., Gutsch, D., and Pagano, J. S. (1991). EBNA-2 transactivates a lymphoid-specific enhancer in the BamHI C promoter of Epstein-Barr virus. J Virol *65*, 2164-2169.

Svergun, D. I. (1992). Determination of the regularization parameter in indirect transformmethods using perceptual criteria. J Appl Cryst *25*.

Svergun, D. I. (1999). Restoring low resolution structure of biological macromolecules from solution scattering using simulated annealing. Biophys J *76*, 2879-2886.

Svergun, D. I., Petoukhov, M. V., and Koch, M. H. J. (2001). Determination of domain structure of proteins from X-ray solution scattering. Biophys J *80*, 2946-2953.

Tamura, K., Taniguchi, Y., Minoguchi, S., Sakai, T., Tun, T., Furukawa, T., and Honjo, T. (1995). Physical interaction between a novel domain of the receptor Notch and the transcription factor RBP-J kappa/Su(H). Curr Biol *5*, 1416-1423.

Tani, S., Kurooka, H., Aoki, T., Hashimoto, N., and Honjo, T. (2001). The N- and C-terminal regions of RBP-J interact with the ankyrin repeats of Notch1 RAMIC to activate transcription. Nucleic Acids Res *29*, 1373-1380.

Taniguchi, Y., Furukawa, T., Tun, T., Han, H., and Honjo, T. (1998). LIM protein KyoT2 negatively regulates transcription by association with the RBP-J DNA-binding protein. Mol Cell Biol *18*, 644-654.

Tong, X., Drapkin, R., Reinberg, D., and Kieff, E. (1995a). The 62- and 80-kDa subunits of transcription factor IIH mediate the interaction with Epstein-Barr virus nuclear protein 2. Proc Natl Acad Sci U S A *92*, 3259-3263.

Tong, X., Drapkin, R., Yalamanchili, R., Mosialos, G., and Kieff, E. (1995b). The Epstein-Barr virus nuclear protein 2 acidic domain forms a complex with a novel cellular coactivatior that can interact with TFIIE. Mol Cell Biol *15*, 4735-4744.

Tsui, S., and Schubach, W. H. (1994). Epstein-Barr virus nuclear protein 2A forms oligomers in vitro and in vivo through a region required for B-cell transformation. J Virol *68*, 4287-4294.
Tun, T., Hamaguchi, Y., Matsunami, N., Furukawa, T., Honjo, T., and Kawaichi, M. (1994). Recognition sequence of a highly conserved DNA binding protein RBP-J kappa. Nucleic Acids Res *22*, 965-971.

Van Stokkum, I. H. M., Spoelder, H. J. W., Bloemendal, M., Van Grondelle, R., and Groen, F. C. A. (1990). Estimation of protein secondary structure and error analysis from CD spectra. Anal Biochem *191*, 110-118.

Wallberg, A. E., Pedersen, K., Lendahl, U., and Roeder, R. G. (2002). p300 and PCAF act cooperatively to mediate transcriptional activation from chromatin templates by notch intracellular domains in vitro. Mol Cell Biol *22*, 7812-7819.

Waltzer, L., Bourillot, P. Y., Sergeant, A., and Manet, E. (1995). RBP-J kappa repression activity is mediated by a co-repressor and antagonized by the Epstein-Barr virus transcription factor EBNA2. Nucleic Acids Res *23*, 4939-4945.

Waltzer, L., Logeat, F., Brou, C., Israel, A., Sergeant, A., and Manet, E. (1994). The human J kappa recombination signal sequence binding protein (RBP-J kappa) targets the Epstein-Barr virus EBNA2 protein to its DNA responsive elements. EMBO J *13*, 5633-5638.

Wang, F., Gregory, C., Sample, C., Rowe, M., Liebowitz, D., Murray, R., Rickinson, A., and Kieff, E. (1990). Epstein-Barr virus latent membrane protein (LMP1) and nuclear proteins 2 and 3C are effectors of phenotypic changes in B lymphocytes: EBNA-2 and LMP1 cooperatively induce CD23. J Virol *64*, 2309-2318.

Wang, F., Gregory, C. D., Rowe, M., Rickinson, A. B., Wang, D., Birkenbach, M., Kikutani, H., Kishimoto, T., and Kieff, E. (1987). Epstein-Barr virus nuclear antigen 2 specifically induces expression of the B-cell activation antigen CD23. Proc Natl Acad Sci U S A *84*, 3452-3456.

Washburn, T., Schweighoffer, E., Gridley, T., Chang, D., Fowlkes, B. J., Cado, D., and Robey, E. (1997). Notch activity influences the alphabeta versus gammadelta T cell lineage decision. Cell *88*, 833-843.

Wettstein, D. A., Turner, D. L., and Kintner, C. (1997). The Xenopus homolog of Drosophila Suppressor of Hairless mediates Notch signaling during primary neurogenesis. Development *124*, 693-702.

Wilson, J. J., and Kovall, R. A. (2006). Crystal structure of the CSL-Notch-Mastermind ternary complex bound to DNA. Cell *124*, 985-996.

Woisetschlaeger, M., Yandava, C. N., Furmanski, L. A., Strominger, J. L., and Speck, S. H. (1990). Promoter switching in Epstein-Barr virus during the initial stages of infection of B lymphocytes. Proc Natl Acad Sci U S A *87*, 1725-1729.

Wu, D. Y., Krumm, A., and Schubach, W. H. (2000). Promoter-specific targeting of human SWI-SNF complex by Epstein-Barr virus nuclear protein 2. J Virol *74*, 8893-8903.

Zhao, B., Marshall, D. R., and Sample, C. E. (1996). A conserved domain of the Epstein-Barr virus nuclear antigens 3A and 3C binds to a discrete domain of Jkappa. J Virol *70*, 4228-4236.

Zhou, S., Fujimuro, M., Hsieh, J. J., Chen, L., Miyamoto, A., Weinmaster, G., and Hayward, S. D. (2000). SKIP, a CBF1-associated protein, interacts with the ankyrin repeat domain of NotchIC to facilitate NotchIC function. Mol Cell Biol *20*, 2400-2410.

Zhou, S., and Hayward, S. D. (2001). Nuclear localization of CBF1 is regulated by interactions with the SMRT corepressor complex. Mol Cell Biol *21*, 6222-6232.

Zimber-Strobl, U., Strobl, L. J., Meitinger, C., Hinrichs, R., Sakai, T., Furukawa, T., Honjo, T., and Bornkamm, G. W. (1994). Epstein-Barr virus nuclear antigen 2 exerts its transactivating function through interaction with recombination signal binding protein RBP-J kappa, the homologue of Drosophila Suppressor of Hairless. EMBO J *13*, 4973-4982.

Zimber-Strobl, U., Suentzenich, K. O., Laux, G., Eick, D., Cordier, M., Calender, A., Billaud, M., Lenoir, G. M., and Bornkamm, G. W. (1991). Epstein-Barr virus nuclear antigen 2 activates transcription of the terminal protein gene. J Virol *65*, 415-423.

Zweifel, M. E., Leahy, D. J., and Barrick, D. (2005). Structure and Notch receptor binding of the tandem WWE domain of Deltex. Structure (Camb) *13*, 1599-1611.

Zweifel, M. E., Leahy, D. J., Hughson, F. M., and Barrick, D. (2003). Structure and stability of the ankyrin domain of the Drosophila Notch receptor. Protein Sci *12*, 2622-2632.

Acknowledgements

I am grateful to the EMBL for having given me the opportunity to do my PhD in the lively international environment of the Hamburg Outstation, which provided a unique scientific and cultural experience. I particularly thank Matthias Wilmanns who kindly took me in his group, for his support and useful discussions. Special thanks go to Bettina Kempkes from GSF in Munich for generously hosting me in her laboratory for extended periods and giving me the opportunity to learn most of what I know about cell biology and supporting my work at the University of Munich.

I thank Dr. Dirk Eick and Prof. Patrick Cramer for accepting to provide expert opinions about my work.

Many thanks go to the members of my thesis advisory committee, especially to Paul Tucker who kindly read the manuscript and made many useful suggestions.

Many people have been supporting me in different ways during the last four years.

The members of Bettina's laboratory have always welcomed and helped me, whenever I was there but often also at a distance. Thanks to Sabine Maier, Claudia Popp and Sarah Valencia for fruitful discussions and suggestions and support in the difficult times, which I guess, arise during any PhD. I am particularly grateful to Sabine and Andrea Hartmann for trying to introduce a structural biologist to the methodology of cell biology.

At the EMBL Hamburg I thank Eleni Mumtsidu and Young-Hwa Song for reading early versions of the manuscript and making useful suggestions. Special thanks go to Eleni for her great help with the insect cell culture and to Dimitri Svergun and his group for their help in the SAXS data collection and evaluation. Christian Neufeld and Robert Janowski introduced me to the software to build and edit structural models.

I am also grateful to Martin von Bergen from the Max-Planck Group for Structural Molecular Biology, who advised me on CD spectroscopy, and Dave Clarke from the SRS Daresbury Laboratory, who did the same with synchrotron CD.

Many thanks go to the entire EMBL staff for their help and kindness during these years.

Beyond strict work I am grateful to Jack and Stephanie King-Scott, Eleni, Rika Werner and Christian Neufeld for their friendship and support – often in edible form - and for the good time we had together.

Finally, I would like to thank my mother and my familiy for providing the best place to recharge the batteries in every respect in good and bad times.

Lebenslauf

PERSÖNLICHE DATEN

Name	**Karen Henning**
Geburtsdatum	**05.10.1976**
Geburtsort	**Brilon**
Familienstand	**ledig**
Nationalität	**Deutsch**

ANSCHRIFT

Straße/Hausnummer	**Mansteinstr. 28**
Postleitzahl, Ort	**20253 Hamburg**

SCHULAUSBILDUNG

1983-1987	**Martin-Luther-Grundschule Brilon**
1987-1990	**Gymnasium Petrinum Brilon**
09.1990 - 06.1996	**Friedrich-Spee-Gynmasium Rüthen mit Abschluss Abitur**

STUDIUM/STUDIENABSCHNITTE

10.1996 – 09.2001	**Universität: Friedrich-Schiller-Universität Jena** **Fach: Biochemie** **Abschluss: Diplom**
09.2000 – 06.2001	**IMB Jena** **Diplomarbeit im Bereich Strukturbiologie**
04.2003 – 01.2006	**Ludwig-Maximilians-Universität München** **Fach: Biologie** **Abschluss: Promotion**

STIPENDIEN

04.1999 – 09.2001	**Konrad-Adenauer-Stiftung**
03.2000 – 07.2000	**Erasmus Programm der Europäischen Union**

SPRACHKENNTNISSE

Deutsch	**Muttersprache**
Englisch	**Fließend**
Französisch	**Konversationsniveau**
Spanisch	**Konversationsniveau**
Japanisch	**Grundkenntnisse**

BERUFSERFAHRUNG

07.1999 – 09.1999	**UC Berkeley, Berkeley, CA** **Praktikum am Institute of Cell Biology**
03.2000 – 06.2000	**Karl-Franzens-Universität Graz,Österreich** **Praktikum am Institut für Vaskuläre Zellbiologie**